ATTACHMENT 1

LICENSE AMENDMENT REQUEST

TO IMPLEMENT

SELECTIVE GAS EXTRACTION (SGE)

TARGET EXPERIMENTAL FACILITY (TEF)

AT THE UNIVERSITY OF MISSOURI

RESEARCH REACTOR

ATTACHMENT 1

TABLE OF CONTENTS

LIST OF FIGURES

LIST OF TABLES

ATTACHMENT 1

1. Selective Gas Extraction Target Experimental Facility Overview

1.1 Proposed Experiment Description

The Selective Gas Extraction (SGE) experiment employs a first-of-a-kind concept for radioisotope production. It is a reactor-driven, low-enriched uranium (LEU)-based system that selectively removes specific isotopes of interest, viz., molybdenum-99 (Mo-99), in gaseous form, that are produced from fission during irradiation of Zircaloy-4 clad target rods containing LEU. The LEU is in the form of uranium dioxide (UO_2) pellets that are nominally enriched to 19.75% in the isotope uranium-235 (U-235). The target rods are contained in Al6061 cartridges that ensure uniform cooling water flow around the target rods and will be located in the graphite reflector region of the University of Missouri Research Reactor (MURR). The SGE Target Experimental Facility (TEF) will be operated by MURR staff in concert with MURR's routine reactor operations.

During SGE experiment operation, one (1) or two (2) target cartridges, holding 11 target rods each, are placed in permanently installed support assemblies in the reactor graphite reflector region. Fission product isotopes, including Mo-99, are generated during target irradiation. At the end of irradiation (0.5 to 3 weeks), and following a short period of cooling (to reduce decay heat), the target rods are removed from their respective cartridge and transferred to a loading/unloading and storage location within the reactor pool. Subsequent target rod transfer to a bank of hot cells inside the reactor containment building will be addressed in the Part 2 license amendment submission.

Figure 1 shows a functional block diagram of the SGE experiment overview for this Part 1 License Amendment submission as well as for the Part 2 submission.

The in-pool (IP) portion of SGE process, the TEF, is the focus of this reactor License Amendment request. A description of these IP systems and associated analyses are presented in this document as follows:

1. Target System including the Target Rods, Cartridge, and Housing (1 or 2 Units)
2. Target Cooling System (TCS)
3. Cartridge Loading/Unloading and Storage Station
4. Instrumentation and Control (I&C) Systems
5. Analyses of Potential Accidents and their Impact on the MURR Facility

The remaining SGE process (ex-pool) systems and associated safety analyses will be described in the Part 2 submission.

Figure 2 and Figure 3 show the layout of the TEF irradiation systems within the MURR reactor pool and containment building.

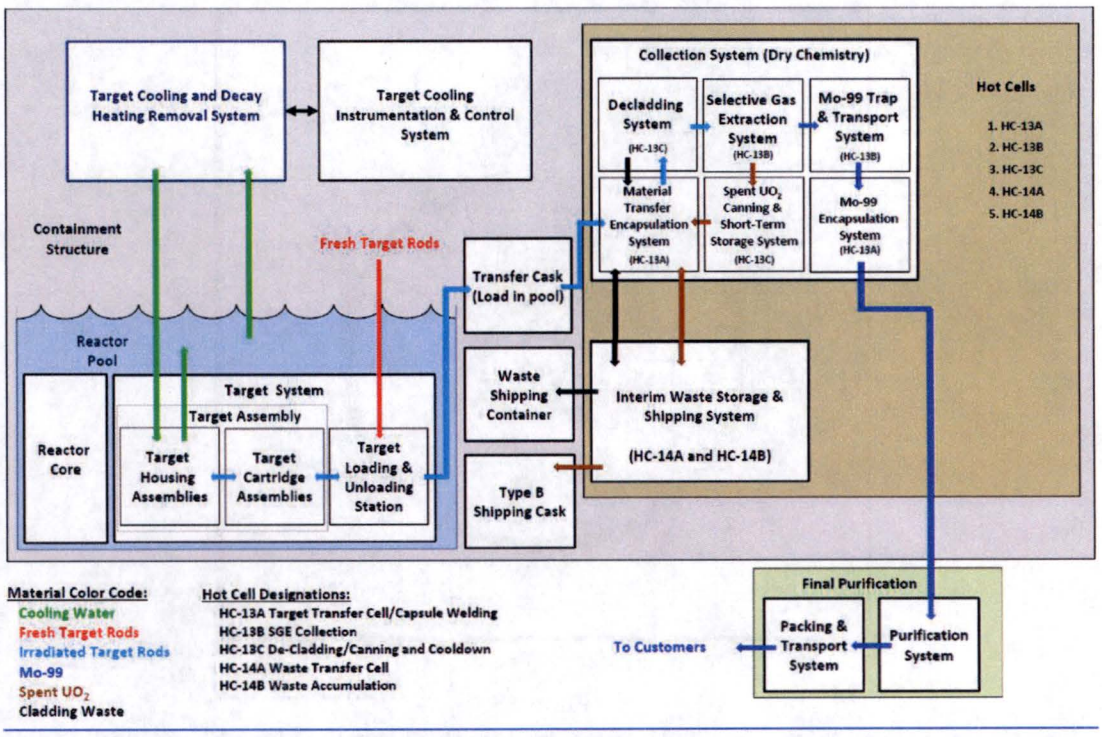

Figure 1
Selective Gas Extraction Process Scope, Functional Relationships and Interfaces

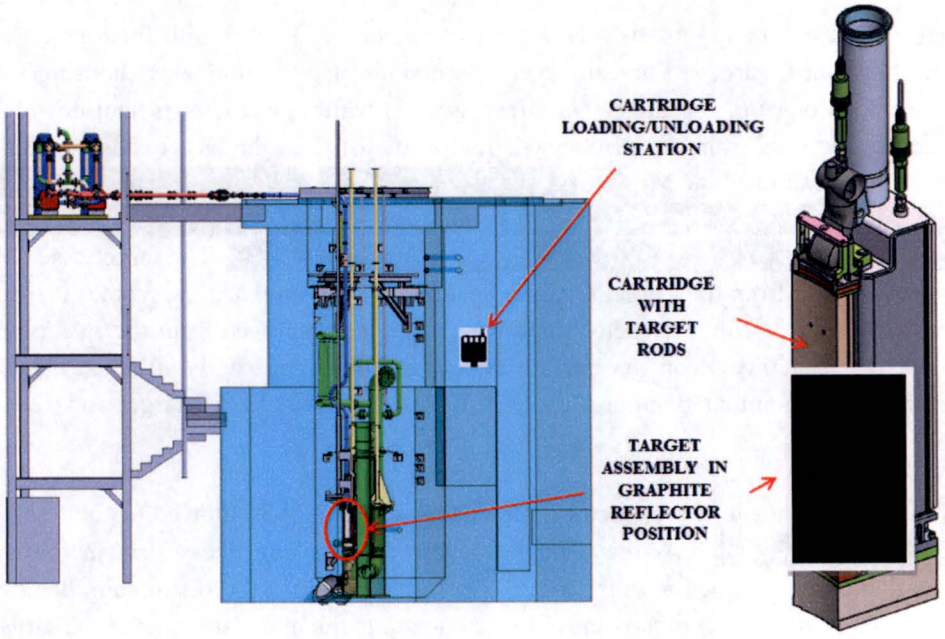

5a, b, d, e, f

Figure 2
Layout of SGE Experimental Facility in the MURR Graphite Reflector Region and Containment

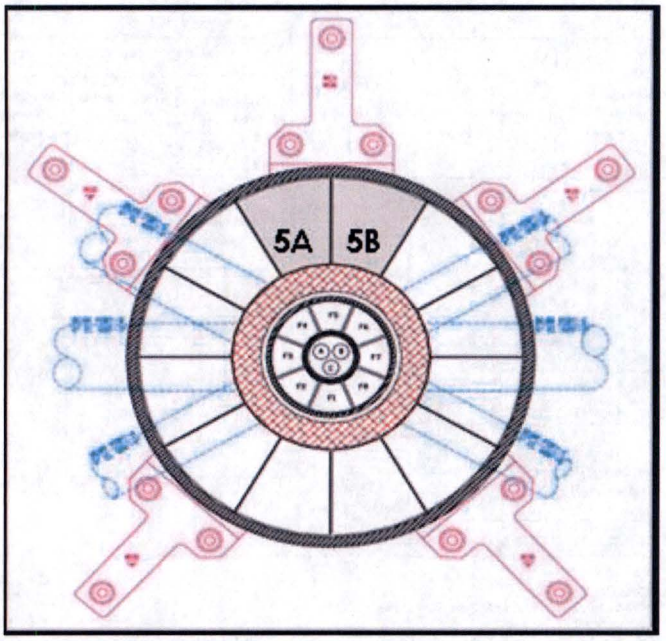

Figure 3
Location of Target Assemblies in MURR Graphite Reflector Positions No. 5A and No. 5B

1.2 Normal Operation

During normal operation, one (1) or two (2) target cartridge(s) are loaded with fresh target rods in the loading station shown in Figure 2. The cartridge(s) is then inserted into the target housing(s) located in graphite reflector positions No. 5A and/or No. 5B (Figure 3) while the reactor is shut down. When the reactor is restarted, neutrons from the reactor will fission the LEU in the target rods generating fission products, including the radioisotope Mo-99. [redacted] The target assemblies (TAs) are cooled by forced flow from the Target Cooling System (TCS) both when the reactor is operating and to remove decay heat during routine reactor shutdowns. The heat removed from the TAs is rejected via the TCS to the existing facility secondary coolant system without significantly affecting the reactor bulk pool temperature. The nominal operation cycle will load and remove 11 target rods per week for processing.

5a, d, e

At the end of the irradiation cycle, the reactor is shut down and the TA is allowed to cool by forced flow from the TCS [redacted]. At this time the level of stored and decay heat in the cartridge is sufficiently low that direct conduction to the reactor pool water is sufficient to maintain the target rods in a safe condition. The cartridge(s) is then moved to the loading/unloading station and the target rods are transferred to in-pool storage or a shielded transfer cask which has been moved to an underwater position near the loading/unloading station for safe transfer. Meanwhile a previously prepared fresh cartridge(s) is loaded into the TA positions No. 5A or/and No. 5B.

5a, d, e

1.3 Design for Loss of Forced Cooling

Loss of forced cooling (LOFC) to the TA could occur by a power failure, pump failure or coolant pipe break. If a LOFC event occurs, a low flow signal (85% of normal flow) or a high flow signal (115% of normal flow) is sent from the SGE TEF to the MURR reactor safety system to scram the reactor. Decay heat removal from the target rods is provided by pool water flowing through automatically-actuated decay heat removal valves into the target cartridge.

1.4 Target Experimental Facility Safety Design Approach

The safety objectives for the SGE TEF are (1) minimization of exposure of occupational workers to radiation from normal system operation, (2) prevention of release of radionuclides to the MURR reactor containment building and the environment from operation of the system, and (3) control of target rod cladding temperatures to prevent cladding failure leading to a fission product release to the reactor containment building and potentially, to the environment.

To meet these objectives, the SGE TEF has been designed to the following top-level requirements to ensure that the safety objectives are met:

- The target rods and cartridges shall be capable of sustained operation with the reactor operating at a steady-state power level of 10.0 MW_t and through anticipated operating transients where the reactor power reaches its scram power limit, without jeopardizing the integrity of barriers that would release radionuclides to the reactor pool water, target cooling water, or the reactor containment building.
- The target cartridges together shall not increase the reactivity worth by more than 0.006 $\Delta k/k$ when inserted into the No. 5A or No. 5B positions of the graphite reflection region.
- The target rods shall be hermetically sealed in cladding that will serve as a barrier against the release of radioisotopes to the reactor pool water, target cooling water, or the reactor containment building.
- In case of a loss of forced flow, natural circulation of the pool water through the TA shall provide an adequate backup means of removing target decay heat without damage to the cladding.
- Normal cooling shall ensure that the minimum critical heat flux ratio (MCHFR) using the Bernath correlation shall not fall below 2.0 for normal operation.
- The SGE TEF shall interface with the MURR reactor safety system to initiate a reactor scram under any condition that threatens the barriers against the release of radionuclides to the reactor pool water, target cooling water, or the reactor containment building.
- The SGE TEF Instrumentation and Control (I&C) System shall incorporate instrumentation to ensure that essential system variables are monitored and are within specified operating ranges at all times.

- The SGE TEF I&C System shall be equipped with a reliable and redundant system that monitors the operation of systems required for safety. Upon detection of conditions that indicate an anomalous state, failure or impending failure of a barrier against the release of radionuclides to the reactor pool or the containment building, the system shall cause a reactor scram, or generate appropriate alarms to cause operator action to the anomalous condition.
- The SGE TEF shall satisfy the facility limits for any releases of radioactivity to the environment.

Target and cladding design temperature limits are shown in Table 1.

Table 1
Temperature Limits for Target Assembly Design

Component	Normal Operation	Transients
Target UO_2 pellets[1]	2400 °C (4352 °F)	2860 °C (5180 °F)
Zircaloy-4 target rod cladding[2]	360 °C (680 °F)	900 °C[3] (1652 °F)
Aluminum target cartridge housing	200 °C (392 °F)	200 °C (392 °F)

[1] The maximum normal operating temperature limit for the target rods is set so that even at their hottest conditions of a maximum power level and a minimum flow rate LOFC event, the maximum pellet temperature will still be below the UO_2 melting temperature of 2860 °C.

[2] Zircaloy-4 is not an ASME code material. General Atomics uses the irradiated properties of Zircaloy-4 contained in Reference 1, which shows adequate strength to 360 °C for normal operations.

[3] This design limit on Zircaloy-4 cladding is the predicted temperature for onset of rapid oxidation of 900 °C (Reference 2). The cladding temperature predicted by transient analysis for the most severe LOFC event (0.5 sec pipe shear in the pool at the target assembly water inlet) is 650 °C, well below the onset of rapid oxidation. Further, the same analysis shows that during this time, retraction of the contained UO_2 pellet eliminates any compromise of the cladding mechanical strength.

The following design features minimize the likelihood of the target cladding exceeding the design temperature limits during irradiation and subsequent processing, and causing a release of radioactivity to the environment:

- The U-235 loading in the target rod is limited to ensure the TAs remain substantially subcritical under normal operation and all credible off-normal conditions.
- The MURR reactor will scram on low or high TA cooling water flow or loss of heat sink (secondary coolant flow) thereby limiting heat generation in the target.
- The TA is designed to permit cooling by natural convection using reactor pool water, in the event of a LOFC transient.
- The heat flux from the target rods is limited by design to ensure the temperature of the Zircaloy-4 cladding does not exceed the design limits.
- The target rod cladding serves as a barrier to the release of radionuclides. A breach of this barrier will be detected by the reactor pool coolant system radioactivity monitoring system.

- In the unlikely event of a leak of radionuclides from the target rods, the reactor pool serves to reduce the amount of both Iodine and noble gas release due to plating out of Iodine, decaying of noble gases by slowing down the time it takes the gas to rise to the pool surface, and gas solubility.

1.5 Design Bases

During the course of target operation the total thermal power and power distribution will depend upon the combination of several independent variables including burnup and location of the fuel elements, age and position of the control blades, age of the beryllium reflector, time in reactor operating cycle and time in target operating cycle. This leads to a near-continuum of core and target states. The target nuclear design analyses are performed for a selected set of conditions that typify the variation in target operating states. No one set of conditions can form a conservative basis for all the safety analyses, but rather the safety design basis was created from a composite of several states to give the conservative worst-case conditions for evaluating the safety performance of the TEF operations.

Design bases, including all assumptions for the design bases, as well as documentation of software verification calculations that form the bases of the design and safety information presented in the License Amendment are provided in the reports listed in Table 2 below.

Table 2
Design Calculation Reports

REPORT NO.	TITLE
30441R00017	ANSYS Target Cartridge, Housing Structural Analysis Design Calculation Report
30441R00019	Target System Cooling Calculation Report
30441R00021	Target Assembly Thermal Analysis
30441R00022	Source Term Analysis Design Calculation Report
30441R00030	Mo-99 Target Cooling System Seismic Analysis Design Calculation Report
30441R00031	Mo-99 Target Assembly Nuclear Design for Once-Through Operation
30441R00032	RELAP Accident Analysis and FRAPTRAN Target Rod Transient Analysis Design Calculation Report
30441R00033	Analysis of Forced Convection Cooling of Target Rods with 2 Phase Considerations
30441R00035	Cooling of the MURR Beryllium Reflector
30441R00038	Computational Fluid Dynamics Analysis of Target Housing Design Calculation Report
30441M00043	ANSYS Thermal Model of RB-MSS Target Rod

1.6 Target Assembly Maximum Power

For normal irradiation operation, the maximum target power determines the coolant flow rate necessary to meet the required TA outlet temperature. The maximum target power also establishes the safety design bases for the fission product source terms and for removal of the residual decay heat from the target rods in case normal flow is lost. The maximum target power therefore establishes the decay heat loads and source terms for safety evaluations.

The calculated maximum thermal power for two (2) TAs in graphite reflector positions No. 5A and No. 5B is [redacted] without margin for uncertainties. This value corresponds to MURR core power at 10 MW_t and a maximum core burnup case (676 MWd). This case produces a peak power in fuel element F5, which is adjacent to the target rods. This value occurs at Day 2 of irradiation and declines with target rod burnup. Nevertheless, this value is conservatively used for the afterheat level and fission product source terms assuming a target irradiation time of three (3) weeks at 160 hours per week. The worst-case control blade tilting and age is assumed (0 years for blades 'A' and 'D' and 8 years for blades 'B' and 'C') and the beryllium reflector age is assumed to be 0 years. This worst-case value conservatively corresponds to a control blade withdrawal position at 17.32 inches (44 cm) despite the fact that the "critical position" is 19.79 inches (50.27 cm). 5a, d, e, f

The estimated 2σ statistical uncertainty in the total power for two (2) TAs is [redacted]. The total uncertainties of the key performance parameters were estimated as a product of statistical error and root-mean-square (RMS) of uncertainties due to fabrication density, enrichment, and target rod position. Uncertainty in impurities was conservatively not included because it is always negative. 5a, d, e,f

An additional heat load for the required cooling is the structural heating from the cartridge [redacted]. The heat from the cartridge [redacted] is 12.7 kW and [redacted] for two (2) TAs, for a total of [redacted]. 5a, d, e,f

The maximum fission power used for the safety analyses is [redacted] for two (2) TAs. 5a, d, e, f

1.7 Target Rod Peak Linear Power

For normal operation, the peak target rod linear power determines the combination of coolant flow velocity, temperature and pressure required to achieve adequate heat transfer margin to prevent film boiling and centerline pellet melting. For abnormal operation, the peak target linear power is a critical parameter for assessing the performance of the target decay heat removal system, especially during the transition from normal cooling to backup cooling after a reactor trip.

The calculated peak linear power is [redacted] without including uncertainties. This value corresponds to a reactor core power at 10 MW_t and an extreme core burnup case (656 MWd). This peak linear power occurs at Day 2 of irradiation and declines with target burnup. Nevertheless, this value is conservatively used for the entire irradiation period. A worst-case control blade age is assumed (0 and 8 years) and the beryllium reflector age is assumed to be 0 years. This worst-case value conservatively corresponds to a 5a, d, e, f

control blade withdrawal position at 11.81 inches (30 cm) despite the fact that the "critical position" is 20.59 inches (52.29 cm).

The estimated 2σ uncertainty in the peak linear power is [redacted] based on the same statistical combination of parameters as for the maximum target power. 5a, d, e, f

The peak linear power to be used for safety analyses is [redacted]. 5a, d, e, f

1.8 Codes and Standards for Design, Fabrication and Operations

The codes and standards; design methods; software; design documentation; quality assurance and software V & V are listed in Attachment 3 to the License Amendment.

2. Detailed Selective Gas Extraction Target Assembly Description and Structural Analysis

This section describes each of the separate subsystems comprising the Target Experimental Facility (TEF): Target Assembly (TA), Target Cooling System (TCS) and target transfer system, including the neutronic and thermal-hydraulic design for the SGE TEF.

2.1 Target Assembly

2.1.1 Functions

The functions of the TA are as follows:

- Produce Mo-99 by the fission of U-235 in UO_2 with a nominal enrichment of 19.75%, but not to exceed 19.9%.
- Provide containment, support, and positioning of the UO_2 target material for irradiation and cooling.
- Guide, direct, and effectively distribute cooling water from the TCS to the surfaces of the clad target rods containing UO_2.
- Prevent fission products from inadvertently entering the reactor pool water and/or containment building.
- Maintain the target pellet configuration such that the TAs are always sub-critical, and ensure that any neutronic coupling between the TAs and the MURR reactor core will continue to meet the reactor license Technical Specification (TS) requirements.
- Enable detachment of the target cartridge from the target housing at the end of irradiation, for short-term transfer to in-pool storage.

2.1.2 Mechanical Design

The two TAs are designed to be installed in the graphite reflector positions No. 5A and No. 5B. The TAs are mirror images of each other and differ only in the position of the inlet cooling water pipe. Each TA consists of a water inlet section, a target housing, a lower plenum, a cartridge, an outlet diffuser, and a cartridge locking mechanism. The housing is held laterally in place by an indicator hole in the reflector support plate and vertically in place by the TCS inlet piping which includes a compressible link. The TA components for the No. 5A TA are shown in Figure 4. The modeling and mechanical design of the TA components in 3D was performed using the commercially available SolidWorks 2016 software package.

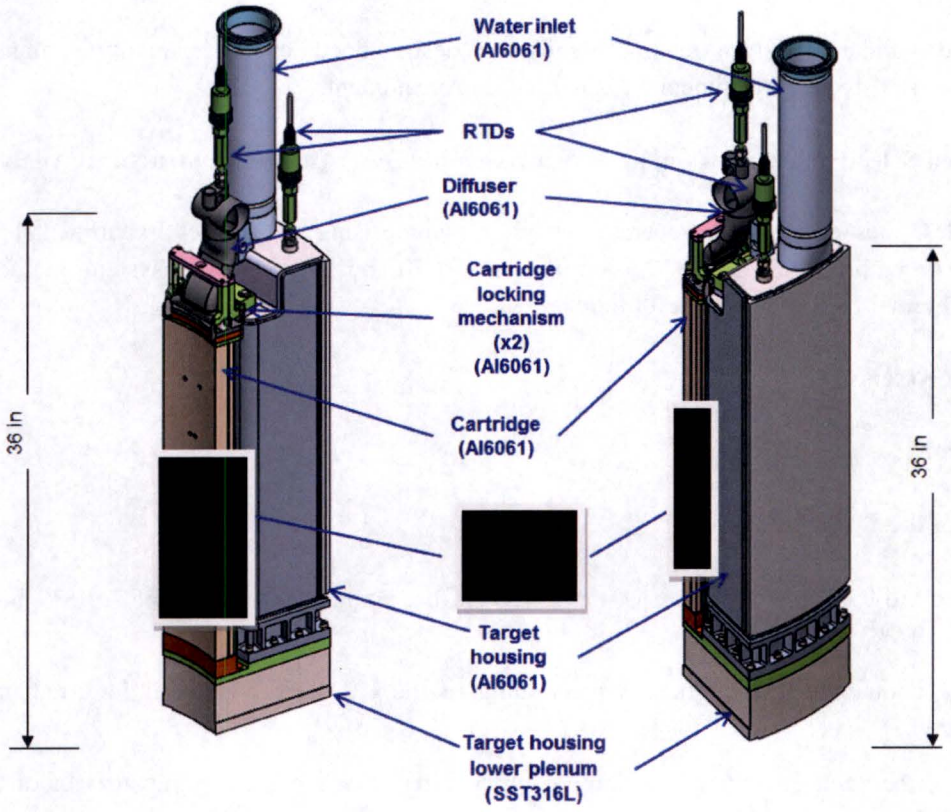

5a, b, d, e, f

Figure 4
Target Assembly (front and back views)

2.1.3 Target Housing

The functions of the target housing are to direct the flow of the cooling water, provide structural support, and position the cartridge within the graphite reflector region. The vertical and plan cutaways of the target housing are shown in Figure 5. The target housing is fabricated from welded Al6061 plates while the lower housing plenum is fabricated from SS316L. Cooling water is fed to the target housing by the TCS through a line at the top of the assembly. The target housing then directs the water flow down

through the lower plenum, up the inside of the cartridge and finally out through the diffuser into the reactor pool. The target housing and the lower housing plenum are bolted together and water leakage is prevented by a metal E-seal that keeps this interface watertight.

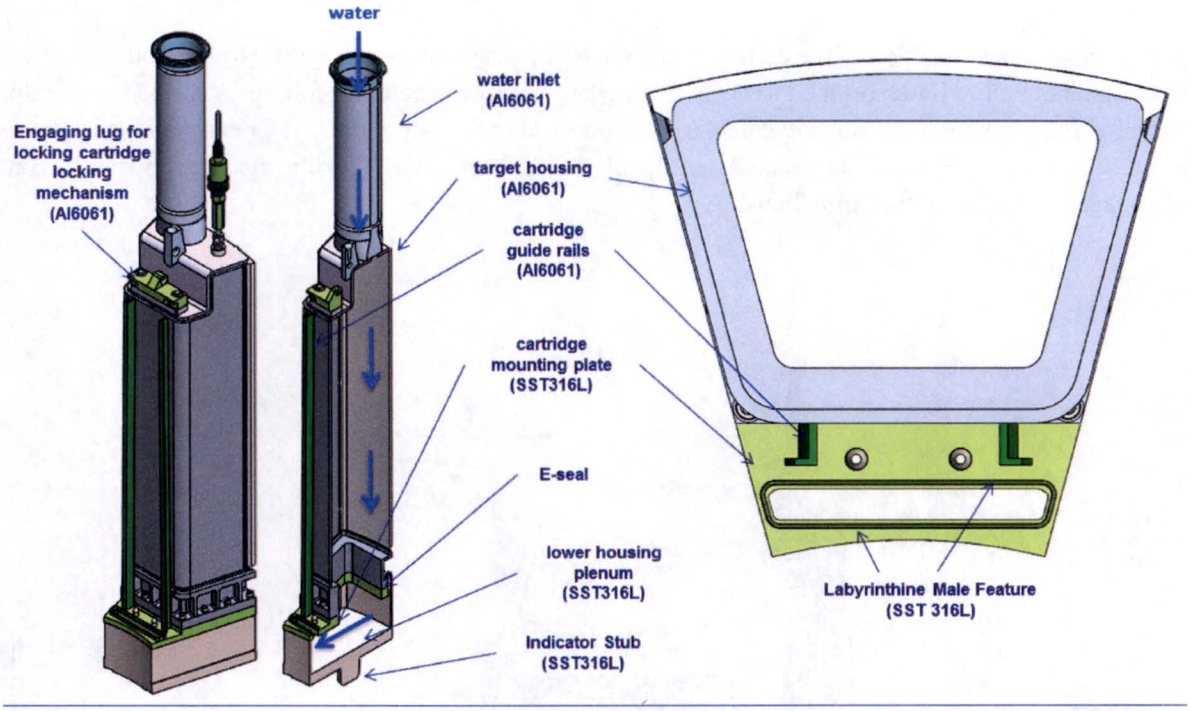

Figure 5
Illustration of Target Housing Elevation and Plan Views

The bottom of the housing has an indicator stub that locates the housing in the reflector support plate, which bears part of the weight of the TA and attached piping. The piping is secured by brackets within the reactor pool and part of the weight load from the piping is transferred to the lower housing plenum by the TA sides.

2.1.4 Target Cartridge

The functions of the cartridge are to (1) position and support the target rods containing the LEU pellets, (2) provide a cooling passage for the target rods, (3) [redacted] and (4) to mix and guide the water outlet flow. The cartridge consists of an Al6061 diffuser on the top, an Al6061 cartridge flow housing, [redacted] an Al6061 lower cartridge flange, a locking mechanism, and 11 Zircaloy-4 clad target rods. The target rods are vertically oriented in a single plane positioned in the target cartridge orthogonal to the direction of the neutron flux (Figure 6).

5a, b, d, e, f

During commissioning operations, it will be necessary to load fewer than 11 UO_2 filled target rods in a cartridge. When fewer than 11 UO_2 filled target rods are loaded, the remaining positions are filled with stainless steel filler rods with the same dimensions to ensure that the flow around all rods is uniform and at design conditions.

The orientation and position of the cartridge relative to the reactor maximizes the Mo-99 production while meeting temperature limits on the target rods. The target rods are held in position by the top and bottom cartridge flanges which allow for the coolant to flow around the target rods. The cartridge is secured in place by a locking mechanism located on top of the diffuser. The locking mechanism engages and disengages to the top of the target housing.

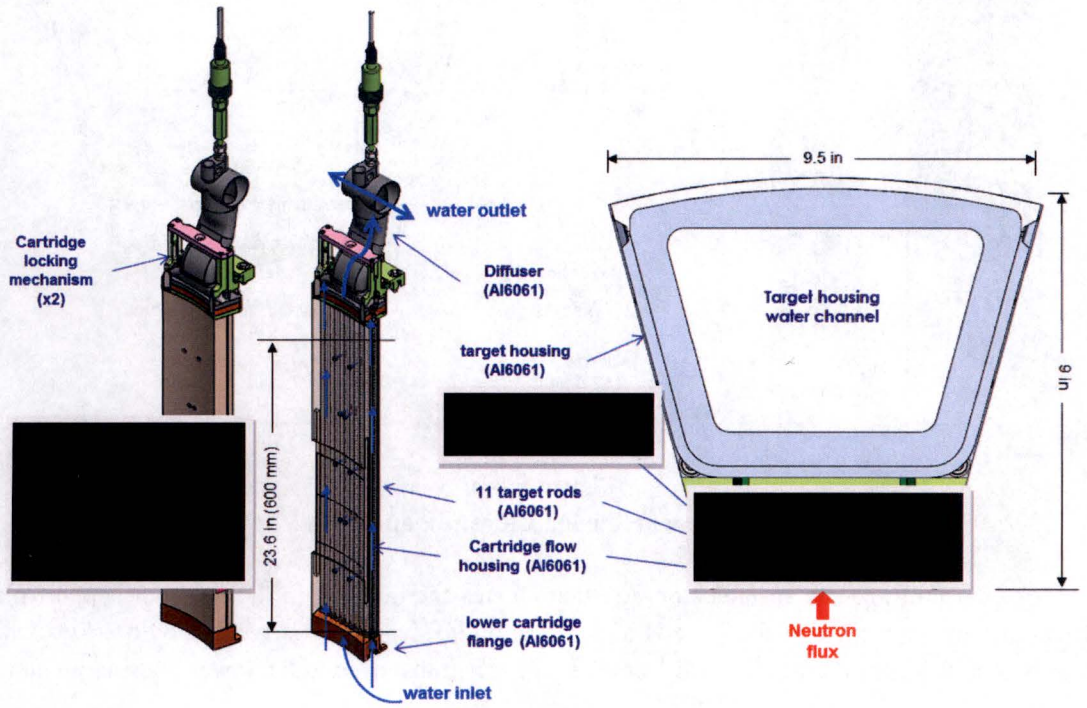

5a, b, d, e, f

Figure 6
Cartridge Configuration and Target System Section View

Figure 7 shows the cartridge upper and lower sections highlighting key components and features of the design. The cartridge design is a clamshell with two seam welds running the length of the cartridge. Five (5) pairs of SS316L pins (3/32 inches in diameter) are located along the center axis of the clamshell assembly to prevent excessive stresses at the weld locations due to the higher internal pressure from cooling water flow. This simplifies the fabrication process as well as allowing more control over the tolerances for the fit between the water cooling channels and the target rods. The cartridge is first located to the target housing by a pair of guide rails that lead to a unique labyrinthine male feature. This feature is part of the target housing lower plenum and receives and places the cartridge in its final position in

relation to the reactor. The cartridge is then held in place by a pair of locking features in the upper TA locking mechanism. The features are actuated via a lever that locks and unlocks the cartridge.

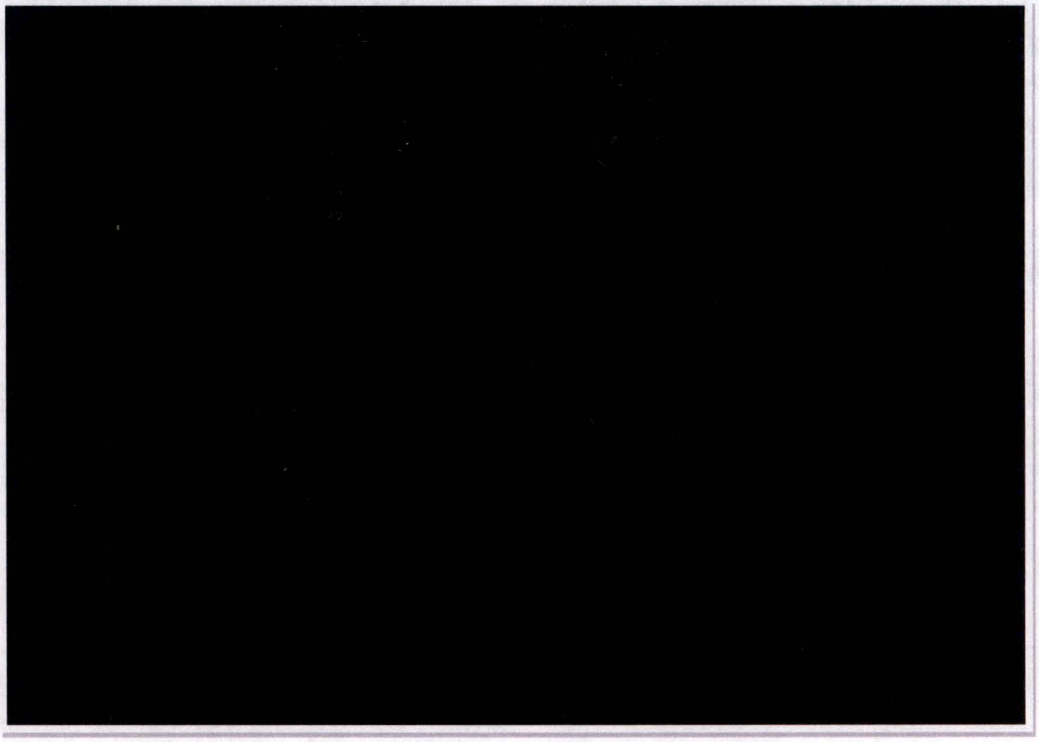

5a, b, d, e, f

Figure 7
Cartridge Upper and Lower Sections

The target rods are fixed on the top (upper endcap) and laterally supported at the bottom (lower endcap) allowing room for axial thermal expansion [redacted] The target rods are expected to thermally grow by < 2 mm (< 0.079 in), leaving [redacted] for margin including mechanical tolerance stack-ups. The target rods are located and held concentric to the water channels by 11 cup features that are fabricated into the lower cartridge flange and can be seen in Figure 8. This ensures even flow velocities around the target rods through the cartridge. The water cutouts on the cup features are smaller than the pointed end cap of the target rod. This eliminates the possibility of the target rod getting stuck on one of these water bypass features when inserting them into the cartridge and ensures the operator can always find the center of the cartridge and guide the target rod into its final position.

5a, b, d, e, f

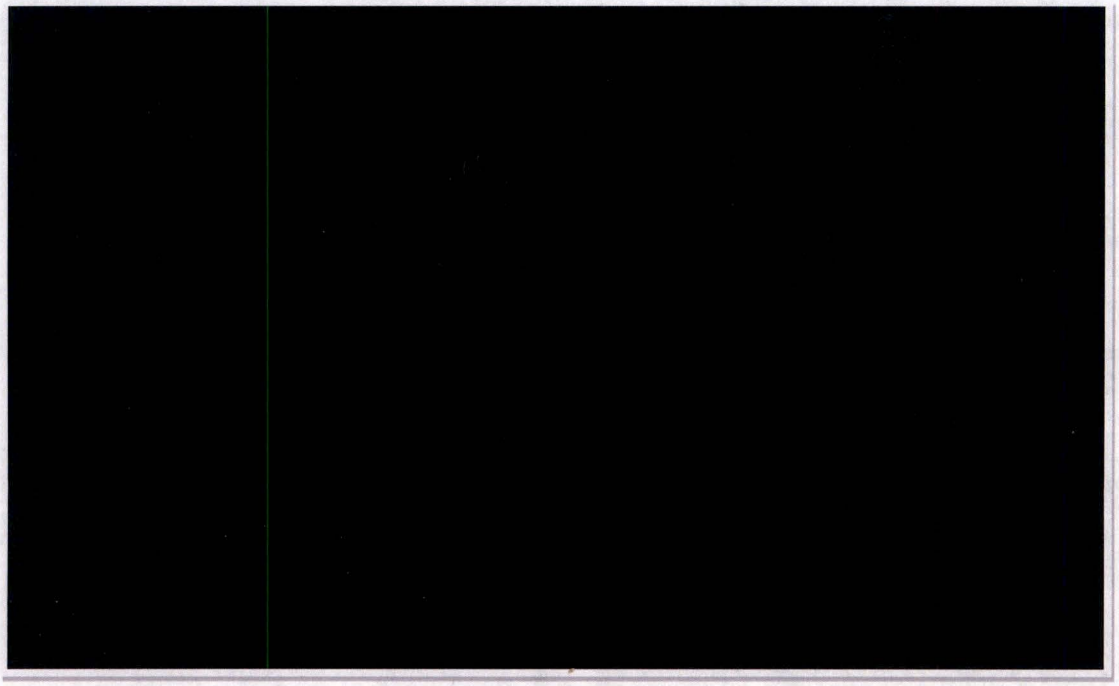

5a, b, d, e, f

Figure 8
Target Rod Lower End Cap Pins Position Rods Relative to Lower Housing Water Plenum

The water cutouts are designed to create near-uniform coolant flow over the target rods as soon as the water enters the cartridge.

2.1.5 Target Rods

Figure 9 shows an individual target rod assembly, which consists of an upper end cap, cladding, a spring, 100 UO_2 target pellets and a lower end cap. The UO_2 target pellets have a nominal active length of 23.6 inches (600 mm) in the cold state. A nominal radial gap of 50 μm exists between the pellet outside diameter (OD) and the cladding inside diameter (ID). This nominal gap offers the best dimensional balance between cladding strain and thermal conductance to the cladding wall. The end caps are fabricated from Zircaloy-4 bar with integrated features designed to optimize installation and extraction from the cartridge. Both end caps are welded to the cladding autogenously (no weld rod) by a standard automated orbital weld head. The stainless steel spring is held captive by the upper end cap, to aid in easier recovery post-irradiation. The individual pellet/clad components and dimensions are listed in Table 3.

The Zircaloy-4 (UNS R60804) cladding will be fabricated and inspected in accordance with seamless alloy tubes for nuclear reactor fuel cladding applications per American Society for Testing and Materials (ASTM) B811. The Zircaloy-4 (UNS R60804) end caps and stainless steel spring will be fabricated from bar material in accordance to ASTM B351.

The filler rods have external dimensions that are identical to the target rods, except that they are fabricated from solid stainless steel (SS316L). The filler rods ensure that the required flow conditions for safe cooling of the target rods are met. The SS316L acts as a neutron absorber to reduce power peaking in the target rod next to the filler rod.

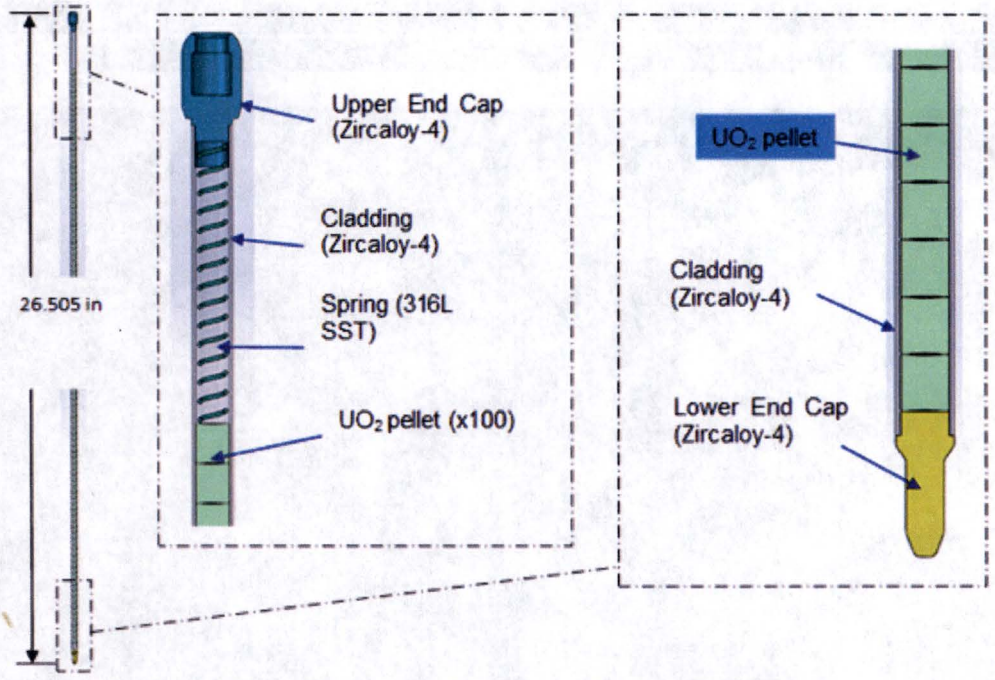

Figure 9
Target Rod Arrangement

Table 3
Target and Filler Rod Dimensions (cold)

Component	Nominal Value in Inches (mm)	
	Target Rod	Filler Rod
Active target rod length (cold)	23.6 (600)	23.6 (600)
Total target rod length	26.505 (673)	26.505 (673)
Pellet height	0.236 (6)	N/A
Pellet outside diameter	0.197 (5)	N/A
Clad ID	0.201 (5.1)	N/A

2.1.6 [redacted]

[redacted]

5a, b, d, e, f

[redacted]

5a, b, d, e, f

Figure 10

[redacted]

2.1.7 Diffuser

The functions of the diffuser are to provide upper support and containment of the target rods, provide water mixing for a bulk outlet water temperature measurement, direct the cooling water exiting the targets away from MURR equipment, and to guide nitrogen-16 (N-16) flow away from the reactor pool surface. The water is mixed in the diffuser's flow mixing zone. The exit temperature measurement is used to determine the power of the TA.

2.1.8 Target Assembly Cooling Water Flow Path

The TA cooling water flow path is shown in Figure 11. Cooling water enters the housing from the inlet pipe and flows into the open lower plenum turning into the lower cartridge flange. The lower cartridge flange has labyrinthine features to minimize water bypassing the target rods during normal operations. The flow then travels along the target rods, into the diffuser and is ultimately rejected to the reactor pool.

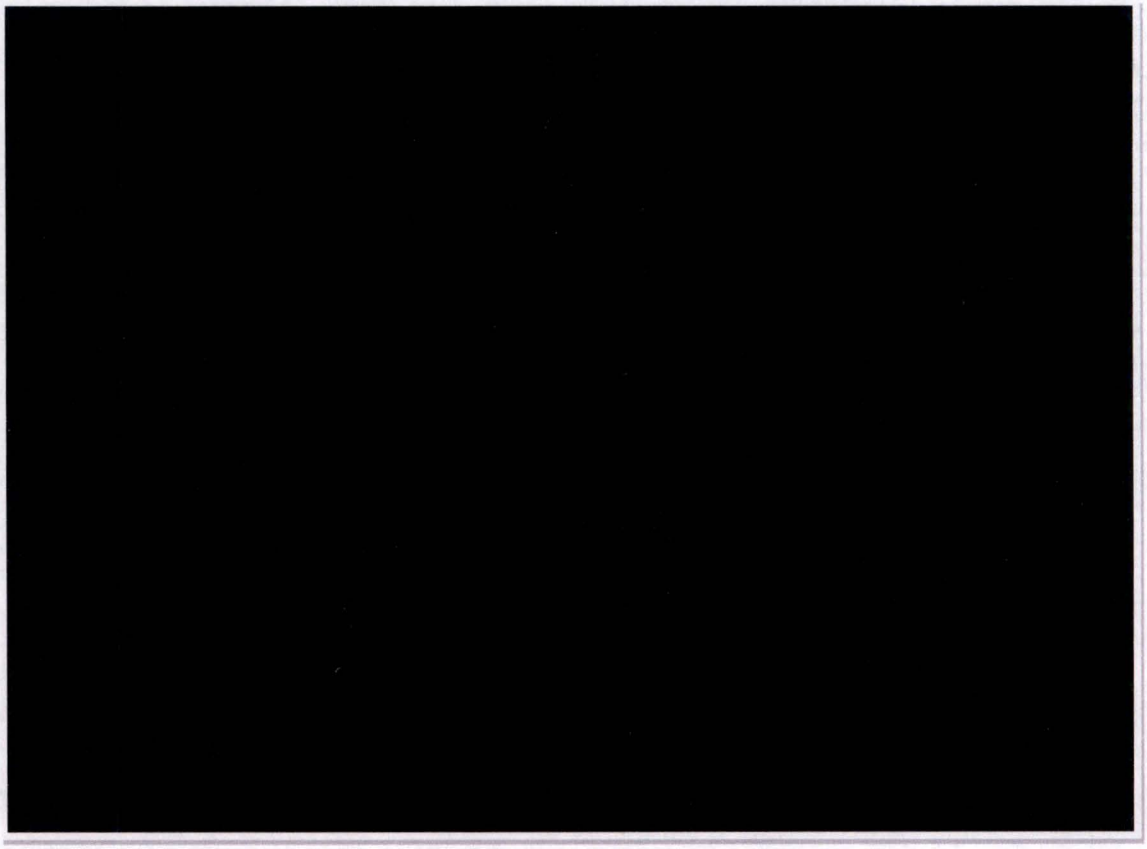

5a, b, d, e, f

Figure 11
Inlet and Outlet Plenums with Method of Attachment (water flow is shown in blue)

2.1.9 Upper Target Housing and Cartridge

The upper target housing, cartridge, and lower section of the diffuser are shown in Figure 12. The lower flange of the diffuser acts as the lid that holds down the target rods and keeps them secured in the cartridge by capturing the target rod's upper end cap. This, along with the lower cartridge flange supporting the target rods, properly constrains the target rods through the installation, irradiation, and transfer to the temporary loading/unloading station in the reactor pool. The lower diffuser flange is welded to the neck portion of the diffuser, which collects the water exiting the cartridge and mixes it before guiding it to the resistance temperature detector (RTD) for measurement of the outlet temperature, and ultimately discharges it to the pool. The mixing of the flow is significant for accurate measurement of the power being generated by the TA. The lower diffuser flange is also designed such that the water cutouts allow the flow to move through the sections have the same cross sectional surface area as the rest of the conical sections of the diffuser all the way to the exit tee. This allows the diffuser to have a minimal pressure drop from the cartridge exit to the reactor pool.

5a, b, d, e, f

Figure 12
Upper Target Cartridge Arrangement (water flow is shown in blue)

When it is time to remove an irradiated cartridge from its target housing for transfer to the in-pool loading/unloading station, the cartridge will be maneuvered and handled remotely in the reactor pool by an operator positioned on top of the pool, using the tools designed for cartridge handling. The cartridge is moved from the TA to the in-pool unloading station, where the diffuser is unlatched from the cartridge to access the target rods for loading into the in-pool storage location. The diffuser is attached to the cartridge by four spring flexures that engage the cartridge upper flange. The flexures are engaged and disengaged by depressing a spring loaded lever located at the top of the diffuser. Tools have been developed to perform such a function within the reactor pool.

2.1.10 Target Pellets

Each target rod contains 100 high density UO_2 pellets, with each pellet containing 1.205 grams of UO_2. The pellets are fabricated using a process similar to light water reactor (LWR) fuel with the pellet dimensions being the only major difference. [redacted]

5a, b, d, e, f

Manufacturing of the target pellets, the loading and welding into the

cladding shall be performed in accordance with the required fabrication, inspection and quality control procedures.

The pellet geometry is shown in Figure 13. Each pellet is nominally 5.0 mm (0.2 in) in diameter and 6.0 mm (0.24 in) high and has a density of greater than 10.42 g/cc (95% TD). The pellets and Zircaloy-4 cladding have a design tolerance to maintain a gap between the pellet and cladding. The gap directly influences the peak pellet temperature and pellet-cladding interaction. Dishing on both ends reduces ratcheting during temperature cycling.

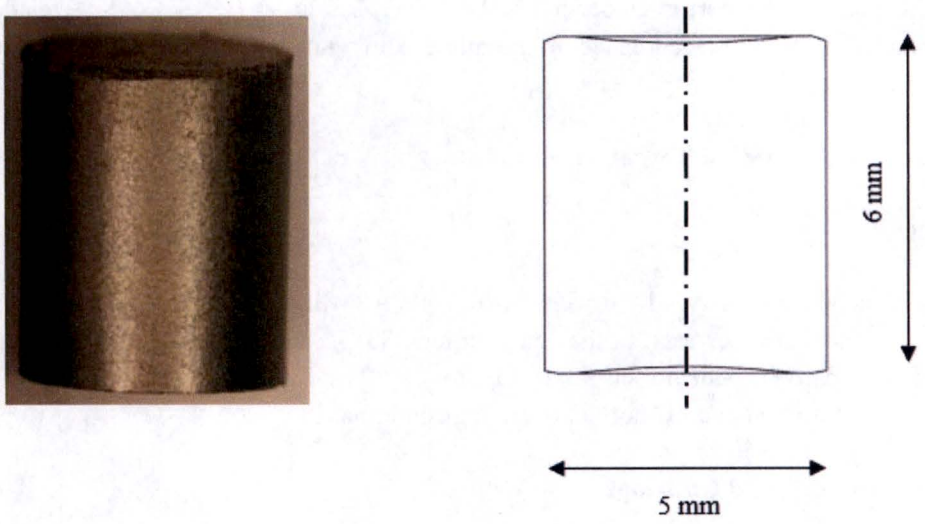

Figure 13
Target Pellet Geometry

2.1.11 Design Basis for Target System Materials

The considerations upon which target system material selections are based are as follows:

- Prior operating experience for target cladding materials in a nuclear reactor irradiation environment is preferable.
- The cladding materials must have good mechanical strength at both normal operating temperatures and at expected temperatures during transients.
- Materials in the neutron flux must have low neutron absorption cross-sections so as not to impede the rate of Mo-99 production.
- Selected alloys must have the properties to readily support fabrication into required shapes and must be readily weldable.

- The material used for the target rod cladding must not undergo undesirable chemical reactions with the target pellet material or fission products within the operating temperature range.

2.1.12 NRC-Approved Fuel Cladding Alloys

The target rods have leak-tight cladding that has proven prior experience for this application, per the design requirements. Alloys that have been approved by the U.S. Nuclear Regulatory Commission (NRC) for fuel cladding in power and research reactors in the United States include Zircaloy, SS304, SS316L, and Al6061. Zircaloy-4 was chosen due to its lower neutron absorption, which results in higher product yield, and proven performance in LWRs. The Zircaloy-4 (UNS R60804) cladding will be fabricated and inspected in accordance to seamless alloy tubes for nuclear reactor fuel cladding applications per ASTM B811.

2.2 Structural Analysis of Target Assembly

2.2.1 General

The TA components are analyzed in accordance with ASME Section VIII Division I and II. The unirradiated allowable stresses used in the analyses for SS316L and Al6061-T6 were obtained from the ASME Section II part D, and are shown in Figure 14. The Zircaloy-4 cladding has been analyzed structurally for both normal and off-normal operating conditions.

2.2.2 Target Housing and Cartridge

The structural analysis for the TA was performed using ANSYS 2016. The calculations confirmed that the target housing and cartridge components are properly sized according to the ASME B&PV Section VIII, Division 1 and Section II-D, for normal and off-normal conditions. Based on this analysis, the structural design life of the target housing is conservatively estimated at 10 years while the design life of the cartridge is conservatively estimated for one (1) year. The target housing and the cartridge, fabricated from Al6061-T6, were analyzed for a maximum design pressure of 148.2 kPa (21.5 psi) and 102.04 kPa (14.8 psi) differential, respectively, to allow for design margins. The normal expected operating differential pressures (100% flow) will be 93.91 kPa (13.62 psi) and 66.40 kPa (9.63 psi) for the housing and cartridge, respectively. However, the flow conditions for which a reactor scram is initiated (115% of normal flow) increases the pressures to 120.11 kPa (17.42 psi) for the housing and to 83.84 kPa (12.16 psi) for the cartridge, respectively. For this 115% flow scenario, the calculated maximum membrane plus bending stresses of 27.07 MPa (3930 psi) for the housing and 49.07 MPa (7120 psi) for the cartridge, show that both the target housing and cartridge aluminum components are well within the allowable limit of 82 MPa (11,893 psi) at expected operating temperatures of ~50 °C (122 °F) (Figure 14).

The SS316L pins in the cartridge see the higher stresses but all are still well within allowables (115 MPa). For the 115% flow condition, the highest maximum principal stress that the SST136L housing components experience is 46.84 MPa (6.79 ksi) while the cartridge pins are subjected to a maximum membrane plus bending stress of 49.07 MPa (7.12 ksi). At these stresses, this design ensures that both

the housing and the cartridge maintain a Factor of Safety (FOS) > 3 for the aluminum components and a FOS > 2 for the stainless steel components before the material begins yielding (241 MPa yield for aluminum and 172 MPa for SS316L per the ASME Code).

This satisfies Section C(1)(c)(3) of Regulatory Guide 2.2, "Development of Technical Specifications for Experiments in Research Reactors," on mechanical stress effects for materials of construction for reactor experiments, which states that materials of construction and fabrication and assembly techniques utilized in experiments "*...should be so specified and used that assurance is provided that no stress failure can occur at stresses twice those anticipated in the manipulation and conduct of the experiment or twice those which would occur as a result of unintended but credible changes of, or within, the experiment.*" Both the housing and the cartridge therefore maintain a FOS > 2 to the yielding allowables which provides plenty of margin to failure stresses as mentioned in Regulatory Guide 2.2.

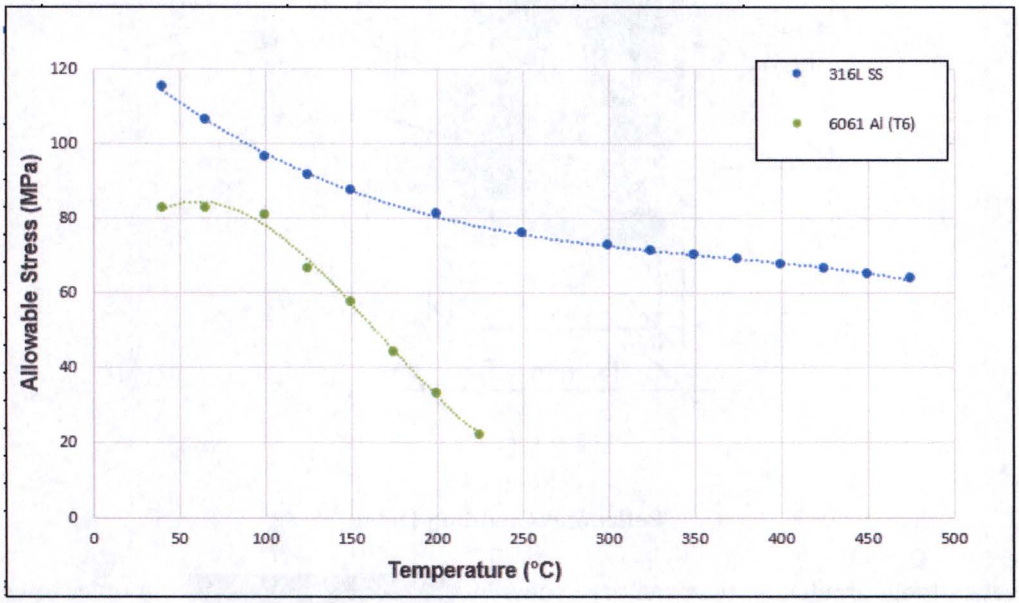

Figure 14
Allowable Strength vs Temperature for Al 6061T6 and SS316L

2.2.3 Pellet-Clad Interaction

Pellet-clad interaction for the target rods have been analyzed using FRAPCON 4.0 to ensure that the target rod performance does not exceed design limiting factors for target pellet melting temperatures and cladding strain cycles. Each target rod consists of 100, 95% dense UO_2 pellets that are encapsulated by the Zircaloy-4 cladding.

The pellets (Figure 15) have been designed for optimum performance with manufacturability in mind. Dishing of both ends was added to address ratcheting effects in the cladding, while chamfers were added for ease of insertion and to eliminate stress concentrations on the cladding from pellet rotation. The pellet

to clad gap was optimized at 50 microns nominal to minimize stress/strain in cladding on one hand and peak centerline temperatures on the other. When adding manufacturing tolerances, the gap varies between [redacted] microns. Additionally, the target rod void space is filled with > 95% He, at ≈1 atmosphere that provides good heat transfer properties to minimize pellet centerline temperatures. 5a, b, f

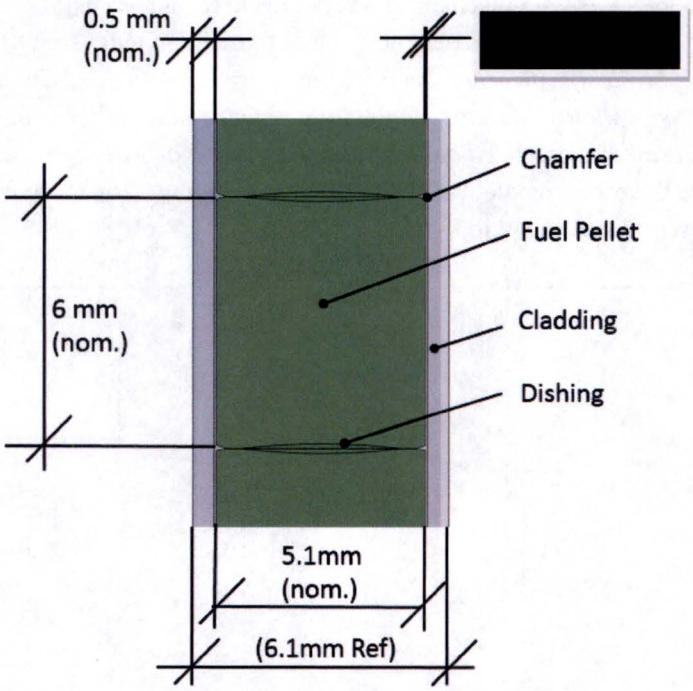

5a, b, f

Figure 15
Pellet and Cladding Details

The target cartridge irradiation time can vary between [redacted]. In order to construct a worst-case operating scenario for pellet-clad interaction analysis, it was assumed that during a [redacted] irradiation period the reactor could see a maximum of [redacted] startups and shutdown cycles, [redacted] per week. The reactor nominal operating power is 10 MW_t, with a reactor shutdown occurring at the end of the [redacted] period. For analysis purposes it is assumed that at the beginning and end of the [redacted] period, the reactor would run at 115% (11.5 MW_t) power for a period of 24 hours. The result, an upsurge in fission gas release, internal pressure rise, and additional thermal growth and pellet relocation are experienced, though the duration and frequency are not enough to cause any design limit to be exceeded. 5a, d, e

The results of the FRAPCON analyses for the above operating scenario are shown in Table 4. Stresses and strains as a result of pellet-clad interaction are highest for the minimal cold gap ([redacted]). The results show that the primary pressure induced stress is 8.1 MPa (1175 psi), which is well within the primary stress limit of Zircaloy-4 of 385 MPa (55,840 psi) at a temperature of 329 °C (624 °F) (Figure 16). With a factor of safety (FOS) of > 47 on primary stresses, the design meets ASME B&PV Code as 5a, b, f

well as Regulatory Guide 2.2, Section C(1)(c)(3) on mechanical stress effects for materials of construction for reactor experiments (FOS against failure of > 2). Primary stresses are therefore not the driver for cladding failure. Secondary stresses as a result of thermal differential expansion and re-location of the cracked pellet on the other hand are the main drivers for cladding longevity. A yield strain for Zircaloy-4 at temperature of about 0.778% is well within the strain range of twice of yield, 1.6%. Therefore, this meets the secondary stress intensity limit. With respect to cyclic fatigue for Zircaloy-4, the maximum number of cycles that the cladding can sustain is 9,000 as shown in Figure 17 (Reference 3), which includes irradiated specimens. With only six (6) expected cycles, the cladding has ample design margin.

Table 4
FRAPCON Results Summary

Gap Size	[redacted]	**50 µm**	[redacted]
Temperature (°C)			
Pellet centerline	2464	2450	2527
Pellet surface	447	438	533
Cladding ID	329	301	327
Cladding OD	177	181	177
Cladding Average	253	241	252
Strain (%)			
Radial	-0.664	-0.281	0.146
Axial	0.409	0.266	0.169
Hoop	0.778	0.499	0.280
Gas Pressure (MPa)			
Cladding Internal	0.72	0.78	0.92

5a, d, e, f

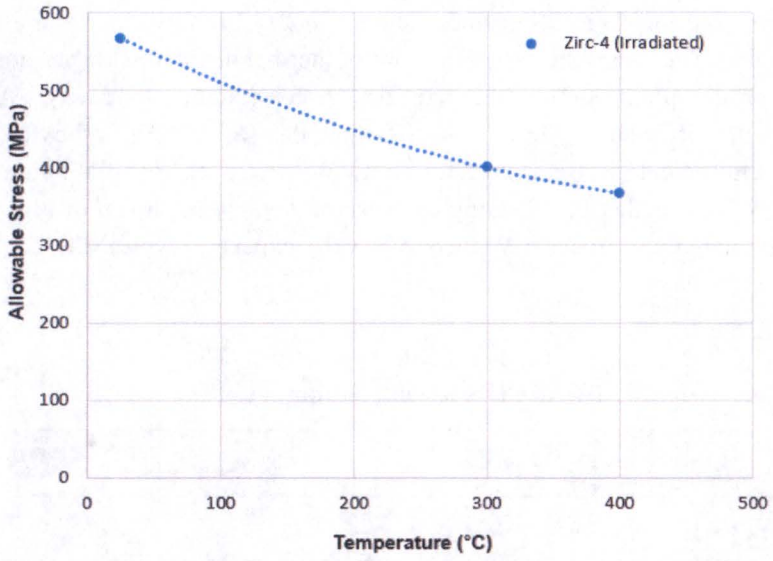

Figure 16
Allowable Stress for Irradiated Zircaloy-4 Based on 2/3rd Yield [Geelhood 2008]

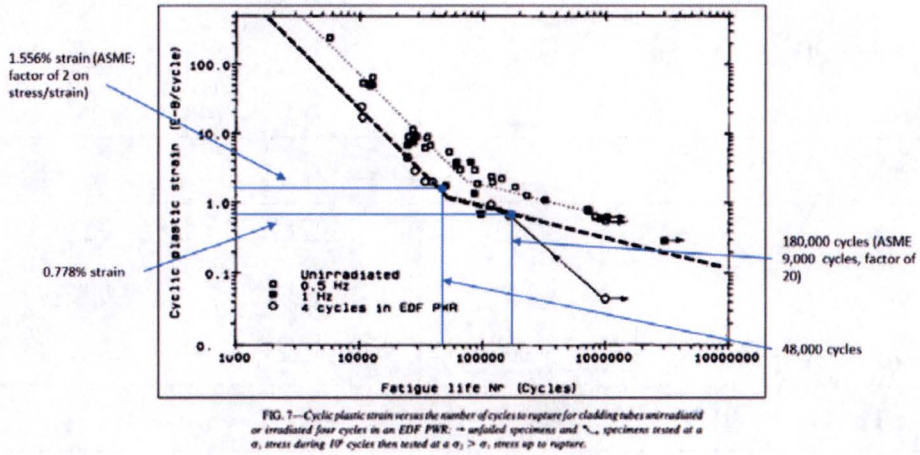

FIG. 7—*Cyclic plastic strain versus the number of cycles to rupture for cladding tubes unirradiated or irradiated four cycles in an EDF PWR: → unfailed specimens and ↘, specimens tested at a σ_1 stress during IP cycles then tested at a $\sigma_2 > \sigma_1$ stress up to rupture.*

Figure 17
Fatigue Chart for Zircaloy-4 at 350 °C (un-irradiated and irradiated)[1]

[1] The reported values for cycles in Figure 4-14 were adjusted in accordance to ASME B&PV Code to provide a factor of 2 on stress/strain and 20 on cycles (whichever is more conservative). With a factor of > 2 on stress/strain, ASME B&PV covers the requirements of Regulatory Guide 2.2. This means that in case of 0.778% strain, applying a factor of 2, or 1.556% strain, the quantity cycles are estimated at 21,000, or in case of 0.778%, using a reduction factor of 20, the expected cycles are 9,000 (180,000 cycles / 20). Note that these are adjustment factors to the experimental data set to obtain estimates of lives of components per NUREG/CR-6815.

In case of the maximum gap of [redacted] microns, the upper limit of manufacturing tolerances, the concern is the centerline temperature of the target pellet. The maximum target pellet centerline temperature is 2527 °C (4581 °F) (Table 4), which will occur at startup when no relocation has occurred. This value is well within the pellet melting temperature of 2860 °C (5180 °F). 5a, b, f

The analyses show that the target rod meets the design requirements and can be safely operated under nominal reactor conditions of 10 MW_t, including the two (2) 11.5 MW_t excursions at the beginning and end of the three (3) weeks. The design incorporates a safety factor of 1,500 for cladding cycles and > 25,000 for pressure-induced primary stress cycles. Additionally, the pellet cladding exhibits a thermal margin of safety of > 140 °C (252 °F), while the contained target pellet exhibits a thermal margin of safety of > 313 °C (595 °F).

2.2.4 Effect of Neutron Irradiation on Target Assembly Structural Materials

The irradiation damage to TA materials of construction Al6061, Zircaloy-4 and SS316L was calculated for full neutron spectrum using damage cross-sections (Reference 4). The maximum damage occurs at the active target vertical mid-plane. The driver neutron flux from the reactor core drops off rapidly as a function of vertical distance from the mid-plane. Table 5 shows the component, location and damage in terms of displacements per atom (dpa).

Table 5
Maximum Irradiation Damage to Target Cartridge Materials

Material	Component	Location	Design Life (weeks)	Fast Neutron (0.1 – 20 MeV) Fluence (n/cm^2)	dpa for Design Life (Ref. 5)
Al6061	Target Cartridge	Front face at active target mid-plane	52	2.0×10^{21}	1.12
Zircaloy-4	Target Rod Cladding	Target rods	3	1.8×10^{20}	0.033
SS316L	Target Cartridge	Front face at active target mid-plane	52	2.2×10^{21}	0.38
Al6061	Target Housing	Front face at active target mid-plane	520	7.6×10^{21}	4.29
SS316L	Lower Plenum	Front face	520	1.4×10^{21}	0.27

The impact of these low levels of irradiation damage on the material structural properties are as follows:

Al6061 – This alloy has a high degree of radiation tolerance and can sustain damage levels in excess of 100 dpa. For damage levels of 1.12 dpa at 50 °C (122 °F), the alloy will experience less than 17% volumetric swelling. The yield and ultimate strengths are increased by ~50% above 0.5 dpa. The alloy

retains good ductility (> 5% failure strain) after irradiation; however, the AL6061 target housing strain is very low at the maximum damage location. The use of non-irradiated properties per the ASME Section II code is appropriate for the use of this alloy in the TA (Reference 6).

Zircaloy-4 – Zircaloy-4 is used reliably as fuel cladding for LWRs with fast fluences in the range of 10^{22} n/cm^2 at 300 to 400 °C (572 to 752 °F). By comparison, the Zircaloy-4 cladding for the target rods will have a maximum fast fluence of 1.8 x 10^{20} n/cm^2 (Table 5) at ~100 to 250 °C, assuming a three (3) week exposure. This results in the displacements per atom (dpa) from fast neutron (E_n = 0.1 – 20 MeV) irradiation of 0.033 dpa. By comparison, LWRs experience peak Zircaloy dpa levels up to 20. However, the effect of irradiation at lower temperature is to lower the rate of annealing. This increases the rate of damage and the level at which thermal-mechanical properties saturate as a function of fluence (or dpa). Reference 7 shows that at LWR temperatures, the properties tend to saturate at a fast neutron fluence of 1 x 10^{21} n/cm^2, but at research reactor temperatures (< 100 °C), some properties will saturate at ~0.5 x 10^{20} n/cm^2, which is lower than the maximum fast fluence experienced by the target. Nevertheless, the total damage to the Zircaloy-4 cladding is not significant for its intended service. The effect on thermal conductivity is negligible (Reference 8). At the lower target operating temperatures, the tensile strength will increase slightly (+20%) at the expense of some loss of ductility (-30%). At 250 °C (482 °F), the irradiation effects will be negligible. These factors are accounted for in the design and structural analysis of the cladding.

SS316L – This alloy will experience a small increase in tensile strength and a corresponding small loss of ductility for the maximum dose of 0.38 dpa at the operating temperature range. This maximum exposure is very small and occurs at the longitudinal center of the cladding. The yield strength increases by about 25% while the failure strain decreases by about 30% (Reference 9). Because the SS316L cladding experiences very low strain along its length, the loss of ductility is not a concern. The fracture toughness will experience a small (< 15%) decrease (Reference 10). This is also an insignificant impact on structural design due to the small negative effect of the low dpa. Therefore, the use of non-irradiated properties per the ASME Section II code is appropriate for the use of this alloy in the TA.

2.2.5 Bowing of Target Rods

The LEU target rods are driven by a directional neutron flux from the reactor core; hence, they can be expected to experience a power gradient across the UO_2 pellet. This will cause a small degree of bowing of the target rods in the radial plane of the core as a result of the following two (2) effects:

1. The reactor core facing side of the rod will have a slightly higher temperature than the opposite side causing differential thermal expansion; and
2. The reactor core facing side of the rod will be exposed to a slightly higher fast neutron flux causing a small degree of differential irradiation induced strain. Conservative evaluations of both effects have been carried out and the estimated bowing is shown to have no effect on rod heat removal.

The power density distribution was analyzed for the target rod where the power density of the front half of the pellets was found to be on average 6% greater than the rear half. At the worst axial location, the front half power density was found to be 16% greater than the rear half. This worst-case assumption is extremely conservative, as only a few pellets throughout both targets come close to this power skew, and the average skew for rods containing those points is much lower. In addition, the entire stack was conservatively assumed to have the maximum power density of [redacted]. The combination of maximum tilt with maximum power density produces a front-to-back temperature difference of about 16.8 °C.

5a, d, e, f

A thermal analysis was performed for the worst power density, showing a total axial growth of the target rod cladding of approximately 0.65 mm. Output from a FRAPCON analysis showed that the irradiation-induced axial growth of the target rod cladding was 0.56 mm. Therefore, it was deemed that the effects of the irradiation induced growth could be captured conservatively in a structural model by doubling the Zircaloy-4 coefficient of thermal expansion in the structural model.

Figure 18 provides a visual depiction of deflection of a target rod for a conservative, worst-case power skew. The figure shows the black wireframe of the un-deformed geometry, with the deformed body colored according to the deflection. The left portion of the figure shows a 1:1 scale of the deflection at its worst point, which shows the maximum deflection of 0.61 mm as slightly greater than the thickness of the cladding (0.5 mm). The right portion of the figure shows the overall deflection of the target rod by magnifying the displacement by a factor of 30.

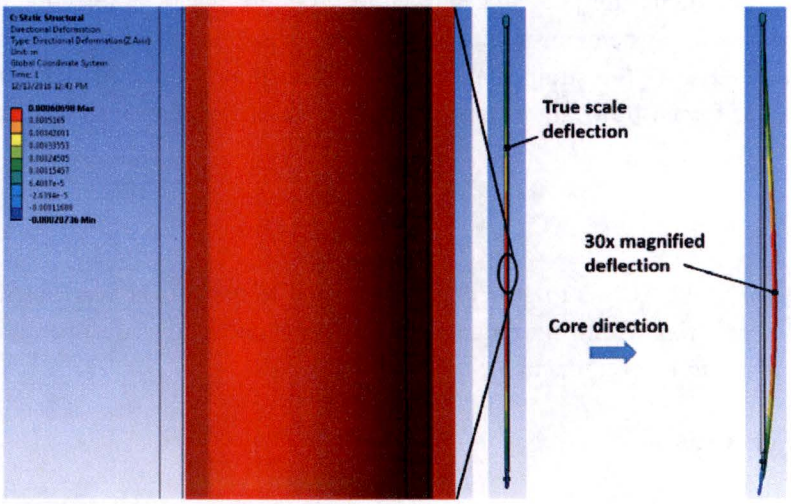

Figure 18
Deflection Due to Target Rod Bowing for Worst-Case Front-to-Back Power Skew

Given that the distance between the target rod and the cartridge wall when centered is about 4.4 mm (0.17 in), no contact would occur. Additionally, flow through the cartridge is highly turbulent and boundary layers are very thin, so this level of deflection would not affect the heat transfer to the coolant. A more realistic average power skew scenario predicts a deflection of only 60 microns, i.e. a factor of ten

less than the conservative case. Given these results, it can be concluded that target rod bowing due to both thermal and irradiation effects will not affect the thermal-mechanical performance of the target rods and cartridge assembly.

3. Target Cooling System

The Target Cooling System (TCS) provides cooling water flow to the two (2) TAs during normal operation and during both planned and unplanned shutdowns. The TCS has two methods of cooling, corresponding to force cooling (pumped) flow during normal operation and natural circulation flow during post loss of forced cooling (LOFC) scenarios.

- Forced Cooling: The reactor is operating and producing fission power in the TAs. The TCS pumps water from the reactor pool, cools it through a heat exchanger that interfaces with the MURR secondary coolant system. The TCS then transports the cooled water to both TAs. The cooling water exits the TAs and flows back to the reactor pool.
- Natural Convection: In the event that pumped flow to the TAs is interrupted, the reactor is shut down and the TA power reverts to decay heat. The TCS transitions to natural circulation flow to the TAs in which valves on the target cooling inlet pipes are opened to allow pool water to flow through the TAs as driven by natural circulation from target decay heat.

The TCS is divided into two subsystems, the target flow assembly and the water cooling module. The flow interface begins at the reactor pool and ends at the TA inlet. The heat rejection interface is with the MURR secondary coolant system for forced cooling operation and with the reactor pool for natural convection operation. The TCS instrumentation also includes inputs to the MURR reactor safety system to scram the reactor if forced flow falls below 85%, or above 115% of normal flow, and on high coolant temperature to the TA.

3.1 Functions

The primary function of the TCS is to provide cooling water to the TAs at a sufficient mass flow rate to maintain the target material within its required temperature range for safe operation. The system is designed to perform the following functions:

3.1.1 Process Functions

- Transfer and reject the target heat to the MURR secondary coolant system during normal operation.
- Maintain sufficient cooling water flow rate and temperature conditions through the target to maintain a large CHFR margin and such that any subcooled nucleate boiling has a negligible impact on target rod integrity.
- Minimize net exchange of heat between the TCS and the reactor pool water during normal operation.

- Provide for reliable transition of target heat removal to the reactor pool via natural circulation in the event of an LOFC.
- Provide instrumentation to assure that flow, temperatures and pressures are within specified conditions for operation.

3.1.2 Safety Functions

- Provide a signal to the MURR reactor safety system to enable a reactor scram in the event that the forced cooling water flow rate falls outside specified ranges for safe operation or for high heat exchanger outlet temperature.
- Provide a corresponding signal to open the decay heat removal valves to initiate natural circulation flow to the TAs that coincides with a reactor scram in the event that the forced cooling water flow rate falls outside specified ranges for safe operation.

Accident analysis shows that even if no natural circulation occurs after an LOFC event, target decay heat will be transported directly to the pool. The targets will remain in a safe condition with no radioactivity released to the reactor pool.

3.2 Target Cooling System Principal Design Parameters

The principal design condition for the TCS corresponds to both TAs loaded with 11 target rods each and the reactor operating at 10 MW_t. The target power levels will vary slightly due to shifts in the driving neutron flux distribution caused by changes in burnup of reactor fuel elements, position of control rods and age of the beryllium reflector. The TCS is designed to accommodate the maximum target thermal power and the maximum linear heat rate. The TCS is designed to maintain an approximate 10 °C (18 °F) cooling water temperature rise across the target cartridge(s) for the maximum power condition. The corresponding flow rate combined with the cartridge design assures the target rod CHFR is greater than 2.0 for the worst-case allowable operating condition.

Table 6 summarizes the principal TCS design parameters assuming the reactor is operating at 10 MW_t and the combined target loading is 22 target rods. The system is controlled to provide [redacted] mass flow which is divided equally to two (2) TAs through manual adjustment of the throttle valves on the supply lines to each TA. This flow rate is held constant for all operating conditions. It includes an additional 5% flow to compensate for any leakage that might occur through the labyrinth seal between the cartridge and the target housing. The inlet temperature is adjusted so that the outlet of each TA is at or slightly above the reactor pool temperature, which is nominally 38.89 °C (102 °F).

5a, d, e, f

Table 6
Target Cooling System Design Parameters for Two Targets [2]

Parameter	One Target Assembly	Two Target Assemblies
Target rods heat generation rate, kWt	[redacted]	[redacted]
Target structure heat generation rate kWt	[redacted]	[redacted]
Target coolant mass flow rate including 5% leakage bypass, kg/s	[redacted]	[redacted]
Target System inlet temp, °C	28.5 (83.4 °F)	28.5 (83.4 °F)
Target System outlet temp, °C (Reference at nominal flow)	38.9 (102 °F)	38.9 (102 °F)

5a, d, e, f

3.3 Target Cooling System Design

The target cooling system (TCS) is comprised of two subassemblies:

- The Target Flow Assembly
- The Water Cooling Module

3.3.1 Target Flow Assembly Design

A process flow diagram of the target flow assembly is shown in Figure 19. The Water Cooling Module (WCM) draws water from the reactor pool through the inlet pipe and cools it to the desired value by rejecting the heat to the MURR secondary coolant system. The cooled water exits the WCM through a single pipe that splits into supply lines to the two (2) TAs. Each supply line has a throttle valve that is manually adjusted to balance the flow between the two (2) TAs or to shutoff flow to the TA. After the flow is balanced, the valves are pinned to prevent inadvertent maladjustment or closure.

Safety-related flow meters on each supply line provide redundant signals to the MURR reactor safety system to enable a reactor scram on high or low flow. RTDs at the TA inlets and the inlet to the WCM are used to control the cooling water inlet temperature to the TAs.

Each supply line has redundant natural circulation bypass valves, which in normal operation are pneumatically held closed, but are spring-loaded to automatically open on a low flow signal from the affected line. This allows reactor pool water to enter into the supply line to initiate natural circulation.

---

[2] The Heat Exchanger will have a capacity of [redacted], or with a ~15% margin, of the total (rods + structure) target heat generation rate.

5a, d, e, f

After flowing through the TAs, the cooling water is returned to the pool through the diffusers located on pipe extensions from the target cartridges. The purpose of the diffusers is to slow down and redirect the flow to allow decay of any N-16 before it can circulate to the pool surface. The diffusers also serve as the mounting point for the RTD to measure the target outlet temperature to provide a caloric measurement of the target power.

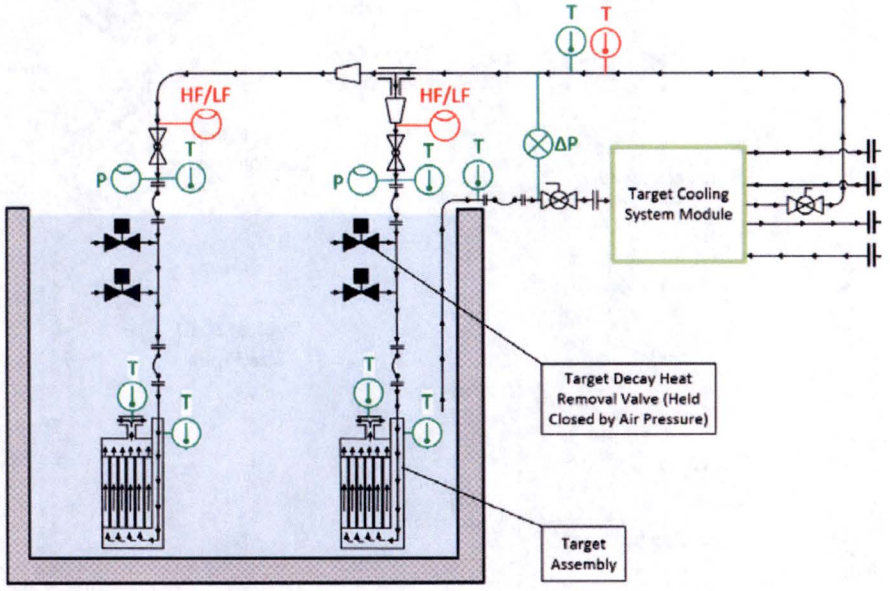

Figure 19
Process Flow Diagram of Target Cooling System

Figure 20 shows an elevation view of the TCS, while Figure 21 shows the TCS superimposed on the reactor in-pool systems and biological shield. The WCM is located on the third level of the Costar Tower in the reactor containment building. The supply line is split at the wye just before the access bridge between the Costar Tower and the reactor biological shield. The individual supply lines to each TA are run parallel to the access bridge to the reactor pool. Flexible couplings are located on each line that crosses from the Costar Tower to the biological shield to accommodate any differential displacement of the two structures. The pipe to the wye is 4-inch SS316L Schedule 40. Downstream of the wye, the piping is 3-inch SS316L Schedule 40 up to the pool surface. There the pipe transitions to Al6061 Schedule 40 via a flanged coupling.

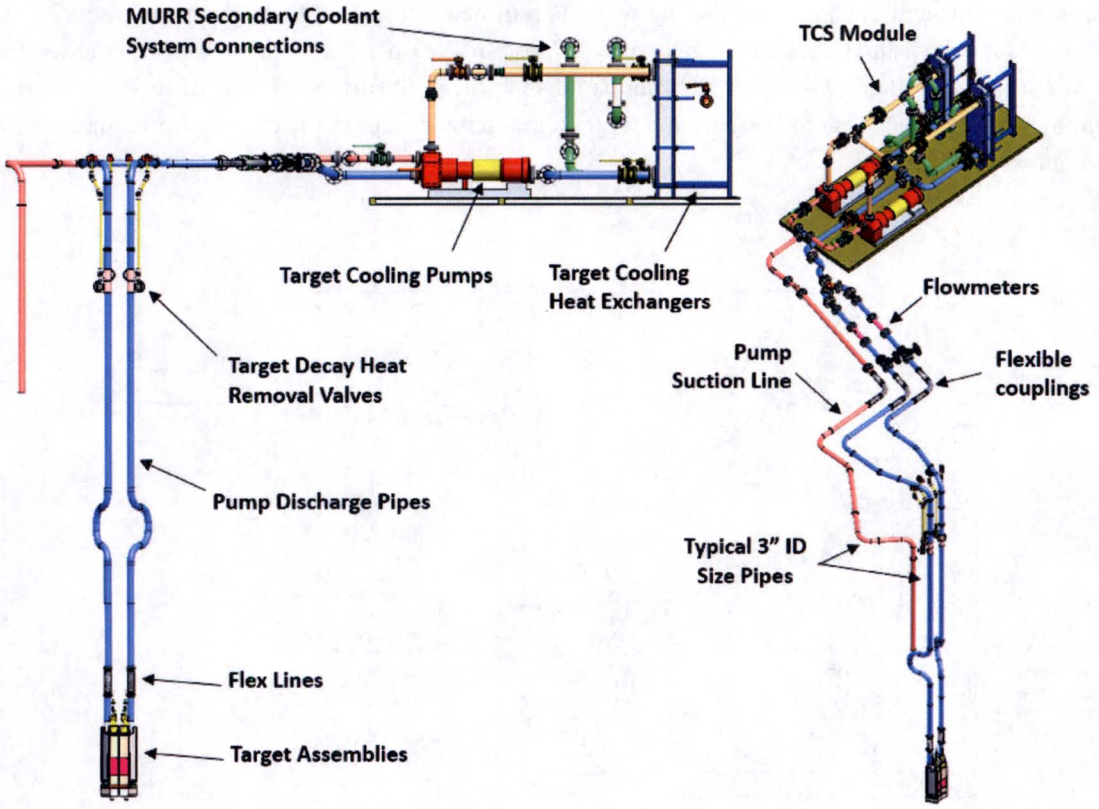

Figure 20
Elevation View of Target Cooling System

The downcomer supply pipes are supported from the floor structure at the top of the biological shield and the TAs are allowed to rest on the reflector support plate. A flexible coupling is located above each TA to accommodate any growth or differential motion between the TA and the pipe upper support.

A single suction line draws water from the pool and is delivered the WCM. The other pump is isolated using a ball valve. The suction line is 3-inch Al6061 Schedule 40 in the reactor pool and transitions to SS316L outside of the pool. The water suction pipe inlet is fitted with a replaceable screen to prevent blockage by debris.

The decay heat removal valves on each supply downcomer are positioned at a submerged location just above the refueling level. These valves are 2-inch butterfly valves with SS316L bodies. Each valve has an actuator rod that extends to a pneumatic actuator located above the pool surface.

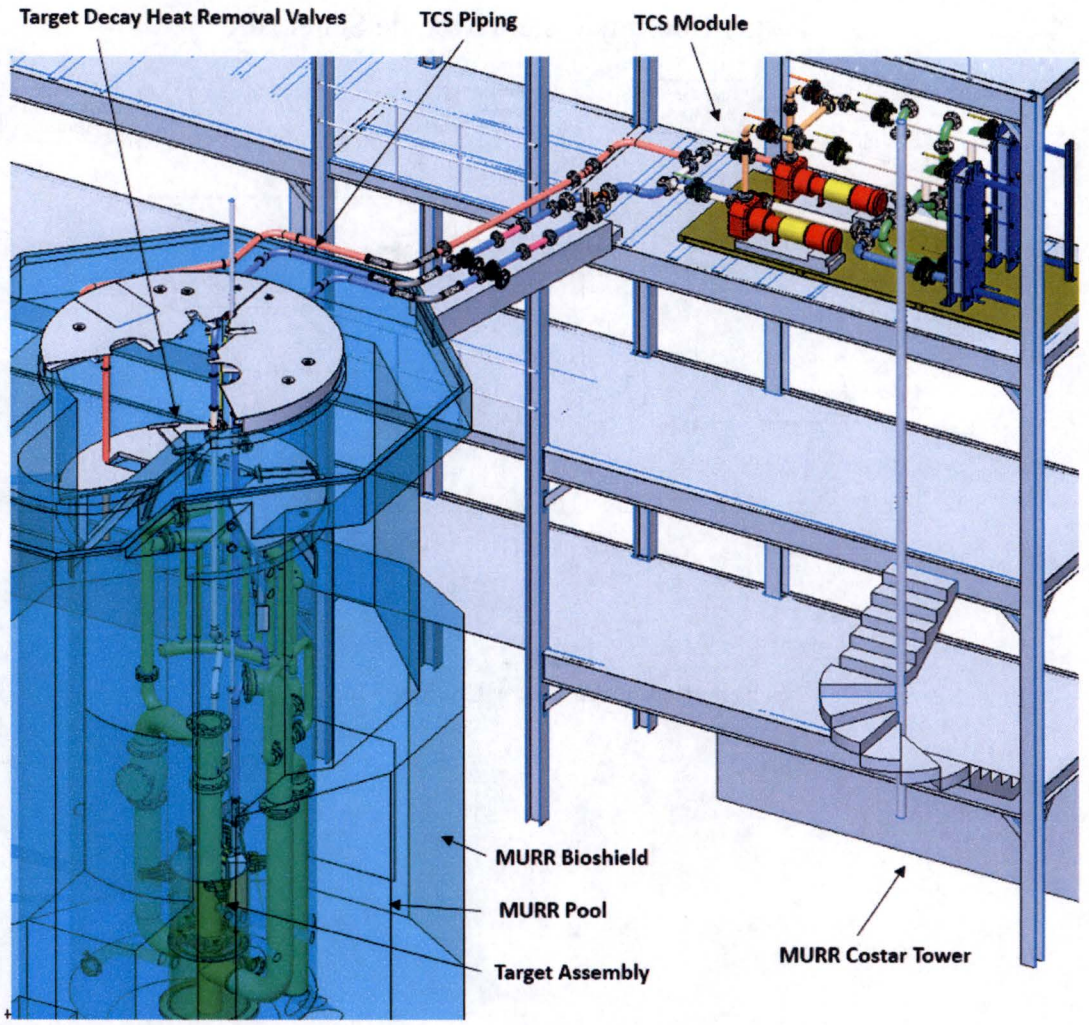

Figure 21
Target Cooling System Superimposed onto MURR Reactor Pool and Biological Shield

3.3.2 Water Cooling Module Design

Figure 22 shows the process flow diagram for the WCM, which incorporates two (2) redundant and cross-connected coolant pumps and heat exchangers. If a pump or heat exchanger is taken out of service, the installed spare component can be placed in operation to permit continued TEF operation. The pumps are self-priming, centrifugal pumps with variable frequency drives (VFD), which are manually controlled to provide the required flow. The heat exchangers are stainless steel, plate-type units. The heat exchangers reject heat to the MURR secondary coolant system. The temperature of the heat exchanger outlet flow is controlled by a flow bypass valve on the secondary side of the heat exchanger. A target system P&ID drawing is presented in Figure 23.

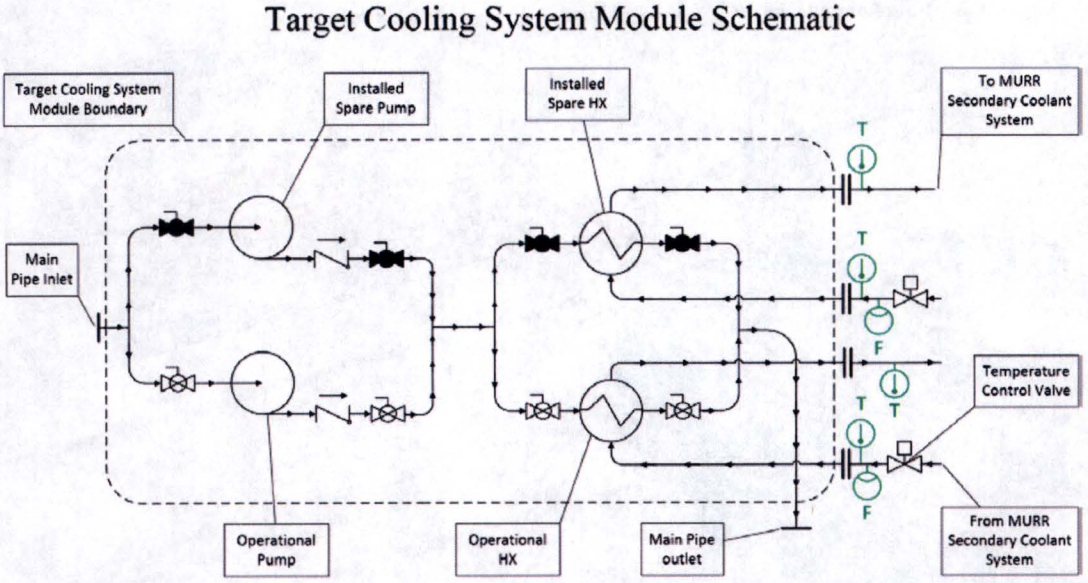

Figure 22
Schematic for the Water Cooling Module

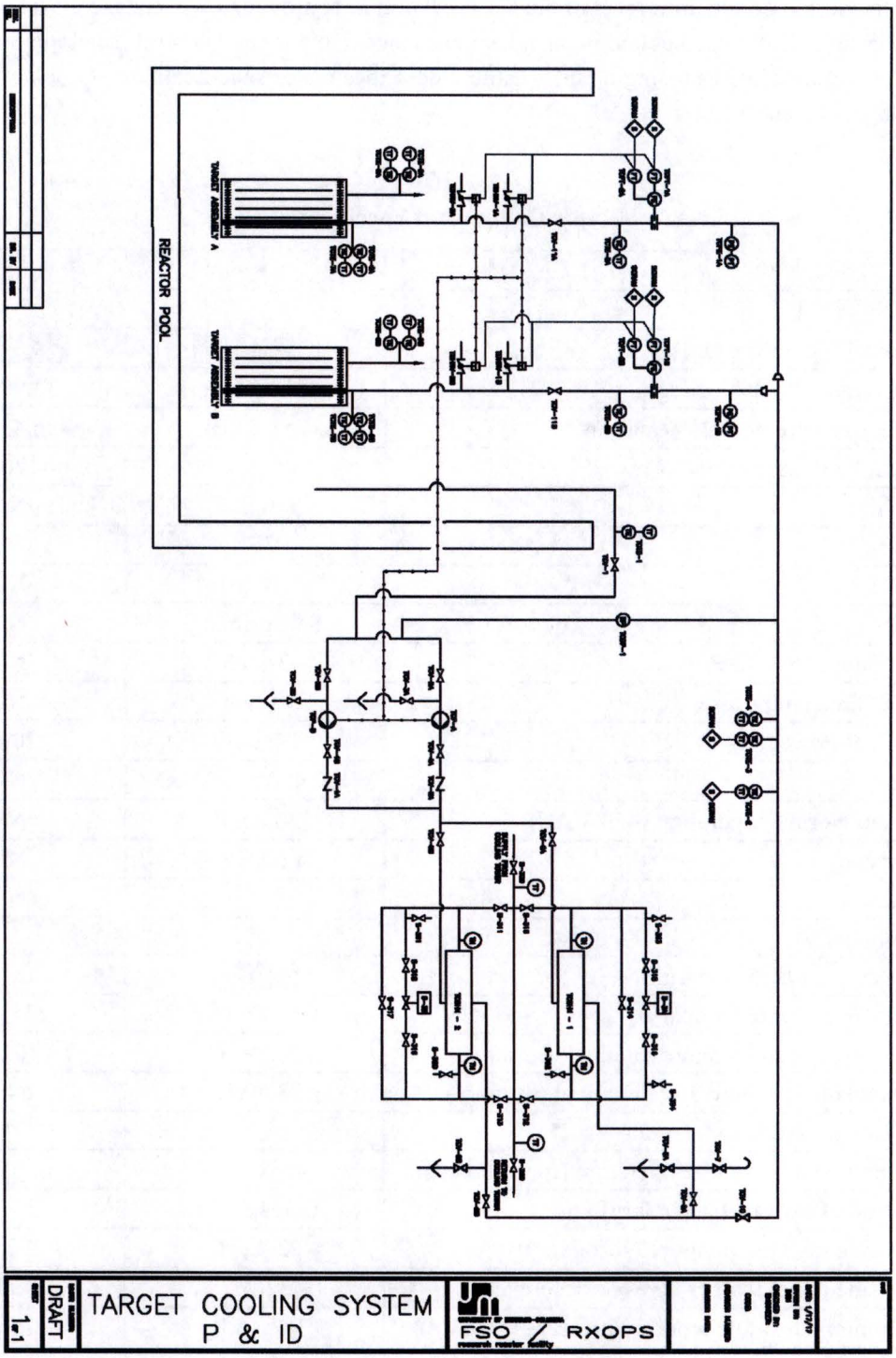

Figure 23
Target Cooling System

The WCM is located on the third level of the Costar Tower at approximately the same elevation as the top of the biological shield. The coolant pumps, heat exchangers, piping and control panel are mounted on a single pallet and installed as a single unit. Table 7 describes major specifications of coolant pumps and heat exchangers for the TCS.

Table 7
Major Component Specifications

Units	SI	English	
Pump			
Nominal Flow Rate (± 15%)	[redacted]	[redacted]	5a, d, e, f
Max Head with 25% margin	262.6 kPa	38.09 psia	
Outlet Pressure with 25% margin	251.6 kPa	36.49 psia	
Max Inlet temperature	48.9 °C	120 °F	
Material	316 SST	N/A	
Drive	VFD	N/A	
NPSH	< 10 psia	N/A	
Pump Type	Self-priming	N/A	
Inlet flange pipe size	3-inch	N/A	
Outlet flange pipe size	4-inch	N/A	
Nominal Power	14.9 kW	20 HP	
Voltage	460/480/500 VAC	N/A	
Current Normal Operation (460 VAC)	20 amps	N/A	
Frequency	60 Hz	N/A	
Phases	3	N/A	
Heat Exchanger			
Heat duty with 15% margin	[redacted]	N/A	5a, d, e, f
Hot side flow rate (primary)	0.0142 m^3/s	225 gpm	
Hot side inlet temperature nominal (primary)	38.89 °C	102 °F	
Hot side outlet temperature nominal (primary)	28.89 °C	84 °F	
Hot side pressure drop (primary)	< 68.9 kPa	< 10 psid	
Differential approach temperature (for reference)	≥ 6.67 °C	≥ 12 °F	
Cold side flow rate (secondary)	0.0142 m^3/s	225 gpm	
Cold side inlet temperature (secondary)	22.22 °C	72 °F	
Cold side outlet temperature (for reference)	~ 32.22 °C	~ 90 °F	
Maximum allowable working pressure (MAWP)	103.4 kPa	15 psi	
Cold side pressure drop	< 68.9 kPa	< 10 psid	
Material	316 SST	N/A	
Type	Plate and frame	N/A	

3.4 Target Cooling System Performance

3.4.1 Thermal-Fluid Performance in Normal Operation, Mode 1

The TCS must be on Mode 1 prior to and during the start of the reactor if the TAs contain active target rods. The process flow diagram with definition of state points for one (of the two) TAs is shown in Figure 24. The figure also provides the flow, temperature and pressure corresponding to each state point.

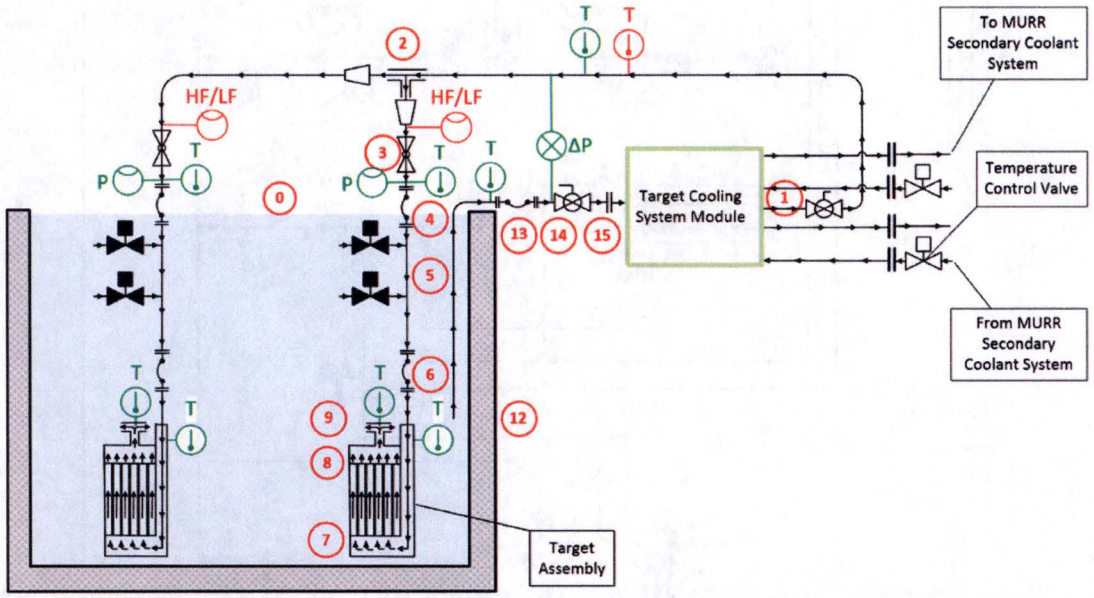

	1	2	3	4	5	6	7	8	9	12	13	14	15
Pressure*, kPa	201.3	199.0	192.4	188.9	202.9	256.8	260.7	186.9	170.8	122.9	86.9	81.1	79.0
Temp,°C	28.5	28.5	28.5	28.5	28.5	28.5	28.5	33.7	38.9	38.9	38.9	38.9	38.9
Flow, m³/s													
Pressure*, psia	29.19	28.86	27.90	27.40	29.42	37.24	37.81	27.10	24.77	17.82	12.60	11.76	11.45
Temp,°F	83.4	83.4	83.4	83.4	83.4	83.4	83.4	92.7	102.0	102.0	102.0	102.0	102.0
Flow, gpm													

5a, d, e, f

Figure 24
State Points within the Target Cooling System

3.4.2 Thermal-Fluid Performance in Natural Circulation Flow, Mode 2

Figure 25 shows a schematic of the TCS operating in the natural circulation mode. In the event of an LOFC, the reactor is tripped by a low flow signal (85% of nominal flow) if the event is cause by a reduction of flow (e.g. loss of offsite power) or a high flow signal (115% of nominal flow) if the event was caused by a pipe break downstream of the sensor. When the reactor is tripped, the driver neutron flux to the targets quickly decays and the target thermal power transitions from fission heat to fission product decay heat. Coincident with the reactor trip, an actuation signal automatically opens the two (2) decay heat removal valves on the affected downcomer pipe(s) such that the downcomer is open to the

reactor pool. This allows natural circulation of pool water to the TA and back to the pool through the diffuser.

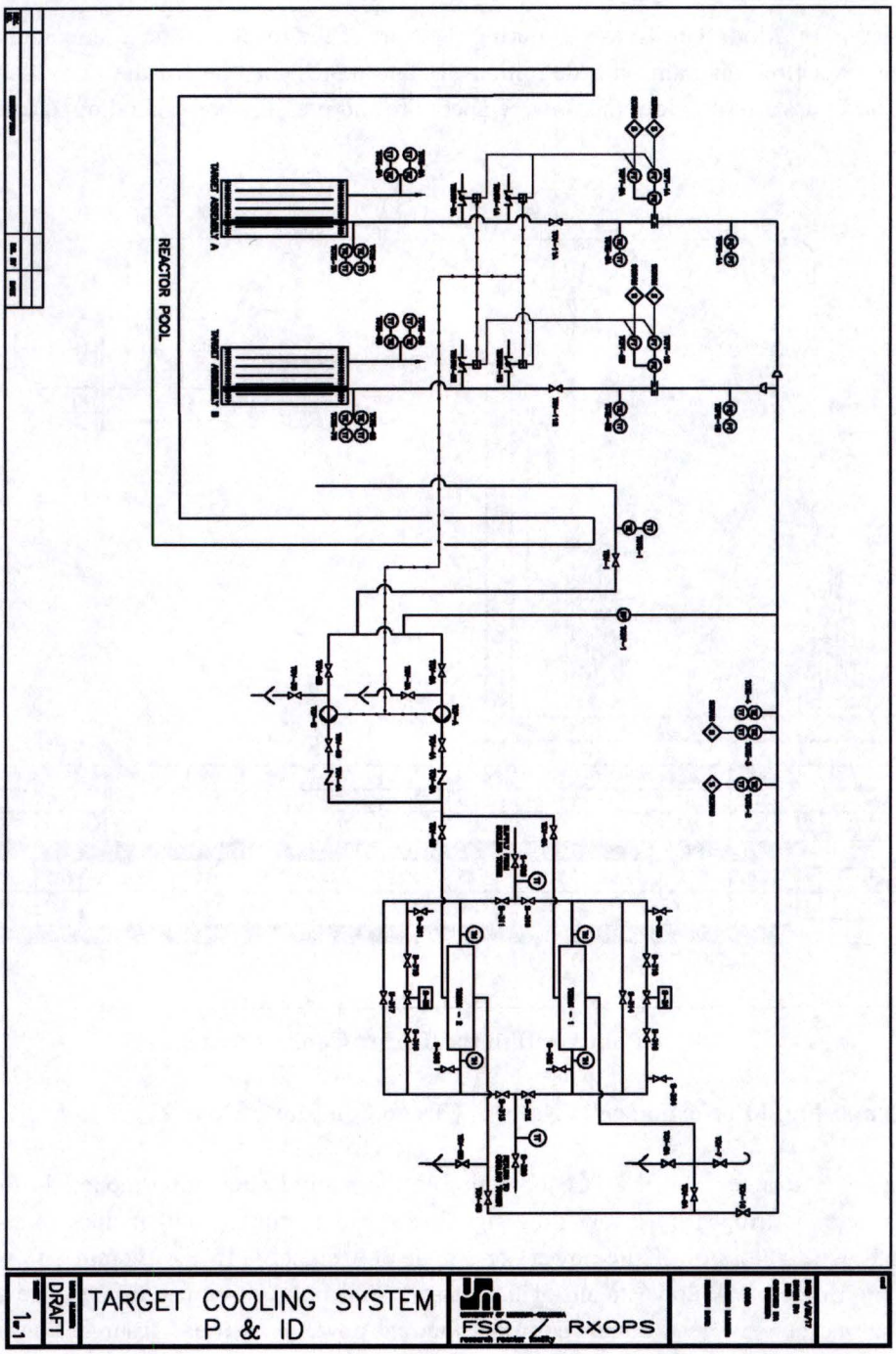

Figure 25
Target Cooling System P&ID

The analysis of the TCS performance in the natural circulation mode for the set of design basis events that can lead to a LOFC is provided later in this document. In all design basis cases, the natural circulation flow to the TA provides the required cooling.

3.4.3 Structural Performance During a Seismic Event

A seismic analysis was performed on the piping components of the TCS based on the acceleration and spectra given in the American Society of Civil Engineering Code 7-10 and interpreted according to American Society of Mechanical Engineering B&PV B31.3. The specified design spectra corresponds to an acceleration of 0.113 g. The analysis was performed using AutoPipe, a specialized nonlinear finite element piping program. The WCM and TA flanged connections where considered idealized anchors. The piping supports are rail-mount vibration damping clamps and are modeled as line supports with no gaps and firmly anchored to the biological shield, the Costar Tower or the bridge.

Figure 26 shows the location and type of pipe supports for piping located above the reactor pool. To account for independent seismic movement of the building to the pool, flexible piping is added at the bridge level. All flexible piping is 11 inches in length and flanged. A guide support is added with the flange connections on the non-flexible piping side. Stiffness values were based on General Atomics' test data. Figure 27 shows the location and type of pipe supports for in-pool piping.

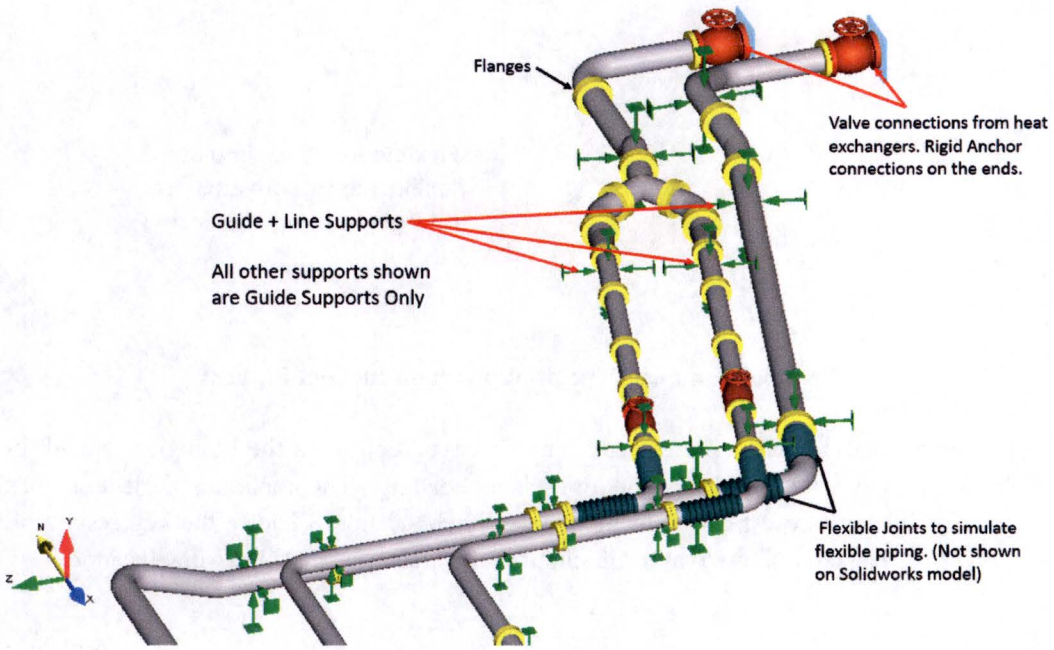

Figure 26
Location and Type of Supports on Above Pool Piping

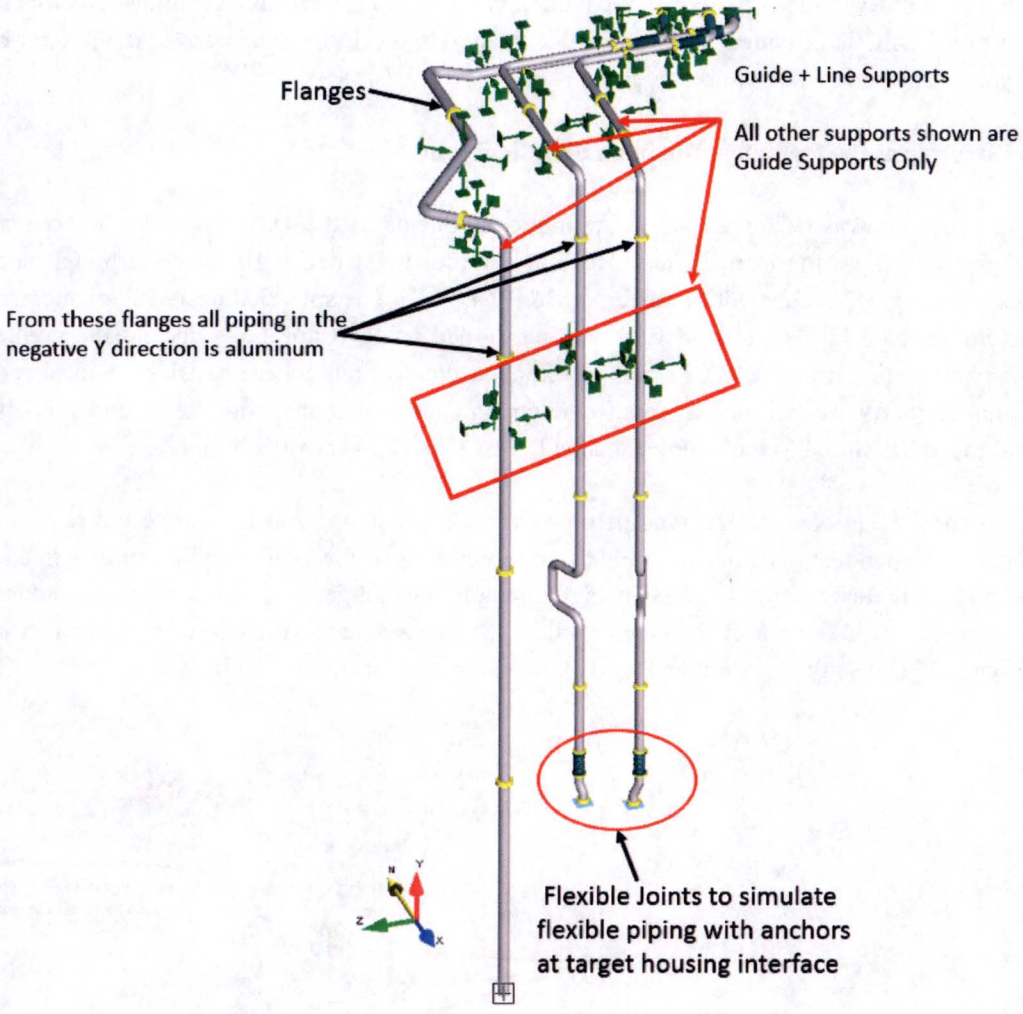

Figure 27
Location and Type of Support on In-Pool Piping

Two (2) types of analyses were performed. The first type considers the biological shield, bridge and Costar Tower as rigid structures due to the low seismic loading. The maximum deflections of structures within areas of interest are estimated to be < $1/16^{th}$ inch. Table 8 shows the key results of the rigid structure analysis. The table shows that the minimum safety factor is 7.8 at the worst location.

Table 8
Results of Rigid Structure Seismic Analysis

Location	Material	Stress (ksi)	Stress Allowable (ksi)	Safety Factor
Y-pipe, before flexible piping	SS316L	0.7	16.7	24
Inside pool, on expansion loop	6061-T6	1.0	16.7	17
At heat exchanger interface	SS316L	3.2	25	7.8
At SS to Al pipe interface	6061-T6	0.2	25.1	126
3-inch to 2-inch Y-pipe	SS316L	0.3	16.7	56
All Al piping	6061-T6	0.3	16.7	56
Y-piping support	SS316L	0.9	22.2	25
Inside pool, on expansion loop	6061-T6	1.0	22.2	22

The second type assumes that the biological shield/pool and Costar Tower combined with the bridge will laterally displace during a seismic event. To demonstrate the effectiveness of the flexible couplings, a hypothetical forced displacement of 2 inches is applied. By comparison, an initial seismic evaluation of the Costar Tower showed a less than $1/8^{th}$ inch lateral movement at the location where the bridge connects. The AutoPipe model showed that the displacement has negligible effects on the stress ratio (max ratio is 0.05) demonstrating that the flexible piping design works as intended.

3.4.4 Secondary Cooling for the Target Cooling System

The heat from the TCS is transferred to the MURR secondary coolant system by means of one of the TCS heat exchangers. The heat is then dissipated to the atmosphere through a cooling tower with seasonal additional cooling provided by a chill water system. The secondary coolant loop that serves the TCS consists of one (1) coolant circulation pump, two (2) heat exchangers, two (2) automatic temperature control valves, one (1) chill water heat exchanger, temperature and flow instrumentation, and associated valves and piping. A piping and instrumentation diagram is shown in Figure 28. The secondary coolant loop that serves the TCS shares a cooling tower, radiation monitoring instrumentation, and chemical control systems with the existing 15 MW capacity MURR secondary coolant system. Only the secondary coolant loop serving the TCS will be described in this section. The secondary coolant system is designed such that a failure or malfunction of any system component will not lead to target rod damage or an uncontrolled release of radioactivity to the environment.

3.4.5 Circulation Pump

The secondary coolant circulation pump for the TCS is a centrifugal, single-stage pump that is direct-connected to a variable speed drive (VSD) unit through a coupling. This pump, designated SP-5, is capable of supplying 500 gpm at a discharge pressure of 50 psig. Three (3) other secondary coolant

pumps are installed in a parallel configuration with each pump capable of supplying 2,200 gpm to the secondary coolant system. In case pump SP-5 failed, TCS secondary coolant flow can be established using a cross-connect pipe to the discharge header of the other three (3) secondary coolant pumps. Additional detail of the SP-5 control system is provided in Instrumentation and Control section of this document.

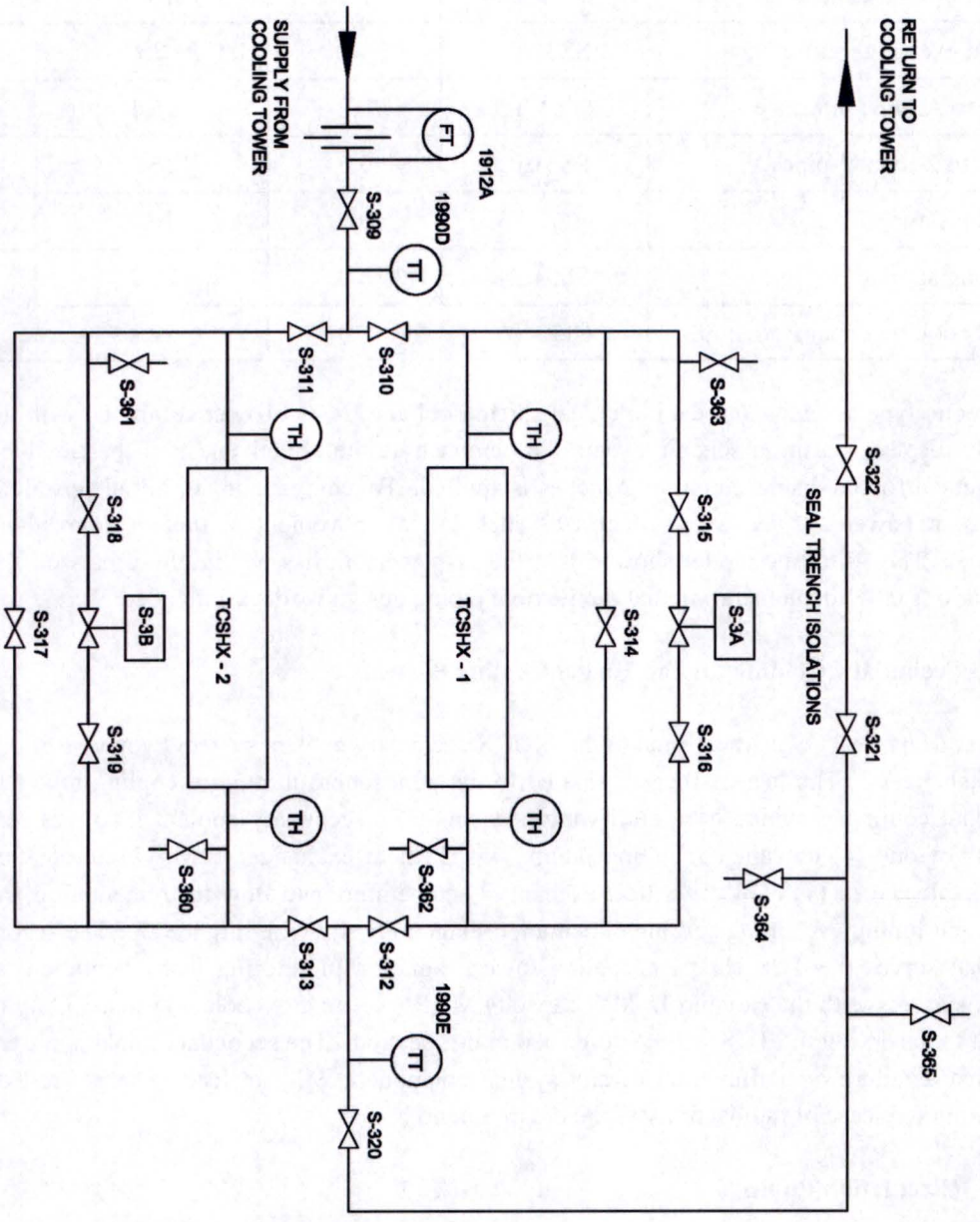

Figure 28
Secondary Cooling for Target Cooling System

3.4.6 Heat Exchangers

The secondary coolant flow makes a single pass on one of the TCS heat exchangers. The TCS heat exchangers are plate-type heat exchangers. On one side of the plates is secondary coolant, and the other side has TCS coolant. Only one TCS heat exchanger is required for TCS operation. The other TCS heat exchanger is an installed spare for operational reliability.

During the summer months, additional cooling to the secondary coolant supply to the TCS may be needed to ensure a sufficient secondary cooling water temperature to maintain proper TCS heat exchanger outlet temperature. This additional cooling to the secondary coolant system is provided by a chill water system via a plate-type heat exchanger.

3.4.7 Automatic Temperature Control Valves

The amount of secondary coolant passing through the TCS heat exchanger is controlled by an automatic temperature control valve located in a bypass line of its associated heat exchanger. The valve is an electro-mechanical butterfly valve which responds to the TCS heat exchanger outlet temperature which maintains a constant cold leg temperature to the TAs. Since only one TCS heat exchanger is operated at any time, only one automatic temperature control valve is in operation at any time. The other valve is an installed spare for operational reliability. The automatic temperature control valves for the TCS heat exchangers are designated as S-3A and S-3B. Additional detail on the operation of the automatic temperature control valves and system is provided in Instrumentation and Control section of this document.

3.4.8 Instrumentation

The secondary coolant inlet and outlet temperatures to both the chill water and TCS heat exchangers and the total flow in the secondary system TCS loop are displayed and recorded in the reactor control room.

3.4.9 Electrical Power System Supporting the TCS

Electrical power to the TCS pumps and their Instrumentation and Controls Uninterruptible Power Supply (I&C UPS) will be supplied by Motor Control Center No. 4 (MCC-4) through a new 480/277 V distribution panel. Normal Electrical Power System Substation B supplies 480-volt, 3-phase, 60-cycle electrical power to MCC-4 through a 250-amp breaker as described in Chapter 8 of the MURR Safety Analysis Report (Reference 11).

The new 480/277 V, 200-amp panel, designated HVP-4, will be connected to MCC-4 in the reactor containment building. Electrical power to the TCS pumps will be provided by HVP-4. HVP-4 will also supply electrical power to a new 120/208-V Distribution Center, designated 120/208V Distribution Center 3, through a 112.5-kVA transformer. A Lighting Panel on 120/208V Distribution Center 3 will supply electrical power to the TCS pumps I&C UPS as shown in Figure 29.

Location of the new electrical wiring will ensure that no electromagnetic interference will exist between the electrical power service and any safety-related I&C circuits.

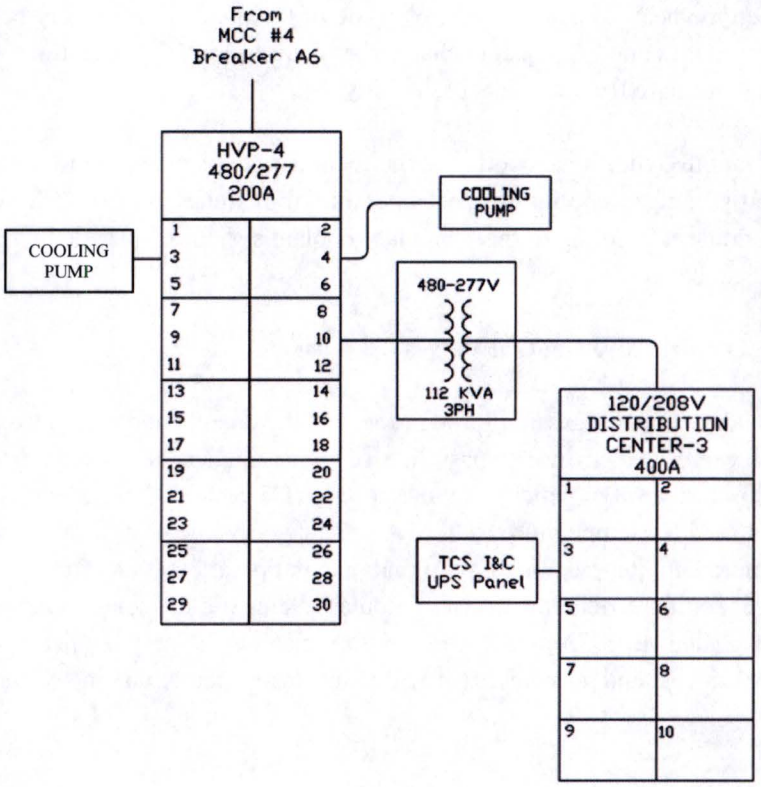

Figure 29
Electric Power Supply to TCS Pumps and I&C UPS

4. Instrumentation and Control System

This section describes the operating characteristics of the TEF Instrumentation and Control (I&C) Systems. These systems assure that the TEF can be safely operated, monitored, and shut down as warranted.

4.1 Summary Description

The TEF I&C Systems are comprised of the sensors, electronic circuitry, displays, and actuating devices available to provide the information and means to safely control the TEF and avoid or mitigate potential accidents that could affect the TEF or the reactor. The TEF I&C systems include the following:

- Target Cooling System (TCS) Control System
- TCS Protection System

- TCS Parameter Indication, Recording, and Alarm System
- TCS Secondary Coolant Control System
- TCS Secondary Coolant Parameter Indication, Recording, and Alarm System
- N-16 Reactor Power Monitoring System
- Pool Coolant Monitoring System

The TCS Control System is designed to control TCS pump speed and the position of the Decay Heat Removal System Automatic Valves. It is a hardwired system that relies on relays, controllers, push buttons, switches, and light indicators. The TCS Control System receives inputs manually and from the TCS Protection System.

The TCS Protection System is designed to prevent operation of the TEF in regions in which target rod damage could occur. This is accomplished by the TCS Protection System which can initiate a reactor scram via the reactor safety system, which instantaneously drops the reactor control rods and takes the reactor subcritical. Therefore, the power of both the TEF and the reactor are quickly reduced. Inputs which govern the TCS Protection System output are supplied by TCS flow and temperature transmitters.

The TCS Parameter Indication, Recording, and Alarm System is designed to provide control room operators with indications of operating parameters for the TCS, to record TCS parameter data for long-term retention or review, and to actuate alarms to alert the operator to abnormal parameters. This is accomplished by parameter current loop signals going to chart recorders which also serve as parameter indication and alarm units. Parameter inputs into the TCS Parameter Indication, Recording, and Alarm System are multiple TCS temperature, pressure, and flow signals.

The TCS Secondary Coolant Control System is designed to control the TCS secondary coolant circulation pump (SP-5) speed and the position of the operating target cooling automatic temperature control valve (S-3A or S-3B). It is a hardwired system that relies on relays, controllers, push buttons, switches, and light indicators. The TCS Secondary Coolant Control System receives inputs manually and from the TCS Parameter Indication, Recording, and Alarm System.

The TCS Secondary Coolant Parameter Indication, Recording, and Alarm System is designed to provide control room operators with indication of parameters convenient for operating the TCS Secondary Coolant Control System, to record TCS secondary coolant parameter data for long-term retention or review, and to actuate alarms to alert the operator to abnormal parameters. This is accomplished by parameter current loop signals going to chart recorders which also serve as parameter indication and alarm units. Parameter inputs into the TCS Secondary Coolant Parameter Indication, Recording, and Alarm System are multiple TCS Secondary Coolant Control System temperature, flow, and valve position signals.

The N-16 Power Monitoring System (N-16 PMS) is designed to provide control room operators with indication of reactor core power by measuring the amount of N-16 produced in the primary coolant system. Reactor fission power is directly proportional to the amount of N-16 atoms produced by the fast

neutron flux in the reactor. Therefore, reactor core power can be measured separate from the TEF power. The N-16 PMS has two (2) reductant detectors located in mechanical equipment room 114 and two (2) redundant displays located in the control room.

The Pool Coolant Monitoring System (PCMS) is designed to provide control room operators with indication and an alarm of elevated iodine-131 (I-131) activity levels in the pool coolant system. Elevated I-131 activity levels in the pool coolant system would be an early indication of a leaking target rod in the reactor pool. The PCMS has a detector, display, and alarms in the entryway to mechanical equipment room 114 and has an indication and alarm in the control room.

4.2 Target Cooling System Control System Description

The TCS Control System is designed to control TCS pump operation and the position of the Target Decay Heat Removal Valves (TDHRVs). From the TCS Control System, the operator can start, stop, and change speed of the TCS pumps. In addition, the TCS Control System contains an interlock between the TCS pumps and the TDHRV position that secures the TCS pumps when any one of the TDHRVs open. The interlock is actuated from a position indication switch located on each TDHRV actuator which opens a contact de-energizing both of the TCS pump control circuits.

The control system architecture for the TCS is shown in Figure 30. A larger image of the TCS Control Panel is shown in Figure 31.

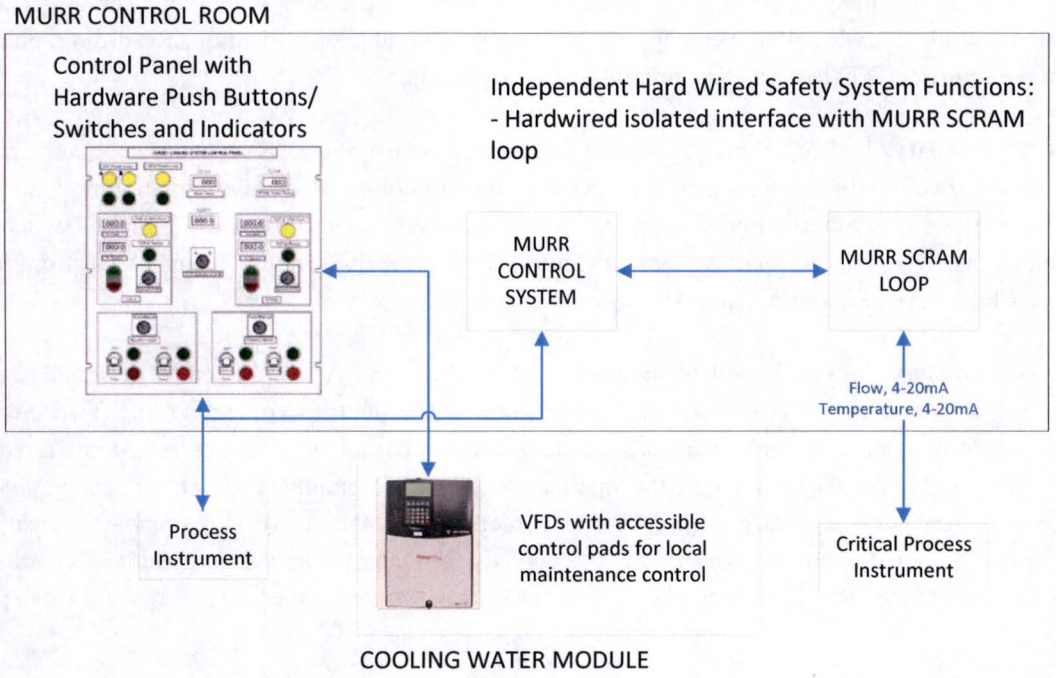

Figure 30
Target Cooling System Control System Architecture

When the TDHRVs are in 'Manual' mode, the operator can individually change the position of each TDHRV as needed for maintenance or testing. In 'Auto' mode, low or high TCS flow will automatically open the two (2) TDHRVs in the associated TCS branch of the abnormal flow condition. When a low or high TCS flow condition occurs in a TCS branch, one or more contacts in the TCS Protection System will open and de-energize the two (2) solenoid-operated valves that are applying air pressure to the TDHRV actuators in that TCS branch. Air pressure will be vented off the TDHRV actuators and spring force will rapidly open the TDHRVs, when required.

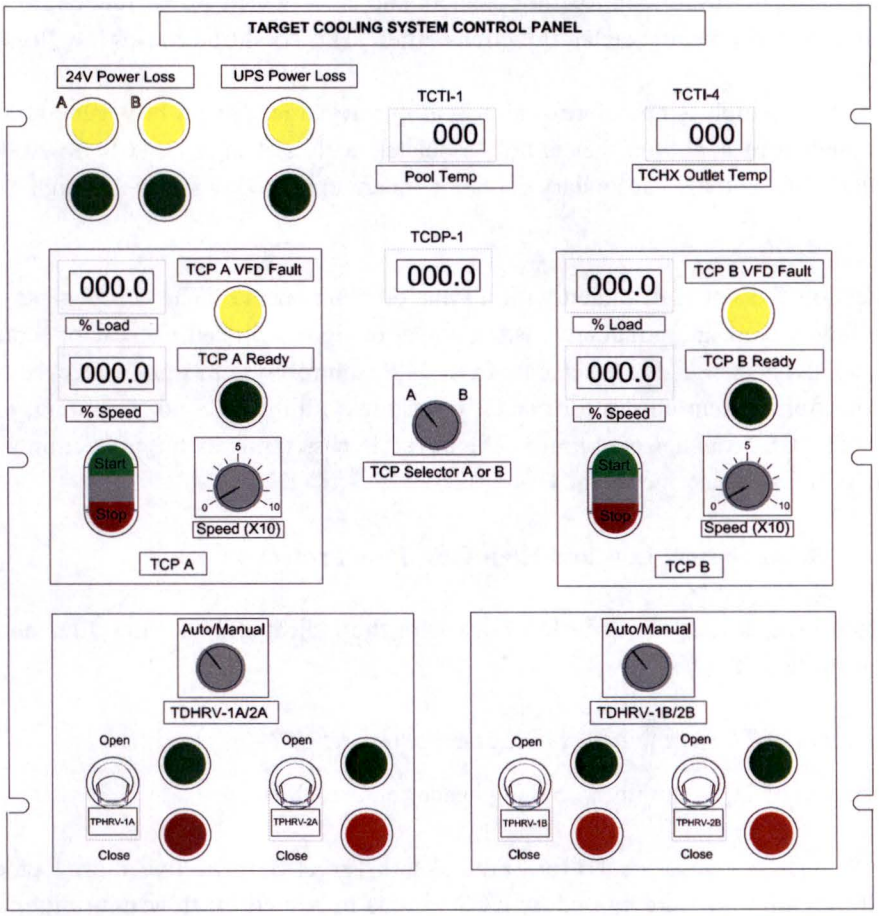

Figure 31
Target Cooling System Control Panel

4.3 Target Cooling System Protection System Description

The TCS Protection System initiates a reactor scram via the reactor safety system to prevent operation of the TEF in regions in which target rod damage could occur. The TCS Protection System will initiate a reactor scram based on low TCS flow rate (< 85% normal flow), high TCS flow rate (> 115% normal

flow), and high TCS heat exchanger outlet temperature (> 105 °F). These set points are based on the limiting conditions used in the thermal-hydraulic safety analysis for the TEF.

The basis for the TCS low flow scram is to ensure target fission heat generation is terminated upon a low flow condition caused by a TCP failure, TCS piping break upstream of the flow transmitters or on the TCP suction, or TCS piping blockage.

The basis for the TCS high flow scram is to ensure target fission heat generation is terminated upon a TCS pipe break between the flow measuring element and a TA which would reduce flow resistance and increase flow indication at the associated flow transmitter. This condition causes low flow to the TAs.

The basis for the TCS high temperature scram is to ensure target fission heat generation is terminated upon a high temperature condition that is not associated with a change in TCS flow rate. Insufficient secondary coolant flow and high secondary coolant temperature could cause such a high TCS temperature to occur.

The TCS Protection System is designed with all analog components. The components and system are designed to be fail-safe, meaning that any loss of power or signal will cause a reactor scram. In addition, all TCS Protection System signals are separate from TCS Control System signals. Keyed bypass switches to the TCS Protection System allows for reactor operation with the TCS not operating, one TCS branch operating, or both TCS branches operating. The keyed bypass removes the protection signal inputs for any part of the TCS that is not operating.

4.3.1 Target Cooling System Low and High Flow Rate Protection

TCS flow is measured at the following locations with the indicated TCS Flow Elements (TCFEs) and TCS Flow Transmitters (TCFTs):

- Downstream of TCS combined cold leg header on branch A
- Downstream of TCS combined cold leg header on branch B

Flow elements TCFE-1A and TCFE-1B for Target A and Target B, respectively, are located in each TCS branch. The differential pressure caused by TCS flow is measured by flow transmitters TCFT-1A and TCFT-2A for TCS branch A and TCFT-1B and TCFT-2B for TCS branch B. The output signal (4 to 20 mA) generated by each flow transmitter is directed to a square root converter which provides a linear output signal for the two dual alarm trip units and a chart recorder in series with the signal.

In addition to providing flow indication and recording, the recorder will initiate a "TCS Lo Flow" alarm when TCS branch flow to either target decreases to 90% of its normal value. If TCS branch flow decreases to 85% normal flow, then the following actions are initiated by the system:

1. Reactor scram;
2. Opening of the two (2) TDHRVs in the associated branch; and

3. Actuation of the "TCS Flow Scram" annunciator alarm.

The low flow dual alarm unit for TCFT-1A opens two (2) contacts:

1. One contact opens in the "Yellow Leg" of the TCS Protection System which in turn opens contact TCS-1 in the "Yellow Leg" of the reactor safety system which causes the reactor scram (See Figure 32).
2. Another contact opens in the TCS Control System that de-energizes both solenoid-operated valves applying air pressure to TDHRV-1A and TDHRV-2A actuators which allows these valves to open. The opening of this contact also activates the "TCS Flow Scram" annunciator alarm.

The low flow dual alarm unit for TCFT-2A opens two (2) contacts:

1. One contact opens in the "Green Leg" of the TCS Protection System which in turn opens contact TCS-2 in the "Green Leg" of the reactor safety system which causes the reactor scram (See Figure 32).
2. Another contact opens in the TCS Control System that de-energizes both solenoid-operated valves applying air pressure to TDHRV-1A and TDHRV-2A actuators which allows these valves to open. The opening of this contact also activates the "TCS Flow Scram" annunciator alarm.

The low flow dual alarm unit for TCFT-1B opens two (2) contacts:

1. One contact opens in the "Yellow Leg" of the TCS Protection System which in turn opens the contact TCS-1 in the "Yellow Leg" of the reactor safety system which causes the scram (See Figure 32).
2. Another contact opens in the TCS Control System that de-energizes both solenoid-operated valves applying air pressure to TDHRV-1B and TDHRV-2B actuators which allows these valves to open. The opening of this contact also activates the "TCS Flow Scram" annunciator alarm.

The low flow dual alarm unit for TCFT-2B opens two (2) contacts:

1. One contact opens in the "Green Leg" of the TCS Protection System which in turn opens contact TCS-2 in the "Green Leg" of the reactor safety system which causes the reactor scram (See Figure 32).
2. Another contact opens in the TCS Control System that de-energizes both solenoid-operated valves applying air pressure to TDHRV-1B and TDHRV-2B actuators which allows these valves to open. The opening of this contact also activates the "TCS Flow Scram" annunciator alarm.

In addition to a low flow condition, the TCS Protection System will provide protection on TCS high flow rate. In this case, the chart recorder will initiate a "TCS Hi Flow" alarm when TCS branch flow to either target increases to 110% of its normal value. If TCS branch flow increases to 115% normal flow, then the following actions are initiated by the system:

1. Reactor scram;
2. Opening of the two (2) TDHRVs in the associated branch; and
3. Actuation of the "TCS Flow Scram" annunciator alarm.

The high flow dual alarm unit for TCFT-1A opens two (2) contacts:

1. One contact opens in the "Yellow Leg" of the TCS Protection System which in turn opens contact TCS-1 in the "Yellow Leg" of the reactor safety system which causes the reactor scram (See Figure 32).
2. Another contact opens in the TCS Control System that de-energizes both solenoid-operated valves applying air pressure to TDHRV-1A and TDHRV-2A actuators which allows these valves to open. The opening of this contact also activates the "TCS Flow Scram" annunciator alarm.

The high flow dual alarm unit for TCFT-2A opens (2) two contacts:

1. One contact opens in the "Green Leg" of the TCS Protection System which in turn opens contact TCS-2 in the "Green Leg" of the reactor safety system which causes the reactor scram (See Figure 32).
2. Another contact opens in the TCS Control System that de-energizes both solenoid-operated valves applying air pressure to TDHRV-1A and TDHRV-2A actuators which allows these valves to open. The opening of this contact also activates the "TCS Flow Scram" annunciator alarm.

The high flow dual alarm unit for TCFT-1B opens two (2) contacts:

1. One contact opens in the "Yellow Leg" of the TCS Protection System which in turn opens contact TCS-1 in the "Yellow Leg" of the reactor safety system which causes the reactor scram (See Figure 32).
2. Another contact opens in the TCS Control System that de-energizes both solenoid-operated valves applying air pressure to TDHRV-1B and TDHRV-2B actuators which allows these valves to open. The opening of this contact also activates the "TCS Flow Scram" annunciator alarm.

The high flow dual alarm unit for TCFT-2B opens (2) two contacts:

1. One contact opens in the "Green Leg" of the TCS Protection System which in turn opens contact TCS-2 in the "Green Leg" of the reactor safety system which causes the reactor scram (See Figure 32).
2. Another contact opens in the TCS Control System that de-energizes both solenoid-operated valves applying air pressure to TDHRV-1B and TDHRV-2B actuators which allows these valves to open. The opening of this contact also activates the "TCS Flow Scram" annunciator alarm.

4.3.2 Target Cooling System High Temperature Protection

TCS combined cold leg header temperature is measured for use in the TCS Protection System at the following location with the indicated TCS Temperature Elements (TCTEs) and TCS Temperature Transmitters (TCTTs):

- Downstream of the TCS Module on the TCS combined cold leg header

Resistance Temperature Detectors (RTDs) TCTE-2 and TCTE-3 are located beside each other in the TCS combined cold leg header. TCS Temperature Transmitters TCTT-2 and TCTT-3 convert the associated RTD signal into 4 to 20 mA output signal providing a linear output temperature signal for a dual alarm trip unit and a chart recorder in series with the signal.

In addition to providing TCS cold leg temperature indication and recording, the chart recorder will initiate a "TCS Hi Temp" alarm when TCS cold leg temperature increases to 100 °F. If TCS cold leg temperature increases to 105 °F, a reactor scram and a "TCS Temp Scram" annunciator alarm are initiated. The high temperature dual alarm unit for TCTT-2 opens a contact in the "Yellow Leg" of the TCS Protection System which in turn opens contact TCS-1 in the "Yellow Leg" of the reactor safety system which causes the scram. The high temperature dual alarm unit for TCTT-3 opens a contact in the "Green Leg" of the TCS Protection System which in turn opens contact TCS-2 in the "Green Leg" of the reactor safety system which causes the reactor to scram (see Figure 32).

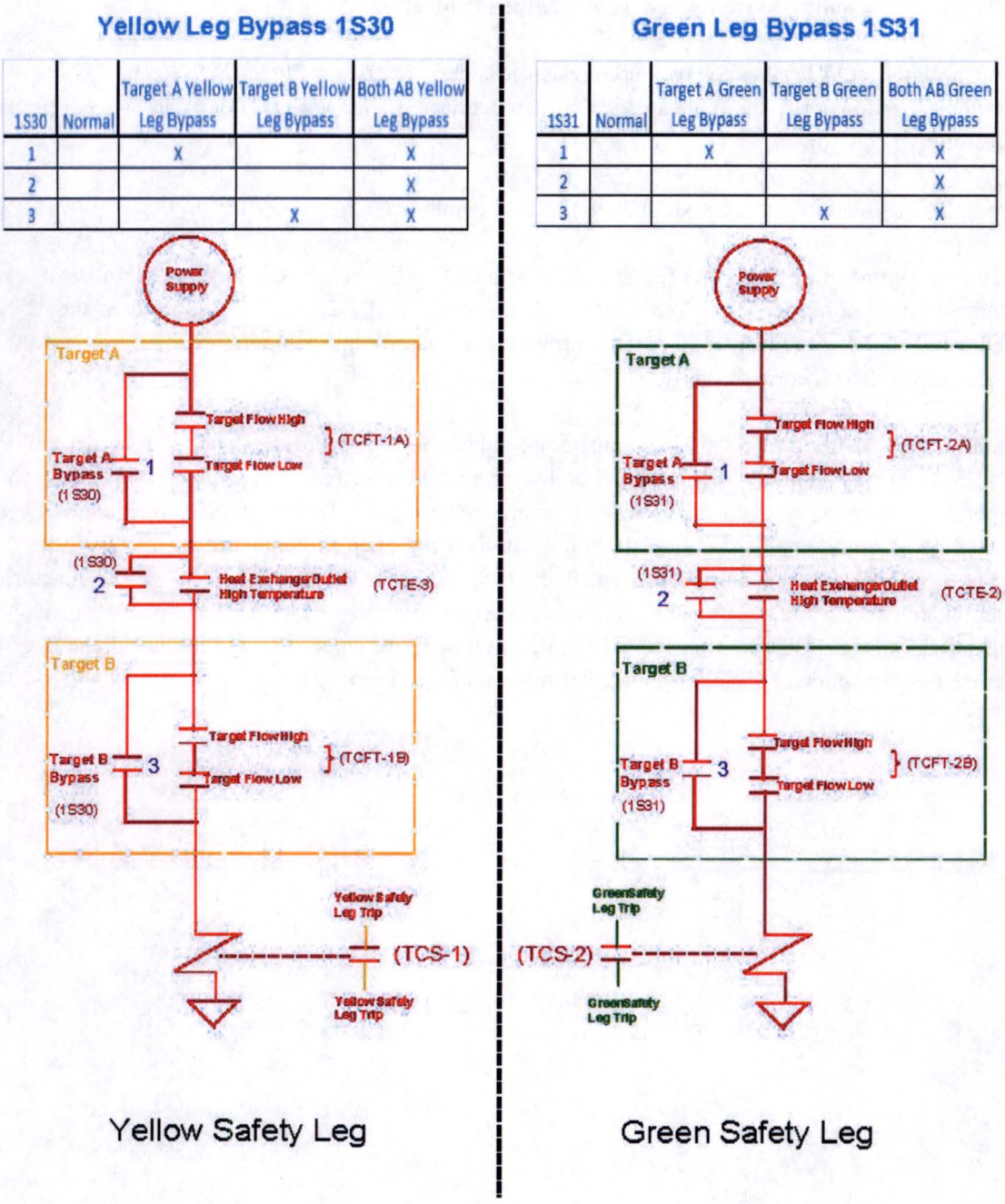

Figure 32
Target Cooling System Protection System Relay Inputs to the MURR Reactor Safety System

4.3.3 Target Cooling System Protection Bypass Capability

When it is desired to operate the reactor without operating one or both of the TAs, two (2) bypass keys will be inserted and switches will be placed in the bypass position for the associated TA's (or assemblies') protection to be bypassed. The bypass switches will be a four-position, standardized keyed-type switch designed 1S30 and 1S31.

With no key in bypass switch 1S30 or 1S31, the switch is locked in the "Normal" position and all TCS protection signals can affect a reactor scram. In addition, the TDHRV to TCS pump interlock is active to shut off the TCS pump when any TDHRV opens.

When a key is in bypass switch 1S30, the switch is able to be positioned in the 'Target A Bypass,' 'Target B Bypass,' or 'Both AB Bypassed' position. With 1S30 in either the 'Target A Bypass' or the 'Target B Bypass' position, the "Yellow Leg" TCS flow protection scram for the bypassed TCS branch is disabled. With 1S30 in either the 'Both AB Bypassed' position, the "Yellow Leg" TCS flow protection scram and the "Yellow Leg" TCS heat exchanger outlet high temperature scram for the bypassed TCS branch are disabled. However, bypass switch 1S30 only disables the "Yellow Leg" protection. Bypass switch 1S31 has the same functions as 1S30, but it only disables the "Green Leg" protection. Therefore, to bypass scram protection from one or more TAs and remove the associated TDHRV to TCS pump interlock, both switches must have their keys installed and positioned correctly. This design ensures that no single switch or single human error will inadvertently remove all scram protection or the TDHRV to TCS pump interlock to a TA that is being irradiated.

For example, if only Target A is to be irradiated, the TCS would be lined up to provide cooling flow to only TCS branch A. TCS branch B would have no flow and the TDHRVs in TCS branch B would be open. Therefore, two keys are inserted and switches 1S30 and 1S31 would be positioned to 'Target B Bypass' so that the no flow condition in branch B would not cause a scram and the open TDHRVs in branch B would not prevent running either TCS pump. When switches 1S30 and 1S31 are in 'Target B Bypass,' relays are energized that close contacts that bypass the reactor safety system contacts actuated by TCFT-1B and TCFT-2B in both legs of the TCS Protection System (See Figure 32). In addition, these energized relays close contacts that bypass the TDHRV-1B and TDHRV-2B valve contacts in the TCS pump controllers thereby allowing the TCS pump to run while the cooling branch B TDHRVs are open (See Figure 33).

If neither Target A nor Target B is to be irradiated, the TCS pumps would both be secured, and all four TDHRVs would be open. The two (2) bypass keys are inserted, and switches 1S30 and 1S31 should be positioned to 'Both AB Bypass' so that the no flow condition in both branches A and B and/or a high heat exchanger outlet temperature would not cause a reactor scram. The open TDHRVs in both branches would prevent running either TCS pump. When switches 1S30 and 1S31 are in 'Both AB Bypass,' relays are energized that close contacts that bypass the reactor safety system contacts actuated by TCFT-1A, TCFT-2A, TCFT-1B, TCFT-2B, TCTE-2, and TCTE-3 in both legs of the TCS Protection System (See Figure 32). However, TDHRV-1A, TDHRV-2A, TDHRV-1B, and TDHRV-2B valve contacts in the TCS pump controllers would be open thereby preventing either TCS pump to run (See Figure 33).

Figure 33
TDHRVs – TCS Pump Interlock Circuit

Finally, if a single switch fails or is placed in the incorrect operating position, the worst condition that could be possible would be to have two (2) TAs operating with one key switch in the 'Normal' position and the other key switch in 'Both AB Bypass.' In this condition, the high and low flow scrams and the high heat exchanger outlet temperature scram would be disabled for only one (1) of the two (2) reductant reactor safety system legs. Any other single switch mis-position or single switch failure with any operating condition would cause less protection to be bypassed. In addition, any single switch mis-position or single switch failure with only one (1) TA operating would cause the operating TCS pump to stop due to the open TDHRVs in the secured TA cooling branch. The stopped TCS pump would reduce target flow and cause a reactor scram.

Administratively, the keys to switches 1S30 and 1S31 will require Reactor Manager's permission to use. Since the MURR is not normally operated with bypass keys installed at the reactor console, the presence of keys will be a noticeable exception from normal operations. Therefore, operator attention to correct operation of the bypass keys will be peaked when they are implemented.

4.3.4 Target Cooling System Parameter Indication, Recording, and Alarm System

The TCS Parameter Indication, Recording, and Alarm System is designed to provide control room operators with indication of parameters convenient for operating the TCS, to record TCS parameter data for long-term retention or review, and to actuate alarms to alert the operator to abnormal parameters. No

safety-related functions are associated with the TCS Parameter Indication, Recording, and Alarm System. Every parameter is detected by a sensor. The sensor signal is converted to a 4-20mA current loop signal going to paperless chart recorders which also serve as parameter indication and alarm units.

4.3.5 Target Cooling System Secondary Coolant Control System

The TCS Secondary Coolant Control System is designed to control the TCS secondary coolant circulation pump (SP-5) speed and the position of the Target Cooling Automatic Temperature Control Valves (S-3A and S-3B). From the TCS Secondary Coolant Control System, the operator can adjust SP-5 to make course secondary coolant flow rate changes to the WCM. However, fine secondary coolant flow rate adjustment through a TCS heat exchanger is made by either S-3A or S-3B that are located in a secondary coolant pipe that bypasses the associated heat exchanger. For simplicity, further explanation of how the Target Cooling Automatic Temperature Control Valves (S-3A and S-3B) operate, S-3A will be assumed operating and its operation will be the example described. S-3B's controls and operation are the same as S-3A.

During steady-state operation, SP-5 provides constant secondary coolant flow to the WCM. S-3A and its associated heat exchanger are in use, and S-3A is in 'Automatic' control. S-3A is located in a secondary coolant bypass line that bypasses the TCS heat exchanger. Therefore, as S-3A closes, less secondary coolant bypasses the heat exchanger resulting in more cooling flow to the heat exchanger. The opposite effect occurs as S-3A opens. The position of S-3A is controlled by a controller that is driven by the TCS heat exchanger outlet temperature transmitter TCTT-4. TCTT-4 receives its temperature measurement from resistance temperature detector TCTE-4. When slight changes to the TCS heat exchanger outlet temperature occur, S-3A moves to regulate the heat exchanger outlet temperature back to the desired set point.

At the TCS Secondary Coolant Control System panel, the operator has manual switches and buttons to start, stop, and adjust the speed of SP-5. During normal operation, the operator will adjust SP-5 speed as necessary to ensure proper automatic operation of S-3A.

S-3A has a 'Manual' control in which TCTT-4 does not affect the valve movement. In 'Manual', only the control room operator has buttons to open or close the valve. Manual control can be used for rapid changes in S-3A during operation, maintenance, or testing.

4.3.6 Target Cooling System Secondary Coolant Parameter Indication, Recording, and Alarm System

The TCS Secondary Coolant Parameter Indication, Recording, and Alarm System is designed to provide control room operators with indication of parameters convenient for operating the TCS Secondary Coolant Control System, to record TCS secondary coolant parameter data for long-term retention or review, and to actuate alarms to alert the operator to abnormal parameters. No safety-related functions are associated with the TCS Secondary Coolant Parameter Indication, Recording, and Alarm System. Parameter current loop signals going to chart recorders which also serve as parameter indication and alarm units. Parameter inputs into the TCS Secondary Coolant Parameter Indication, Recording, and

Alarm System are multiple TCS Secondary Coolant Control System temperature, flow, and valve position signals.

4.3.7 N-16 Power Monitoring System

The N-16 Power Monitoring System (PMS) is designed to provide control room operators with indication of reactor core power by means of measuring the amount of N-16 produced in the primary coolant system. Reactor fission power is directly proportional to the amount of N-16 atoms produced by the fast neutron flux in the reactor. Therefore, reactor core power can be measured separate from the TEF power. The N-16 PMS has two (2) redundant detectors located in mechanical equipment room 114 and two (2) redundant displays located in the control room. The detectors will be placed in a shield with a collimator facing the primary coolant outlet pipe. The detectors are sealed stainless steel ionization chambers capable of measuring the dose rates at the designated measurement point.

The N-16 PMS detectors are located on the reactor primary coolant hot leg piping at a distance corresponding to the time delay for primary coolant exiting the core to reach the measuring point of 1.35 times the N-16 half-life. This power measurement is calibrated by performing a series of power calorimetric calculations to determine reactor core power while not operating the TEF. This method of power measurement is used by several domestic and international research reactors and has been found to be stable and reliable.

4.3.8 Pool Coolant Monitoring System

The Pool Coolant Monitoring System (PCMS) provides display and alarm functions both locally at the entryway to mechanical equipment room 114 and remotely in the control room based on I-131 activity concentration in the pool coolant system. Elevated I-131 activity levels in the pool coolant system would be an early indication of a leaking target rod in the reactor pool. The PCMS has a detector in room 114 entryway.

The PCMS continuously monitors pool coolant activity anytime the pool coolant system is in operation. The monitor receives ~1 gpm of pool coolant from a ½-inch vent line connection on the pool coolant circulation pump combined discharge header downstream of the pool coolant circulation pumps. The pool coolant water flows through a filter and a cation resin bed before it is monitored by a gamma scintillation detector in a 2.7-liter volume of the system. Once the pool coolant leaves the monitored volume, the coolant returns to the pool coolant system via ½-inch vent piping on the pool water holdup tank.

Given a 1 gpm flow rate, the overall time for the PCMS to detect I-131 in the pool coolant system is approximately 13 minutes. The 13 minutes is based on the I-131 taking more than 11 minutes to get to the PCMS detector volume and almost two (2) minutes for the detector to recognize the increased I-131 concentration.

5. Target Assembly Nuclear Design Analysis

The target physics model predicts the production of Mo-99 as a function of the dimension, location and loading of the target rods and the neutron flux distribution in the target position. The physics model also provides the distribution of power densities in the UO_2 pellets for the thermal-hydraulic design of the TA. The target physics model incorporated both the TAs and the MURR reactor core and examined the full range of MURR operations to develop the target physics design cases.

5.1 Analytical Methods

The nuclear design calculations were conducted using Monte Carlo code MCNP6 (Reference 12) and ENDF/B-VII.1 (References 13 and 14) to obtain eigenvalue and neutron flux distributions. The MCNP6 calculations also produce heating rates for the reactor fuel elements and target rods, which are used for the nuclear design and analyses to obtain the TA power. For the determination of the TA uranium-235 enrichment distribution in MCNP6, 100 million source histories (10,000×10,000 neutrons) were used to obtain converged eigenvalue and power distributions.

5.2 Target Assembly Physics Model

The TAs are loaded in graphite reflector positions No. 5A and No. 5B. The physics design and analyses of the TAs utilized the "MURR 2015 reflector model" (Reference 15), which includes the reactor core and associated structures such as detailed modeling of the control blades (CB), regulating blade, beam tubes, beryllium (Be) reflector, graphite reflector, and experimental holes. The MCNP6 model of the MURR core with two (2) TAs is shown in Figure 34.

The target rod physical dimensions used for the nuclear design calculations are summarized in Table 3. The physical dimensions utilized in the nuclear design are exactly the same as those of the mechanical design, which includes 11 target rods per target rod cartridge (flow channel), cartridge top and bottom fixture, cartridge guide rail, neutron shield, channel housing, and water plenum. The cartridge locking device, water diffuser, and incoming water pipe are not included in the physics model as they are expected to have little influence on the analyses. The physics model of the TA is shown in Figure 35 at the axial mid-plane, and target numbering is shown in Figure 36 for the baseline TA model. [redacted] 5a, d, e, f

The target rod model includes target pellets, pellet-clad gap, cladding, top plenum spring, and the top and bottom endcaps. In the physics model, four (4) pellets are defined as a single axial node (2.4 cm). The effective isotopic densities of UO_2 pellet consider 1.78% of open pore due to the pellet's dish and chamfer design. The plenum spring was homogeneously mixed with the helium filling gas. Due to the complexity of the geometry of the top and bottom fixtures, the physics model of these components was designed to preserve the outer dimension and mass of the Zircaloy-4 material.

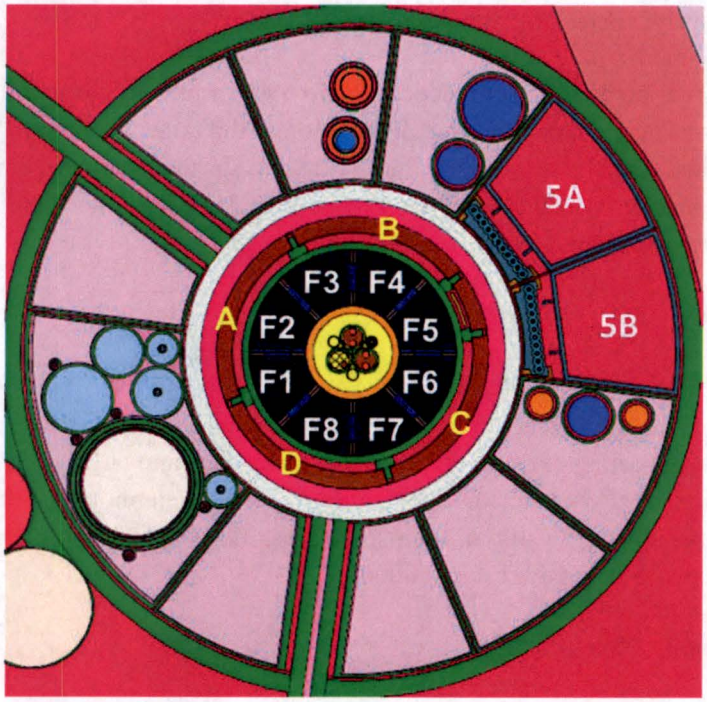

Figure 34
MCNP6 Model of MURR with Driver Fuel and Reflector Element Numbers at Axial Mid-Plane

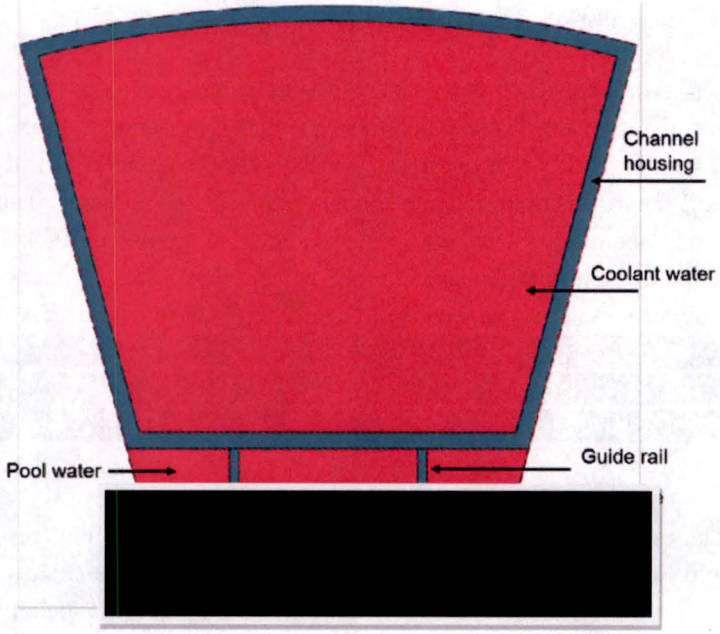

5a, d, e, f

Figure 35
MCNP6 Model of Target Assembly at Axial Mid-Plane

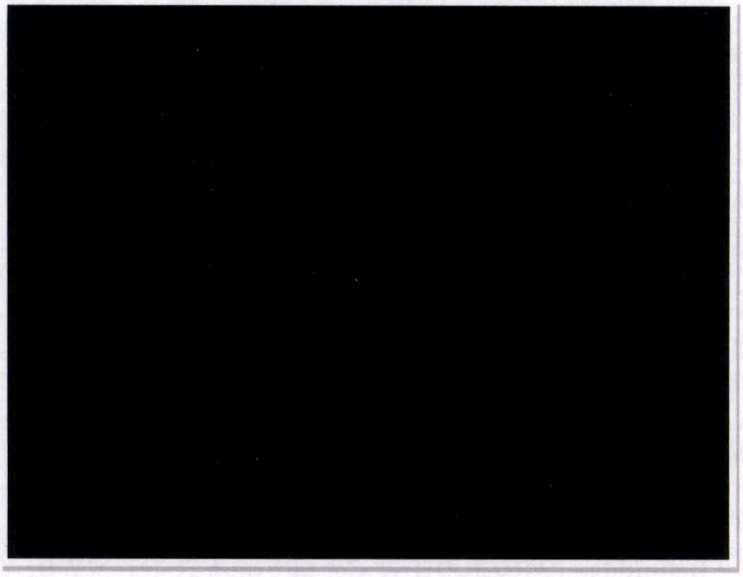

5a, b, d, e, f

Figure 36
Target Rod Numbering for Two Target Assemblies (baseline model)

5a, b, d, e, f

Figure 37

5.2.1 MURR Driver Core States

The physics design evaluates the target cartridge performance as well as the reactivity insertion to the MURR reactor core and driver fuel power changes due to TA loading and changes of the MURR core states. The TA design was conducted for the equilibrium core represented by its minimum, average and maximum burnup as summarized in Table 9. The extreme burnup core represents an anticipated driver fuel burnup distribution that can create the worst power peaking in both the driver fuel and target pellets, which has been generated from the maximum burnup core case without xenon. The critical CB position (distance from its fully inserted position) is the lowest at beginning-of-cycle (BOC) and withdraws as the driver fuel depletes and fission products accumulate in the core. For the typical 1-week operating cycle, the CB reaches its equilibrium height about 48 hours (Day 2 state) after startup and slowly withdraws until the end-of-cycle (EOC).

Table 9
Definition of MURR Driver Core Burnup States (MWD)

Driver Fuel Element	Extreme Burnup Core <core_ext>	Minimum Burnup Core <core_min>	Average Burnup Core <core_avg>	Maximum Burnup Core <core_max>
F1	0	0	19	3
F2	117	20	92	122
F3	67	18	60	68
F4	142	142	130	145
F5	0	0	19	3
F6	117	20	92	123
F7	67	18	60	68
F8	142	142	130	144
Core total (MWD)	652	360	600	676

- Depending on reactor operating conditions, especially CB insertion height, the flux level in the reflector region could appreciably change. During 2014 – 2015 operations, the lowest startup and highest shutdown critical position was recorded at CB heights of 32.69 cm (12.87 in) and 61.6 cm (24.25), respectively (Reference 16). These two CB positions are bounding values that include various reactor perturbations such as Be reflector installation, CB replacement and adjacent experiment loading/unloading. The CB movement during a 19-month period of operation in 2014 and 2015 is shown in Figure 38. The CB average age during this period is 4.7 to 5.7 years. In order to conservatively conduct the core and target power calculations, the limiting core configuration has been constructed to use a fresh Be reflector that will result in a higher neutron flux in the target region, in addition to the variations of driver fuel burnup.

- The CB age is tilted such that A and D are fresh and B and C are eight (8) years old, which will result in a higher power peaking in the TA.
- The CB tip position is tilted so that the tip position of CB B and C is higher than that of A and D by 2.54 cm (1 in), which results in a higher power peaking in the TA.
- The central flux trap is loaded with sample materials.
- Equilibrium xenon is used for the maximum and average burnup driver fuels.
- No xenon is used for the extreme and minimum burnup driver fuels.

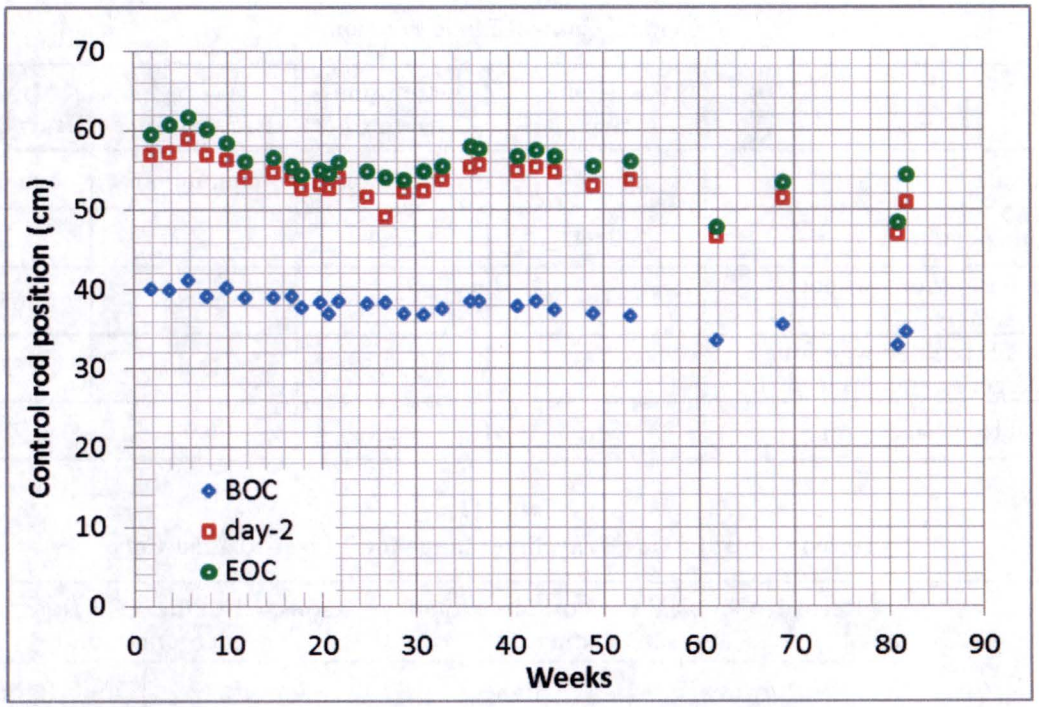

Figure 38
MURR Control Blade Travel between January 13, 2014 and September 15, 2015

Typically, the CB travels over 10 cm (3.94 in) during the first two (2) days after startup and then slowly continues to withdraw. The driver fuel elements also have two (2) distinct states: clean fuel and equilibrium xenon. The xenon-free core burnup is provided in Table 10. The core burnup of an equilibrium xenon state core is approximately 20 MWD higher than that of the xenon-free core. Because the pellet enrichment is fixed at nominally 19.75 wt%, the target cartridge design process searched for the target rod position that satisfies the thermal design limits of the target rod and cartridge during normal operating conditions (accident conditions presume operation at the allowable design limits). The selected target rod position is 26.37 cm (10.38 in) from the core center.

The critical CB positions and expected CB travel range of the equilibrium core are summarized in Table 10 and Table 11. When the TAs are loaded, the CBs are inserted deeper into the core. The estimated additional CB insertion depth is 3 to 9 cm (1.2 to 3.5 in) depending on the core states. When these offset values are applied to the lowest and highest CB position during 2014 to 2015 operation, the lowest and highest critical CB position with a two (2) TA loading is expected to be 33.7 cm (13.27 in) and 51.9 cm (20.43 in), respectively (Table 11). Here, the CB offset values of <core_ext> and <core_max> were applied to BOC and EOC cases, respectively, while that of <core_avg> was approximately used for Day-2 CB position.

Table 10
Critical Control Blade Positions

	Extreme Burnup Core	Minimum Burnup Core	Average Burnup Core	Maximum Burnup Core
Xenon state	no xenon	no xenon	equilibrium	equilibrium
Regulating blade (cm)	25.4	25.4	38.1	38.1
Critical CB position without target assembly	41.67	35.09	59.87	65.00
Critical CB position with full (2 fresh) target assemblies loaded	38.75	32.75	52.89	55.28
Control blade offset (cm)	2.92	2.34	6.98	9.72

Table 11
Expected Control Blade Travelling Range for Target-Loaded Core

	Recorded Critical CB Position without Target Loading		Expected Critical CB Range with Target Loading	
	Lowest	Highest	Lowest	Highest
BOC	36.6	42.6	33.7	39.6
Day-2	49.1	58.8	42.1	51.8
EOC	53.6	61.6	43.9	51.9

5.2.2 Target Assembly Criticality

A conservative estimate of K_{eff} for two (2) TAs was performed using the MURR core model by replacing the driver fuel with water and assuming the control and regulating blades are completely withdrawn from the core. The calculated values of K_{eff} for the target cartridge located in reflector position No. 5A (single TA), and No. 5B (single TA) are 0.65868±0.00014 and 0.65870±0.00018, respectively. When both 5A and 5B are loaded, the K_{eff} is 0.65875±0.00018, indicating that the TAs will be subcritical with a large margin for uncertainty. The uncertainties are given in 2 standard deviations (2σ) as a 95% confidence level.

5.2.3 Impact of Target Assembly Loading on MURR Reactor Core

Loading two TAs in the MURR graphite reflector region causes perturbations in neutronic and thermal performance of the MURR core as follows:

- The MURR core excess reactivity will increase slightly, which will be compensated by the reactivity control devices.
- The neutron flux and power of the adjacent F5 fuel element will increase even though the total core power is maintained at 10 MW.
- The thermal power generated by the target rods will not affect the reactor core primary or pool cooling capability. The heat generated by the targets that is discharged to the reactor pool will be adequately removed by the reactor pool coolant system without impacting the pool temperature.

5.2.4 Reactivity Insertion

The reactivity insertion due to target cartridges being loaded in graphite reflector positions No. 5A and No. 5B is summarized in Table 12. The reactivity worth was calculated by replacing the water in the TA cartridge with fresh, clean, cold target rods. Under the hot operating condition, the reactivity insertion due to a single cartridge loading is less than 0.31% Δk/k. The maximum reactivity insertion due to a hot target rod is the same as that of the cold target rod for all core burnup states.

Table 12
K_{eff} and Reactivity Insertion Values for Single Target Assembly

	5A/5B filled with structure and water (K_{eff})	Target in 5A		Target in 5B	
		K_{eff}	Δk/k (%)	K_{eff}	Δk/k (%)
Maximum with equilibrium xenon	0.99368	0.99658	0.29	0.99660	0.29
Average with equilibrium xenon	0.99392	0.99673	0.28	0.99677	0.29
Minimum without xenon	0.99385	0.99662	0.28	0.99690	0.31
Extreme without xenon	0.99382	0.99667	0.29	0.99685	0.31

5.2.5 Driver Fuel Power Peaking

The target cartridge loading in the graphite reflector positions has a relatively small impact on power peaking of the MURR core driver fuel. Table 13 compares the distribution of MURR driver fuel power with and without TA loading and provides the location of the largest peaking factors in the reactor core. For most of core states, the fuel element F5 (closest to the TAs, see Figure 34 for driver fuel identification) peaking factor is the highest because the fuel burnup is the lowest and the fuel is located close to the TA. For the F5 fuel element, the peaking factor of the inner plate is always higher than that

of the outer plate. When two (2) TAs are loaded, the increase of peaking factor is less than 4% for the inner plate, while the maximum increase of peaking factor is ~11% for the outer plate. However, the absolute value of the outer plate peaking factor is always less than that of the inner plate peaking factor.

Table 13
MURR Core Maximum Power Peaking Due to Target Assembly Loading

	Number of Target Rods	Inner Fuel Plate		Outer Fuel Plate	
		Axial Node[1] (Fuel Element)	Peaking Factor	Axial Node (Fuel Element)	Peaking Factor
Maximum with equilibrium xenon	0	13 (F5)	2.541	13 (F1)	2.064
	22	11 (F5)	2.637	11 (F5)	2.218
Average with equilibrium xenon	0	11 (F5)	2.426	12 (F1)	1.999
	22	8 (F5)	2.511	11 (F5)	2.155
Minimum without xenon	0	10 (F1)	2.968	9 (F6)	2.444
	22	9 (F5)	3.031	9 (F6)	2.565
Extreme without xenon	0	10 (F5)	2.905	9 (F1)	2.200
	22	10 (F5)	2.976	8 (F5)	2.397

[1]Axial nodes 1 and 24 correspond to the bottom and top of MURR driver fuel plate, equally spaced.

5.2.6 Reactivity Coefficients

Though the core power distribution and power peaking factors are altered when two (2) target cartridges are loaded in the graphite reflector region, the core reactivity characteristics do not change significantly due to target rods being loaded in the reflector region. The reactivity coefficients of the core with two (2) fresh TAs were calculated for the fuel temperature coefficient, coolant temperature coefficient and void reactivity and are summarized in Table 14.

The driver fuel temperature coefficient was calculated by increasing the fuel temperature by 906.4 °C (1663.5 °F), i.e. from 20.44 °C (68.8 °F) to 926.84 °C (1700.3 °F). The fuel temperature coefficients are consistent with core burnup state and kept negative. Due to the limitations in cross section data, however, the temperature dependence of lumped fission products (all fission products except ^{135}I, ^{135}Xe, ^{149}Pm, ^{149}Sm) was not considered. The coolant temperature coefficient was calculated by changing the coolant temperature from 20.44 °C (68.8 °F) to 76.84 °C (170.3 °F), where the coolant density changes from 0.99815 to 0.97378 g/cm^3. The principal cross section data used for the calculations are basically the same for both the lower and higher coolant temperature conditions, but the S(α,β) thermal scattering was correctly treated. The coolant void reactivity of the core was calculated by removing 99.9% of coolant from the core.

The statistical uncertainty (2σ) of the reactivity coefficient is ~0.026% when the error propagation rule is used. The least negative values are -1.03×10^{-6} and -1.69×10^{-4} $\Delta k/k/°C$ for the fuel and coolant temperature coefficient, respectively.

Negative reactivity coefficients of coolant void and temperature limit the peak power during a reactivity transient. Using the lowest magnitude of these negative reactivity coefficients for a positive reactivity insertion accident analysis is conservative because the subsequent power transient is larger than if nominal values were used.

Table 14
Reactivity Coefficients of the Reactor Core with Two Fresh Target Assemblies

Core Burnup State	Fuel Temperature Coefficient ($\Delta k/k/°C$)	Coolant Temperature Coefficient ($\Delta k/k/°C$)	Coolant Void Reactivity ($\Delta k/k/\%void$)
Maximum with equilibrium xenon	-1.20×10^{-6}	-1.69×10^{-4}	-3.40×10^{-3}
Average with equilibrium xenon	-1.16×10^{-6}	-1.73×10^{-4}	-3.40×10^{-3}
Minimum without xenon	-1.27×10^{-6}	-1.85×10^{-4}	-3.40×10^{-3}
Extreme without xenon	-1.03×10^{-6}	-1.79×10^{-4}	-3.40×10^{-3}

5.2.7 Reactivity Device Worth

The impact of TA loading on the existing reactivity control devices (control and regulating blades) were estimated for their reactivity worth and subcriticality margin as summarized in Table 15. Reactivity worth of the regulating blade was calculated from fully inserted and fully withdrawn conditions while the CB is kept at its critical position. For the selected core states, the lowest worth of the regulating blade is 3.41×10^{-3} $\Delta k/k$.

The CB subcriticality margin was at first calculated for the average burnup core. Among four (4) CB's (A, B, C and D), the subcriticality margin of C is the lowest even though it is almost the same as that of B. The subcriticality margin increases as the core burnup increases due to effective neutron flux changes. The lowest subcriticality margin with the most reactive CB (i.e. A) and regulating blade fully withdrawn is 0.055 $\Delta k/k$ for the minimum burnup core.

Table 15
Reactivity Control Device Worth with Two Fresh Target Assemblies

	Subcriticality Margin of Control Blade (Δk/k)	Regulating Blade Worth (Δk/k)
Maximum with equilibrium xenon	0.109	3.55×10^{-3}
Average with equilibrium xenon	0.106	3.41×10^{-3}
Minimum without xenon	0.055	3.69×10^{-3}
Extreme without xenon	0.076	4.02×10^{-3}

5.2.8 Core Excess Reactivity

The excess reactivity of the core with two (2) fresh TAs was calculated for the minimum burnup core which has the largest excess reactivity. All CB's and regulating blade are fully withdrawn from the core. The excess reactivity of the cold core (all at room temperature) is 0.072 Δk/k, while that of the hot operating core is 0.067 Δk/k.

5.2.9 Kinetic Parameters

The kinetic behavior of the core is dominated by the driver fuel elements, which is slightly perturbed by the presence of two (2) TAs in the graphite reflector region. The effective (or adjoint weighted) neutron generation time (Λ_{eff}) and effective delayed neutron fraction (β_{eff}) were generated for different burnup states of the core with and without (Reference 17) TAs as summarized in Table 16. The neutron generation time tends to increases when the two (2) TAs are loaded, but very slightly. The effective delayed neutron fractions of the core with and without TAs are very close to each other within the uncertainty range ($\pm 2\sigma$). From the viewpoint of point kinetics, the TA loading won't deteriorate the slope of power increase (or inverse reactivity period) during the reactivity induced transient.

Table 16
Kinetic Parameters of the Reactor Core with and without Target Assemblies

Target Loading	Core Burnup State	Λ_{eff} (μsec)	STD (1σ)	β_{eff}	STD (1σ)
No Target Assemblies	Maximum	62.3	0.273	0.00723	0.00015
	Average	60.6	0.278	0.00731	0.00015
	Minimum	53.7	0.244	0.00749	0.00016
	Extreme	57.0	0.248	0.00732	0.00015
Two Target Assemblies	Maximum	62.7	0.237	0.00730	0.00013
	Average	61.5	0.235	0.00745	0.00013
	Minimum	54.7	0.215	0.00766	0.00014
	Extreme	58.4	0.220	0.00769	0.00014

5.2.10 Structural Component Heating

The structural component heating was estimated by MCNP6 code using the kinetic energy deposited by the fission fragments, prompt neutrons and delayed neutrons. In addition to the neutron data used for neutron flux calculation, the heating calculation uses photon-atomic data (mcplib04) (Reference 18), photon-nuclear data (endf7u) (Reference 19), electron data (el03) (Reference 20), and delayed neutron/gamma data (cinder.dat, delay_library.dat, cindergl.dat, delay_library_v2.dat) (References 21 and 22). MCNP6 adopts the CINDER'90 model to calculate delayed particle emissions from all of the radionuclides in the decay chain for a fission product. The photon emission time for delayed-neutron and delayed-photon emission was adjusted to 10^5 sec (the default value is 10^{10} sec), under which the statistical uncertainty (1σ) of the calculated heat deposited in the Be reflector is ~5%.

The Be reflector heating is higher for the maximum burnup core by 3.3% when compared with the minimum burnup core. For the maximum burnup core, the Be reflector heating is 216.2 kW and 205.7 kW with and without two (2) TAs, respectively.

The heat from the cartridge and neutron absorber shield is 12.7 kW and 7.6 kW respectively, when two (2) TAs are loaded (Table 17).

Table 17
Component Radiation Heating Due to Target Assembly Loading for Maximum Burnup Core

Target Loading	Component	Neutron Heating (kW)	Photon Heating (kW)	Electron Heating (kW)	Total (kW)
No Target Assemblies	Be reflector	41.6	81.9	82.2	205.7
Two Target Assemblies	Be reflector	42.9	86.2	87.1	216.2
	Al cartridge	0.27	6.2	6.2	12.7
	Steel shield	0.05	3.8	3.8	7.6

5.3 Target Assembly Flux and Power

5.3.1 Fresh Target Assemblies in Both Positions No. 5A and No. 5B (Base Loading Pattern)

The neutron flux in a TA is dominated by incoming neutrons from the reactor core even though the TA produces neutrons from fission reactions. Figure 39 and Figure 40 show 4-group axial neutron flux distributions of the target rods 6 and 17, i.e. the middle of each 11 target rod bundle (see Figure 36 for target rod numbering), when two fresh target cartridges are loaded in graphite reflector positions No. 5A and No. 5B, respectively. The upper energy boundaries of the 4-group are 20 MeV (Group 1), 0.1 MeV (Group 2), 5.53 keV (Group 3), and 0.625 eV (Group 4). The solid and hollow symbols in each figure indicate the MURR core states, i.e. <core_ext> and <core_max>, respectively. Axial nodes 1 and 25 correspond to the bottom and top pellet, respectively. As can be seen, the neutron flux drops at the bottom and top section of the target rod. The neutron flux is suppressed even more in the top section due to the CBs, which is relaxed to a certain extent when the CBs are pulled out in the maximum burnup core. The thermal neutron flux is effectively flattened in the vertical middle section, from node 5 to 20, due to the presence of the SS316L absorber.

Figure 41 shows neutron flux in the azimuthal direction, from target rod 1 to 11 (position No. 5A) and from rod 12 to 22 (position No. 5B), at axial middle plane. The neutron population is suppressed at the assembly edge region due to elongated neutron absorber material on the cartridge edge. For the average burnup core, the peak neutron fluxes of the target pellet are [redacted]

5a, d, e, f

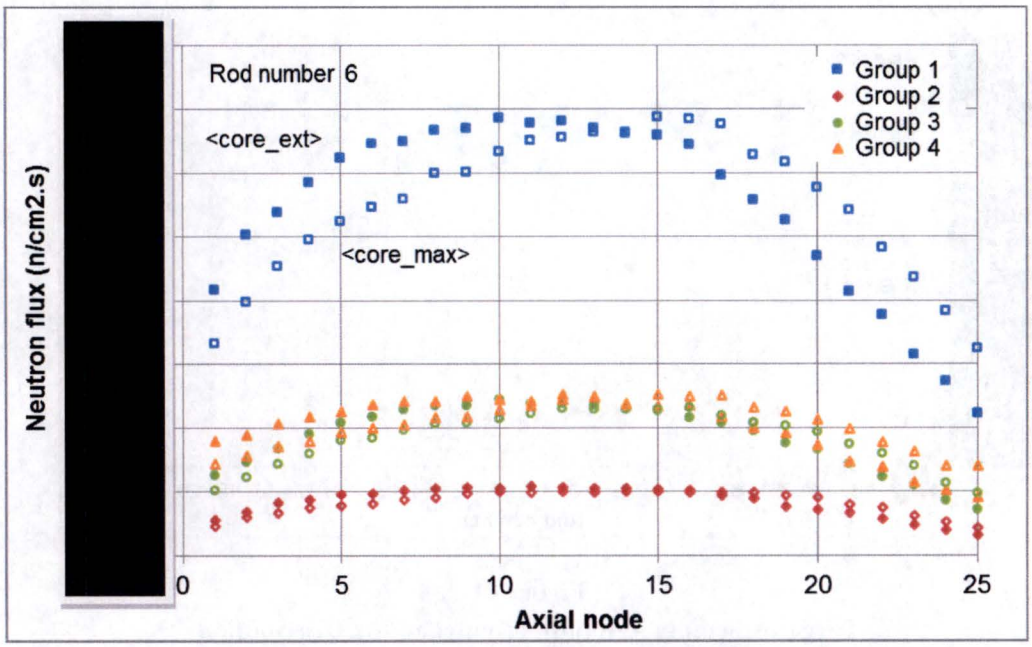

5a, d, e, f

Figure 39
Target Rod 6 Axial Neutron Flux Distribution in Position No. 5A

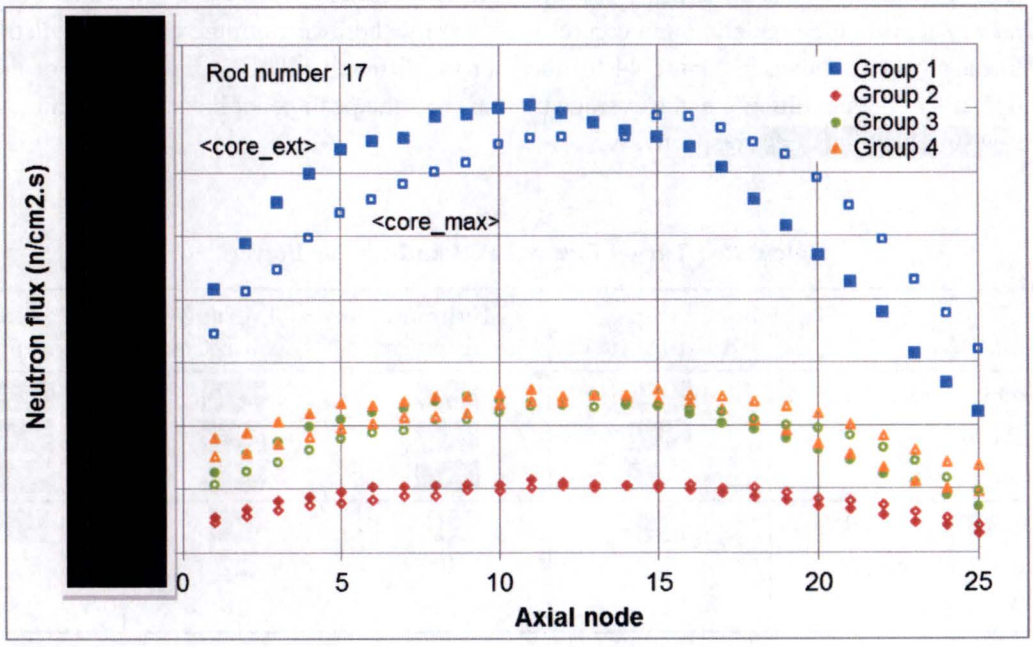

5a, d, e, f

Figure 40
Target Rod 17 Axial Neutron Flux Distribution in Position No. 5B

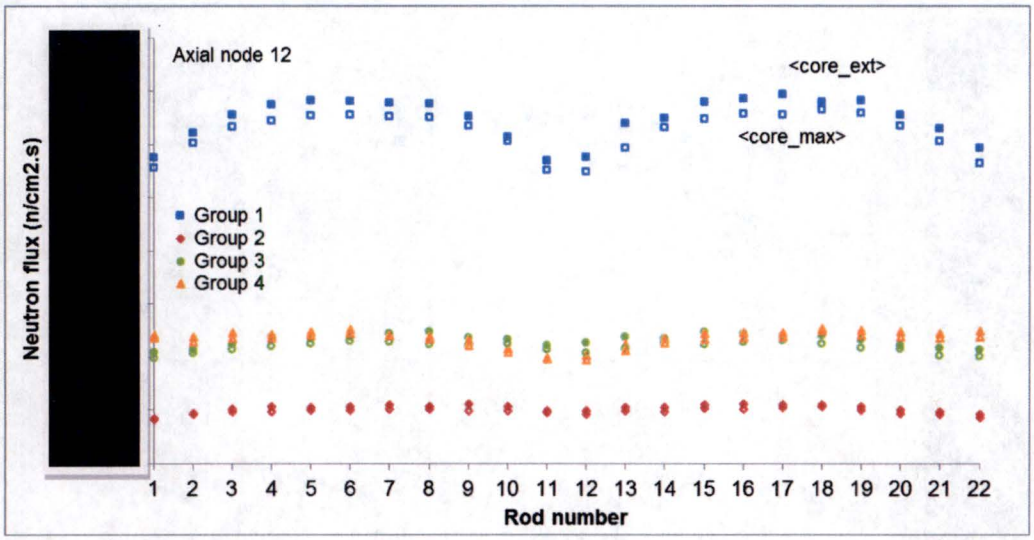

5a, d, e, f

Figure 41
Target Assembly Azimuthal Neutron Flux Distribution

Calculated target power and pellet linear power when two (2) fresh TAs are being irradiated are given in Table 18. Figure 42 and Figure 43 show the pellet linear power envelope of the extreme and maximum burnup cores respectively. The axial power profile is initially bottom-peaked and gradually changes to middle-peaked shape as the regulating and control blades are withdrawn from the core. The distribution of pellet linear power is shown in Figure 44 for the four (4) different MURR core states. For the most probable operating core condition, i.e. the average burnup core, the peak pellet linear power and total TA power are [redacted], respectively.

5a, d, e, f

Table 18
Calculated Target Power Level and Linear Power

	Extreme Burnup Core	Minimum Burnup Core	Average Burnup Core	Maximum Burnup Core
Assembly Power (kW)	[redacted]	[redacted]	[redacted]	[redacted]
Assembly in 5A	[redacted]	[redacted]	[redacted]	[redacted]
Assembly in 5B	[redacted]	[redacted]	[redacted]	[redacted]
Peak Linear Power (kW/m)	[redacted]	[redacted]	[redacted]	[redacted]
Target Rod Number	18	20	22	22
Axial Node*	11	10	18	18

5a, d, e, f

*Axial nodes 1 and 25 correspond to bottom and top node, equally spaced.

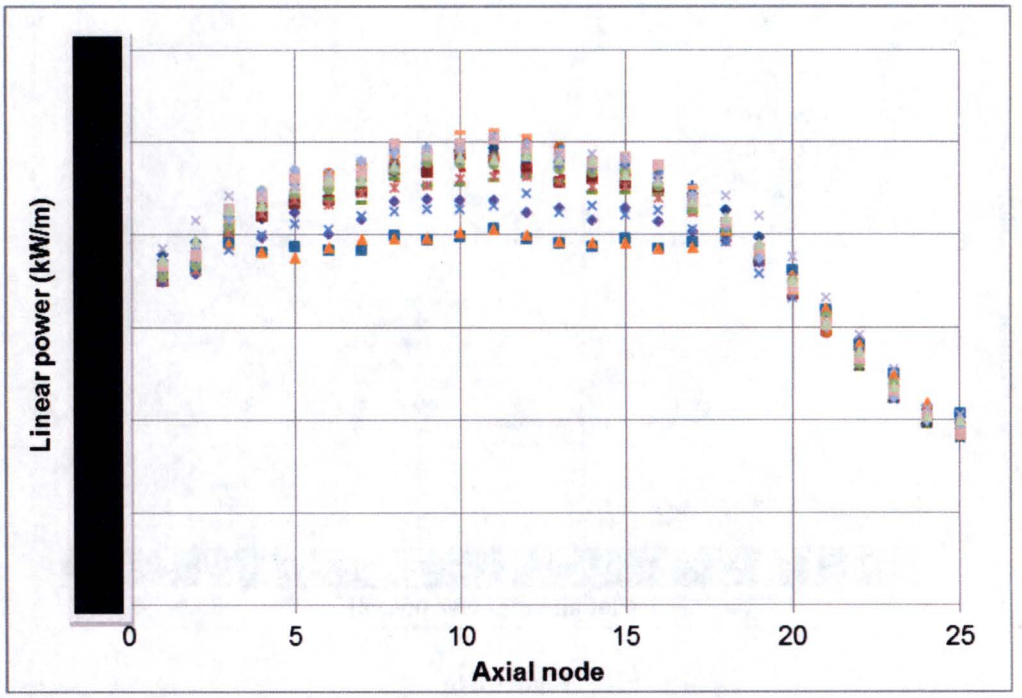

5a, d, e, f

Figure 42
Power Envelope of the Base Target Loading for the Extreme Burnup Core Case

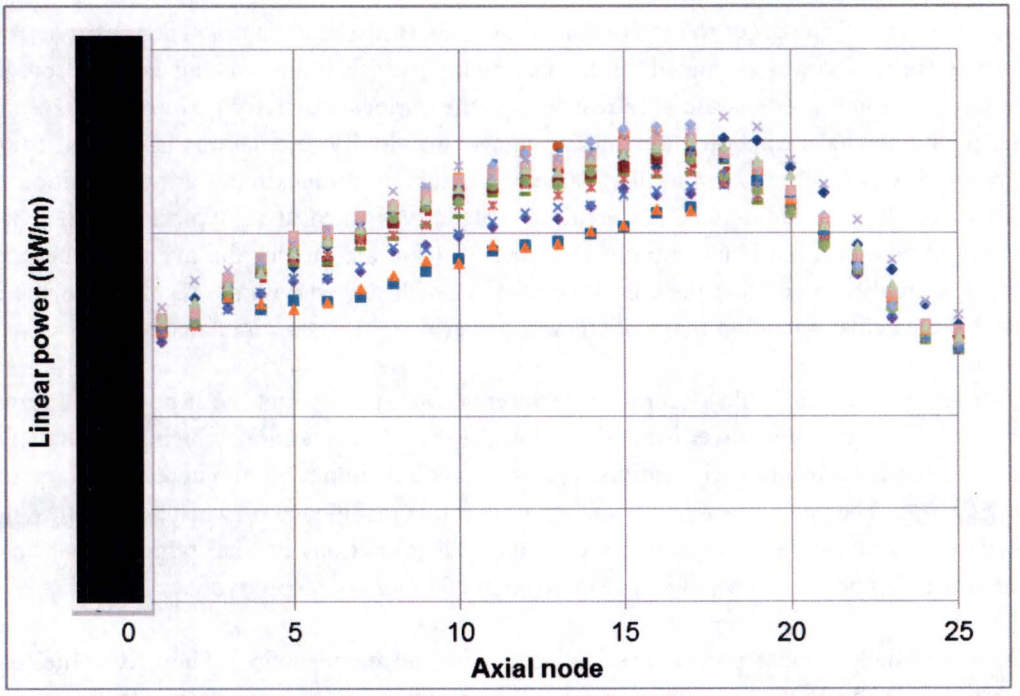

5a, d, e, f

Figure 43
Power Envelope of the Base Target Loading for the Maximum Burnup Core Case

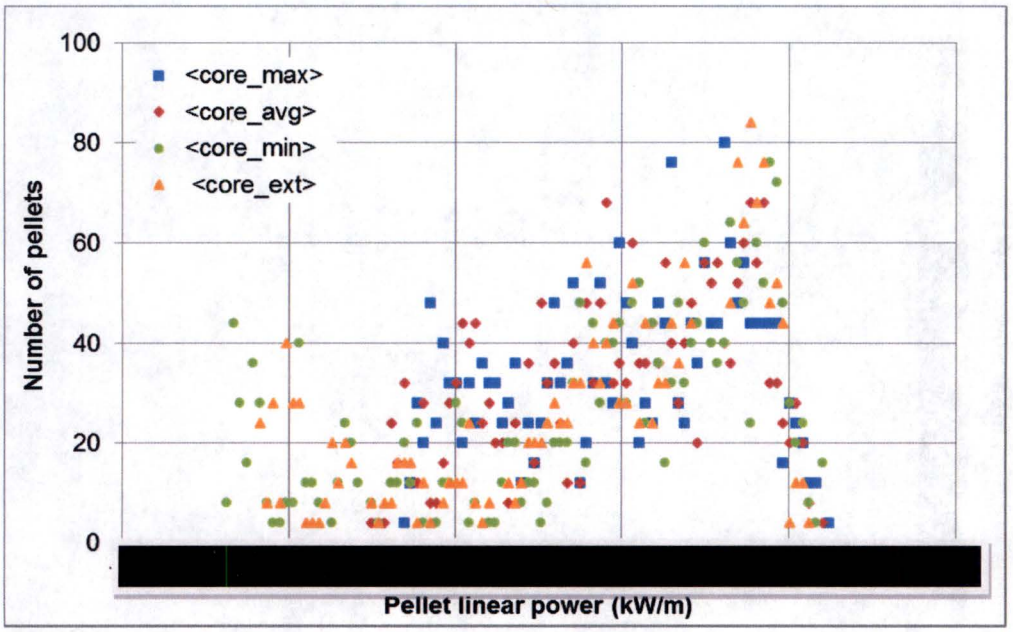

5a, d, e, f

Figure 44
Target Assembly Pellet Linear Power Distribution for Base Target Loading Case

5.3.2 Sensitivity to Control Blade Position for Full Target Assembly Loading

The peak linear power of the target rod is dominated by the CB insertion depth. The sensitivity of peak linear power to CB position was estimated for the maximum, average, minimum and extreme core burnup states. The CB position represents the core response to the various reactivity perturbations seen by the reactor core, including fuel depletion and material aging. Sensitivity calculations have been conducted for a wide range of CB positions beyond the expected minimum and maximum critical position for the target-loaded core. In this simulation, the regulating blade was fixed at its typical position: 25.4 cm (10 in) for the extreme and minimum burnup core and 38.1 cm (15 in) for the average and maximum burnup core. It should be noted that the CB movement is synchronized with the regulating blade in real operation so that the actual operating range of CB will be narrower than the simulated one.

The results are summarized in Table 19 for the total target power, peak target linear power and driver fuel peaking factors. The total target power is relatively low for the BOC condition, which is a relatively short term period. For the equilibrium fuel conditions (average and maximum burnup cores), the target power stays below [redacted]. The peak linear power of the target rod is maintained between [redacted] for the simulated equilibrium core states and CB position. The variations in total target power and peak linear power versus CB position are shown in Figure 45 and Figure 46, respectively.

5a, d, e, f

The MURR driver fuel element power peaking occurs in fuel element F5. The driver fuel element peaking is higher for the BOC state when the CB and regulating blade are deep into the core. The calculated maximum peaking factor is 3.231 for the inner plate. For the outer plate that faces the target,

the maximum peaking factor is 2.636, which is lower than that of the inner plate for all core state and CB positions. The variations of driver fuel element peaking factor vs CB position are shown in Figure 47.

The effect of CB position has also been studied for the critical core configurations by changing the CB average age from 0 to 8 years. For all the critical core cases, the calculated total target power and the maximum linear power are less than those of non-critical core cases. For the extreme burnup core, the maximum linear power is [redacted] for the non-critical and critical core, respectively, when the average CB age is the same (4 years) for both cases. The extreme burnup core becomes critical at CB height of 32.28 cm (12.71 in) when the age of all the CBs is 8 years. The maximum linear power of the extreme burnup core with CB at ~32 cm (12.6 in) is [redacted] for the non-critical and critical core, respectively. It should be noted that the CB age tilt is 8 years for the non-critical case while it is 0 for the critical case, which reduces the neutron population in the TA to a certain extent; and both the total target power and the maximum linear power are reduced in the critical core when compared with the non-critical core.

5a, d, e, f

The critical core calculations have shown that the non-critical core calculations conservatively estimate the target power and the maximum linear power. However, it should also be noted that the critical core simulation here is limited by the range of CB age and its tilt and therefore, the variation of CB position is smaller when compared with the expected CB traveling range. This means that variation of CB age (as well as CB age tilt) is not sufficient to realistically model all the critical core cases. It is also true that in the actual core the CB position could be even higher or lower than those used for the critical core calculations due to Be reflector aging and other reactivity perturbations. Finally, it is also reasonable to assume that the target power and its axial shape are dominated by CB position.

Therefore, the limiting core configuration has been selected from the non-critical core configurations. The maximum linear power found from the sensitivity calculation is [redacted] for the extreme burnup core with the CBs positioned at 30 cm (11.81 in) and the regulating blade positioned at 25.4 cm (10 in), which is used for the target thermal-hydraulics and CHF analyses. The maximum TA power is [redacted] for the maximum burnup core with CB at 44 cm (17.32 in) and regulating blade at 38.1 cm (15 in), which is the recommended case for the TA cooling analysis.

5a, d, e, f

Table 19
Target Assembly Power and Core Peaking Factors

Core State	CB Position (cm)	Target Power (kW)	Peak Linear Power (kW/m)	Inner Plate Peaking	Outer Plate Peaking
Maximum burnup with equilibrium xenon	62	[redacted]	[redacted]	2.573	2.147
	60	[redacted]	[redacted]	2.577	2.173
	58	[redacted]	[redacted]	2.605	2.192
	56	[redacted]	[redacted]	2.622	2.208
	54	[redacted]	[redacted]	2.662	2.239
	52	[redacted]	[redacted]	2.674	2.273
	50	[redacted]	[redacted]	2.709	2.302
	48	[redacted]	[redacted]	2.755	2.348
	46	[redacted]	[redacted]	2.792	2.385
	44	[redacted]	[redacted]	2.861	2.441
Average burnup with equilibrium xenon	56	[redacted]	[redacted]	2.488	2.109
	54	[redacted]	[redacted]	2.505	2.131
	52	[redacted]	[redacted]	2.529	2.163
	50	[redacted]	[redacted]	2.575	2.192
	48	[redacted]	[redacted]	2.609	2.240
	46	[redacted]	[redacted]	2.648	2.263
	44	[redacted]	[redacted]	2.684	2.310
	42	[redacted]	[redacted]	2.757	2.374
	40	[redacted]	[redacted]	2.781	2.393
Minimum burnup without xenon	42	[redacted]	[redacted]	2.790	2.386
	40	[redacted]	[redacted]	2.857	2.419
	38	[redacted]	[redacted]	2.898	2.453
	36	[redacted]	[redacted]	2.944	2.489
	34	[redacted]	[redacted]	3.046	2.546
	32	[redacted]	[redacted]	3.055	2.576
	30	[redacted]	[redacted]	3.120	2.609
Extreme burnup without xenon	42	[redacted]	[redacted]	2.906	2.301
	40	[redacted]	[redacted]	2.930	2.351
	38	[redacted]	[redacted]	2.991	2.403
	36	[redacted]	[redacted]	3.053	2.475
	34	[redacted]	[redacted]	3.130	2.539
	32	[redacted]	[redacted]	3.182	2.594
	30	[redacted]	[redacted]	3.231	2.636

5a, d, e, f

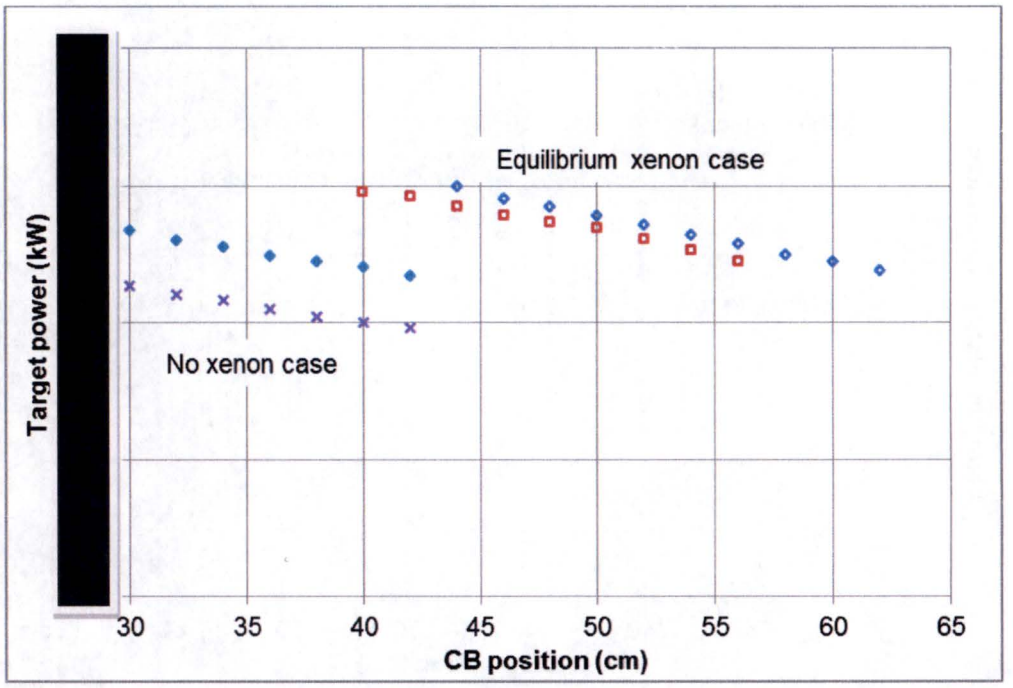

5a, d, e, f

Figure 45
Variation of Target Power vs. Control Blade Position

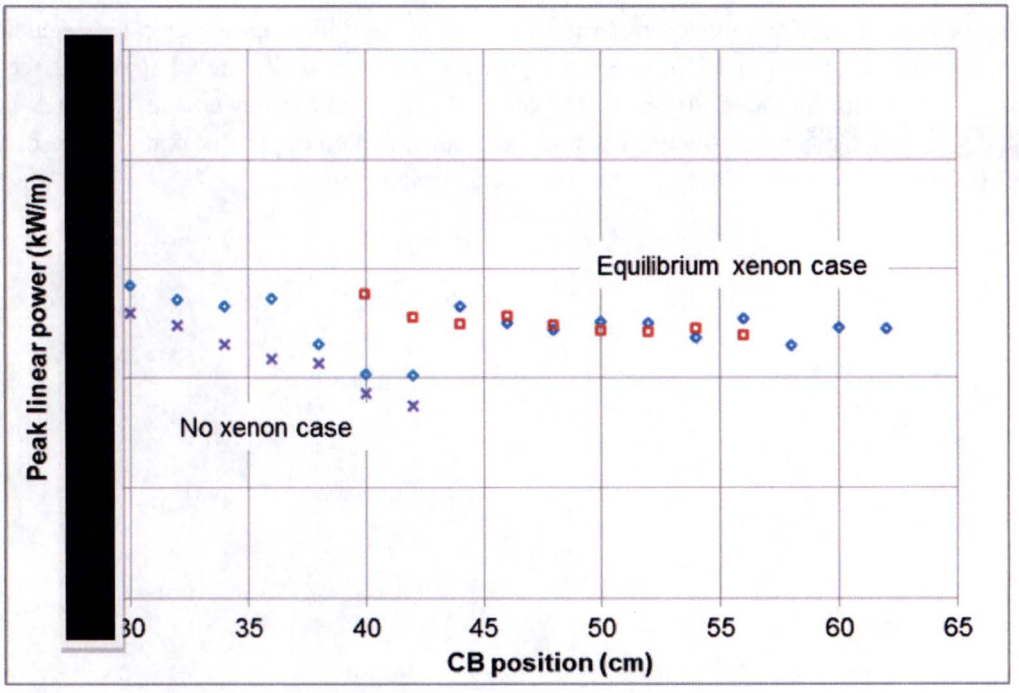

5a, d, e, f

Figure 46
Variation of Peak Linear Power vs. Control Blade Position

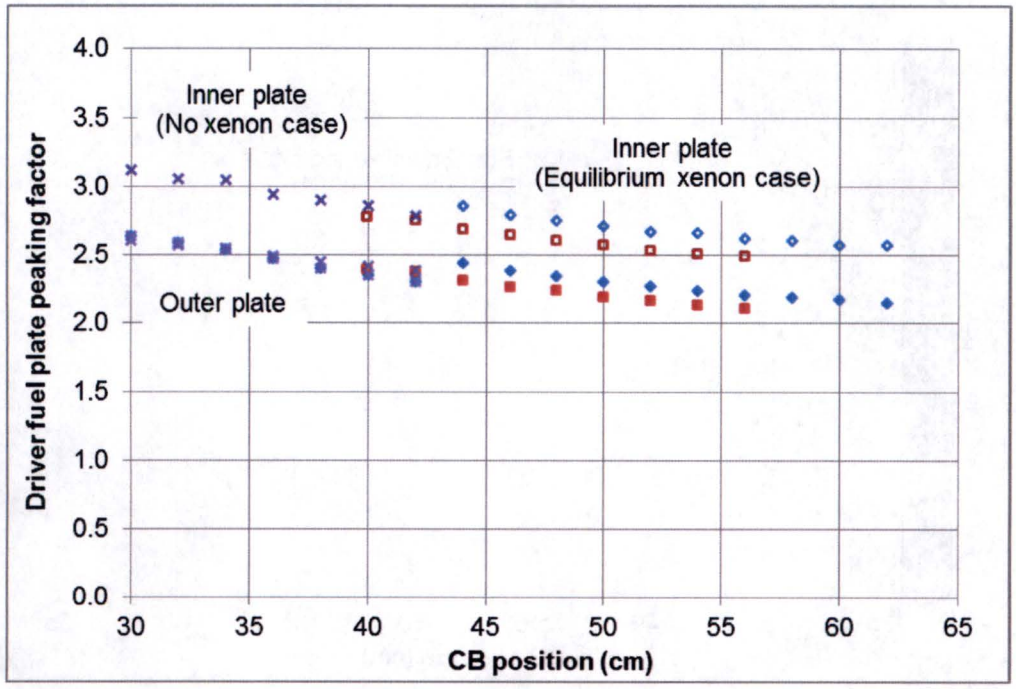

Figure 47
Variation of Driver Fuel Element Peaking Factor vs. Control Blade Position

The effect of regulating blade movement was assessed for the critical core. Two (2) regulating blade positions, i.e. low (25.4 cm) and high (38.1 cm), were considered while the CBs were at their critical positions. The results in Table 20 show that the pellet peak linear power and total TA power are [redacted], respectively. The maximum inner and outer plate peaking factors of the driver fuel are 3.043 and 2.576, respectively, for the minimum burnup core.

5a, d, e, f

Table 20
Effect of Regulating Blade on Pellet Peak Linear Power and Target Assembly Power

Core State	Regulating Blade (cm)	Target Power (kW)	Peak Linear Power (kW/m)	Inner Plate Peaking	Outer Plate Peaking
Maximum burnup with equilibrium xenon	38.1	[redacted]	[redacted]	2.637	2.218
	31.75	[redacted]	[redacted]	2.641	2.147
	25.4	[redacted]	[redacted]	2.638	2.046
Average burnup with equilibrium xenon	38.1	[redacted]	[redacted]	2.511	2.155
	31.75	[redacted]	[redacted]	2.542	2.093
	25.4	[redacted]	[redacted]	2.528	1.973
Minimum burnup without xenon	38.1	[redacted]	[redacted]	3.037	2.576
	31.75	[redacted]	[redacted]	3.043	2.563
	25.4	[redacted]	[redacted]	3.031	2.565
Extreme burnup without xenon	38.1	[redacted]	[redacted]	2.988	2.531
	31.75	[redacted]	[redacted]	2.999	2.507
	25.4	[redacted]	[redacted]	2.976	2.397

5a, b, e, f

5.3.3 Uncertainties

The neutronics analysis has an inherent uncertainty due to the solution method employed in the MCNP6 code. The standard deviation (1σ) of the pellet power is [redacted] for almost all the pellet numerical nodes when 100 million particles are used for the calculation. For the total target power, the standard deviation (1σ) is as small as [redacted]. Other uncertainties considered are impurities of constituent materials, pellet density, fissile content and target rod position due to manufacturing tolerance. Table 21 shows impurities of of the target pellet, cladding, cartridge and neutron shield. For the aluminum (cartridge) and stainles steel (neutron shield), the impurity was assumed to be 10 part per million (ppm) natural boron.

5a, b, e, f

Table 21
Material Impurities for Uncertainty Analysis

	Uranium (wt%)	Zircaloy-4 (wt%)	Aluminum (ppm)	Stainless Steel (ppm)
^{232}U	2×10^{-7}	N/A	N/A	N/A
^{234}U	0.26	N/A	N/A	N/A
^{236}U	0.46	N/A	N/A	N/A
Boron	3 ppm	0.00005	10	10

The uncertainties of the peak linear power and total target power were estimated for the four (4) critical cores. In order to estimate the sensitivity of the core and target performance parameters, the uncertainties of design parameters were defined as follows:

- For the statistical uncertainty of the solution method, ±2σ value is used to estimate the eigenvalue, total target power and peak linear power with a 95% confidence level.
- The impurity always reduces the target power and is regarded as a bias. The uncertainty is estimated as 95% of the performance parameter change due to the maximum impurity level of the target uranium, assuming a flat distribution of impurity between its minimum and maximum values.
- The manufacturing tolerances of the pellet density and fissile content are [redacted] and [redacted] wt%, respetively. The target performance is relatively insensitive to the variation of these parameters. For conservatism, the tolerance value is taken as the uncertainty. In this simulation, only a positive value is used as a bias to estimate the power increases. 5a, b, e, f
- The uncertainty of the target rod position is [redacted], which is 2/3 of the manufacturing/ installation tolerance [redacted], i.e. approximately a 2σ value when a triangular distribution is assumed between the minimum and maximum values with the mode (average) at 0. The [redacted] means that the rod is closer to the core by [redacted]. Though the target rod could be either closer to or farther from the core, [redacted] is used as a bias to estimate the power increase of the target. 5a, b, e, f

The estimated uncertainties (positive components) of the core eigenvalue, peak linear power and total target power due to the statistical and manufacturing uncertainties are summarized in Table 22, Table 23, and Table 24, respectively. The impact of the pellet fabrication density and fissile content uncertainty on the core eigenvalue and target peak linear power is very small, which makes it difficult to obtain consistent results by direct perturbation calculations. Therefore, large manufacturing uncertainties [redacted] were used for the direct calculation and the results were linearly interpolated. 5a, b, e, f

The uncertainty (positive variation) of the eigenvalue due to manufacturing tolerances (pellet density and fissile content) is estimated to be less than 11 per cent mille (pcm). The impact of target rod position uncertainty mostly dominates the total uncertainty for all core states.

For the peak linear power, the statistical uncertainty prevails over uncertainties of the pellet density and fissile content, while it is comparable to the target rod position uncertainty. Arithmetic summation of these uncertainties, excluding the impurity effect, results in a total uncertainty of [redacted] for the peak linear power in the extreme burnup core, which is very conservative. Specifically, for the extreme burnup core, the uncertainty due to the most dominant contributor, i.e. rod position uncertainty, is [redacted], which is [redacted] of the peak linear power. 5a, b, e, f

For the total target power, the statistical uncertainty is relatively small, while the target rod position uncertainty dominates the total uncertainty. The estimated maximum increase of target power due to uncertainties associated with manufacturing tolerances (pellet density and enrichment) is [redacted] (for the 5a, b, e, f

maximum burnup core), which is 1.1% of the total power. The effect of target rod position uncertainty is 1.5% of the total target power for the maximum burnup core.

- The total uncertainties of the key performance parameters were estimated as a product of statistical error and root-mean-square (RMS) of uncertainties due to fabrication density, enrichment, and target rod position. Here, the uncertainty due to impurity is neglected for conservatism. For the limiting core configurations, the total uncertainty (excluding the impurity effect) is applied to the target design power such as:

$$P=P_0(1+\sigma_s)\left(1+\sqrt{\sigma_d^2+\sigma_e^2+\sigma_p^2}\right)$$

where P and P_0 are power with and without uncertainty, respectively. Subscripts s, d, e, and p refer to the uncertainties due to statistical, density, enrichment, and position, respectively.

- For the eigenvalue, the estimated uncertainty is [redacted] for the maximum burnup core.
- For the total target power, the estimated uncertainty is [redacted] for the maximum burnup core. The estimated upper bound for the total target fission power is then [redacted] when considering uncertainties (cf. 549.8 kW without uncertainty). 5a, b, e, f
- For the peak linear power, the estimated uncertainty is [redacted] for the extreme burnup core. The estimated upper bound for the peak linear power is then [redacted] when considering uncertainties (cf. 54.2 kW/m without uncertainty).

Table 22
Uncertainties in Core Eigenvalue (Bias)

Core Burnup State	Statistical Uncertainty (pcm)	Impurity (pcm)	Fabrication Density (pcm)	Fissile Content (pcm)	Target Rod Position (pcm)
Maximum with equilibrium xenon	[redacted]	[redacted]	[redacted]	[redacted]	[redacted]
Average with equilibrium xenon	[redacted]	[redacted]	[redacted]	[redacted]	[redacted]
Minimum without xenon	[redacted]	[redacted]	[redacted]	[redacted]	[redacted]
Extreme without xenon	[redacted]	[redacted]	[redacted]	[redacted]	[redacted]

5a, b, e, f

Table 23
Uncertainties in Peak Linear Power (Bias)

Core Burnup State	Statistical Uncertainty (%)	Impurity (%)	Fabrication Density (%)	Fissile Content (%)	Target Rod Position (%)
Maximum with equilibrium xenon	[redacted]	[redacted]	[redacted]	[redacted]	[redacted]
Average with equilibrium xenon	[redacted]	[redacted]	[redacted]	[redacted]	[redacted]
Minimum without xenon	[redacted]	[redacted]	[redacted]	[redacted]	[redacted]
Extreme without xenon	[redacted]	[redacted]	[redacted]	[redacted]	[redacted]

5a, b, e, f

Table 24
Uncertainties in Target Power (Bias)

Core Burnup State	Statistical Uncertainty (%)	Impurity (%)	Fabrication Density (%)	Fissile Content (%)	Target Rod Position (%)
Maximum with equilibrium xenon	[redacted]	[redacted]	[redacted]	[redacted]	[redacted]
Average with equilibrium xenon	[redacted]	[redacted]	[redacted]	[redacted]	[redacted]
Minimum without xenon	[redacted]	[redacted]	[redacted]	[redacted]	[redacted]
Extreme without xenon	[redacted]	[redacted]	[redacted]	[redacted]	[redacted]

5a, b, e, f

5.3.4 Nominal Operating Cycle (Staggered Loading Pattern)

The nominal operating cycle will load and remove 11 target rods per week for processing. In a nominal operating cycle, one (1) fresh TA (11 rods) is loaded in one graphite reflector position (No. 5A or No. 5B) and is irradiated for 2 weeks (152-hour irradiation + 16-hour shutdown + 152-hour irradiation as a nominal operating condition). However, after a 1-week operation, a second TA is loaded in the other reflector position. Therefore, both reflector positions are fully occupied during nominal operation with target rods. The difference between nominal operations and operations with all fresh targets is the burnup states of TAs: a fresh TA is in one reflector position and 1-week-burned TA is in the other reflector

position (i.e. staggered loading pattern). Therefore, it is expected that the TA power and the impact on the MURR driver fuel elements of the nominal, or staggered, loadings are always less severe when compared with the fresh target rod loading case.

Figure 48 and Figure 49 show 4-group axial neutron flux distributions of the target rods 6 and 17, respectively, when a fresh TA is loaded in reflector position No. 5A of the reference and extreme burnup core. The axial flux shape of the staggered target loading is almost the same as that of the fresh target loading. Figure 50 shows the azimuthal flux variation on the axial middle plane, which shows a slight decrease of neutron flux level in position No. 5B.

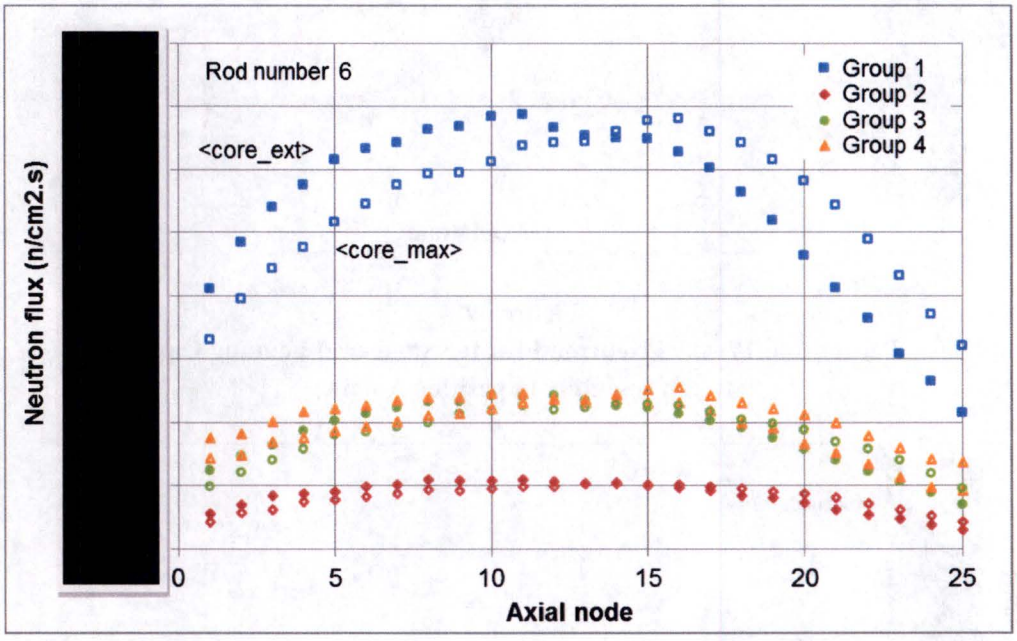

5a, d, e, f

Figure 48
Target Rod 6 Axial Neutron Flux for Staggered Loading Case
(fresh assembly in position No. 5A)

For the nominal loading with a fresh TA in position No. 5B (a 1-week-burned assembly is in position No. 5A), the 4-group axial neutron flux distributions of target rods 6 and 17 are shown in Figure 51 and Figure 52, respectively. The azimuthal fluxes are shown in Figure 53.

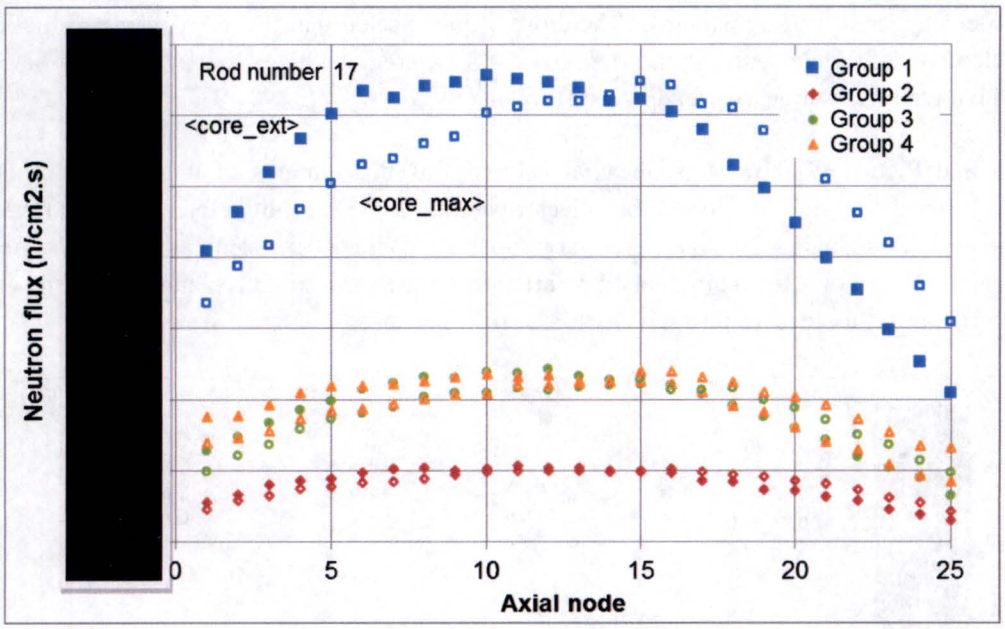

5a, d, e, f

Figure 49
Target Rod 17 Axial Neutron Flux for Staggered Loading Case
(fresh assembly in position No. 5A)

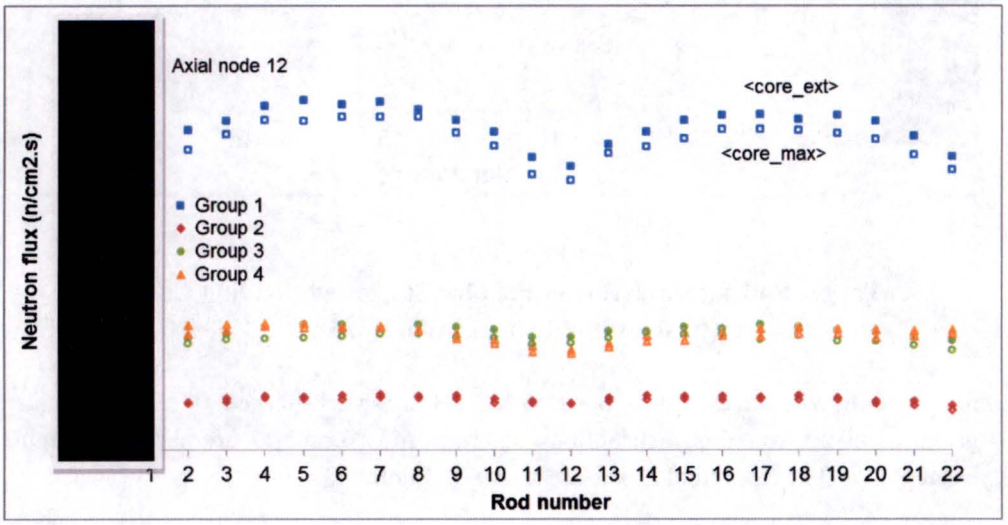

5a, d, e, f

Figure 50
Target Assembly Azimuthal Neutron Flux for Staggered Loading Case
(fresh assembly in position No. 5A)

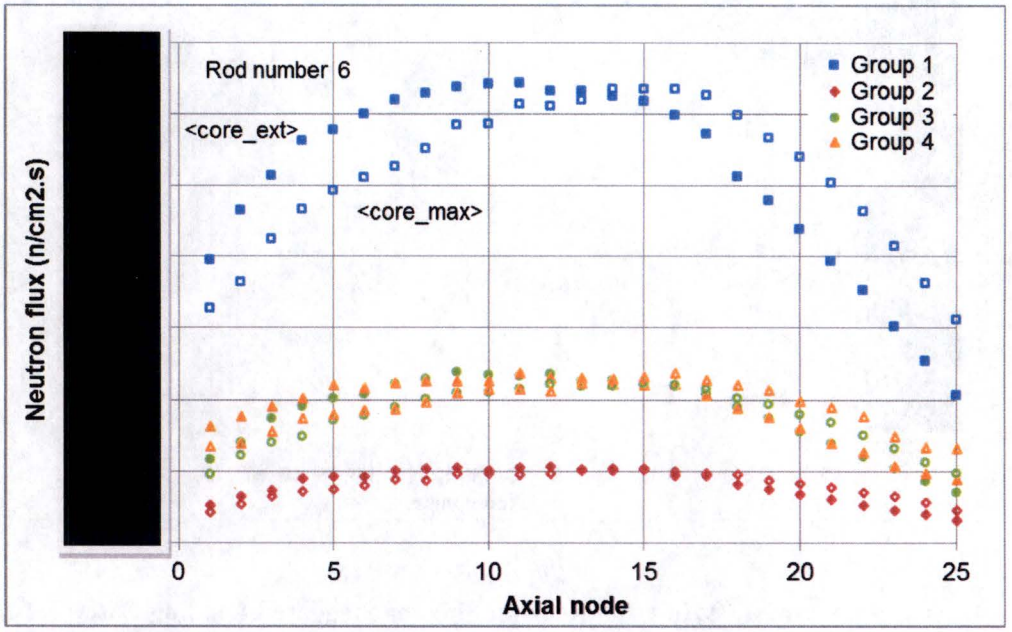

5a, d, e, f

Figure 51
Target Rod 6 Axial Neutron Flux for Staggered Loading Case
(fresh assembly in position No. 5B)

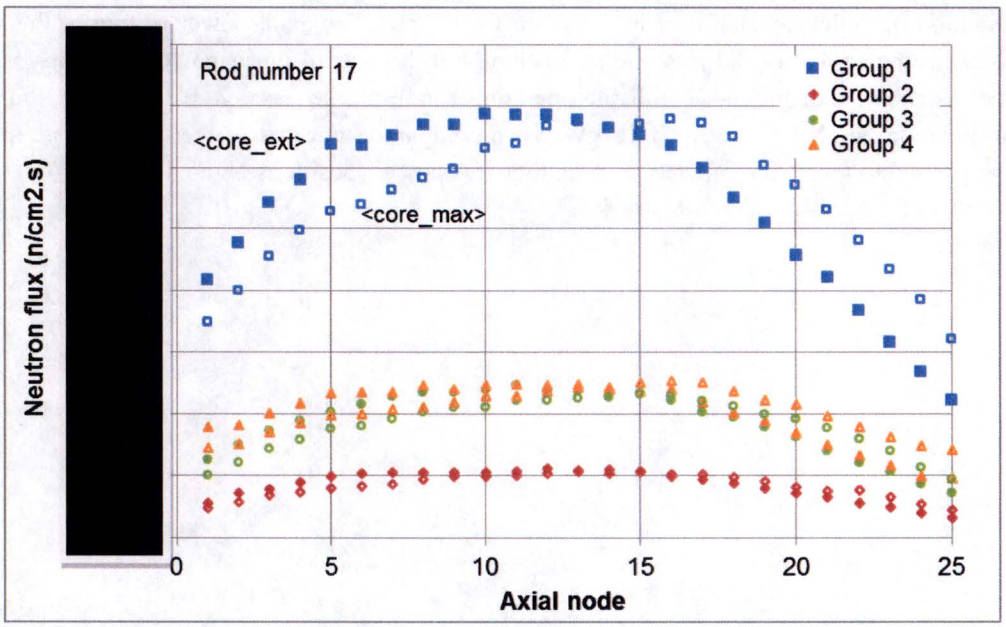

5a, d, e, f

Figure 52
Target Rod 17 Axial Neutron Flux for Staggered Loading Case
(fresh assembly in position No. 5B)

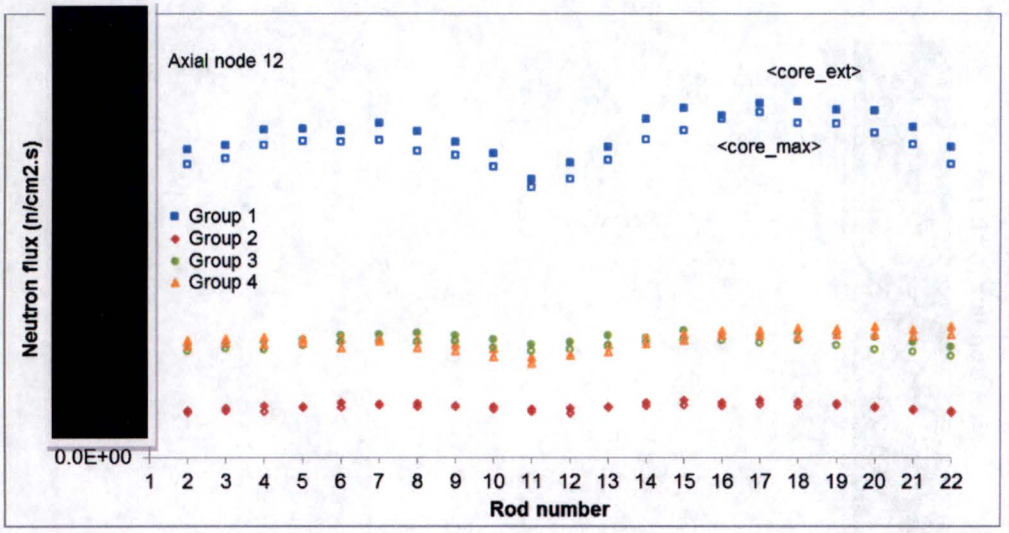

5a, d, e, f

Figure 53
Target Assembly Azimuthal Neutron Flux for Staggered Loading Case
(fresh assembly in position No. 5B)

TA power and rod linear power of the staggered TA loading is summarized in Table 25 when the fresh assembly is in graphite reflector position No. 5A. The pellet linear power envelopes of the staggered loading are shown in Figure 54 and Figure 55 for the extreme and maximum burnup core, respectively. The distribution of pellet linear power is shown in Figure 56. The axial power profile of the staggered loading is the same as that of the fresh target loading, but the overall linear power is slightly reduced in the burned assembly. For the most probable operating condition, i.e. average burnup core, the power of the TA in position No. 5B is lower by 11 kW when compared with that of the TA in position No. 5A, which is attributed to target fuel depletion. The total TA power (positions No. 5A and No. 5B) is slightly lower than that of the fresh TA loading by 4%.

Table 25
Calculated Target Power Level and Pellet Linear Power for the Staggered Loading

Core Burnup State	Target Power	Staggered Loading (fresh target in 5A)	Staggered Loading (fresh target in 5B)
Maximum with equilibrium xenon	Assembly Power (kW)	[redacted]	[redacted]
	Assembly in 5A	[redacted]	[redacted]
	Assembly in 5B	[redacted]	[redacted]
	Peak Linear Power (kW/m)	[redacted]	[redacted]
	Target Rod Number	6	22
	Axial Node	16	19
Average with equilibrium xenon	Assembly Power (kW)	[redacted]	[redacted]
	Assembly in 5A	[redacted]	[redacted]
	Assembly in 5B	[redacted]	[redacted]
	Peak Linear Power (kW/m)	[redacted]	[redacted]
	Target Rod Number	5	22
	Axial Node	16	18
Minimum without xenon	Assembly Power (kW)	[redacted]	[redacted]
	Assembly in 5A	[redacted]	[redacted]
	Assembly in 5B	[redacted]	[redacted]
	Peak Linear Power (kW/m)	[redacted]	[redacted]
	Target Rod Number	6	22
	Axial Node	8	10
Extreme without xenon	Assembly Power (kW)	[redacted]	[redacted]
	Assembly in 5A	[redacted]	[redacted]
	Assembly in 5B	[redacted]	[redacted]
	Peak Linear Power (kW/m)	[redacted]	[redacted]
	Target Rod Number	7	20
	Axial Node	11	12

5a, d, e, f

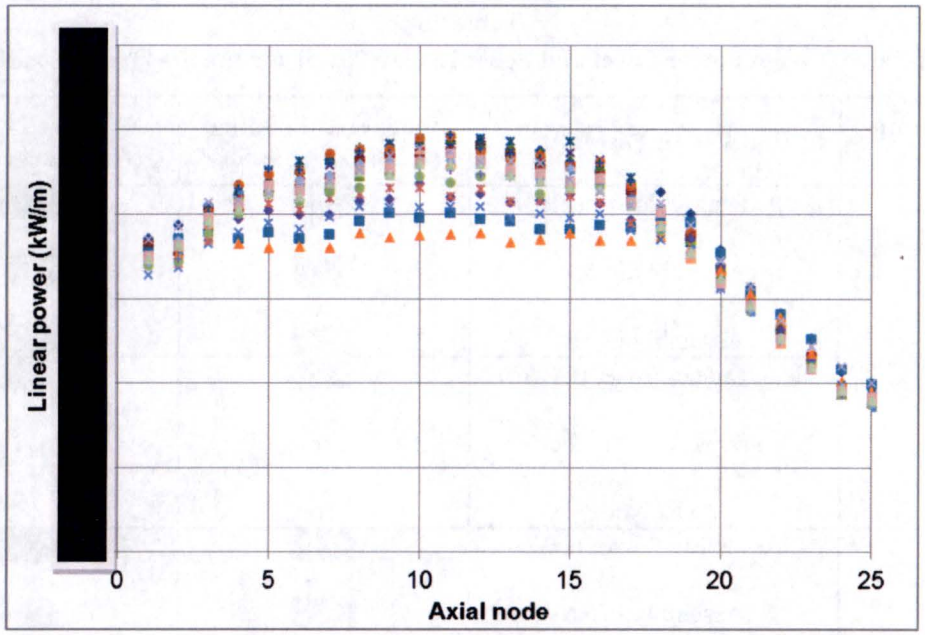

5a, d, e, f

Figure 54
Power Envelope of the Staggered Loading for the Extreme Burnup Core Case (fresh assembly in position No. 5A)

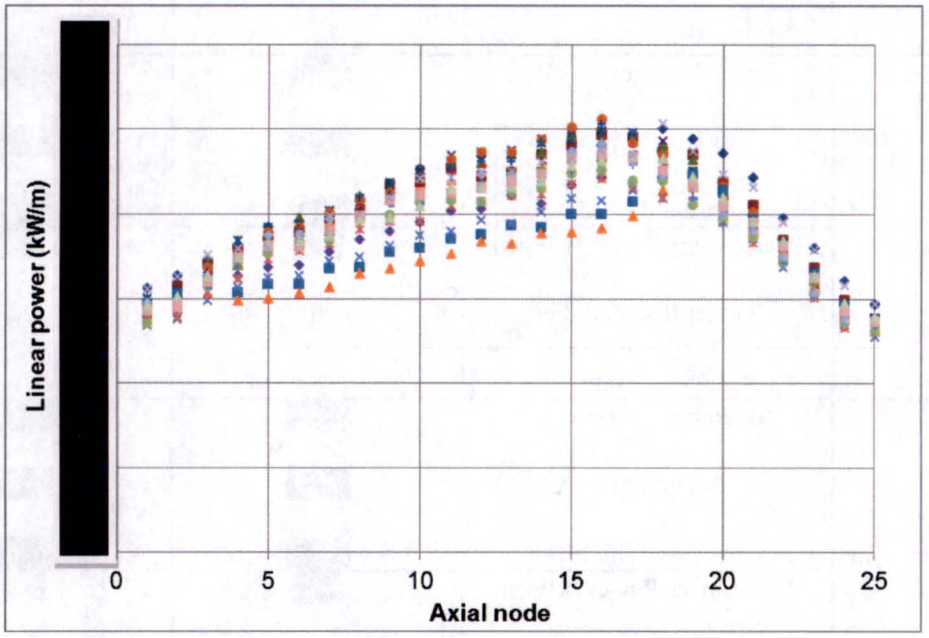

5a, d, e, f

Figure 55
Power Envelope of the Staggered Loading for the Maximum Burnup Core Case (fresh assembly in position No. 5A)

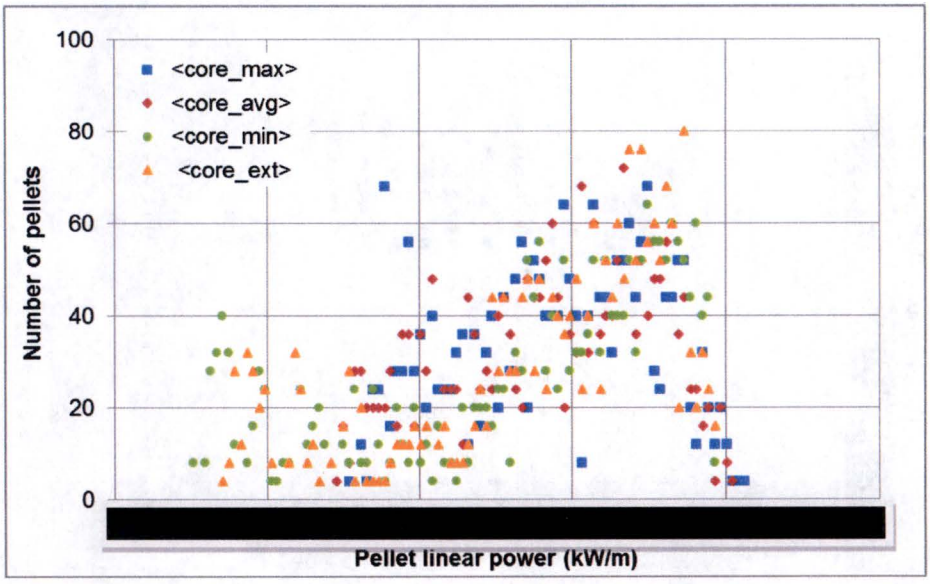

5a, d, e, f

Figure 56
Target Assembly Pellet Linear Power Distribution for the Staggered Loading Case (fresh assembly in position No. 5A)

The pellet linear power envelopes of the staggered loading with a fresh TA in position No. 5B are shown in Figure 57 and Figure 58 for the extreme and maximum burnup core, respectively, and their distribution is plotted in Figure 59. The total TA power of the staggered target loading with fresh target rods in position No. 5A and No. 5B are almost the same. The power from the TA in position No. 5B is higher by 18.6 kW when compared with that from the TA in position No. 5A.

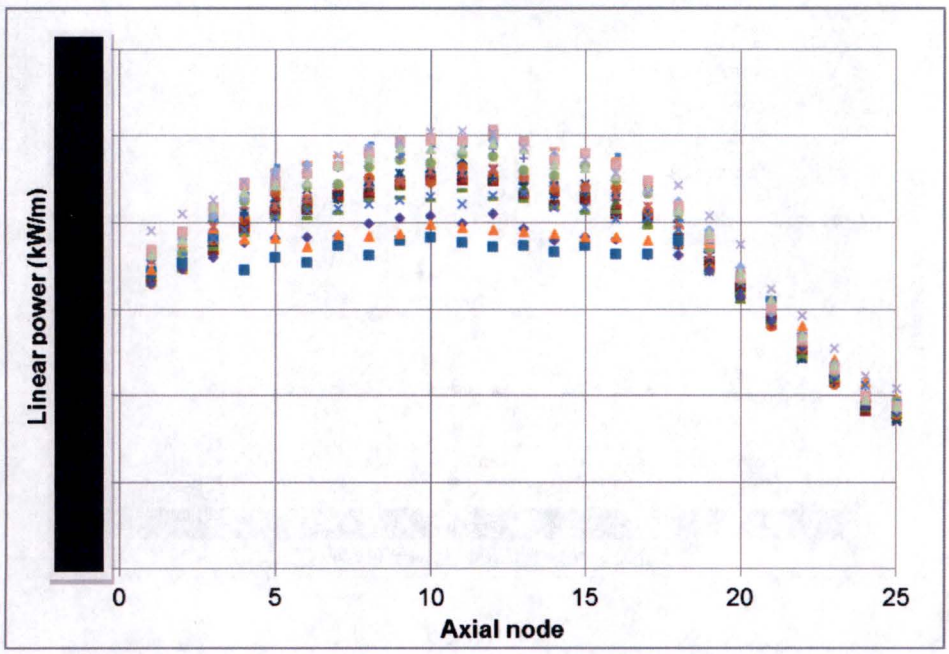

5a, d, e, f

Figure 57
Power Envelope of the Staggered Loading for the Extreme Burnup Core Case (fresh assembly in position No. 5B)

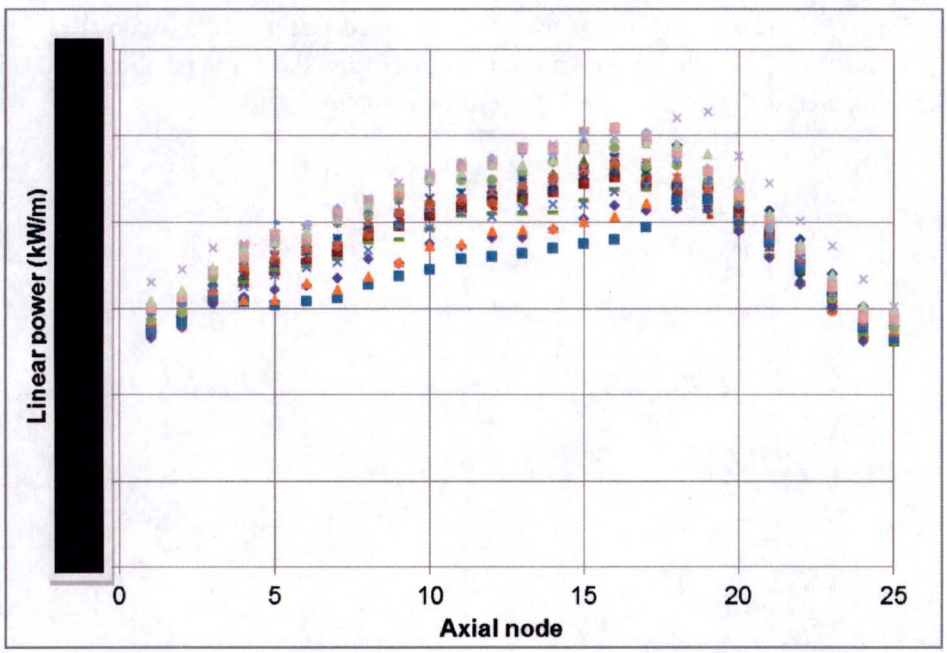

5a, d, e, f

Figure 58
Power Envelope of the Staggered Loading for the Maximum Burnup Core Case (fresh assembly in position No. 5B)

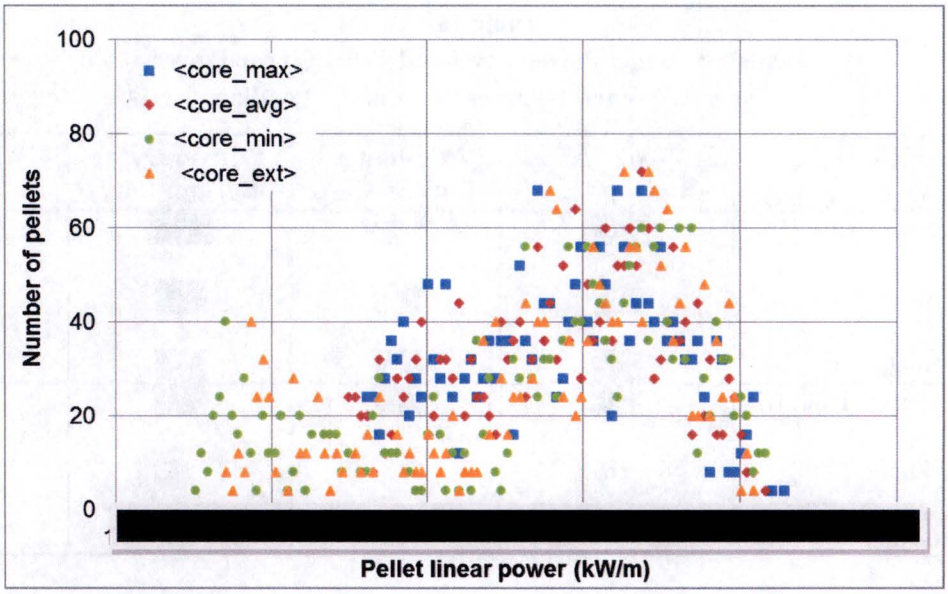

5a, d, e, f

Figure 59
Target Assembly Pellet Linear Power Distribution for the Staggered Loading Case (fresh assembly in position No. 5B)

5.3.5 Target Assembly Flux and Power of Partial Target Assembly Loading

The number of target rods loaded in a TA may be less than 11 during commissioning. For that purpose, the neutron flux and power distribution of the TA were simulated for the case of a 3-target rod loading for each 11-rod cartridge. Target rod positions 5 to 7 and 16 to 18 were selected to maintain the symmetry. Other rods positions are loaded with filler rods to avoid excessive neutron thermalization while maintaining the nominal flow conditions.

The 4-group axial neutron flux distributions of target rods 6 and 17 are shown in Figure 60 and

, respectively. The azimuthal fluxes are shown in Figure 62. TA power and pellet linear power are summarized below in Table 26. The pellet linear power envelopes of the extreme and maximum burnup core are shown in Figure 63 and Figure 64, and their distribution is plotted in Figure 65.

Table 26
Calculated Target Power Level and Pellet Linear Power
for a Reference 3-Target Rod Partial Loading

	Extreme Burnup Core	Minimum Burnup Core	Average Burnup Core	Maximum Burnup Core
Assembly Power (kW)	[redacted]	[redacted]	[redacted]	[redacted]
Assembly in 5A	[redacted]	[redacted]	[redacted]	[redacted]
Assembly in 5B	[redacted]	[redacted]	[redacted]	[redacted]
Peak Linear Power (kW/m)	[redacted]	[redacted]	[redacted]	[redacted]
Rod Number	18	18	18	18
Axial Node	15	10	15	17

5a, d, e, f

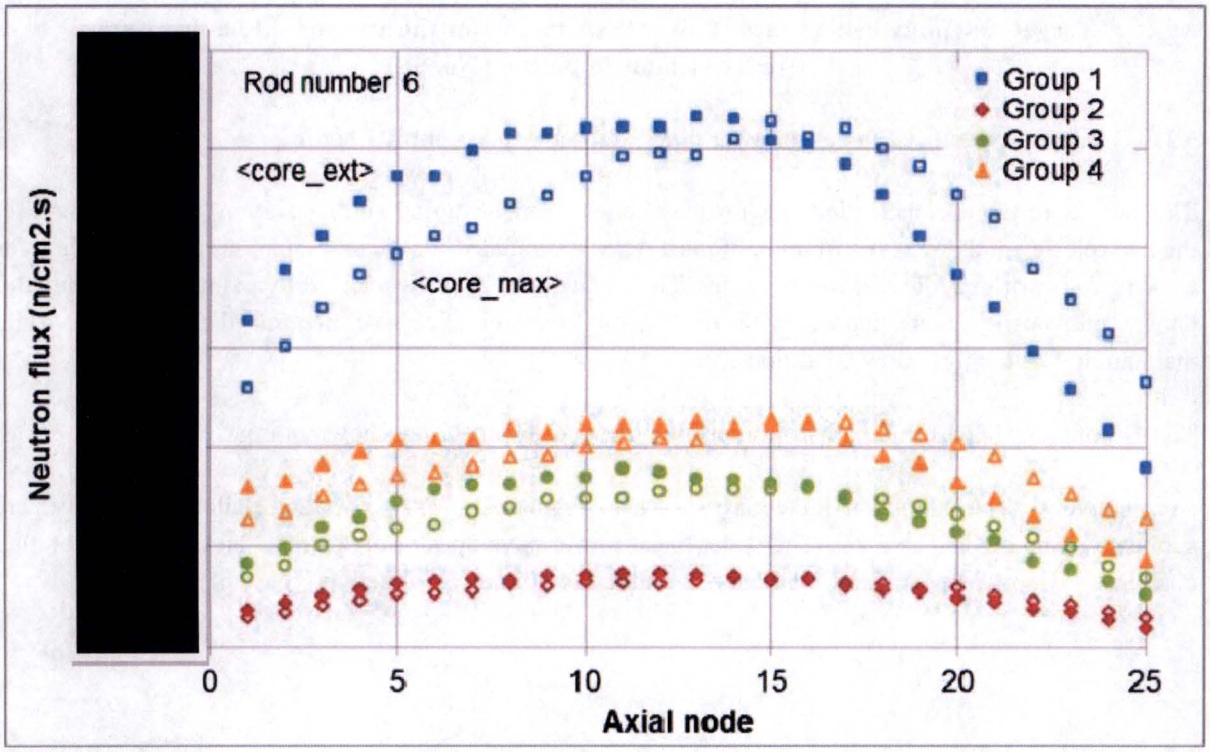

5a, d, e, f

Figure 60
Target Rod 6 Axial Neutron Flux for Partial Loading Case

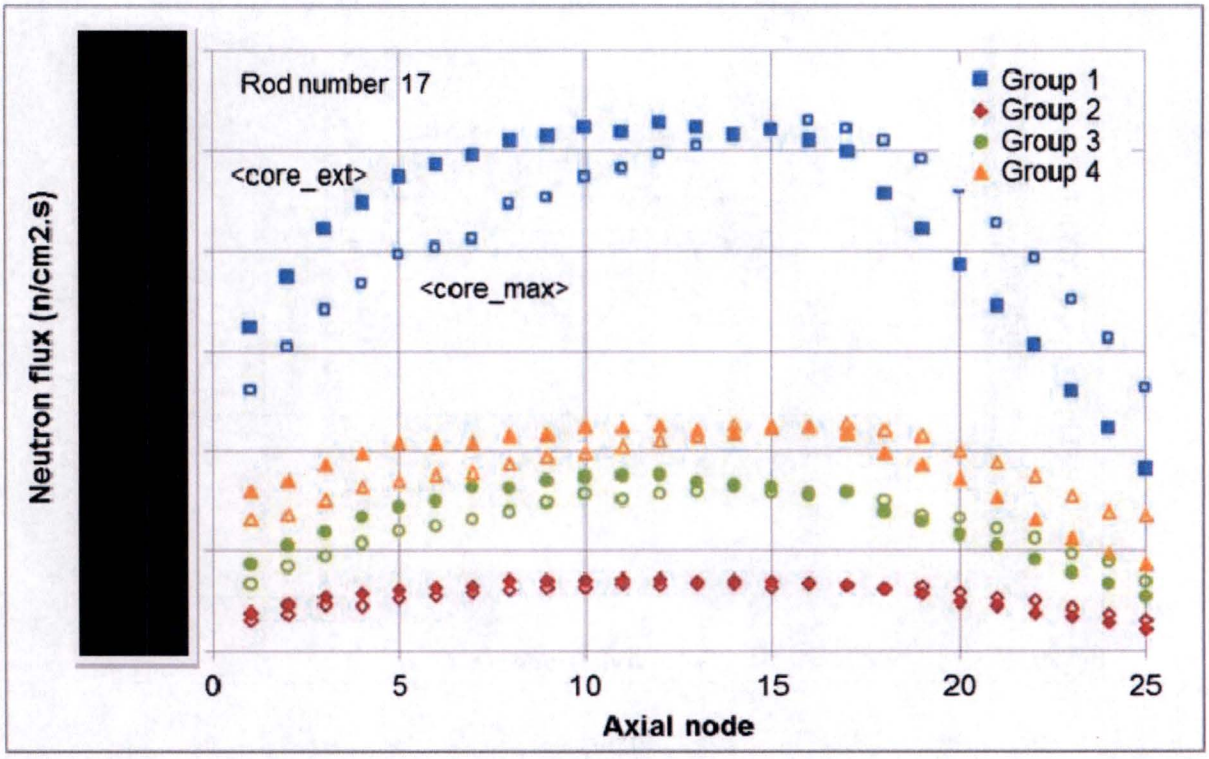

5a, d, e, f

Figure 61
Target Rod 17 Axial Neutron Flux for Partial Loading Case

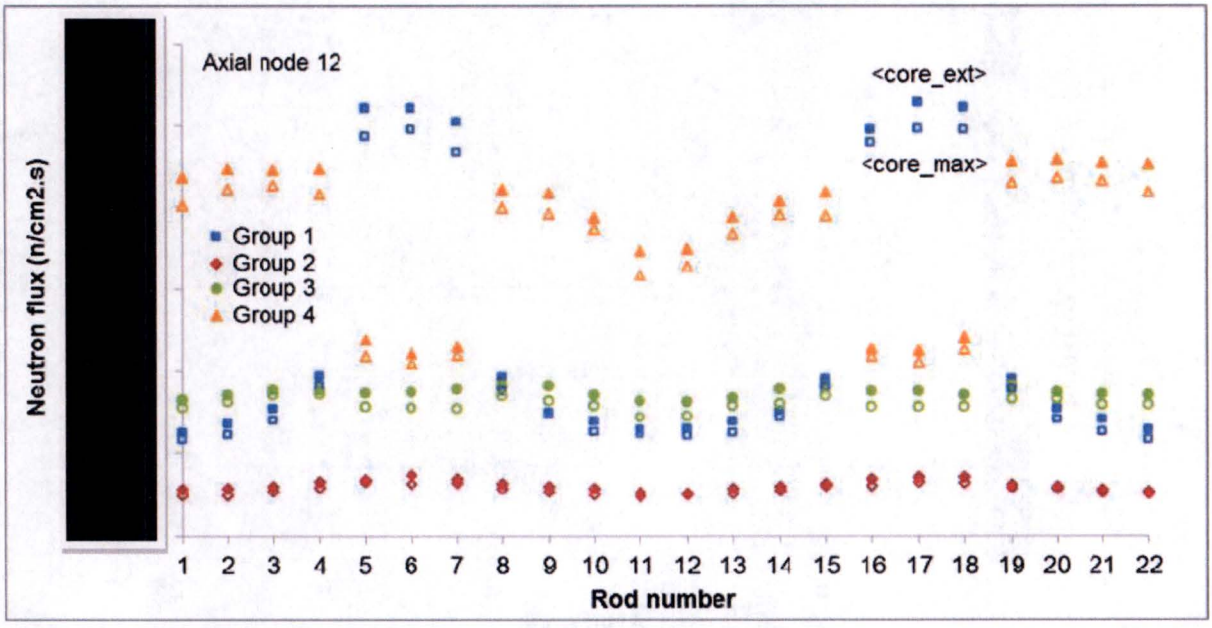

5a, d, e, f

Figure 62
Target Assembly Azimuthal Neutron Flux for Partial Loading Case

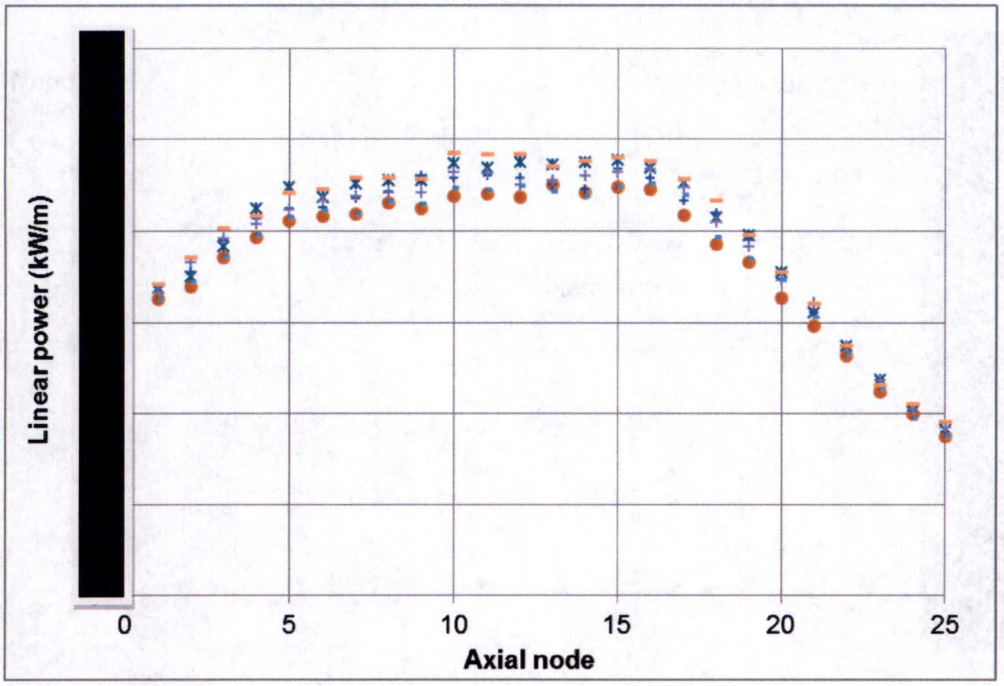

5a, d, e, f

Figure 63
Power Envelope for Partial Loading for the Extreme Burnup Core Case

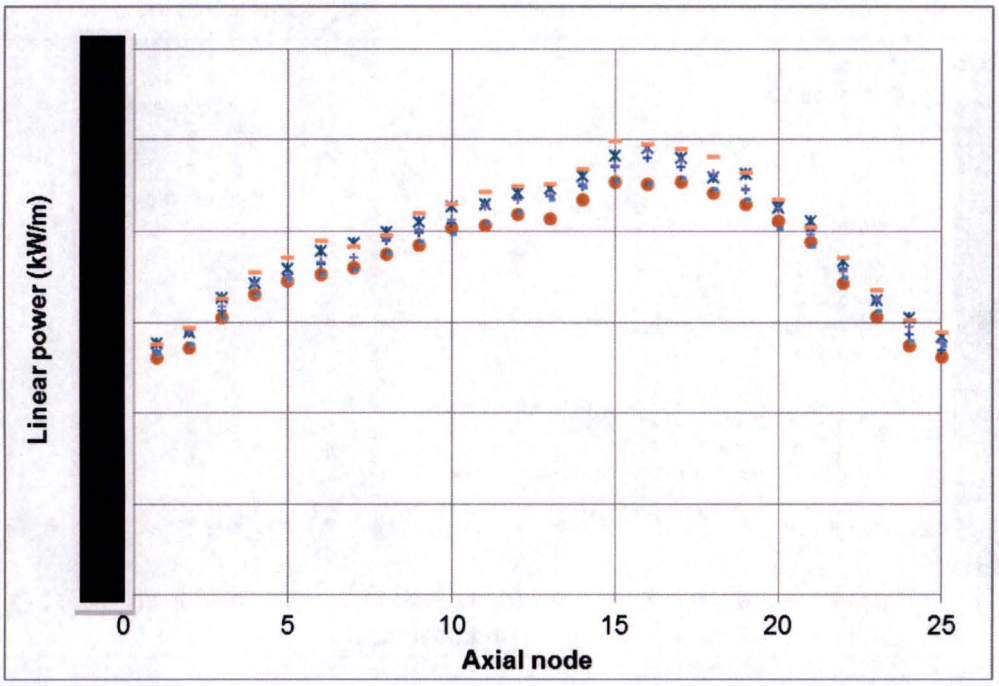

5a, d, e, f

Figure 64
Power Envelope of the Partial Loading for the Maximum Burnup Core Case

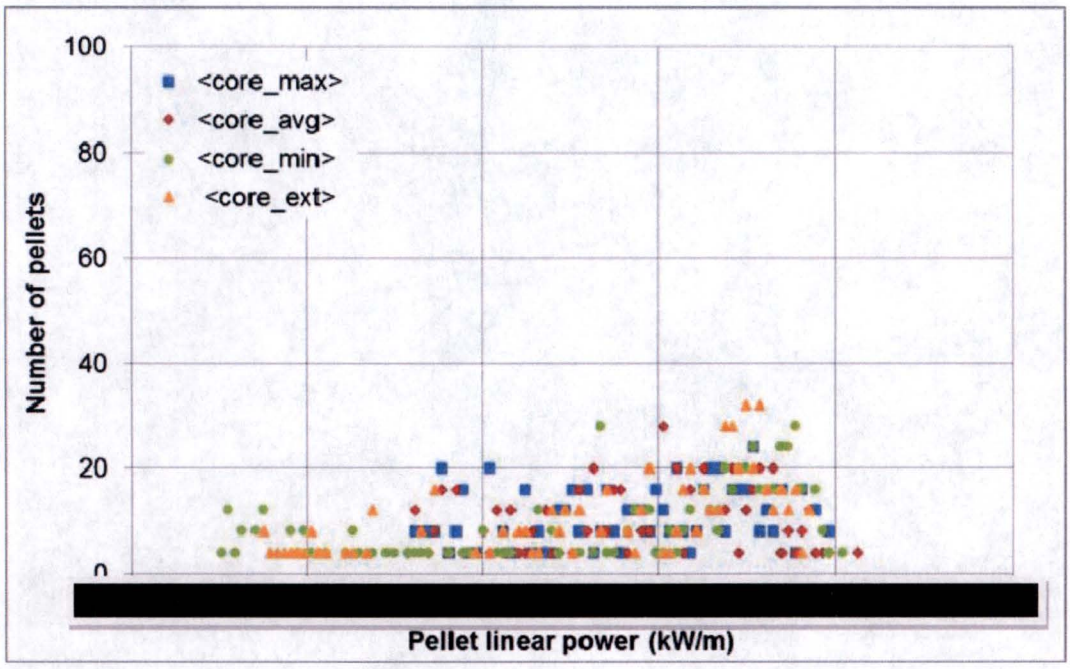

5a, d, e, f

Figure 65
Target Assembly Pellet Linear Power Distribution for Partial Loading Case

5.3.6 Target Assembly Material Depletion

As the fissile material burns in the target rods from irradiation by the incident neutron flux from the reactor core, the TA power steadily decreases. Table 27 lists the isotopic mass of two (2) TAs for the average burnup core, which is the most likely core state.

As the fissile uranium depletes, the TA power also decreases linearly as shown in Figure 66. At the end of a 2-week irradiation, the TA power drops to [redacted], which corresponds to a 1.7% reduction when compared to the initial power of [redacted] for the commercial loading. The target pellet burnup is [redacted] Megawatt day per ton heavy metal (MWd/tHM).

5a, d, e, f

Table 27
Material Content and Burnup of the Base Target Loading for Average Burnup Core State

Calendar Day	Operation	Burnup (MWd/tHM)	^{235}U (grams)	^{238}U (grams)	^{239}Pu (grams)
[redacted]	[redacted]	[redacted]	461	1,874	0
[redacted]	[redacted]	[redacted]	457	1,874	0.21
[redacted]	[redacted]	[redacted]	457	1,874	0.21
[redacted]	[redacted]	[redacted]	453	1,874	0.42

5a, d, e, f

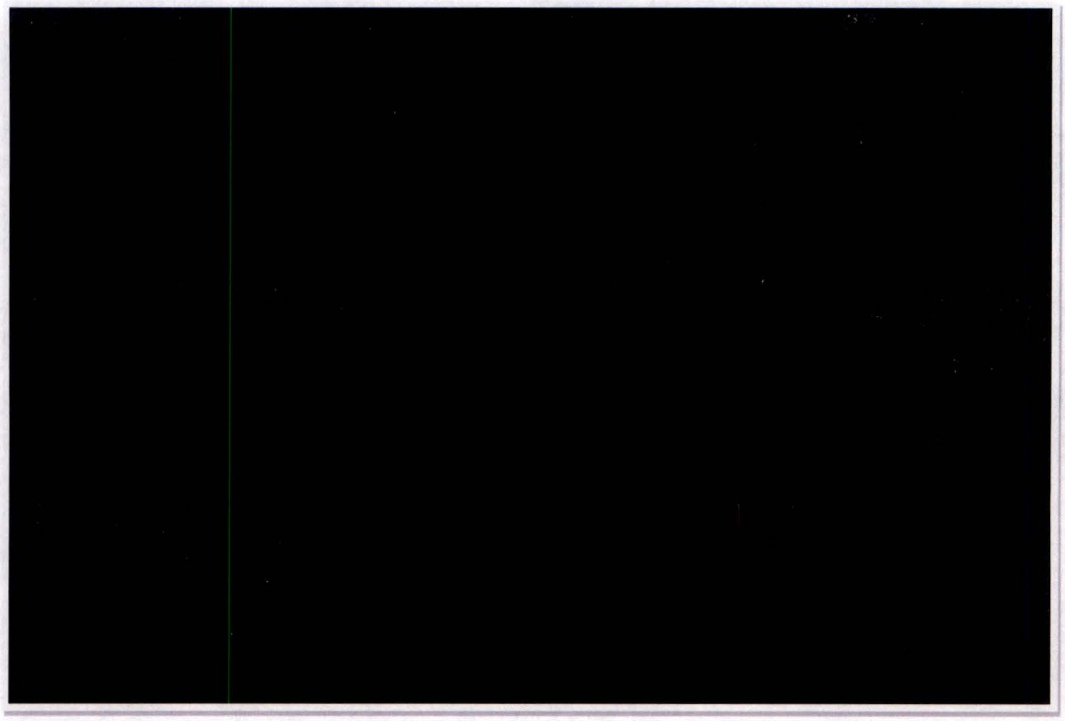

5a, d, e, f

Figure 66
Change of 2-Target Assembly Power for [redacted] Operation

5.3.7 Summary of Target Assembly Nuclear Design Evaluation

The nuclear performance of the TA has been evaluated using a single target pellet enrichment of 19.75 wt% and an 11-rod target loading per cartridge housed in the TA. The evaluation results of the baseline TA model are as follows:

- Two stand-alone target cartridges together are sufficiently subcritical, with a K_{eff} below 0.659.
- The MURR driver fuel element power peaking factor is less than 3.27 when two (2) fresh TAs are loaded.
- The variation of target pellet linear power and total TA power due to CB movement is small. For the equilibrium core conditions, the peak linear power and total TA power change from [redacted] to [redacted] (~4.4%) and from [redacted] (~5.7%), respectively, when the CBs travel from position 46 cm (18.11 in) to 62 cm (24.41 in). 5a, d, e, f

[redacted]The uncertainty due to pellet fabrication does not exceed 0.0001 Δk/k due to either [redacted] 5a, d, e, f

- The uncertainty due to mechanical tolerance of the target rod loading [redacted] is [redacted] and [redacted] for the peak linear power of the extreme burnup core and total target power of the maximum burnup core, respectively.

- The peak linear power and total target power for operations with the staggered target loading or partially loaded target cartridges are less than those of the full fresh loading of target rods in the cartridge.

Nuclear compatibility of the target cartridges and assembly with the MURR core has been assessed based on applicable MURR Technical Specifications. In general, because the thermal power from the two TAs is relatively small (~5.5% of the nominal MURR core thermal power) and the target rods are loaded in the graphite reflector region outside the Be reflector, the effect of target rods on the core reactivity characteristics is small as summarized below for representative core burnup states with the base target loading:

- The least negative reactor core temperature coefficient of reactivity is -1.69×10^{-4} Δk/k/°C, which is more negative than Technical Specification 5.3.a value of -1.08×10^{-4} Δk/k/°C (-6.0×10^{-5} Δk/k/°F). The primary coolant temperature range in this calculation was from 20.44 °C (68.79 °F) to 76.84 °C (170.31 °F).
- The reactor core void coefficient of reactivity is -3.4×10^{-3} Δk/k/%void, which is more negative than Technical Specification 5.3.b value of -2.0×10^{-3} Δk/k/%. The primary coolant density in the calculation was changed from 100% nominal to 0.1%.
- The highest regulating blade reactivity worth is 4.02×10^{-3} Δk/k, which is less than Technical Specification 5.3.d limit of 6.0×10^{-3} Δk/k.
- The lowest subcriticality margin of the core with the most reactive shim blade and regulating blade fully withdrawn is 0.055 Δk/k, which is greater than Technical Specification 3.1.e value of 0.02 Δk/k.
- The excess reactivity of the cold, clean minimum burnup core with cold, fresh, base TA loading is 0.072 Δk/k, which is less than Technical Specification 3.1.a value of 0.098 Δk/k referenced to the cold, clean critical core.
- A single target cartridge insertion into the MURR graphite reflector regions adds 0.31% Δk/k to the MURR core, which is lower than allowed reactivity worth of each secured removable experiment, 0.6% Δk/k (Technical Specification: 3.1.a).

6. Target Assembly Thermal Hydraulic Design Analysis

This section provides information that demonstrates that adequate cooling capacity is available to keep the TA in a thermally safe condition during all operational states. The TCS design is described in detail in Section 3.

For 10 MW_t reactor power, the peak linear power, including margin for uncertainties, is [redacted], which corresponds to a local target cartridge power density of [redacted]. The target rod with this power density is located in the middle of the cartridge, and has an average power density of [redacted]. The two (2) TAs generate [redacted] for the conditions that yield the highest peak linear power. 5a, d, e, f

The highest total power target rod is located at the edge of the cartridge. It has a peak linear power, including margins for uncertainty, of [redacted], and an average power density of [redacted] with a local maximum of [redacted]. The two (2) TAs generate [redacted] for the conditions that yield the maximum fission power. 5a, d, e, f

Both the peak power and the maximum total heat cases were investigated in these analyses to ensure safe operations.

In addition to the power generated in the target rods, [redacted] are produced directly in the cartridge itself (Table 17). This heat is also absorbed by the target cartridge rod cooling water and removed by the TCS. 5a, d, e, f

The maximum local target rod powers ([redacted] at peak linear power and [redacted] at maximum power) are used to determine the local peak temperatures and heat fluxes; the cartridge power is used to determine the total coolant heat absorption and hence, flow rate and outlet temperatures. 5a, d, e, f

The pellet with the peak linear heat rate has that peak approximately 30% of the rod length above the coolant entrance, at a point where 35.4% of the target rod heat is generated. The target rod with the highest total power has its maximum power pellet approximately 46% of the rod length above the coolant entrance, at a point where 47.9% of the rod heat is generated. Analyses were performed for both target rods at their point of maximum heat generation rate, at the local water temperature and pressure. Margins were added to account for uncertainties in flow rate, pressure drop and temperature measurements.

All analyses were performed assuming one (1) day of burnup ([redacted]) which is the burnup experienced for the maximum power density pellet (greater burnup rates increase the relocation of the pellet, with a resultant reduction in the pellet/clad gap, which results in colder UO_2 temperatures). It has no effect on the CHFR. Varying burnup rates were considered in the transient analyses performed on the structure. 5a, d, e, f

Steady-state, one-dimensional, axisymmetric analyses were performed at the location of the maximum UO_2 pellet power density. The effect of reactor power (10 MW_t nominal and 11.5 MW_t maximum), coolant flow rate (100% and 85% of nominal), pellet/cladding gap ([redacted], 50 μm nominal and [redacted]), cartridge channel diameter (14.12 mm minimum, 14.45 mm nominal, and 14.82 mm maximum) and the number of active target rods per cartridge (11 maximum, 3 minimum) were investigated to verify that all system temperatures, as well as the CHFR, were in safe regimes. 5a, d, e, f

6.1 Thermal-Hydraulic Design Basis

6.1.1 Normal Conditions of Operation

The mechanical design, dimensions and tolerances for the target rods are given in Table 3. The nominal (cold) gap between the pellet and the cladding is 50 μm. The minimum/maximum (cold) gap is 36/64 μm, respectively. The pellet/clad gap is filled with helium at 1 atm pressure when cold.

The target rods are placed in a scalloped cartridge which allows "annular" flow axially along the length of the rod. The target rod spacing is 11.63 mm, center to center, and the nominal cartridge flow "full" hole size is 14.45 mm. Thus, on each side of the rod, the "annulus" defining the flow along the target rod shall be open and intersecting the adjacent scallop over an angle of 72.77° for the nominal geometry. This gives a cartridge flow channel with a hydraulic diameter of 10.01 mm. For the minimum channel diameter of 14.12 mm, the hydraulic diameter will be 9.62 mm. For the maximum channel diameter of 14.8 mm, the hydraulic diameter will be 10.02 mm. (Channel diameter variations are the result of manufacturing processes as well as cartridge pressure during operation.)

The target cooling water will flow through the cartridge at a flow rate that will have a nominal heat rise of 10 °C (18 °F). For a cartridge with 11 target rods, a target water mass flow rate of [redacted]) will produce a nominal fluid velocity of 5.20 m/sec as it flows through the section of maximum heat flux. In order to minimize the thermal impact on the reactor pool, the nominal target coolant outlet temperature is set to be the same as the pool water temperature, nominally 102 °F (38.89 °C). Thus, the nominal target cooling water inlet temperature is 28.89 °C (84 °F). The secondary coolant system, which is common to the MURR primary and pool coolant systems and the SGE TCS, will ensure that even on the hottest summer days, the required target inlet temperature is achieved.

5a, d, e, f

6.1.2 Subcooled Nucleate Boiling

For both the peak linear power target rod and the maximum total power rod, the nominal heat flux at the surface of the Zircaloy-4 cladding will be approximately [redacted], which will cause subcooled nucleate boiling at the cladding wall surface. To examine the boiling effects and ensure safe target rod operation, multiple boiling convection models using the ANSYS FLUENT computational fluid dynamics (CFD) computer code were developed (Reference 23). In addition, a literature search was carried out to find relevant experiments to validate the analyses.

5a, d, e, f

The closest case found in the literature is that of Del Valle and Kenning (Reference 24) who studied subcooled nucleate boiling on flat plates under forced convection. For their experiments, they utilized water at 116.7 kPa (16.9 psia), with subcooling between 24 and 84 °C, and coolant velocities between 0.8 and 2.0 m/sec, at heat fluxes up to 4.6 MW/m^2. The 84 °C maximum subcooling in their experiments matches the target system well (82 - 88 °C), while the coolant pressure and velocity are lower. Therefore, their results should be conservative.

Del Valle and Kenning's data show heat flux rising faster than other boiling correlations, such as Jens-Lottes and Chen (Reference 25). The Jens-Lottes correlation, used in the following thermal analysis, is an empirical correlation for fully-developed subcooled nucleate boiling, whereas the Chen model is a broader correlation which combines single phase forced convection and surface boiling effects. The Chen model is used in RELAP5 for nuclear thermal-hydraulic calculations.

Del Valle and Kenning give several important observations from their photographic study of the bubble formation in their experiment. The photographic study was done for the 84 °C subcooling, 1.7 m/s coolant velocity condition. These are summarized below:

- **At high subcooling, the flow remains in a bubbly regime up until burnout.** "All runs at 84 °C subcooling remained in the bubbly flow regime up to burnout, the bubbles retaining their identities except for occasional coalescences leading to small, short-lived vapour patches."
- **The bubbles formed are small.** "The maximum diameters were normally distributed (class interval 0.1 mm) with a mean value of 0.4 mm [redacted] independent of heat flux."
- **The bubbles are short-lived.** "Even at the maximum camera speed [of 10,000 frames per second], individual bubbles appeared in only 3 - 5 frames."

5a, d, e, f

These observations indicate that while bubble nucleation is expected, the bubbles are small and collapse quickly. This agrees with an earlier publication by Unal (Reference 26), who writes, "*The bubbles formed at high subcooling do not leave the heated surface, although they attain their maximum diameter. They slide along the heated surface or collapse, as observed visually by Gunther.*"

Therefore, it is expected that while some subcooled nucleate boiling will occur in the high heat flux regions of the target section, there will be minimal vapor generation, and given the expected bubble lifetime and high subcooling, there will be no vapor present in the coolant exiting the target. The correlations above do not make predictions on vapor formation.

To corroborate the work of Del Valle and Kenning, ANSYS FLUENT CFD models were used to examine the presence of vapor in the target coolant. These models used an Eulerian multiphase model to track the balance of liquid water and vapor throughout the fluid domain of the target housing. The heat transfer at the wall was determined by what is known as the "RPI model," developed at Rensselaer Polytechnic Institute (RPI). The RPI model partitions the heat flux into boiling and convective effects, much like the Chen correlation (Reference 27). The results from these CFD models were in line with the observations of Del Valle and Kenning, in that the presence of vapor was confined to the cladding rod surfaces and that the total amount of vapor generated was very small. The resulting vapor volume fractions at the maximum heat flux rod in the worst case operating conditions are shown in Figure 67. The graph shows that the maximum local vapor volume faction is about 5 parts per million. This is lower than the 100 parts per million shown in Del Valle and Kenning's experiments, although the difference is reasonable given that the coolant pressure and velocity are higher in the target (the latter by nearly a factor of 3). Additionally, the results show that all vapor bubbles collapse outside of the high heat flux region at the rod surface, and water exiting the target housing contains no vapor. Note that the large downward spikes around 0.36 m are due to the presence of a structural support pin, which causes local flow acceleration that depresses the vapor generation.

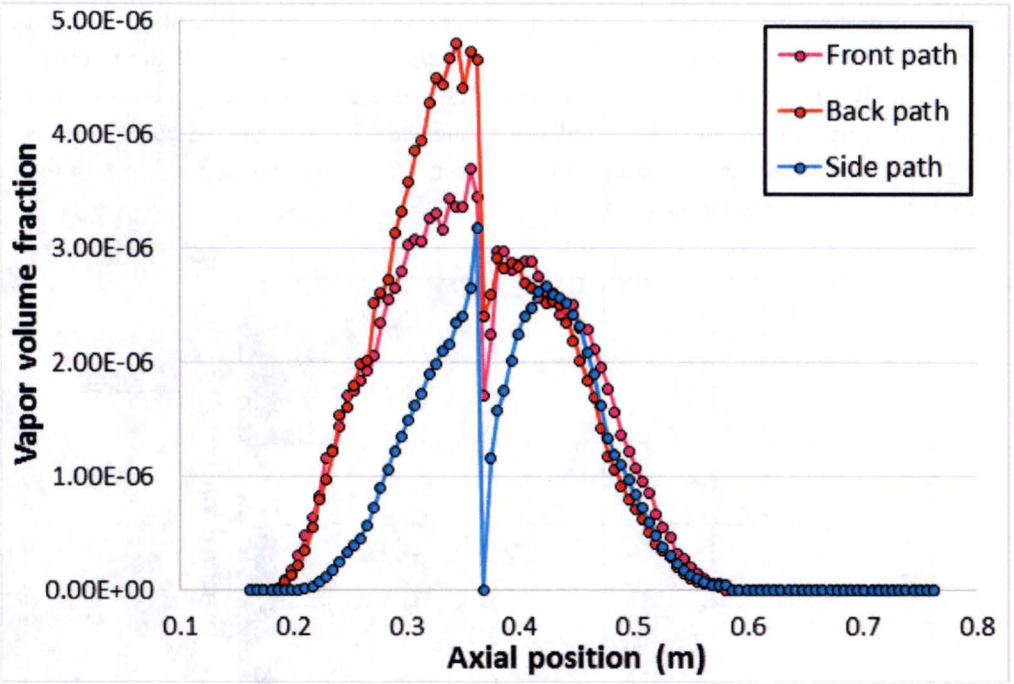

Figure 67
Vapor Fraction at Cladding Wall for Worst-Case Conditions in FLUENT RPI Wall Boiling Model

Both the CFD modelling and Del Valle and Kenning's work give compelling evidence to show that vapor formation in the target is minimal and confined only to the highest heat flux regions of the target rods. To confirm this evidence, experiments are planned to replicate the exact conditions that the target rods will experience in the MURR graphite reflector region, and provide data regarding CHF and subcooled nucleate boiling behavior, which should confirm that two-phase flow is not a concern in the target.

The TA thermal design and analysis ensures that vapor bubbles do not coalesce together forming a vapor film at the cladding surface. This phenomenon occurs when the surface heat flux reaches the CHF value at the transition from nucleate boiling to partial film boiling (Reference 28). Three correlations, Bernath (Reference 29), Macbeth (Reference 30) and Groeneveld (Reference 31) have been used to assure that the target operates in a safe heat transfer regime. The Bernath correlation is very conservative (in predicting low critical heat fluxes) and is an industry-wide standard for such calculations. The Macbeth correlation incorporates data at the low pressures of this system, and it is one of the correlations recognized in the NRC light water reactor fuel rod analysis code FRAPTRAN. The Groeneveld correlation, a lookup table based on the most extensive set of data available, is generally considered the most accurate. All three (3) predictions were found to be in close agreement. The lowest CHF of the three (3) correlations (in every case, Bernath) was used to calculate the CHFR, defined as the CHF divided by the actual heat flux. Recognizing the large amount of scatter and uncertainty in CHF data, a CHFR > 2.0 is required and has been assigned for the design. With a subcooling margin greater than 80 °C, the TA is normally operating at the transition point from convection to nucleate boiling, well below the value of heat flux where transition from nucleate to partial film boiling occurs.

The thermal analysis first calculates the single phase convective heat transfer from the cladding surface. If the surface temperature is higher than that required to initiate subcooled nucleate boiling per the Jens Lottes correlation (Reference 25), then the water at the surface is assumed to be boiling. Its surface temperature is set at the Jens-Lottes suggested value, and the CHFR is calculated. Figure 68 shows the CHFR, heat flux and enthalpy as a function of the axial location in the target rod for both the peak linear power (PLP) rod and the maximum heating (MH) rod.

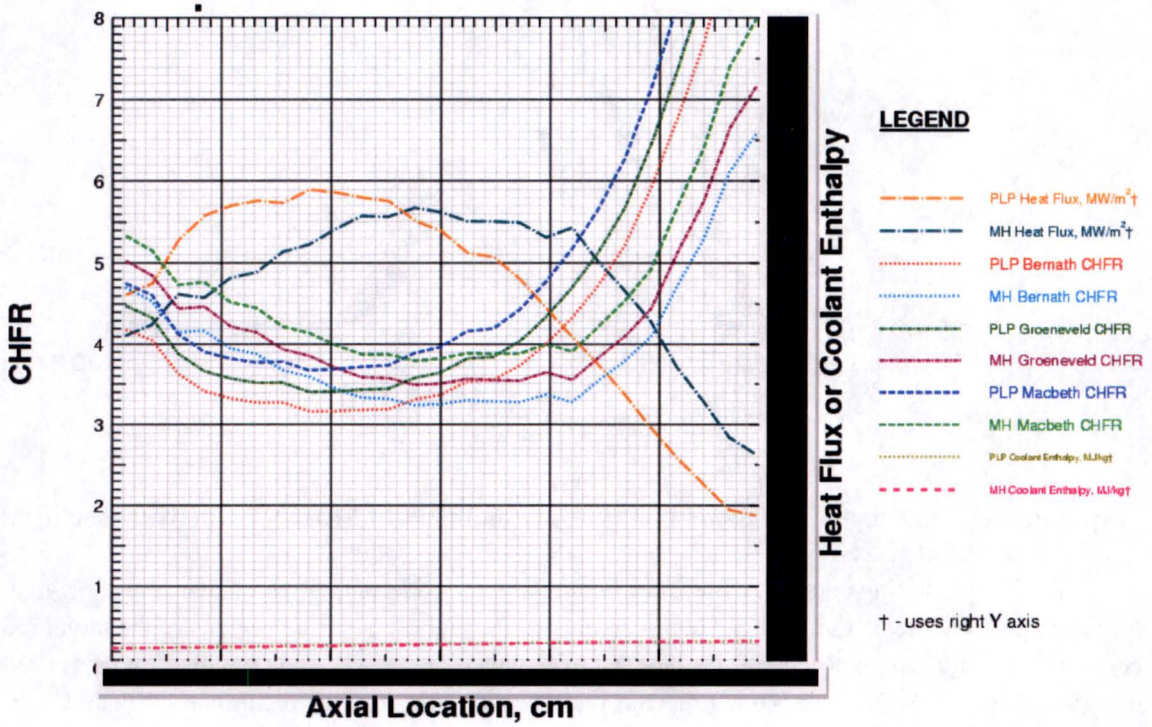

5a, d, e, f

Figure 68
Heat Flux and CHFR as a Function of Axial Location for Peak Power Target Rods

The red dotted line shows the CHFR (Bernath) for the peak linear power target rod. The blue dotted line shows the CHFR (Bernath) for the maximum power rod. In all these analyses, the Bernath CHFR was consistently the most conservative. Although maximum heat flux occurs at different points along the PLP and MH rods, the minimum CHFR is almost the same for both rods. The small temperature rise of the coolant yields an almost constant line for the coolant enthalpy as a function of rod axial location. Thus, the point of the minimum CHFR coincides with the location of the maximum heat flux in the rod.

6.1.3 Design Margins for Uncertainties

In addition to a safety margin of 10% on heat transfer coefficients, several additional margins to account for operating measurement uncertainties were included in these analyses:

1. The pressure drops through the entire TA that were calculated using CFD were *reduced* by 5% for the thermal analyses as this will reduce the water saturation temperature and give a lower predicted CHFR.
2. A control system uncertainty of +2 °C (3.6 °F) was applied to the cooling water inlet temperature. As with the pressure drop reduction, this reduces the predicted CHFR.
3. An uncertainty of -5% was applied to the system flow rate to account for possible errors in measurement – this also reduces the predicted CHFR.

Multiple analyses were performed to investigate the possible variations of operating parameters and geometric tolerances. Each analysis was performed for both the nominal parameters and with the above margins for operating uncertainties. The first set of results represents the most accurate possible engineering solution of the case analyzed. The second set of results represents the worst possible stacking of all the operating uncertainties. The thermal design is required to have a CHFR > 2.0 for the combined application of uncertainties for the worst possible operating condition. A CHFR of 2.0 is a 100% margin by itself.

6.1.4 Target Assembly Steady-State Operations

The water flow rate to the TA has a value of [redacted] and is 10 °C (18 °F) below the pool temperature. It is conservatively assumed that 5% of the flow leaks out at the labyrinthine seal at the junction of the removable cartridge and the target housing. This leakage will be determined by ex-reactor testing on the unit. The target flow rate is therefore [redacted] After flowing through the cartridge, it exits to the reactor pool at a pool depth of 6.85 m (22.5 ft). The absolute pressure at the diffuser exit is 1.66 atm and the pressure of the water at the mid-height of the target (location of maximum heat flux) is approximately 2.15 atm for [redacted] flow. This sets the local water saturation temperature at 123 °C (253.4 °F).

5a, d, e, f

The nominal water inlet and outlet temperatures are 28.89 °C (84 °F) and 38.89° C (102 °F), respectively. This corresponds to a reactor pool temperature of 38.89 °C (102 °F). The 10 °C (18 °F) temperature rise corresponds to 11 UO_2 filled target rods in the cartridge, each dissipating an average of [redacted]. During ramp up to full scale operation, between 1 and 11 UO_2 filled rods will be present in the cartridge, with the balance occupied by non-heat generating filler rods. In order to maintain the TA water outlet temperature equal to the pool temperature, the TA inlet temperature is automatically adjusted so that:

5a, d, e, f

$$T_{out,\,mixed} = T_{POOL} = [n \times (T_{inlet} + 10) + (11\text{-}n) \times T_{inlet}] / 11.\ \text{Hence,}$$

$$T_{inlet} = T_{out,\,mixed} - 10/11 \times n = T_{POOL} - 0.9091 \times n.$$

Table 28 shows the variation in coolant temperatures as the active rod count varies.

Table 28
Variation of Coolant Inlet Temperature with Active Target Rod Count

Active Rods	Non Heating Rods	T_{in} (°C)	T_{in} (°F)	T_{out} (°C)	T_{out} (°F)	Mixed T_{out} (°C)	Mixed T_{out} (°F)
3†	8	36.16	97.09	46.16	115.09	38.89	102.00
4	7	35.25	95.46	45.25	113.46	38.89	102.00
5	6	34.34	93.82	44.34	111.82	38.89	102.00
6	5	33.44	92.18	43.44	110.18	38.89	102.00
7	4	32.53	90.55	42.53	108.55	38.89	102.00
8	3	31.62	88.91	41.62	106.91	38.89	102.00
9	2	30.71	87.27	40.71	105.27	38.89	102.00
10	1	29.80	85.64	39.80	103.64	38.89	102.00
11	0	28.89	84.00	38.89	102.00	38.89	102.00

†Operations with less than 11 active rods will only be allowed during system commissioning. At no time will less than 3 active rods be irradiated to ensure critical heat flux ratios are always above 2 at maximum power/minimum flow conditions.

To achieve a cartridge mixed outlet temperature equal to a nominal pool temperature of 38.89 °C (102 °F) the range for T_{inlet} will be 28.89 °C (84 °F) to 36.16°C (97.09 °F). For each additional degree of initial temperature rise of the pool, the cartridge inlet temperature will need to increase by the same number of degrees. For these analyses, it was assumed that three (3) active target rod operation would not occur if the pool temperature exceeded 42.22 °C (108 °F). This limit is dictated by the requirement to maintain CHFR's above 2.0 for all operational scenarios. As can be seen from Table 28, both the inlet and outlet coolant temperatures rise with decreasing active target rod counts, the most severe operating conditions are those with the least number of active rods.

As the system heats up, the gap between the UO_2 pellet and the Zircaloy-4 cladding will be set by the relative expansion of the pellet and the cladding, as well as the physical expansion of the UO_2 because of relocations in the pellet due to the stresses experienced during fuel burnup. Changes in the gap also change the volume occupied by the helium between the pellet and the cladding, which, along with temperature changes, increase the pressure of the gap helium. It is noted that the thermal conductivity of helium is a function of temperature, but in very small gaps such as these, it is also a function of the gap size and pressure.

Properties used for these analyses are shown in Figure 69, Figure 70, and Figure 71.

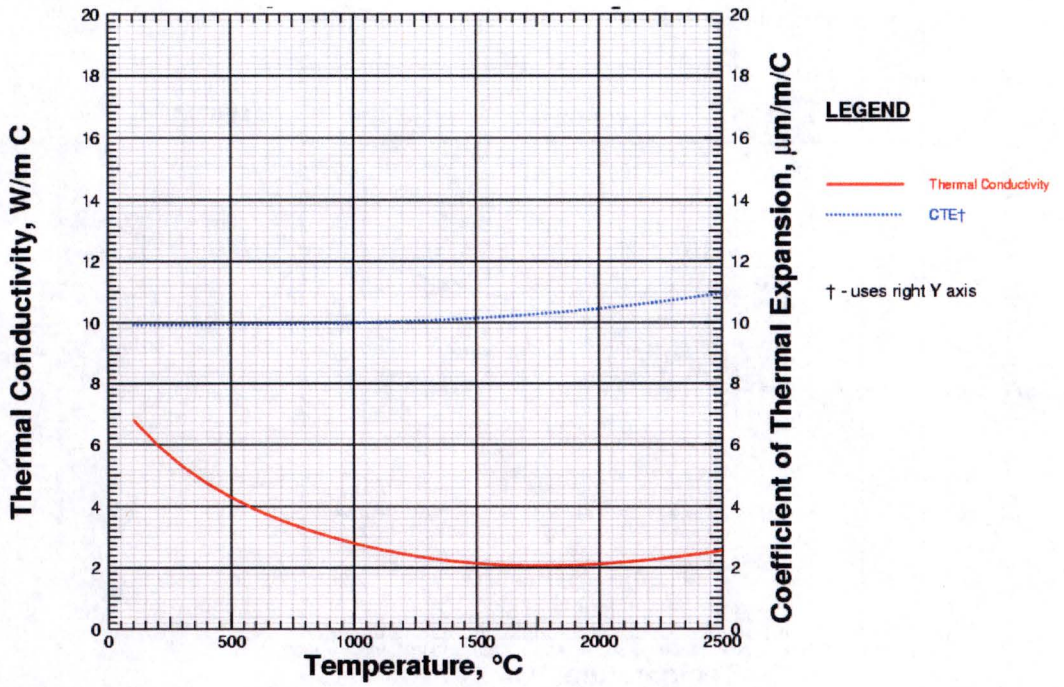

Figure 69
UO_2 Thermal Conductivity and Thermal Expansion Coefficient at 95% Theoretical Density

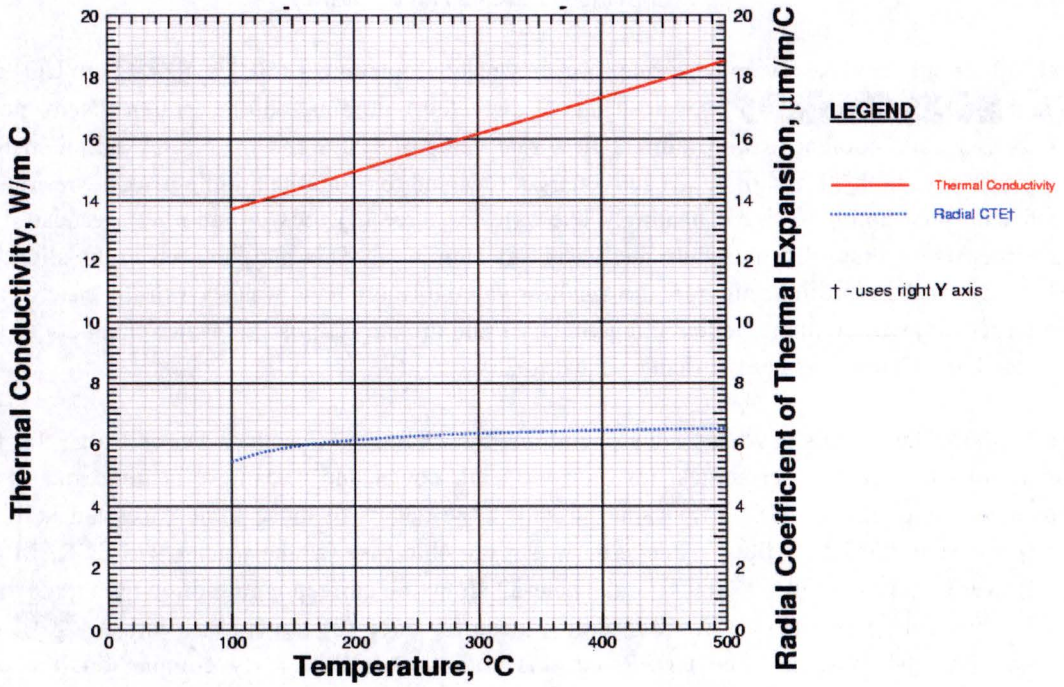

Figure 70
Zircaloy-4 Thermal Conductivity and Radial Thermal Expansion Coefficient

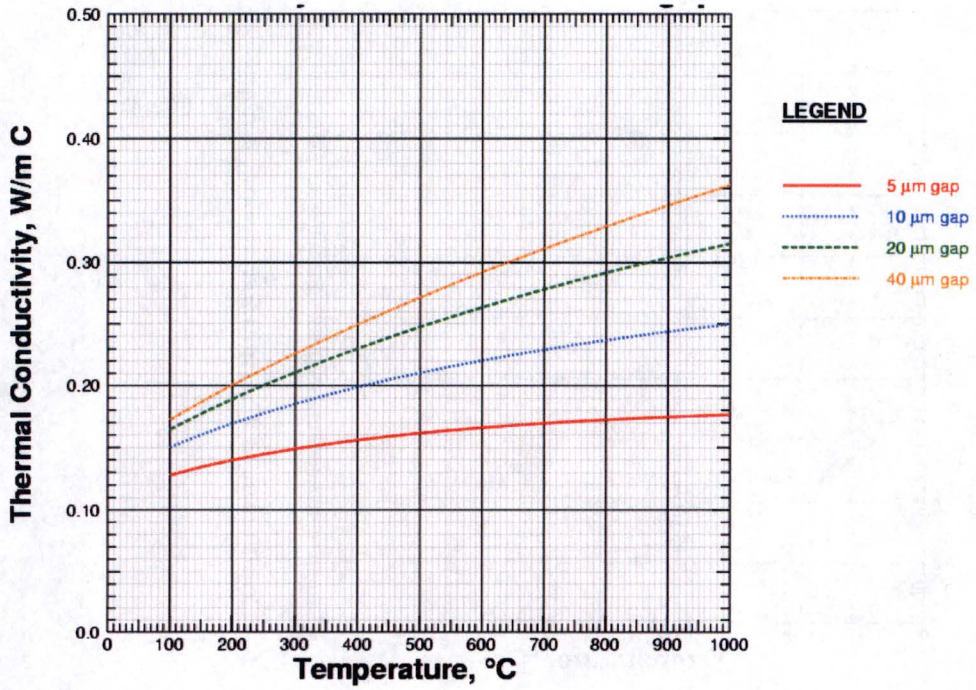

Figure 71
Helium Thermal Conductivity in Small Gaps
(2 atm pressure used as an example)

Target rod thermal analyses were performed for dimensional tolerances (50, [redacted] µm UO_2/cladding gaps and [redacted] water channel diameters), nominal and maximum reactor power (10 and 11.5 MW) and coolant flows (nominal flow rate value of 100% and the SCRAM limited flow rate value of 85%) for both 11 and three (3) active target rods and for both the middle peak power rod and the end rod with the maximum linear heating. The case for three (3) rods is important because it has the highest inlet temperature thus reducing the margin to saturation. This may be seen in the slightly lower CHFR's. Of all the cases investigated, the smallest value of the CHFR was seen in the case of the peak power target rod; with nominal pellet/clad geometries and the largest possible water channel. In all cases investigated, the CHFR was greater than or equal to 2.0.

5a, d, e, f

Table 29 shows the details of steady-state operations for 11 active target rods per cartridge, for both the nominal and worst case uncertainties, for both the peak power and maximum heating rods at 10 MW reactor power with 100% TCS flow. Table 30 shows the details of those same cases but at 11.5 MW_t reactor power and 85% TCS flow. This is the worst possible case (as the reactor will SCRAM at either higher power or lower flow). Table 31 and Table 32 show the corresponding three (3) target rod cases. Table 33 shows the worst (lowest CHFR) cases, those for three (3) target rods, with a [redacted] gap and added calculational margin. The CHFR for this condition is 2.07. By comparison, the expected minimum CHFR is 2.92 per Table 29.

5a, d, e, f

Table 29
Predicted Thermal Performance for 11 Active Target Rods, 10 MWt Reactor Power, 100% Flow

	Peak Power Rod, No Added Margin	Peak Power Rod, Maximum Added Margin	Max Linear Heating Rod No Added Margin	Max Linear Heating Rod, Maximum Added Margin
Reactor power, MW_t	10	10	10	10
Flow %	100	100	100	100
Active rods	11	11	11	11
Pool temperature, °C	38.9	40.9	38.9	40.9
Target inlet temperature, °C	28.9	30.9	28.9	30.9
Cold gap	Nominal	Nominal	Nominal	Nominal
Rod type	Peak Linear	Peak Linear	Max Heating	Max Heating
Rod location	Middle	Middle	End	End
Added error margin	None	Maximum	None	Maximum
Scallop diameter	Nominal	Maximum	Nominal	Maximum
Cold gap, μm	50	50	50	50
UO_2 radial growth, μm	40.06	40.01	38.7	38.66
Cladding radial growth, μm	2.92	2.9	2.88	2.86
Relocation growth, μm	5.11	5.11	4.94	4.94
Hot gap, μm	7.76	7.79	9.24	9.26
Helium gap pressure, atm	1.74	1.74	1.71	1.71
Plenum height, mm (Cold)	35	35	35	35
Plenum height, mm (Hot)	32.61	32.61	32.55	32.56
Axial CTE UO_2, μm/(m°C)	9.87	9.87	9.87	9.87
Radial CTE UO_2, μm/(m°C)	10.47	10.47	10.44	10.44
Radial CTE Zircaloy, μm/(m°C)	6.17	6.16	6.16	6.16
UO_2 centerline temperature, °C	2000.1	1998.7	1942.4	1941.1
UO_2 average temperature, °C	1117	1115.8	1097.4	1096.4
UO_2 surface temperature, °C	423.6	422.9	433.0	432.4
Helium temperature, °C	345.2	344.2	348.1	347.2
Cladding temperature at ID, °C	263.0	261.8	258.4	257.2
Mean cladding temperature, °C	206.0	204.7	203.4	202.2
Cladding temperature at OD, °C	156.1	154.8	155.4	154.1

Table 29
Predicted Thermal Performance for 11 Active Target Rods, 10 MWt Reactor Power, 100% Flow (continued)

	Peak Power Rod, No Added Margin	Peak Power Rod, Maximum Added Margin	Max Linear Heating Rod No Added Margin	Max Linear Heating Rod, Maximum Added Margin
UO_2 gap conductance, W/(m^2 C)	22160.5	22092.4	19603.2	19539.5
Coolant HTC, W/(m^2 C)	[redacted]	[redacted]	[redacted]	[redacted]
Water (scallop) OD, mm	14.45	14.823	14.45	14.823
D_h, mm	10.243	10.746	9.14	9.555
Re (D_h)	[redacted]	[redacted]	[redacted]	[redacted]
Local coolant velocity, m/s	[redacted]	[redacted]	[redacted]	[redacted]
Mass flow per rod, kg/s	[redacted]	[redacted]	[redacted]	[redacted]
Mass flow per target, kg/s	[redacted]	[redacted]	[redacted]	[redacted]
Mass flow per target, gpm	[redacted]	[redacted]	[redacted]	[redacted]
Coolant inlet temperature, °C	28.89	30.89	28.89	30.89
Local coolant temperature, °C	32.52	34.71	34.02	36.29
Coolant outlet temperature, °C	39.14	41.68	39.61	42.17
Local saturation temperature, °C	124.53	123.15	124.11	122.78
Peak pellet power density, W/cc	[redacted]	[redacted]	[redacted]	[redacted]
Heat (modeled) per rod, W	[redacted]	[redacted]	[redacted]	[redacted]
Heat flux at cladding OD, W/m^2	[redacted]	[redacted]	[redacted]	[redacted]
Bernath CHF, W/m^2	[redacted]	[redacted]	[redacted]	[redacted]
Bernath CHFR	3.17	2.93	3.18	2.92
Macbeth CHF, W/m^2	[redacted]	[redacted]	[redacted]	[redacted]
Macbeth CHFR	3.67	3.60	4.06	4.00
Groeneveld CHF, W/m^2	[redacted]	[redacted]	[redacted]	[redacted]
Groeneveld CHFR	3.40	3.13	3.50	3.24
Minimum CHFR	3.167	2.933	3.176	2.924
Pressure at CHFR, atm	2.2588	2.1645	2.2299	2.1400

5a, d, e, f

Table 30
Predicted Thermal Performance for 11 Active Target Rods, 11.5 MWt Reactor Power, 85% Flow

	Peak Power Rod, No Added Margin	Peak Power Rod, Maximum Added Margin	Max Linear Heating Rod No Added Margin	Max Linear Heating Rod, Maximum Added Margin
Reactor power, MW_t	11.5	11.5	11.5	11.5
Flow %	85	85	85	85
Active rods	11	11	11	11
Pool temperature, °C	38.9	40.9	38.9	40.9
Target inlet temperature, °C	28.9	30.9	28.9	30.9
Cold gap	Nominal	Nominal	Nominal	Nominal
Rod type	Peak Linear	Peak Linear	Max Heating	Max Heating
Rod location	Middle	Middle	End	End
Added error margin	None	Maximum	None	Maximum
Scallop diameter	Nominal	Maximum	Nominal	Maximum
Cold gap, μm	50	50	50	50
UO2 radial growth, μm	45.16	45.11	43.79	43.75
Cladding radial growth, μm	3.03	3.01	2.98	2.97
Relocation growth, μm	5.11	5.11	4.94	4.94
Hot gap, μm	2.77	2.79	4.25	4.27
Helium gap pressure, atm	1.85	1.85	1.82	1.82
Plenum height, mm (Cold)	35	35	35	35
Plenum height, mm (Hot)	32.87	32.88	32.79	32.79
Axial CTE UO_2, μm/(m°C)	9.86	9.86	9.86	9.86
Radial CTE UO_2, μm/(m°C)	10.57	10.57	10.55	10.55
Radial CTE Zircaloy, μm/(m°C)	6.19	6.18	6.18	6.17
UO_2 centerline temperature, °C	2204.7	2203.6	2150.8	2149.8
UO_2 average temperature, °C	1181.0	1180.0	1165.7	1164.9
UO_2 surface temperature, °C	379.3	378.7	394.2	393.8
Helium temperature, °C	328.5	327.8	333.9	333.2
Cladding temperature at ID, °C	277.2	276.2	272.1	271.2
Mean cladding temperature, °C	212.1	211.1	209.3	208.4
Cladding temperature at OD, °C	154.9	153.9	154.2	153.3

Table 30
Predicted Thermal Performance for 11 Active Target Rods, 11.5 MWt Reactor Power, 85% Flow (continued)

	Peak Power Rod, No Added Margin	Peak Power Rod, Maximum Added Margin	Max Linear Heating Rod No Added Margin	Max Linear Heating Rod, Maximum Added Margin
UO_2 gap conductance, W/(m^2 C)	40111.0	39965.3	32241.7	32132
Coolant HTC, W/(m^2 C)	[redacted]	[redacted]	[redacted]	[redacted]
Water (scallop) OD, mm	14.450	14.823	14.450	14.823
D_h, mm	10.243	10.746	9.140	9.555
Re (D_h)	[redacted]	[redacted]	[redacted]	[redacted]
Local coolant velocity, m/s	[redacted]	[redacted]	[redacted]	[redacted]
Mass flow per rod, kg/s	[redacted]	[redacted]	[redacted]	[redacted]
Mass flow per target, kg/s	[redacted]	[redacted]	[redacted]	[redacted]
Mass flow per target, gpm	[redacted]	[redacted]	[redacted]	[redacted]
Coolant inlet temperature, °C	28.89	30.89	28.89	30.89
Local coolant temperature, °C	33.81	36.06	35.83	38.19
Coolant outlet temperature, °C	42.76	45.49	43.39	46.16
Local saturation temperature, °C	122.06	121.00	121.74	120.73
Peak pellet power density, W/cc	[redacted]	[redacted]	[redacted]	[redacted]
Heat (modeled) per rod, W	[redacted]	[redacted]	[redacted]	[redacted]
Heat flux at cladding OD, W/m^2	[redacted]	[redacted]	[redacted]	[redacted]
Bernath CHF, W/m^2	[redacted]	[redacted]	[redacted]	[redacted]
Bernath CHFR	2.47	2.31	2.47	2.29
Macbeth CHF, W/m^2	[redacted]	[redacted]	[redacted]	[redacted]
Macbeth CHFR	3.24	3.18	3.59	3.53
Groeneveld CHF, W/m^2	[redacted]	[redacted]	[redacted]	[redacted]
Groeneveld CHFR	2.69	2.51	2.79	2.62
Minimum CHFR	2.473	2.307	2.465	2.286
Pressure at CHFR, atm	2.0921	2.0240	2.0712	2.0063

5a, d, e, f

Table 31
Predicted Thermal Performance for 3 Active Target Rods, 10 MWt Reactor Power, 100% Flow

	Peak Power Rod, No Added Margin	Peak Power Rod, Maximum Added Margin	Max Linear Heating Rod No Added Margin	Max Linear Heating Rod, Maximum Added Margin
Reactor power, MW_t	10	10	10	10
Flow %	100	100	100	100
Active rods	3	3	3	3
Pool temperature, °C	42.2	44.2	42.2	44.2
Target inlet temperature, °C	39.5	41.5	39.5	41.5
Cold gap	Nominal	Nominal	Nominal	Nominal
Rod type	Peak Linear	Peak Linear	Max Heating	Max Heating
Rod location	Middle	Middle	End	End
Added error margin	None	Maximum	None	Maximum
Scallop diameter	Nominal	Maximum	Nominal	Maximum
Cold gap, µm	50	50	50	50
UO2 radial growth, µm	40.06	40.01	38.7	38.66
Cladding radial growth, µm	2.92	2.9	2.88	2.86
Relocation growth, µm	5.11	5.11	4.94	4.94
Hot gap, µm	7.76	7.79	9.24	9.26
Helium gap pressure, atm	1.74	1.74	1.71	1.71
Plenum height, mm (Cold)	35	35	35	35
Plenum height, mm (Hot)	32.61	32.61	32.55	32.56
Axial CTE UO_2, µm/(m°C)	9.87	9.87	9.87	9.87
Radial CTE UO_2, µm/(m°C)	10.47	10.47	10.44	10.44
Radial CTE Zircaloy, µm/(m°C)	6.17	6.16	6.16	6.16
UO_2 centerline temperature, °C	2000.1	1998.7	1942.4	1941.1
UO_2 average temperature, °C	1117	1115.8	1097.4	1096.4
UO_2 surface temperature, °C	423.6	422.9	433	432.4
Helium temperature, °C	345.2	344.2	348.1	347.2
Cladding temperature at ID, °C	263	261.8	258.4	257.2
Mean cladding temperature, °C	206	204.7	203.4	202.2
Cladding temperature at OD, °C	156.1	154.8	155.4	154.1

Table 31
Predicted Thermal Performance for 3 Active Target Rods, 10 MWt Reactor Power, 100% Flow (continued)

	Peak Power Rod, No Added Margin	Peak Power Rod, Maximum Added Margin	Max Linear Heating Rod No Added Margin	Max Linear Heating Rod, Maximum Added Margin
UO_2 gap conductance, W/(m^2 C)	22160.5	22092.4	19603.2	19539.5
Coolant HTC, W/(m^2 C)	[redacted]	[redacted]	[redacted]	[redacted]
Water (scallop) OD, mm	14.450	14.823	14.450	14.823
D_h, mm	10.243	10.746	9.140	9.555
Re (D_h)	[redacted]	[redacted]	[redacted]	[redacted]
Local coolant velocity, m/s	[redacted]	[redacted]	[redacted]	[redacted]
Mass flow per rod, kg/s	[redacted]	[redacted]	[redacted]	[redacted]
Mass flow per target, kg/s	[redacted]	[redacted]	[redacted]	[redacted]
Mass flow per target, gpm	[redacted]	[redacted]	[redacted]	[redacted]
Coolant inlet temperature, °C	39.49	41.49	39.49	41.49
Local coolant temperature, °C	43.12	45.31	44.62	46.89
Coolant outlet temperature, °C	49.74	52.28	50.21	52.77
Local saturation temperature, °C	124.53	123.15	124.11	122.78
Peak pellet power density, W/cc	[redacted]	[redacted]	[redacted]	[redacted]
Heat (modeled) per rod, W	[redacted]	[redacted]	[redacted]	[redacted]
Heat flux at cladding OD, W/m^2	[redacted]	[redacted]	[redacted]	[redacted]
Bernath CHF, W/m^2	[redacted]	[redacted]	[redacted]	[redacted]
Bernath CHFR	2.90	2.68	2.91	2.67
Macbeth CHF, W/m^2	[redacted]	[redacted]	[redacted]	[redacted]
Macbeth CHFR	3.53	3.47	3.91	3.85
Groeneveld CHF, W/m^2	[redacted]	[redacted]	[redacted]	[redacted]
Groeneveld CHFR	3.16	2.91	3.26	3.02
Minimum CHFR	2.905	2.683	2.909	2.671
Pressure at CHFR, atm	2.2588	2.1645	2.2299	2.1400

5a, d, e, f

Table 32
Predicted Thermal Performance for 3 Active Target Rods, 11.5 MWt Reactor Power, 85% Flow

	Peak Power Rod, No Added Margin	Peak Power Rod, Maximum Added Margin	Max Linear Heating Rod No Added Margin	Max Linear Heating Rod, Maximum Added Margin
Reactor Power, MW_t	11.5	11.5	11.5	11.5
Flow %	85	85	85	85
Active rods	3	3	3	3
Pool Temperature, °C	42.2	44.2	42.2	44.2
Target inlet temperature, °C	39.5	41.5	39.5	41.5
Cold Gap	Nominal	Nominal	Nominal	Nominal
Rod Type	Peak Linear	Max Heating	Max Heating	Max Heating
Rod location	Middle	End	End	End
Added Error Margin	None	Maximum	None	Maximum
Scallop Diameter	Nominal	Maximum	Nominal	Maximum
Cold Gap, µm	50	50	50	50
UO2 radial growth, µm	45.16	43.75	43.79	43.75
Cladding radial growth, µm	3.03	2.97	2.98	2.97
Relocation Growth, µm	5.11	4.94	4.94	4.94
Hot Gap, µm	2.77	4.27	4.25	4.27
Helium Gap pressure, atm	1.85	1.82	1.82	1.82
Plenum height, mm (Cold)	35	35	35	35
Plenum height, mm (Hot)	32.87	32.79	32.79	32.79
Axial CTE UO_2, µm/(m°C)	9.86	9.86	9.86	9.86
Radial CTE UO_2, µm/(m°C)	10.57	10.55	10.55	10.55
Radial CTE Zircaloy, µm/(m°C)	6.19	6.17	6.18	6.17
UO_2 centerline temperature, °C	2204.7	2149.8	2150.8	2149.8
UO_2 average temperature, °C	1181.0	1164.9	1165.7	1164.9
UO_2 surface temperature, °C	379.3	393.8	394.2	393.8
Helium temperature, °C	328.5	333.2	333.9	333.2
Cladding temperature at ID, °C	277.2	271.2	272.1	271.2
Mean cladding temperature, °C	212.1	208.4	209.3	208.4
Cladding temperature at OD, °C	154.9	153.3	154.2	153.3

Table 32
Predicted Thermal Performance for 3 Active Target Rods, 11.5 MWt Reactor Power, 85% Flow (continued)

	Peak Power Rod, No Added Margin	Peak Power Rod, Maximum Added Margin	Max Linear Heating Rod No Added Margin	Max Linear Heating Rod, Maximum Added Margin
UO_2 gap conductance, W/(m^2 C)	40111.0	32132.0	32241.7	32132.0
Coolant HTC, W/(m^2 C)	[redacted]	[redacted]	[redacted]	[redacted]
Water (scallop) OD, mm	14.450	14.823	14.450	14.823
D_h, mm	10.243	9.555	9.140	9.555
Re (D_h)	[redacted]	[redacted]	[redacted]	[redacted]
Local coolant velocity, m/s	[redacted]	[redacted]	[redacted]	[redacted]
Mass flow per rod, kg/s	[redacted]	[redacted]	[redacted]	[redacted]
Mass flow per target, kg/s	[redacted]	[redacted]	[redacted]	[redacted]
Mass flow per target, gpm	[redacted]	[redacted]	[redacted]	[redacted]
Coolant inlet temperature, °C	39.49	41.49	39.49	41.49
Local coolant temperature, °C	44.40	48.79	46.43	48.79
Coolant outlet temperature, °C	53.36	56.75	53.99	56.75
Local saturation temperature, °C	122.06	120.73	121.74	120.73
Peak pellet power density, W/cc	[redacted]	[redacted]	[redacted]	[redacted]
Heat (modeled) per rod, W	[redacted]	[redacted]	[redacted]	[redacted]
Heat flux at cladding OD, W/m^2	[redacted]	[redacted]	[redacted]	[redacted]
Bernath CHF, W/m^2	[redacted]	[redacted]	[redacted]	[redacted]
Bernath CHFR	2.26	2.08	2.25	2.08
Macbeth CHF, W/m^2	[redacted]	[redacted]	[redacted]	[redacted]
Macbeth CHFR	3.13	3.41	3.46	3.41
Groeneveld CHF, W/m^2	[redacted]	[redacted]	[redacted]	[redacted]
Groeneveld CHFR	2.50	2.45	2.60	2.45
Minimum CHFR	2.261	2.080	2.250	2.080
Pressure at CHFR, atm	2.0921	2.0063	2.0712	2.0063

5a, d, e, f

Table 33
Predicted Thermal Performance for 3 Active Target Rods, Worst-Case Operations

	Peak Power Rod, No Added Margin	Peak Power Rod, Maximum Added Margin	Max Linear Heating Rod No Added Margin	Max Linear Heating Rod, Maximum Added Margin
Reactor power, MW_t	10	10	11.5	11.5
Flow %	100	100	85	85
Active rods	3	3	3	3
Pool temperature, °C	44.2	44.2	44.2	44.2
Target inlet temperature, °C	41.5	41.5	41.5	41.5
Cold gap	Minimum	Minimum	Minimum	Minimum
Rod type	Peak Linear	Max Heating	Peak Linear	Max Heating
Rod location	Middle	End	Middle	End
Added error margin	Maximum	Maximum	Maximum	Maximum
Scallop diameter	Maximum	Maximum	Maximum	Maximum
Cold gap, µm	36	36	36.25	36.25
UO2 radial growth, µm	33.75	32.79	43.85	40.64
Cladding radial growth, µm	2.90	2.85	3.01	2.96
Relocation Growth, µm	3.68	3.56	3.68	3.56
Hot gap, µm	1.47	2.50	0.00	0.00
Helium gap pressure, atm	1.66	1.64	1.70	1.70
Plenum height, mm (Cold)	35	35	35	35
Plenum height, mm (Hot)	33.14	33.07	32.99	33.04
Axial CTE UO_2, µm/(m°C)	9.85	9.86	9.86	9.86
Radial CTE UO_2, µm/(m°C)	10.26	10.25	10.52	10.44
Radial CTE Zircaloy, µm/(m°C)	6.17	6.16	6.18	6.18
UO_2 centerline temperature, °C	1796.6	1746.0	2169.9	2061.7
UO_2 average temperature, °C	964.5	952.2	1149.8	1093.4
UO_2 surface temperature, °C	334.6	346.6	359.9	351.7
Helium temperature, °C	298.6	302.4	318.5	311.9
Cladding temperature at ID, °C	262.5	258.0	277.1	272.0
Mean cladding temperature, °C	205.1	202.5	211.5	208.8
Cladding temperature at OD, °C	154.9	154.2	153.9	153.3

Table 33
Predicted Thermal Performance for 3 Active Target Rods, Worst-Case Operations
(continued)

	Peak Power Rod, No Added Margin	Peak Power Rod, Maximum Added Margin	Max Linear Heating Rod No Added Margin	Max Linear Heating Rod, Maximum Added Margin
UO_2 gap conductance, W/(m^2 C)	49643.1	38796.47	49643.1	49643.1
Coolant HTC, W/(m^2 C)	[redacted]	[redacted]	[redacted]	[redacted]
Water (scallop) OD, mm	14.823	14.823	14.823	14.823
D_h, mm	10.779	9.581	10.779	9.581
Re (D_h)	[redacted]	[redacted]	[redacted]	[redacted]
Local coolant velocity, m/s	[redacted]	[redacted]	[redacted]	[redacted]
Mass flow per rod, kg/s	[redacted]	[redacted]	[redacted]	[redacted]
Mass flow per target, kg/s	[redacted]	[redacted]	[redacted]	[redacted]
Mass flow per target, gpm	[redacted]	[redacted]	[redacted]	[redacted]
Coolant inlet temperature, °C	41.49	41.49	41.49	41.49
Local coolant temperature, °C	45.32	46.90	46.68	48.81
Coolant outlet temperature, °C	52.31	52.80	56.13	56.79
Local saturation temperature, °C	123.15	122.78	121.00	120.73
Peak pellet power density, W/cc	[redacted]	[redacted]	[redacted]	[redacted]
Heat (modeled) per rod, W	[redacted]	[redacted]	[redacted]	[redacted]
Heat flux at cladding OD, W/m^2	[redacted]	[redacted]	[redacted]	[redacted]
Bernath CHF, W/m^2	[redacted]	[redacted]	[redacted]	[redacted]
Bernath CHFR	2.66	2.65	2.09	2.07
Macbeth CHF, W/m^2	[redacted]	[redacted]	[redacted]	[redacted]
Macbeth CHFR	3.44	3.83	3.05	3.38
Groeneveld CHF, W/m^2	[redacted]	[redacted]	[redacted]	[redacted]
Groeneveld CHFR	2.89	3.00	2.32	2.43
Minimum CHFR	2.665	2.653	2.090	2.067
Pressure at CHFR, atm	2.1645	2.1400	2.0240	2.0063

5a, d, e, f

6.1.5 Flow Induced Vibrations

An analysis of the displacement of target rods caused by vibration due to the surrounding flow was performed. Ignoring the stiffening effects of the tube filled with the target pellets, the fixed-end Zircaloy-4 tubes have a natural frequency of 26 Hz and a maximum displacement of 65 μm, using the correlations of Paidoussis, which is also the ASME B&PV recommended method (Reference 32). A maximum displacement of 4 μm is calculated using Farmer et.al (Reference 33). In either case, it can be concluded that vibrations are not an issue for the target systems.

6.1.6 Cooling of the Beryllium Reflector during Operations with Target Rods

The Be reflector rests between the TA and the outer reactor pressure vessel. Nuclear, fluid flow and heat transfer analyses were performed to show the effect of the TAs in the two (2) graphite reflector positions. The important consideration is the increased heating of the Be reflector and the effect on cooling of the Be surfaces. The MURR Be reflector generates up to 200 kW of heat, primarily due to neutron scattering and absorption of high energy photons from the reactor core. With the target rods installed, the MCNP analyses show that the 22 targets rods will increase the reflector power density by as much as 24% at the reactor core elevation centerline (its hottest point). This heat is then rejected to the MURR pool coolant system.

It is not possible to measure the flow velocity around the Be reflector. Therefore, a model of the reflector cooling flow was created that accounts for these distinct flow paths.

1. Through the flux trap inside the annular core pressure vessel, which has a minimal effect on the reflector cooling.
2. Flow that travels between a 0.56-inch (14.2 mm) gap between the outer reactor pressure vessel and the inner wall of the Be reflector. The reactor regulating and control blades also reside in this gap and were accounted for.
3. The flow that passes through the gaps around the graphite reflector elements (and TAs) and down through holes and slots in the reflector support plate. A portion of this flow contacts the outer wall of the beryllium reflector, and thus is relevant to the reflector cooling.

Measurements show the pressure drop across the reflector assembly is 0.78 psi (5.38 kPa), which will serve as the basis for determining the flow rate in the reflector region. The flows through the three (3) flow paths were iterated in the model until all flow paths had the measured pressure drop and the total flow equaled the measured flow.

The flow surrounding the Be reflector, the predicted power density in the reflector, and the resulting heat transfer were examined to determine if the pool coolant system provides adequate cooling to the Be reflector in the presence of two TAs installed in graphite reflector positions No. 5A and No. 5B (Reference 34). Worst-case control/regulating blade positions, reflector age and estimated power densities were used. The results show that the reflector maintains a 20 °C (36 °F) margin from surface temperature to coolant saturation temperature in the presence of both TAs and hence there is no impact on

cooling of the Be reflector. Additionally, the driving pressure head was shown to have a small effect on the flow rate, indicating that it is unlikely the surface temperature of the Be will increase significantly if the pressure head changed.

7. In-Pool Target Transfer System

7.1 Cartridge Loading/Unloading Station Design

This section presents a description of the equipment and process that will take place to move target rods from/to target storage to/from the target cartridge at the cartridge loading/unloading station.

7.1.1 Cartridge Loading/Unloading Station Description

The cartridge loading/unloading station is located in the weir area of the reactor pool. It is an aluminum structure designed to bolt to the existing pool structure and contains storage for 33 target rods, four (4) target cartridges, and two (2) target diffusers. Figure 72 shows the location of the in-pool storage area within the MURR reactor pool and how it is positioned in relation to the reactor.

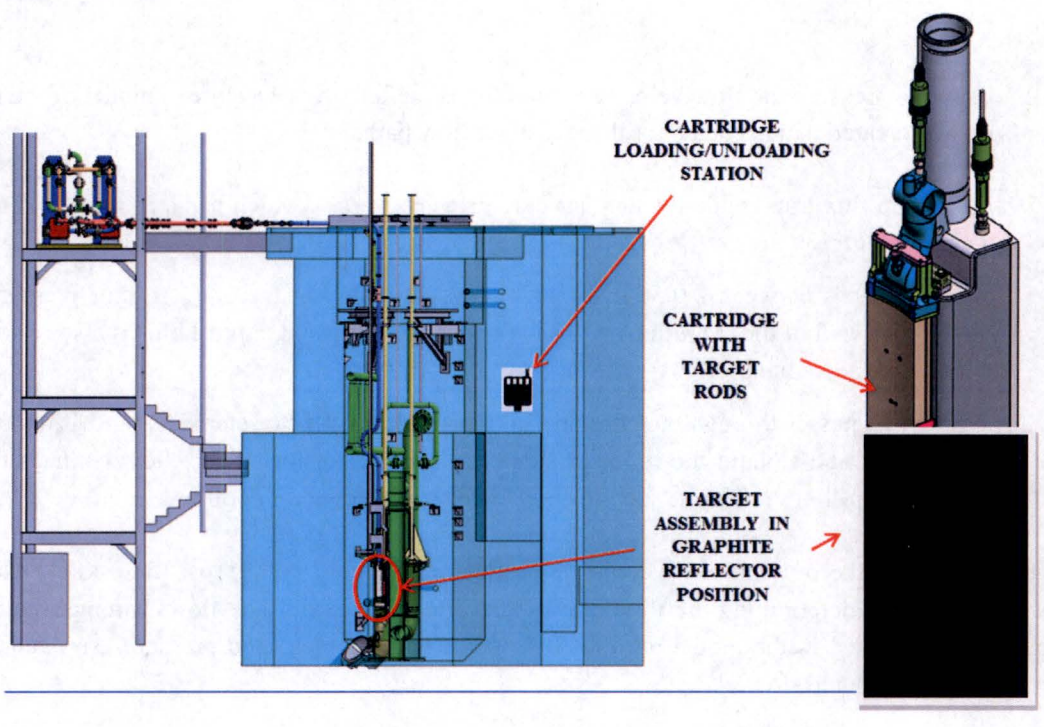

5a, b, d, e, f

Figure 72
Target Rod Loading/Unloading/Storage Location

The cartridge loading/unloading station has three functions (Figure 73):

1. It provides a location for the removal and installation of the diffuser from the cartridge;

2. It holds the cartridge while target rods are removed or installed into the cartridge; and
3. It provides an approved target rod storage location that places the target rods in a geometry to ensure a large margin to criticality.

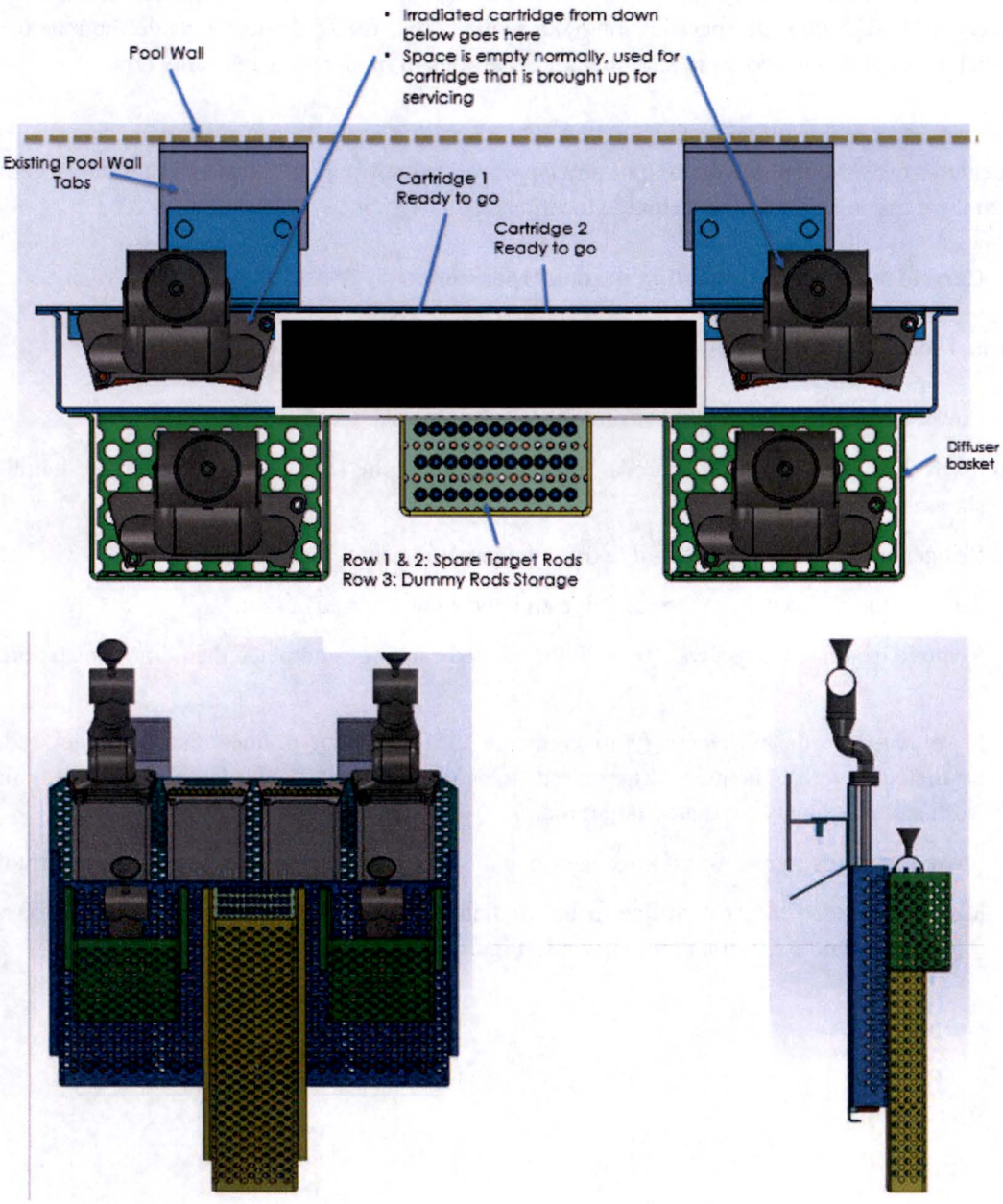

5a, b, d, e, f

Figure 73
Representation of the Cartridge Loading/Unloading Station

During normal operations, no more than 22 target rods will be either in a cartridge or in target storage at the cartridge loading/unloading station. Of those 22 target rods, only 11 of them will be fresh. However, the performed criticality analysis assumes 33 target storage positions and two (2) nearby target cartridges with 11 positions each filled with fresh target rods for a total of 55 fresh target rods in the station at the same time. The criticality analysis shows a maximum K_{eff} of 0.57 under all conditions of moderation and reflection. MURR Technical Specification 5.4.a requires that fueled devices outside the reactor core be stored such that the K_{eff} is less than 0.9 under all conditions of moderation and reflection.

Administrative controls similar to the MURR administrative controls for reactor fuel handling will be implemented to ensure that the location of any target rod is known at all times and that the target rods are placed in the correct irradiation and storage locations.

7.1.2 Cartridge Loading/Unloading Station Operation

The normal sequence of operation at the cartridge loading/unloading station will be:

1. Lower 11 or less fresh target rods into the station storage location.
2. Insert 11 or less fresh target rods into a cartridge at the station using the remote handling tool shown in Figure 71.
3. Bring an irradiated target cartridge from the target housing.
4. Remove the diffuser from the cartridge and place into storage basket.
5. Remove irradiated target rods from the irradiated cartridge and place them into the station storage location.
6. Move target rods as necessary to complete the placement of the next 11 target rods to be irradiated. (Note: The next 11 target rods to be irradiated may be all fresh or may be a mixture of fresh and previously irradiated target rods.)
7. Move the diffuser from the storage basket and install it onto the target cartridge to be irradiated.
8. Move the loaded target cartridge to be irradiated into the target housing at the reactor reflector (target rod remote handling tool shown in Figure 74).

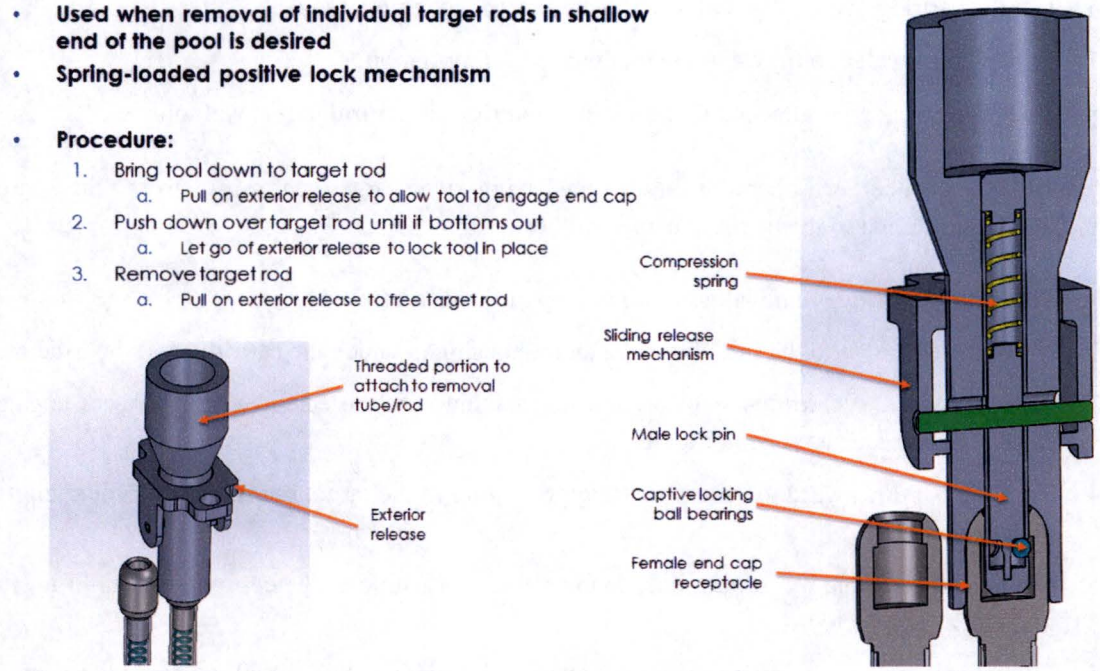

Figure 74
Target Rod Remote Handling Tool

7.2 Installation and Removal of the Target Cartridge Into/From the Target Housing

7.2.1 Target Cartridge Description

A detailed description for the target cartridge and how it fits into the target housing is provided in Section 2.1.4.

7.2.2 Cartridge Installation and Removal Into/From the Target Housing Operation

The normal sequence of operation for transferring the irradiated target cartridge from the target housing to the cartridge loading/unloading station will be:

1. Shut down the reactor.
2. To allow sufficient cooling and decay, keep the target cartridge in the target housing for a minimum of one (1) hour after reactor shutdown prior to unlatching the cartridge.
3. Remove the RTD at the top of the diffuser and secure it out of the way of cartridge movement operations.
4. Thread the cartridge removal tool into the top of the diffuser.
5. Unpin the cartridge by turning bolt-connected levers with a socketed, long tool.

6. Lift the cartridge vertically with the attached cartridge removal tool.
7. Move the cartridge to the cartridge loading/unloading station.
8. Once the cartridge is attached to the station, unthread the cartridge removal tool.

The normal sequence of operation for transferring the target cartridge from the cartridge loading/unloading station to the target housing will be:

1. Thread the cartridge removal tool into the top of the diffuser
2. Move the cartridge to the just above the target housing in which the cartridge will be irradiated.
3. Slowly lower the cartridge into the housing making sure the cartridge rail features engage the target housing rails as seen in Figure 5.
4. Gently push downward to ensure cartridge is resting in the target housing with proper alignment pin engagement.
5. Secure the cartridge by turning bolt-connected levers with a socketed, long tool until no further movement is detected.
6. Pull upward and push downward on the attached cartridge removal tool to ensure the cartridge is secured and cannot move.
7. Visually observe the proper position of the cartridge locking mechanism.
8. Unthread the cartridge removal tool.
9. Install the RTD at the top of the diffuser.

8. Radiological Protection Evaluation for the SGE Target Experimental Facility Operations

This section discusses and analyzes the expected radiological consequences related to normal operations from the production of Mo-99 using the SGE TEF. Included are the principal discussions of the MURR facility program to control radiation and expected radiation exposures due to operation, maintenance, and use of the irradiation hardware associated with the TEF. This section also outlines the methods for quantitative assessment of radiation doses in the restricted and unrestricted areas; application of these methods to all applicable radiation sources related to the operation of the TEF; and the program and provisions for protecting the health and safety of all individuals present at MURR, the general public and the environment. This section does not discuss the Radiation Protection Aspects of the MURR Health Physics program as related to the processing of the LEU targets for the Selective Gaseous Extraction (SGE) of Mo-99 from the TEF. That will be covered under the Part 2 License Amendment submission for processing the LEU target rods and the extraction of Mo-99.

The MURR Radiation Protection Program (RPP) has been established to protect the health and safety of all individuals present at MURR, the general public and the environment. In accordance with 10 CFR 20.1101, this program has been developed, documented, and implemented to a level commensurate with the scope and extent of licensed activities at MURR, and is sufficient to ensure compliance with the

regulations in 10 CFR 20. A primary component of this program is the fundamental principle of maintaining individual radiation exposures and releases of radioactive effluents as low as is reasonably achievable (ALARA). Responsibility for maintaining the MURR ALARA Program extends to all individuals who are granted access to the reactor facility.

Renewed Facility Operating License No. R-103 is the primary license that covers the authority and responsibilities associated with the reactor and the majority of radioactive materials produced at MURR. It is under the auspices of this license that operation of the TEF will occur. Radioactive Material use is further supplemented by the authorization of an NRC-issued Broad Scope license (24-00513-39) and is used to support the research and development mission of the MURR for materials and activities which may not be currently produced or covered under license No. R-103.

The radiation sources that are expected to be generated during irradiation of the TEF fall under the administrative control of the MURR Radiation Protection and Radioactive Waste Management Programs and can be categorized as airborne, liquid, or solid. While each of these categories is discussed individually in the following paragraphs, the major contributors to each category can be summarized as follows:

8.1 Airborne Sources

Airborne – Potential airborne sources consists mainly of the fission product gasses of the bromine, iodine, krypton and xenon species. Of these, iodine-131 (I-131) has the lowest Derived Air Concentration (DAC) and Effluent Release limits due to potential thyroid exposure while krypton-85 (Kr-85) has the longest half-life (10.76 years); however, Kr-85 is a noble gas and as such is minimally active with regards to human and non-human biological effects. All potential airborne sources from the SGE TEF are confined by the target rod cladding and are not expected to be released during routine operations.

Currently, during normal operation of MURR, argon-41 (Ar-41) is the principal source of airborne radioactivity (> 99%) released through the facility ventilation exhaust stack. However, similar to the irradiation of reactor fuel, there exists the possibility to release any one of the fission products created during the fission process from the TEF. Such release would likely be limited to noble gases (krypton and xenon) and the halogens iodine and bromine that exist in the "gap" between the LEU pellets and the target cladding. These releases could occur during two (2) points of the irradiation and use of the targets; (1) during the actual irradiation of the target rods in the graphite reflector region (this would occur if a leak occurs in the cladding of the target rod, thereby allowing the gap fission gases to escape), and (2) during handling of the target rods in the reactor pool pre- and post-irradiation.

8.2 Liquid Sources

Liquid – Liquid sources would include primary and pool coolant used in the reactor coolant systems and the TEF target cooling water, which is essentially reactor pool water that has been pumped to a separate cooling system to facilitate target heat removal. The water becomes activated and contaminated by direct neutron activation of the water molecule itself (H-3) along with any activation of impurities contained in the water due to its use as a coolant. The pool water would also contain contaminants due to its direct

contact with the reactor and pool coolant system components. Since primary and pool coolant is, by design, contained to the maximum extent possible, there are no substantial releases of these liquids directly into the environment. However, certain reactor maintenance activities along with TEF cooling system maintenance could result in small volumes of liquid (containing mainly tritium) being directed to the existing liquid waste retention system. Limited and strictly controlled quantities of liquid radioactive waste are released to the sanitary sewer in accordance with the requirements of 10 CFR 20.2003; this effluent may contain small quantities of pool and primary water. Thus the operation of the TEF would add little to existing liquid waste effluent streams.

All potentially radioactive aqueous liquid wastes are directed to a liquid waste retention and disposal system located at a level below the main grade of the MURR laboratory building. Liquid waste is then retained or mechanically processed until an assay indicates that activity concentration levels are less than the limits specified in 10 CFR 20, Appendix B for disposal by release into sanitary sewerage. Tritium currently accounts for about 81% of the total activity released each year. Historically, H-3 release is < 5% of the annual release limit of 5 Ci.

Pool coolant is the only radioactive liquid source expected to be impacted by the TEF. Radioactivity in this liquid occurs by the same mechanisms as described above: neutron interactions with hydrogen and oxygen in the water and neutron interactions with system and structural components, with the subsequent transfer into the pool coolant. Table 34 contains a list of the predominant radionuclides and their typical measured concentrations present in the pool coolant at 10 MW.

Table 34
Predominant Radionuclides in the MURR Pool Coolant and Their Measured Concentrations at 10 MW

Radionuclide	Half-Life	Typical Measured Concentration[1]
Magnesium-27 (^{27}Mg)	9.45 minutes	1.10×10^{-2} Ci/ml
Sodium-24 (^{24}Na)	14.96 hours	4.64×10^{-3} Ci/ml
Manganese-56 (^{56}Mn)	2.58 hours	2.54×10^{-3} Ci/ml
Technetium-101 (^{101}Tc)	14.2 minutes	4.70×10^{-5} Ci/ml
Technetium-99m (^{99m}Tc)	6.01 hours	9.73×10^{-6} Ci/ml
Antimony-122 (^{122}Sb)	2.70 days	1.01×10^{-5} Ci/ml
Xenon-135 (^{135}Xe)	9.10 hours	1.22×10^{-5} Ci/ml
Silver -110m (^{110m}Ag)	248.9 days	1.10×10^{-5} Ci/ml

[1]Listed values are typical of the measured concentrations that exist in the pool coolant at 10 MW, 2 to three days after reactor startup.

Due to the structural components that will be used in the target rods and assemblies, it is anticipated that any additional activity added to the pool water will be similar in nature to those found in the table above

with the exception of the potential addition of isotopes of zirconium, most likely Zr-95 and Zr-97 with half-lives of 64.02 days and 16.75 hours, respectively; as zirconium is the main constituent in the target rod cladding, as Zircaloy-4. Overall, however, it is anticipated that any increase in activity will not be greater than 6%, as determined by ratio of the TEF thermal power to the MURR core thermal power. It should be noted that the pool water will still be diverted to a pool clean up system (as is currently in place) that has anion-cation removal capability in order to ensure that the pool water is relatively free of contamination. This slight increase in pool water activity is not expected to warrant additional engineering or administrative controls beyond the control currently in place at the MURR.

For the purposes of the TEF, cooling water will flow from the WCM, located outside of the reactor pool, through piping located in the pool and then enter at the top of the TA. After traveling down through the housing the water will then pass upwards through the target rod region where it removes the fission heat from the target rods. The water will then be discharged out of the TA into the pool near the top of the assembly through a diffuser back into the bulk pool water region. Here the water will intermingle with the reactor pool water and circulate through the pool hold-up tank system prior to entering the pool coolant heat exchangers as noted earlier. A portion of that pool water will be diverted off to the TEF cooling system and then cooled further before being reintroduced into the TA. By utilizing existing reactor-related cooling and decay systems for the reduction of N-16, the addition of any N-16 produced by the TAs will not add any appreciable source term to the overall inventory of N-16 that must be decayed and/or shielded in order to protect reactor staff.

8.3 Solid Sources

Solid – Solid sources are a bit more diverse, but for the most part are very typical of a research reactor facility. Such sources include the reactor fuel in use in the core, irradiated fuel stored in the reactor pool, and new, unirradiated fuel. Additionally, fueled target rods used to produce the Mo-99 will be an additional solid radiation source. At any one time, there will be a maximum of 22 target rods each containing 106.2 grams of uranium nominally enriched to 19.75% in the isotope U-235 being irradiated. After irradiation, the target rods will be transferred to a dedicated hot cell system and then processed to extract Mo-99 through the SGE process. Any sources of radioactivity germane to the SGE process would be further described in the Part 2 licensing action and not included herein. Thus, the target rods (irradiated and unirradiated) would solely add to the current uranium inventory at MURR.

The solid radioactive sources associated with normal operation of MURR are summarized in Table 35. Because the actual inventory of reactor fuel, SGE target rods and other radioactive sources continuously change as part of the normal operation of the reactor and the experimental program, the information presented in Table 35 should be considered representative rather than an exact inventory. Disposition of the irradiated LEU-target material will be discussed in the Part 2 License Amendment submission and is expected to be coordinated through a Uranium Lease Take-Back agreement between MURR and the U.S. Department of Energy (DOE).

Table 35
Representative Radioactive Sources at MURR

Source Description	Radionuclide(s)	Nominal Activity (Ci)	Physical Characteristics	Wt% Uranium	Approximate Total (grams)	
					U-235	Total U
8 MURR Fuel Elements	Highly Enriched Uranium	N/A	In 10 MW Core - Irradiated	93	6,200	6,656
45 MURR Fuel Elements	Highly Enriched Uranium	N/A	In Pool Storage - Irradiated	93	34,875	37,440
4 MURR Fuel Elements	Highly Enriched Uranium	N/A	In Storage - New	93	3,100	3,328
22 SGE Target Rods	Low-Enriched Uranium (LEU)	N/A	In Irradiation Position	19.75	526	2,662

8.4 Radioactive Waste Management Program

MURR has a comprehensive Radioactive Waste Management Program that supports operation of the reactor, its ancillary facilities, and their utilization programs. All radioactive waste materials released from the facility through the Ventilation and Air Treatment System, the Radioactive Liquid Waste Retention and Disposal System, and the Solid Radioactive Waste Program are identified, assessed, and released or disposed of in conformance with all applicable regulations and in a manner that protects the health and safety of the general public and the environment. It is the policy of the reactor facility to keep the volume of waste materials being generated to the absolute minimum by the efficient use of experiment materials, by the use of proper techniques, and by any other means available.

It is not anticipated that additional radiation safety training programs will need to be developed for this portion of the License Amendment request for the irradiation of the LEU target rods. Operations personnel that will be responsible for and perform the actual handling of the individual target rods and assemblies are well versed in the underwater manipulation of materials as demonstrated by the years of successful handling of fuel elements essential to the operation of MURR over the past 50 years of operational experience.

At this time, minimal additional Health Physics (HP) procedures are anticipated to need development for the irradiation phase of the SGE target rods. Current reviewed and approved HP procedures related to the operation of the reactor are deemed to be sufficient to protect both the staff and general public during the irradiation phase of this project as it is not significantly different than the actual current operation of the reactor.

Any permanently installed radiation monitoring equipment at the reactor facility specifically installed to support the SGE TEF is discussed in detail in Section 4. Any HP-related radiation monitoring equipment

used at the MURR is much the same as that described in the MURR SAR. Little additional equipment is anticipated to be needed in order to support the addition and operation of the SGE TEF.

Additionally, no changes are anticipated for the MURR HP monitoring and survey program as a result of the irradiation of the target rods nor are any significant number of additional records anticipated to be generated as a result of this activity.

Shielding is the paramount design feature used in controlling radiation exposure during operation of the reactor. Shielding has been installed to keep radiation levels in areas occupied by all personnel ALARA. All shielding thicknesses are based on an operating power level of 10 MW. Fuel storage and handling requirements are based on 40-day continuous operation at 10 MW prior to shutting down and removing fuel. With over 50 years of operational history, the installed radiation shielding has performed more than adequately as designed and analyzed. This same shielding will be used to provide radiation exposure protection from the two (2) target assemblies that will be operating in the graphite reflector region directly outside the reactor pressure vessel and beryllium reflector region. It should be noted however that one entire TEF assembly (11 target rods) used for the production of Mo-99 via the SGE process contains approximately 263 grams of U-235; approximately 30% of the U-235 contained in one single fresh MURR fuel element. Thus, two (2) full target assemblies with 11 target rods each would contain approximately 7.5 % of the U-235 that is contained in the reactor core with eight (8) fresh fuel elements. This does not count the fuel elements in the reactor pool that are being cooled for either reuse within the reactor or awaiting sufficient cooling and decay for shipment as spent fuel. Thus the addition of the two (2) target assemblies adds less than 7.5% to the entire source term that is contained in the pool due to the use and storage of fuel elements located there.

Similar calculations were performed using the computer program MicroShield® to predict the dose resulting from the movement of a target cartridge to a position underneath the pool water surface that allows handling and removal of the individual target rods for eventual placement into the transfer cask. These doses are summarized in Table 36 below and provide the worst-case estimate of exposure rates from target cartridge movement activities (e.g., one hour after the end of a three week irradiation of 22 target rods). MURR staff is not expected to be present in the fields given in Table 36 below on a routine or regular basis. Target cartridge movement activities are anticipated to happen twice a week for periods not greater than 30 minutes per occurrence. It is also expected that each handling activity will be rotated amongst several staff members throughout the year. The maximum expected dose rates are presented in Table 36.

Table 36
Maximum Expected Dose Rates from Target Cartridge Movement Activities One Hour after EOI

Dose Location	Surface Exposure Rate (mR/hr)	1 foot Exposure Rate (mR/hr)	1 meter Exposure Rate (mR/hr)
Reactor Pool	127	100	61
Biological Shield at Handling Station	18	13	6.5

In conclusion, it is not apparent that any additional major changes are required to the MURR RPP due to the addition of the irradiation facilities that will be used for the SGE TEF.

9. Conduct of Operations

9.1 Procedures

Standard Operating Procedures (SOP) will be developed that are specific for operation and maintenance of the SGE TEF and also reactor operation with the TEF. The following topics will be incorporated into procedures for TEF systems installation, testing, operation, and maintenance.

- TEF component/systems installation and testing
- TEF startup plan
- Target cartridge loading, unloading, and in-pool transfer
- Target rod receiving, inspection, and storage
- TCS operation
- TEF preventative maintenance and inspection
- Surveillance procedures required by the Technical Specifications

Table 37 lists the SOPs that are expected to be used for routine operation of the facility.

Table 37
Standard Operating Procedures

No.	Title	Contents
1	TEF Installation and Checkout	• Receiving and inspection of equipment • Installation checkout of Water Cooling Module • Piping installation • Welding and inspection procedures • Instrumentation and control installation and checkout • Target housing installation
2	TEF Commissioning and Startup	• Cold commissioning with filler rods • Safety interlock checkout • Hot commissioning • Hot acceptance procedure • Checklists
3	Target Rod Loading and Unloading	• Transfer from storage • Cartridge loading • Target assembly loading and unloading • Cartridge unloading and temporary cooling • Checklists
4	Target Rod Receiving, Inspection and Storage	• Material control procedure • Unpacking and inspection • Acceptance criteria • Storage procedure
5	TEF Normal Operations	• Pre-operational checkout • Startup procedure • Monitors and data recording • Safety interlocks and alarms • Shutdown and standby
6	TEF Maintenance and Inspection	• Routine maintenance and inspection • Planned equipment replacement • Equipment performance monitoring • Instrumentation checkout and calibration

9.2 Target Experimental Facility Commissioning Plan

A high-level commissioning plan is presented in this section. A detailed startup and commissioning plan will be prepared and approved by the Reactor Safety Procedure Review Subcommittee (a subcommittee of the Reactor Advisory Committee) prior to startup of the TEF. Appropriate hold points will be identified in the plan for review of data and for approval to proceed to the next step of the startup plan.

9.2.1 Assumptions

- Secondary Coolant System modifications complete
- TCS installation complete outside of the reactor pool
- Interface with the MURR reactor safety system ready to be connected
- Experimental Facilities ready to be installed
- Both filler and target rods on hand

9.2.2 Phase 1: Installation and Initial Testing with One TEF Target Assembly

- Reactor shutdown
- Reactor startup with reference core configuration to 50 kW (log ECP control blade heights)
- Reactor shutdown
- Remove current graphite reflector element from position No. 5A
- Install one new experimental facility target housing
    - Connect forced cooling loop
    - Connect interface to reactor safety system
    - Install cartridge with 11 filler rods loaded
    - Complete coolant system testing including all reactor safety system Technical Specification surveillances
- After all cooling testing is complete, remove cartridge with 11 filler rods
- Reactor startup to 50 kW
    - Calculate reactivity worth with new facility experimental facility target housing
- Reactor shutdown
- Install cartridge with 11 filler rods
- Make coolant system adjustments due to flow restriction changes
- Reactor startup to 50 kW
    - Calculate reactivity worth of cartridge and 11 filler rods
- Continue reactor startup to 10 MW with forced flow and 11 filler rods

9.2.3 Phase 2: Loading of One Cartridge with 3 Target Rods and 8 Filler Rods

- Reactor shutdown

- Reactor startup with reference configuration to 50 kW with all filler target rods
- Reactor shutdown
- Reactor startup with 3 target rods to 10 kW with thermocouple. Check thermocouple temperature and target thermal calculations. Verify excess reactivity, shutdown margin, and secured experiment reactivity.
- Increase power to 50 kW – check thermocouple temperature and target thermal calculations
- Increase power to 100 kW – check thermocouple temperature and target thermal calculations
- Increase power to 250 kW – check thermocouple temperature and target thermal calculations
- Increase power to 500 kW – check thermocouple temperature and target thermal calculations
- Increase power to 1 MW – check thermocouple temperature and target thermal calculations
- Increase power to 2 MW – check thermocouple temperature and target thermal calculations
- Increase power to 5 MW – check thermocouple temperature and target thermal calculations
- Increase power to 10 MW – check thermocouple temperature and target thermal calculations
- Operate at 10 MW all week with 3 target rods and 8 filler rods
- Visually inspect each target rod at the end of the week after removal

9.2.4 Phase 3: Loading of One Cartridge with 11 Target Rods

- Reactor shutdown
- Reactor startup with reference configuration to 50 kW with all filler target rods
- Reactor shutdown
- Reactor startup with 11 target rods to 10 kW with thermocouple. Check thermocouple temperature and target thermal calculations. Verify excess reactivity, shutdown margin, and secured experiment reactivity. Vary coolant inlet temperature between max and min temperatures to verify effect on reactivity.
- Increase power to 50 kW – check thermocouple temperature and target thermal calculations
- Increase power to 100 kW – check thermocouple temperature and target thermal calculations
- Increase power to 250 kW – check thermocouple temperature and target thermal calculations
- Increase power to 500 kW – check thermocouple temperature and target thermal calculations
- Increase power to 1 MW – check thermocouple temperature and target thermal calculations
- Increase power to 2 MW – check thermocouple temperature and target thermal calculations
- Increase power to 5 MW – check thermocouple temperature and target thermal calculations

- Increase power to 10 MW – check thermocouple temperature and target thermal calculations
- Operate at 10 MW all week with 11 target rods
- Visually inspect each target rod at the end of the week after removal

9.2.5 Phase 4: Installation of Second TEF Target Assembly and Initial Testing and Conduct Full 22-Target Rod Experiment Run

- Reactor shutdown
- Reactor startup with reference configuration to 50 kW
- Reactor shutdown
- Remove current graphite reflector element from position No. 5B
- Install second new experimental facility with filler target rods in both target cartridges
    - Connect forced cooling loop
    - Connect interface to reactor safety system
    - Install cartridge with 11 filler rods loaded
    - Complete coolant system testing including all reactor safety system Technical Specification surveillances
- After all cooling testing is complete, remove cartridge with 11 filler rods
- Install both cartridges with 22 target rods
- Reactor startup to 10 kW with thermocouples. Check thermocouples temperature and target thermal calculations. Verify excess reactivity, shutdown margin, and secured experiment reactivity.
- Increase power to 50 kW – check thermocouple temperature and target thermal calculations
- Increase power to 100 kW – check thermocouple temperature and target thermal calculations
- Increase power to 250 kW – check thermocouple temperature and target thermal calculations
- Increase power to 500 kW – check thermocouple temperature and target thermal calculations
- Increase power to 1 MW – check thermocouple temperature and target thermal calculations
- Increase power to 2 MW – check thermocouple temperature and target thermal calculations
- Increase power to 5 MW – check thermocouple temperature and target thermal calculations
- Increase power to 10 MW – check thermocouple temperature and target thermal calculations
- Operate at 10 MW all week with 22 target rods
- Visually inspect each target rod at the end of the week after removal

9.3 Material Control & Accounting

The LEU target rods will be controlled and accounted for under MURR's existing material control and accounting procedures. The fresh target rods will be stored in the same storage area as reactor fuel. Irradiated target rod material control will be discussed in the Part 2 License Amendment application.

10. Target Experimental Facility Accident Analyses

Accidents affecting the SGE TEF while it is in the reactor pool can occur either during reactor operation or after reactor shutdown when the irradiated target rods are being transferred in the reactor pool. Accidents can be initiated by a failure either in the TEF or in the MURR reactor facility. Potential accidents initiated by the TEF include breach of target rod cladding, loss of target coolant from a pipe break, loss of target cooling flow, or mishandling of the target. Accidents initiated by the reactor facility include insertion of excess reactivity, loss of primary coolant flow, loss of primary coolant, loss of pool coolant or loss of offsite electrical power. The breach of target rod cladding has been identified as the TEF maximum hypothetical accident (MHA).

10.1 Target Experimental Facility Maximum Hypothetical Accident

An accident resulting in a significant release of fission products to the environment from operating the SGE TEF is considered highly improbable. The redundant safety measures, strictly controlled quality and administrative procedures in the design, fabrication and operation of the facility give high confidence in the improbable nature of such a release. Nevertheless, inadvertent physical damage to the TEF from manufacturing defects or damage from handling must be considered and analyzed for licensing purposes with a defined, enveloping event that can be used for bounding the radiation hazard.

For the TEF, such an enveloping event, the MHA, is a postulated breach of a target rod cladding during full power operation. The initiating event for this is hypothesized to be caused by a defect in the cladding or a defect in either of the welds that attach the upper and lower end fittings. It is further postulated that this accident occurs at the worst possible time at the end of an approximate three-week irradiation which maximizes the fission product inventory in the gas gap between the target material and the cladding.

10.1.1 Description of Maximum Hypothetical Accident Scenario

The scenario for the MHA is a postulated breach from a defective weld or cladding at the end of a three-week irradiation. The fission gas in the void volume of the target rod is released to the target cooling water which is then discharged to the reactor pool water, then into the reactor containment building, and ultimately a release to the outside environment.

During operation, fission of the LEU UO_2 target material produces a variety of fission products including the fission gases krypton, xenon, and iodine. These fission gases can diffuse out of the UO_2 target material and into the void spaces within the target rod. As the target rod burns its U-235, there is an accumulation of fission gases in these void spaces. A breach of a target rod at the end of its three-week design life will release this accumulated fission gas inventory. Originally, the helium pressure inside the

target rods is 101 kPa (14.7 psia). Temperature, thermal expansion and fission gas release raise the pressure to 550 kPa (80 psia). Therefore, a breach of the target rod rapidly releases the fission gap gas into the target cooling water which is then discharged to the reactor pool immediately above the target rods.

10.1.2 Source Term

The radionuclide inventory in the target rods at the end of irradiation was calculated by using MCODE, a code to couple MCNP6 and ORIGEN2, to predict isotopic concentration at the end of irradiation. A Once Through Source Term Model (OTSTM) was developed to predict the evolution of radionuclides after irradiation (Reference 35). This program uses an analytic solution to a generalized Bateman equation to calculate the nuclide inventory as a function of time. In addition, OTSTM calculates the decay heat from the actinides and fission products according to ANSI/ANS-5.1-2014, "Decay Heat Power in Light Water Reactors" (Reference 36), and the fraction of the volatile nuclides that may be released from a target rod gap if the cladding is breached according to ANSI/ANS-5.4-2011, "Method for Calculating the Fractional Release of Volatile Fission Products from Oxide Fuel" (Reference 37).

The subsequent decay of 1307 nuclides as they move through the TEF was also modeled using OTSTM. In the OTSTM fission products diffuse out of the UO_2 matrix and into the pellet-cladding gap during irradiation. This "gap gas" can then escape into the atmosphere if the cladding is breached during an accident and is the bases for the MHA source term. The source term for the gap gas is calculated using the factor of 5X conservatism on the release to birth ratios, as recommended in ANSI/ANS-5.4-2011 (Reference 37) and to be conservative, the source term for the gap gas is calculated using power density and temperature profiles in the target rod at the beginning and the burnup at the end of a three-week irradiation. The temperature is highest at the beginning because the power density is highest in the fresh pellets and the burnup is highest at the end, giving the highest pellet surface to volume ratio. In addition, the release fraction for the hottest, highest power target rod is used for calculating the gap gas for all the rods in a set.

The total activity of all isotopes of iodine, krypton and xenon in the gap gas of the hottest target rod is 396 Ci at 0 hours (End of Irradiation). Note that the sum of the activities of the individual nuclides in Table 38 below is slightly less than the total activity because Table 38 does not include some short lived nuclides with minor radiological consequence. The activity in a 22 target rod set is obtained by multiplying the activity in the hottest rod by 21.45, which is the ratio of the total fission power in a 22 rod set to the fission power in the hottest rod.

Note that most of the fission products are volatile during irradiation due to the very high temperatures inside the rods. However, we assume that only isotopes of iodine, krypton and xenon are volatile after irradiation or upon target rod cladding failure because the rods are then much cooler. Nonetheless, the decay and progeny of non-volatile nuclides, such as Te-132, does contribute to the activities shown in Table 38.

More detailed information about the source term calculation, including the input and output files for the codes used, can be found in GA Report 30441R00022, "Source Term Analysis Design Calculation Report" (Reference 38). However, for ease of reviewability the source term output applicable to the MHA is repeated in Table 38.

Table 38
Activity of Volatile Fission Products in the Gap Gas of the Hottest Target Rod

Fission Product	Half-life	Activity at EOI (Ci)	Activity at 6 hours (Ci)
Kr-85m	4.481 h	5.9623	2.3670
Kr-85	10.72 y	0.0316	0.0316
Kr-87	1.272 h	6.2891	0.2400
Kr-88	2.839 h	12.0723	2.7903
Kr-89	3.15 m	2.2661	0.0000
Kr-90	32.32 s	0.8907	0.0000
I-131	8.041 d	26.2934	25.8531
I-132	2.3 h	144.6951	84.4133
I-133	20.8 h	45.7961	37.9656
I-134	52.6 m	26.0561	0.7470
I-135	6.611 h	30.5511	16.2867
Xe-133	5.245 d	64.8080	64.0750
Xe-135	9.089 h	8.1066	13.3210
Xe-135m	15.29 m	5.5078	2.6087
Xe-137	3.818 m	3.0510	0.0000
Xe-138	14.08 m	5.9110	0.0000
Xe-139	39.68 s	1.0359	0.0000
	Totals:	**389.3242**	**250.6993**

10.1.3 Dose Assessment

The methodology applied for the dose assessment calculations presented throughout this section are based on the fueled experiment failure methodology submitted by MURR to the NRC as part of relicensing efforts.

10.1.4 Radionuclide Concentration in Reactor Pool Water

A breach of the target rod with the highest power generation at the end of a three-week irradiation cycle will release the iodine, krypton and xenon gap activities shown in Table 39 into the MURR reactor pool.

Fission products released into the reactor pool will be detected by the pool surface and ventilation system exhaust plenum radiation monitors. However, for the purposes of this analysis, it is assumed that a reactor scram and actuation of the containment building isolation system occurs by action of the pool surface radiation monitor. Actuation of the isolation system will prompt Operations personnel to ensure that a total evacuation of the containment building is accomplished promptly, usually within two (2) to two and a half (2.5) minutes. A conservative 5 minute evacuation period is used as the basis for the stay time in the dose calculations for personnel that are in containment during target failure.

Table 39
Iodine and Noble Gas Activities Released to MURR Reactor Pool

Activity (μCi)		
^{131}I - $2.63 \times 10^{+07}$	^{85}Kr - $3.16 \times 10^{+04}$	^{133}Xe - $6.48 \times 10^{+07}$
^{132}I - $1.45 \times 10^{+08}$	^{85m}Kr - $5.96 \times 10^{+06}$	^{135}Xe - $8.11 \times 10^{+06}$
^{133}I - $4.58 \times 10^{+07}$	^{87}Kr - $6.29 \times 10^{+06}$	^{135m}Xe - $5.51 \times 10^{+06}$
^{134}I - $2.61 \times 10^{+07}$	^{88}Kr - $1.21 \times 10^{+07}$	^{137}Xe - $3.05 \times 10^{+06}$
^{135}I - $3.06 \times 10^{+07}$	^{89}Kr - $2.27 \times 10^{+06}$	^{138}Xe - $5.91 \times 10^{+06}$
	^{90}Kr - $8.91 \times 10^{+05}$	^{139}Xe - $1.04 \times 10^{+06}$

The iodine released into the reactor pool over a 5 minute period is conservatively assumed to be instantly and uniformly mixed into the 20,000 gallons (75,708 l) of bulk pool water, which then results in the following pool water concentrations for the iodine isotopes (Table 40). The water solubility of the krypton and xenon noble gases released into the pool over this same time period is conservatively ignored. The gas bubble rise time in the reactor pool from where the TEF is situated in the graphite reflector region to the pool surface has been measured at 17 seconds, so it is assumed the earliest any of the radioisotopes from the TEF, including radioiodine nuclides, enters into the containment building air volume is after 17 seconds. It is also assumed when the radioactivity enters the containment air volume it instantaneously forms a uniform concentration in the isolated containment structure.

Table 40
Iodine Concentrations in Pool Water

Concentration (μCi/gal)
^{131}I - $1.31 \times 10^{+03}$
^{132}I - $7.23 \times 10^{+03}$
^{133}I - $2.29 \times 10^{+03}$
^{134}I - $1.30 \times 10^{+03}$
^{135}I - $1.53 \times 10^{+03}$

10.1.5 Radionuclide Concentration in Containment

When the reactor is at 10 MW and the containment building ventilation system is in operation, the evaporation rate from the reactor pool is approximately 80 gallons (302.8 L) of water per day. For the purposes of this calculation, it is assumed that a total of 20 gallons (75.7 L) of pool water containing the previously listed iodine concentrations evaporates into the containment building over the 5 minute period. Containment air with a temperature of 75 °F (23.9 °C) and 100% relative humidity contains H_2O vapor equal to 40 gallons (151.4 L) of water. Since the air in containment is normally at about 50% relative humidity, thus containing 20 gallons (75.7 L) of water vapor, the assumed addition of 20 gallons (75.7 L) of water vapor will not cause the containment air to become supersaturated. It is also conservatively assumed that all of the iodine activity in the 20 gallons (75.7 L) of pool water instantaneously forms a uniform concentration in the containment building air. When distributed into the containment building, this would result in the following iodine concentrations in the 225,000 ft^3 (6,371.3 m^3) containment air volume:

Example calculation of the average ^{131}I concentration released into the containment air during the first minute:

= ^{131}I concentration in pool water/gal × 20 gal/5 min × 0.5 min x EXP(-0.693 × (17+30 sec) / (8.02 day × 8.64 × 10^{+04} sec/day)) / (225,000 ft^3 × 28,317 ml/ft^3)

= 1.31 × 10^{+03} µCi/gal × 2 gal × 0.99995 / (6.371 × 10^{+09} ml)

= 4.13 × 10^{-07} µCi/ml

The same calculation is used for the other iodine isotopes listed below and was performed for each 1-minute interval in the 5 minute period. The average radioiodine concentrations over the 5 minute evacuation period is the average of the five 1-minute intervals in the 5 minute period (Table 41).

Table 41
Average Iodine Concentrations in the Containment Building Air During the 5 Minute Evacuation Period

Concentration (µCi/cc)
^{131}I - 2.06 × 10^{-06}
^{132}I - 1.12 × 10^{-05}
^{133}I - 3.59 × 10^{-06}
^{134}I - 1.95 × 10^{-06}
^{135}I - 2.38 × 10^{-06}

As noted previously, the krypton and xenon gases released into the reactor pool from the SGE TEF during the 5 minute evacuation period following a cladding failure are assumed to have no absorption in the pool

water, rise through the pool in 17 seconds (thus slightly decaying) and enter the containment building air volume where they are assumed to instantaneously form a uniform concentration in the isolated structure. Based on the 225,000-ft^3 volume of containment building air, and the previously listed curie quantities of these gases released into the reactor pool, the average noble gas concentrations in the containment structure over the 5 minute evacuation period would be calculated as follows:

Example calculation of the average ^{85}Kr concentration in containment during the first minute after the gas enters the containment air:

= ^{85}Kr activity × EXP(-0.693 × (17+ 30 sec) / (10.76 yrs × 3.156 × 10^{+07} sec/yr)) / (225,000 ft^3 × 28,317 ml/ft^3)

= 3.16 × 10^{+04} µCi × 0.99999 / (6.371 × 10^{+09} ml)

= 4.96 × 10^{-06} µCi/ml

The same calculation is used for the other krypton and xenon isotopes listed below in Table 42 and was performed for each 1-minute interval in the 5 minute period. The average concentrations over the five minute evacuation period are the average of the five 1-minute intervals in the 5 minute period.

Table 42
Average Noble Gas Concentrations in the Containment Building Air during the 5 Minute Evacuation Period

Concentration (µCi/cc)	
^{85}Kr - 4.96 × 10^{-06}	^{133}Xe - 1.02 × 10^{-02}
^{85m}Kr - 9.29 × 10^{-04}	^{135}Xe - 1.27 × 10^{-03}
^{87}Kr - 9.63 × 10^{-04}	^{135m}Xe - 7.64 × 10^{-04}
^{88}Kr - 1.87 × 10^{-03}	^{137}Xe - 2.99 × 10^{-04}
^{89}Kr - 2.02 × 10^{-04}	^{138}Xe - 8.11 × 10^{-04}
^{90}Kr - 1.41 × 10^{-05}	^{139}Xe - 2.19 × 10^{-05}

10.1.6 Dose Assessment in Restricted Area

The objective of this calculation is to present a worst-case occupational dose assessment for an individual who remains in the containment building for 5 minutes following the MHA. Therefore, as noted previously, the radioactivity in the evaporated pool water is assumed to be instantaneously and uniformly distributed into the building once released into the air.

Based on the source term data provided, it is possible to determine the radiation dose to the thyroid from radioiodine and the dose to the whole body resulting from submersion in the airborne noble gases and radioiodine inside the containment building.

Because the airborne radioiodine source is composed of five different iodine isotopes, it will be necessary to determine the dose contribution from each individual isotope and to then sum the results. Dose multiplication factors were established using the Derived Air Concentrations (DACs) for the "listed" isotopes in Appendix B of 10 CFR 20 and calculated values for the "unlisted" submersion isotopes (Kr-89, Kr-90, Xe-137, and Xe-139). The submersion DAC values that were calculated were done in accordance with the data and methodology as supplied in Federal Guidance Report No. 12.

Example calculation of thyroid dose due to ^{131}I:

The DAC can also be defined as 50,000 mrem (thyroid target organ limit) / 2,000 hr, or 25 mrem/DAC-hr. Additionally, 5 minutes of one DAC-hr is 8.33×10^{-02} DAC-hr.

^{131}I concentration in containment $= 2.06 \times 10^{-06}$ µCi/ml

^{131}I DAC (10 CFR 20) $= 2.00 \times 10^{-08}$ µCi/ml

Dose Multiplication Factor $= (^{131}I \text{ concentration}) / (^{131}I \text{ DAC})$

$= (2.06 \times 10^{-06} \text{ µCi/ml}) / (2.00 \times 10^{-08} \text{ µCi/ml})$

$= 1.03 \times 10^{+02}$

Therefore, the 5-minute thyroid exposure from ^{131}I is:

= Dose Multiplication Factor × DAC Dose Rate × 5 minutes of a DAC-hr

$= 1.03 \times 10^{+02} \times (25 \text{ mrem/DAC-hr}) \times (8.33 \times 10^{-02} \text{ DAC-hr})$

$= 2.15 \times 10^{+02}$ mrem

The same calculation sequence was repeated for all iodine isotopes and is summarized in Table 43.

Table 43
Derived Air Concentration Values and 5-Minute Exposures for Iodine

Radionuclide	Derived Air Concentration (μCi/ml)	5-Minute Exposure (mrem-CDE)
^{131}I	2.00×10^{-08}	$2.15 \times 10^{+02}$
^{132}I	3.00×10^{-06}	$7.74 \times 10^{+00}$
^{133}I	1.00×10^{-07}	$7.47 \times 10^{+01}$
^{134}I	2.00×10^{-05}	2.03×10^{-01}
^{135}I	7.00×10^{-07}	$7.09\times 10^{+00}$

Doses from the krypton and xenon radionuclides present in the containment building are assessed in much the same manner as the iodines, and the dose contribution from each individual radionuclide must be calculated and then added together to arrive at the final noble gas dose. Because the dose from the noble gases is only an external dose due to submersion, and because the DACs for these radionuclides are based on this type of exposure, the individual noble gas doses for 5 minutes in containment were based on their average concentration in the containment air and the corresponding DAC.

The whole body dose due to ^{85}Kr is calculated as follows:

The DAC can also be defined as 5,000 mrem/2,000 hrs, or 2.5 mrem/DAC-hr. Additionally, 5 minutes of one DAC-hr is 8.33×10^{-02} DAC-hr.

^{85}Kr concentration in containment = 4.96×10^{-06} μCi/ml

^{85}Kr DAC (10 CFR 20) = 1.00×10^{-04} μCi/ml

Dose Multiplication Factor = (^{85}Kr concentration) / (^{85}Kr DAC)

= $(4.96 \times 10^{-06}$ μCi/ml) / $(1.00 \times 10^{-04}$ μCi/ml)

= 4.96×10^{-02}

Therefore, a 5 minute whole body exposure from ^{85}Kr is:

= Dose Multiplication Factor x DAC Dose Rate x 5 minutes of a DAC-hr

= $4.96 \times 10^{-02} \times$ (2.5 mrem/DAC-hr) $\times$ $(8.33 \times 10^{-02}$ DAC-hr)

= 1.03×10^{-02} mrem

The same calculation sequence was repeated for all noble gases and is summarized in Table 44.

Table 44
Derived Air Concentration Values and 5 Minute Exposures – Noble Gases

Radionuclide	Derived Air Concentration (μCi/ml)	5-Minute Exposure (mrem-CEDE)
^{85}Kr	1.00×10^{-04}	1.03×10^{-02}
^{85m}Kr	2.00×10^{-05}	$9.68 \times 10^{+00}$
^{87}Kr	5.00×10^{-06}	$4.01 \times 10^{+01}$
^{88}Kr	2.00×10^{-06}	$1.95 \times 10^{+02}$
^{89}Kr	1.90×10^{-06}	$2.22 \times 10^{+01}$
^{90}Kr	2.80×10^{-06}	$1.05 \times 10^{+00}$
^{133}Xe	1.00×10^{-04}	$2.12 \times 10^{+01}$
^{135}Xe	1.00×10^{-05}	$2.64 \times 10^{+01}$
^{135m}Xe	9.00×10^{-06}	$1.77 \times 10^{+01}$
^{137}Xe	2.00×10^{-05}	$3.11 \times 10^{+00}$
^{138}Xe	4.00×10^{-06}	$4.22 \times 10^{+01}$
^{139}Xe	3.70×10^{-06}	$1.24 \times 10^{+00}$

To finalize the occupational dose in terms of Total Effective Dose Equivalent (TEDE) for a 5 minute exposure in the containment building during the MHA, the doses from the iodines and noble gases must be added together. This summation results in the following TEDE values presented in Table 45.

Table 45
5-Minute Dose from Radioiodines and Noble Gases in the Containment Building

Iodine – Committed Dose Equivalent (Thyroid)	**304 mrem**
Iodine – Committed Effective Dose Equivalent (CDE x 0.03)	**9 mrem**
Noble Gas – Committed Effective Dose Equivalent	**380 mrem**
Total Effective Dose Equivalent	**389 mrem**

By comparison of the maximum TEDE and Committed Dose Equivalent (CDE) for those occupationally-exposed during a TEF failure and the MHA to applicable NRC dose limits in 10 CFR 20, the final values are shown to be well within the published regulatory limits, in fact, less than 10% of any occupational limit.

10.1.7 Dose Consequences to Members of the Public

As noted earlier in this chapter, the containment building ventilation system will shut down and the containment building will be isolated from the surrounding areas upon actuation of the isolation system. A breach of target rod cladding will not cause an increase in pressure inside the reactor containment structure; therefore, any air leakage from the building will occur as a result of normal changes in atmospheric pressure and pressure equilibrium between the inside of the containment structure and the outside atmosphere. It is highly probable that there will be no pressure differential between the inside of the containment building and the outside atmosphere, and consequently there will be no air leakage from the building and no radiation dose to members of the public in the unrestricted area. However, to develop what would clearly be a worst-case scenario, this analysis assumes that a barometric pressure change has occurred in conjunction with the target failure. A reasonable assumption would be a pressure change on the order of 0.7 inches of Hg (25.4 mm of Hg at 22 °C), which would then create a pressure differential of about 0.33 psig (2.28 kPa above atmosphere) between the inside of the isolated containment building and the inside of the adjacent laboratory building, which surrounds most of the containment structure. Making the conservative assumption that the containment building will leak at the Technical Specification leakage rate limit, 10% of the contained volume over a 24-hour period from an initial overpressure of 2.0 psig (13.8 kPa above atmosphere), the air leakage from the containment structure in standard cubic feet per minute (scfm) as a function of containment pressure can be expressed by the following equation:

$$LR = 17.68 \times (CP-14.7)^{1/2};$$

where:

LR = leakage rate from containment (scfm); and

CP = containment pressure (psia).

The minimum Technical Specification free volume of the containment building is 225,000-ft^3 at standard temperature and pressure. At an initial overpressure of 2.0 psig (13.8 kPa above atmosphere), the containment structure would hold approximately 255,612 standard cubic feet (scf) of air.

When applying the Technical Specification leakage rate equation to the assumed initial overpressure condition of 0.33 psig (2.28 kPa above atmosphere), it would take approximately 16.5 hours for the leak rate to decrease to zero from an initial leakage rate of approximately 10.25 scfm, which would occur at the start of the event. Determination of the average leakage rate is subdivided into multiple intervals within the total 16.5 hour leak duration to provide a more accurate calculation of release concentrations from the facility using the Technical Specification leakage rate equation. The average containment building leakage rate for each of the first five (5) 1-hour intervals and for the following three (3) 4-hour intervals is provided below in Table 46.

Table 46
Average Containment Building Leakage Rate

Hours:	0-1	1-2	2-3	3-4	4-5	5-9	9-12	12-16.5
scf/hr:	595.6	558.7	521.8	485.0	448.1	355.8	207.9	67.9

Several factors exist that will mitigate the radiological impact of any air leakage from the containment building following target failure. First of all, most leakage pathways from containment discharge into the reactor laboratory building, which surrounds the containment structure. Since the laboratory building ventilation system continues to operate during target failure, leakage air captured by the ventilation exhaust system is mixed with other building air, and then discharged from the facility through the exhaust stack at a rate of approximately 30,500 cfm. Mixing of containment air leakage with the laboratory building ventilation flow, followed by discharge out the exhaust stack and subsequent atmospheric dispersion, results in extremely low radionuclide concentrations and very small radiation doses in the unrestricted area. A tabulation of these concentrations and doses is given below.

A second factor which helps to reduce the potential radiation dose in the unrestricted area relates to the behavior of radioiodine, which has been studied extensively in a containment mockup facility at Oak Ridge National Laboratory (ORNL). From these experiments, it was shown that up to 75% of the iodine released will be deposited in the containment vessel. For the purposes of this analysis a conservative value from Regulatory Guide 1.3, "Assumptions Used for Evaluating the Potential Radiological Consequences of a Loss of Coolant Accident for Boiling Water Reactors," was used and provides a reduction factor of 50% for plate-out and deposition of iodine within the containment building. Thus, due to this 50% iodine deposition in the containment building, each cubic foot of air released from containment has a iodine concentration that is fifty percent of each cubic foot within the containment building air.

Example calculation of average ^{131}I concentration in containment during the first hour:

= (^{131}I concentration in pool water/gal x 20 gal) × EXP[(-0.693 × 0.5 hr) / (^{131}I $T_{1/2}$)] / (scf in containment)

= $(1.31 \times 10^{+03}$ µCi/gal x 20 gal) × 0.99820 / (229,800 scf)

= 1.14×10^{-01} µCi/scf

The average ^{131}I concentration in containment over the first hour is then further reduced by the 50% iodine plate-out reduction factor prior to escaping from containment at the average leak rate and further diluted in 30,500 scfm of laboratory building exhaust ventilation prior to being released from the facility.

Example calculation of average ^{131}I concentration in air released from the facility during the first hour:

= (average ^{131}I concentration in containment µCi/scf × average leak rate × 0.5 reduction factor) / (30,500 scfm × 60 min/hr × 28,317 ml/scf)

= $(1.14 \times 10^{-01}$ µCi/scf × 595.6 × 0.5) / $(5.18 \times 10^{+10})$

= 6.56×10^{-10} µCi/ml

The average of first five (5) 1-hour intervals and the following three (3) 4-hour intervals is then summed and averaged over the entire 16.5 hour duration to calculate an average of the air concentration released from the facility. The same calculation is used for the other radioiodines and is provided in Table 47.

Table 47
Average Iodine Concentrations in Air Exiting the Exhaust Stack

Activities (µCi/ml)
^{131}I - 3.38×10^{-10}
^{132}I - 5.89×10^{-10}
^{133}I - 5.01×10^{-10}
^{134}I - 4.60×10^{-11}
^{135}I - 2.39×10^{-10}

Calculation of nobles gases released through the exhaust stack is identical to the calculation of the radioiodines released except no credit is taken for activity absorbed by pool water or reduction via plate-out inside of the containment building.

Example calculation of average ^{85}Kr concentration in containment during the first hour:

= ^{85}Kr activity × EXP[(-0.693 × 0.5 hr) / (^{85}Kr $T_{1/2}$)] / (scf in containment)

= $3.16 \times 10^{+04}$ µCi × 0.99999 / (229,800 scf)

= 1.38×10^{-01} µCi/scf

Example calculation of average ^{85}Kr concentration in air released from the facility during the first hour:

= (average ^{85}Kr concentration in containment µCi/scf × average leak rate) / (30,500 scfm × 60 min/hr × 28,317 ml/scf)

= $(1.38 \times 10^{-01}$ µCi/scf × 595.6) / $(5.18 \times 10^{+10})$

= 1.58×10^{-09} µCi/ml

The average of the first five (5) 1-hour intervals and the following three (3) 4-hour intervals is then summed and averaged over the entire 16.5 hour duration to calculate an average of the air concentration released from the facility. The same calculation is used for the other noble gasses and is provided in Table 48.

Table 48
Noble Gas Concentrations in Air Exiting the Exhaust Stack

Activities (μCi/ml)	
^{85}Kr - 8.29×10^{-10}	^{133}Xe - 1.65×10^{-06}
^{85m}Kr - 7.67×10^{-08}	^{135}Xe - 1.44×10^{-07}
^{87}Kr - 3.13×10^{-08}	^{135m}Xe - 4.57×10^{-09}
^{88}Kr - 1.16×10^{-07}	^{137}Xe - 4.00×10^{-11}
^{89}Kr - 9.34×10^{-12}	^{138}Xe - 4.31×10^{-09}
^{90}Kr - 4.56×10^{-26}	^{139}Xe - 7.10×10^{-23}

10.1.8 Dose Assessment in Unrestricted Area

Assuming that (1) the above provided average leak rates from the reactor containment building, (2) the leak continues for about 16.5 hours in order to equalize the containment building pressure with atmospheric pressure, (3) the flow rate through the facility's ventilation exhaust stack is 30,500 scfm, (4) the reduction in concentration from the point of discharge at the exhaust stack to the point of maximum concentration in the unrestricted area is a factor of 292 (explained below) and (5) there is no decay of any iodines or noble gases, then the following concentrations of iodines and noble gases with their corresponding radiation doses will occur in the unrestricted area. The values listed are at the point of maximum concentration in the unrestricted area assuming uniform, semi-spherical cloud geometry for noble gas submersion and further assuming that the most conservative (worst-case) meteorological conditions exist for the entire 16.5-hour period of containment leakage following target failure. Radiation doses are calculated for the entire 16.5-hour period. Dose values for the unrestricted area were obtained using the same methodology that was used to determine doses inside the containment building, and it was assumed that an individual was present at the point of maximum concentration for the full 16.5 hours that the containment building was leaking.

A worst-case scenario dilution factor of 292 for effluent dilution using the Pasquill-Guifford Model for atmospheric dilution is used in this analysis. It is assumed that all offsite (public) doses occur under these atmospheric conditions at the site of interest, i.e. 760 meters North of MURR. This point conservatively assumes a Stability Class F; which normally occurs only 11.4% of the time when the wind blows from the south. Thus, this calculation is conservative.

10 CFR 20 Appendix B Effluent Concentration Limits are used for the "listed" isotopes. Effluent Concentration Limits were calculated for each of the four (4) "unlisted" noble gases (Kr-89, Kr-90, Xe-137 and Xe-138) using the data and methodology contained in Federal Guidance Report No. 12 for submersion isotopes. The DAC value was first calculated and then a factor of 219 was applied using 10 CFR 20, Appendix B, methodology for effluent values from submersion isotopes. Exposure at 1 DAC equates to 5000 mrem per year whereas the Effluent Concentration Limit is 50 mrem per year. Thus, there is a factor of 100 times lower allowable dose for the Effluent Concentration Limit as compared to the DAC. Exposure at the effluent concentration limit assumes a person is in that effluent concentration for 8760 hours per year. Thus, the time assumed for exposure to the effluent concentration limit is a factor of 4.38 longer than the 2000 hours per year that defines a DAC. No credit is taken for transit time from the stack to the receptor point. In the case of Kr-89 and Xe-137 the transit time alone would be approximately one (1) half-life while the transit time for Kr-90 and Xe-139 would be at least four (4) half-lives.

Example calculation of whole body dose in the unrestricted area due to ^{131}I:

Conversion Factor: (Public dose limit of 50 mrem/yr) × (1 yr/8760 hours) = 5.71×10^{-03} mrem/hr

^{131}I concentration	= 3.38×10^{-10} µCi/ml
^{131}I effluent concentration limit	= 2.00×10^{-10} µCi/ml
^{131}I Conversion Factor	= 5.71×10^{-03} mrem/hr

Therefore, a 16.5-hour whole body exposure from ^{131}I at the maximum receptor site is:

= (^{131}I concentration / 292 dilution factor) / (^{131}I effluent concentration limit) × (Conversion Factor × 16.5 hrs)

= $(3.38 \times 10^{-10}$ µCi/ml / 292) / $(2.00 \times 10^{-10}$ µCi/ml) × $(5.71 \times 10^{-03}$ mrem/hr × 16.5 hrs)

= 5.45×10^{-04} mrem

The same calculation is used for the other isotopes (iodines and noble gases) and results are listed in Table 49 and Table 50.

Table 49
Effluent Concentration Limits, Concentrations at Point of Maximum Concentration and Radiation Doses in the Unrestricted Area – Iodine

Radioiodine	Effluent Limit (µCi/ml)	Concentration[1] at Maximum Receptor Site (µCi/ml)	Radiation Dose (mrem)
^{131}I	2.00×10^{-10}	1.16×10^{-12}	5.45×10^{-04}
^{132}I	2.00×10^{-08}	2.02×10^{-12}	9.51×10^{-06}
^{133}I	1.00×10^{-09}	1.72×10^{-12}	1.62×10^{-04}
^{134}I	6.00×10^{-08}	1.58×10^{-13}	2.48×10^{-07}
^{135}I	6.00×10^{-09}	8.18×10^{-13}	1.28×10^{-05}
			Total = 0.000729

Note 1: Concentrations are the average radioiodine concentrations leaking from the containment building and exiting the exhaust stack reduced by a dilution factor of 292.

Table 50
Effluent Concentration Limits, Concentrations at Point of Maximum Concentration and Radiation Doses in the Unrestricted Area – Noble Gases

Radioisotope	Effluent Limit (µCi/ml)	Concentration[1] at Maximum Receptor Site (µCi/ml)	Radiation Dose (mrem)
^{85}Kr	7.00×10^{-07}	2.84×10^{-12}	3.82×10^{-07}
^{85m}Kr	1.00×10^{-07}	2.63×10^{-10}	2.48×10^{-04}
^{87}Kr	2.00×10^{-08}	1.07×10^{-10}	5.06×10^{-04}
^{88}Kr	9.00×10^{-09}	3.97×10^{-10}	4.15×10^{-03}
^{89}Kr	2.00×10^{-08}	3.20×10^{-14}	3.51×10^{-07}
^{90}Kr	2.00×10^{-08}	1.56×10^{-28}	1.23×10^{-21}
^{133}Xe	5.00×10^{-07}	5.64×10^{-09}	1.06×10^{-03}
^{135}Xe	7.00×10^{-08}	4.94×10^{-10}	6.64×10^{-04}
^{135m}Xe	4.00×10^{-08}	1.57×10^{-11}	3.69×10^{-05}
^{137}Xe	2.00×10^{-08}	1.37×10^{-13}	1.42×10^{-07}
^{138}Xe	2.00×10^{-08}	1.48×10^{-11}	6.96×10^{-05}
^{139}Xe	2.00×10^{-08}	2.43×10^{-25}	1.43×10^{-18}
			Total = 0.00674

Note 1: Concentrations are the average noble gas concentrations leaking from the containment building and exiting the exhaust stack reduced by a dilution factor of 292.

To finalize the unrestricted dose in terms of TEDE, the doses from the iodines and noble gases must be added together. Results are provided in Table 51.

Table 51
Dose from Iodines and Noble Gases in the Unrestricted Area

Committed Effective Dose Equivalent (Iodine)	**0.000729 mrem**
Committed Effective Dose Equivalent (Noble Gases)	**0.00674 mrem**
Total Effective Dose Equivalent	**0.00747 mrem**

Summing the doses from the noble gases and the iodines simply substantiates earlier statements regarding the low levels in the unrestricted area should a failure of the TEF occur and subsequent containment building leakage following such an event. The overall TEDE is much less than 1 mrem, a value far below the 100 mrem regulatory limit within 10 CFR 20 for the unrestricted area.

10.1.9 Radiation Shine through Containment

An evaluation of radiation shine through the containment building has also been performed to ensure whole body doses are of minimal concern during an accident scenario. The radiation shine model uses MicroShield Ver. 8.02 (Grove Software) for shielding and exposure rate calculations to evaluate radiation shine through the containment structure under accident conditions, and to determine dose consequences to the public and MURR staff. Calculations of exposure rate from the TEF failure were performed using a Rectangular Volume – External Dose Point geometry for the representation of the containment structure.

The exposure rate values provided below represents the radiation fields at 1 foot (30 cm) from a 12-inch thick ordinary concrete containment wall and at the Emergency Planning Zone (EPZ) boundary of 150 meters (492.1 ft) representing the anticipated exposure rates in the restricted and unrestricted area respectively. The airborne concentrations used in calculating the exposure rate values were derived from the total activities of the gap gas nuclides provided in Table 52 divided by the containment free volume of 225,000 scf. Therefore, all radiation shine exposure rate values provided are very conservative as solubility of the iodine nuclides in the pool water, and decay of all nuclides is ignored. The source term also assumes a homogenous mixture of the nuclides within the containment free volume.

Table 52 provides the exposure rates external to the containment building at 1 foot and 150 meters from the building surface.

Table 52
Radiation Shine through the Containment Building

Exposure Rate at 1-Foot from Containment Building Wall	**67 mR/hr**
Exposure Rate at Emergency Planning Zone Boundary (150 meters)	**0.32 mR/hr**

10.2 Insertion of Excess Reactivity

Because of (1) the subcriticality of the target cartridges and (2) the physical impossibility of removing a target cartridge without scramming the reactor, a reactivity accident associated with the removal or insertion of the target cartridges is not considered credible. Removal and insertion of the target cartridges only occurs when the MURR reactor is shutdown.

Two (2) different reactivity insertion accidents for the MURR reactor core would have an impact on the TA. First, a step insertion of positive reactivity based upon the maximum step insertion that the MURR core can withstand with no core damage, and second, a continuous ramp insertion of positive reactivity based on the continuous withdrawal of MURR's four (4) shim control blades.

10.2.1 Rapid Insertion of Positive Reactivity

For the Insertion of Excess Reactivity accident analysis, the licensed maximum power level of 10 MW was originally used in the reactor SAR as the starting assumption since MURR does not, nor can it legally, operate above this power level. NUREG-1537, Part 2, page 13-9, *Standard Review Plan and Acceptance Criteria*, states for Insertion of Excess Reactivity accident, that "*The accident scenario assumes that the reactor has a maximum load of fuel (consistent with the technical specifications), the reactor is operating at full licensed power, and the control system...*" The accident was reanalyzed at a much more conservative starting power level (11.5 MW) than is required by NUREG-1537 and the results are provided below. 11.5 MW was chosen, instead of the Limiting Safety System Setting (LSSS) set point of 12.5 MW, because the rod run-in system will initiate a rod run-in at 11.5 MW (Technical Specification 3.2.f.1) and shut down the reactor prior to reaching the LSSS SCRAM set point of 125%.

The third paragraph on Page 13-17 of the SAR lists the various reactivity coefficients assumed for the Insertion of Excess Reactivity accident analysis.

For both the reactor SAR analyses, as well as for the updated analysis presented here, the CB insertion times are based on the current and relicensing Technical Specification 3.2.c requirement of insertion to the 20% withdrawn position in less than 0.7 seconds. The insertion rate was calculated based on the shim CBs travelling from 26 inches (fully withdrawn) to 5.2 inches (20% withdrawn or 80% inserted) in 0.7 seconds. This is a conservative assumption because monthly control blade drop time verifications performed at MURR have always yielded insertion times of 0.6 seconds or less.

Similar to the reactor SAR analysis, the Reactivity Transient Analysis program PARET (V7.5), maintained and distributed by the Nuclear Engineering Division of Argonne National Laboratory (ANL) was used. For the Insertion of Excess Reactivity accident analysis, two (2) channels were modeled in PARET; a hot channel representing worst-case conditions inside the core and an average channel representing the rest of the core experiencing "average" conditions. As indicated earlier, the transient was started from an initial power level of 11.5 MW with core coolant flow rate as well as core coolant inlet temperatures set at their LSSS values of 3,200 gpm and 155 °F, respectively. Also, pressurizer pressure was at 75 psia (LSSS value). Since the Insertion of Excess Reactivity transient was analyzed from a

starting power level of 11.5 MW, the rod run-in that would be initiated by the rod run-in system at 11.5 MW was bypassed and only the high power scram set point of 12.5 MW was modeled. Also, a delay of 150 milliseconds was incorporated into the CB scram model so that the CBs would only start to insert 0.15 seconds after the power level had exceeded the scram set point of 12.5 MW.

The results of a step reactivity insertion of 600 pcm (+0.006 Δk/k) are shown below in Figure 75. As expected, due to the higher starting core power level, much lower core coolant flow rate and much higher than normal core coolant inlet temperature conditions assumed for this updated analysis, the peak power during the transient momentarily reaches approximately 37.4 MW compared to a value of approximately 33.0 MW reported in prior SAR analyses for the same 600 pcm step reactivity insertion.

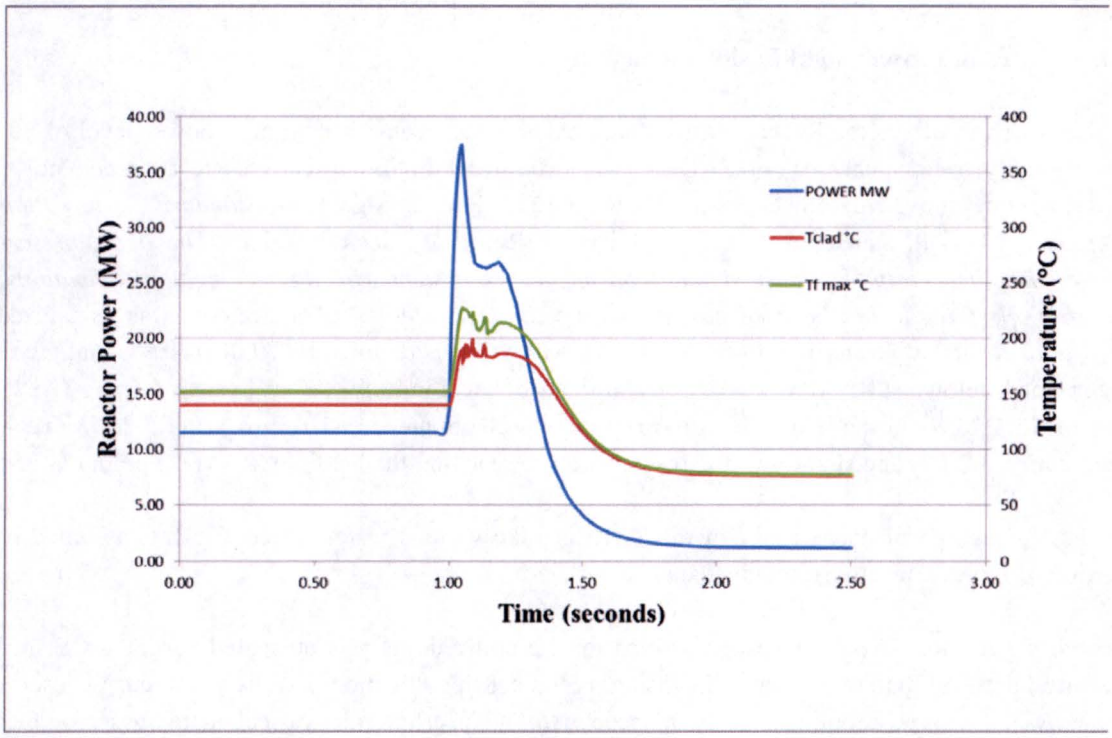

Figure 75
Reactor Power, Fuel and Cladding Temperatures vs. Time
for a Positive Reactivity Step Insertion of 0.006 Δk/k

The power generation in the TAs would follow the same proportional power transient that the reactor core experiences because the TAs are driven by the neutron flux generated by the reactor core.

The target rod analysis for the positive reactivity step insertion examines the maximum powered target rod at the beginning and end of a three-week irradiation. A steady-state analysis of the three-week irradiation was performed using FRAPCON to establish the initial conditions for the transient analysis. The FRAPCON analysis assumed that the first and last day of the three-week irradiation are at 115% power and the rest of the operating period is at 100% power. The FRAPCON analysis also

assumes that the TA flow rate is 85% of nominal during the first and last day of operation. Mid-week and weekend shutdowns are also included in the power history of the TA. The transient analysis was performed using the FRAPTRAN code. FRAPCON and FRAPTRAN are two NRC-sponsored computer codes that can model the steady-state and transient thermal-mechanical behavior of light water reactor oxide fuel. Phenomena modeled by the codes include heat transfer through fuel and cladding to coolant, cladding elastic/plastic deformation, fuel-cladding mechanical interaction, fission gas release, rod internal pressure, and cladding oxidation.

The FRAPCON steady-state analysis defines the burnup, UO_2 and cladding deformation, and fission gas release that form the starting point for the FRAPTRAN analysis. The FRAPTRAN analysis increases the power to 115% and decreases the flow rate to 85% within 40 seconds. Twenty-one seconds later, the 600 pcm (+0.006 Δk/k) step reactivity insertion is simulated. The target cooling water inlet temperature to the TA was assumed to be at 102 °F (38.9 °C) which corresponds to an outlet temperature at the maximum pool temperature of 120 °F (48.9 °C) during nominal conditions. The maximum cladding strain occurs with the minimum gap tolerance of [redacted] The maximum cladding strain also occurs at the end of the [redacted] due to the effects of burnup on gap closure and fission gas release. The FRAPCON and FRAPTRAN analysis also use the maximum tolerance on the scallop diameter that forms the flow area of the target cartridge. This tolerance results in the minimum coolant velocity consistent with the minimum gap. The analysis also uses the maximum pellet outer diameter, minimum cladding inner diameter, and maximum cladding thickness. The strain transient that the cladding is predicted to undergo during the positive step reactivity insertion is shown in Figure 76. The hoop strain increases from about 0.61% to just over 0.79% but remains under the 1% strain limit.

5a, b, f

Maximum temperatures occur with the maximum gap tolerance of [redacted] rather than the minimum gap tolerance. Burnup effects reduce the gap so that the maximum pellet temperature occurs at the beginning of irradiation. The analysis also uses the minimum pellet outer diameter, maximum cladding inner diameter, maximum cladding thickness, and maximum cladding outer diameter in order to obtain the maximum gap tolerance or to maximize peak pellet temperature. The peak target temperature transient is shown in Figure 77. The peak target temperature increases from 2541 °C (2743 °F) to 2743 °C (4969 °F) in less than 0.4 seconds. This peak UO_2 temperature is 97 °C (175 °F) below the melting temperature of 2840 °C (5144 °F).

5a, b, f

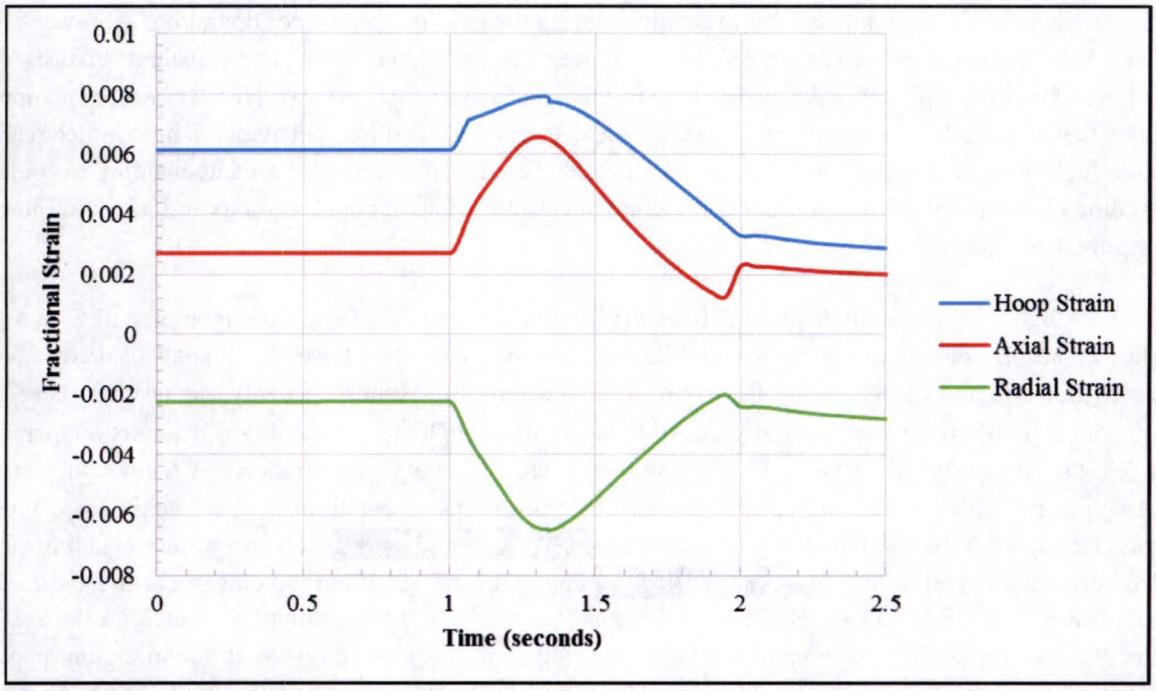

Figure 76
Cladding Strains at Peak Pellet Location During a Positive 0.006 Δk/k Reactivity Insertion

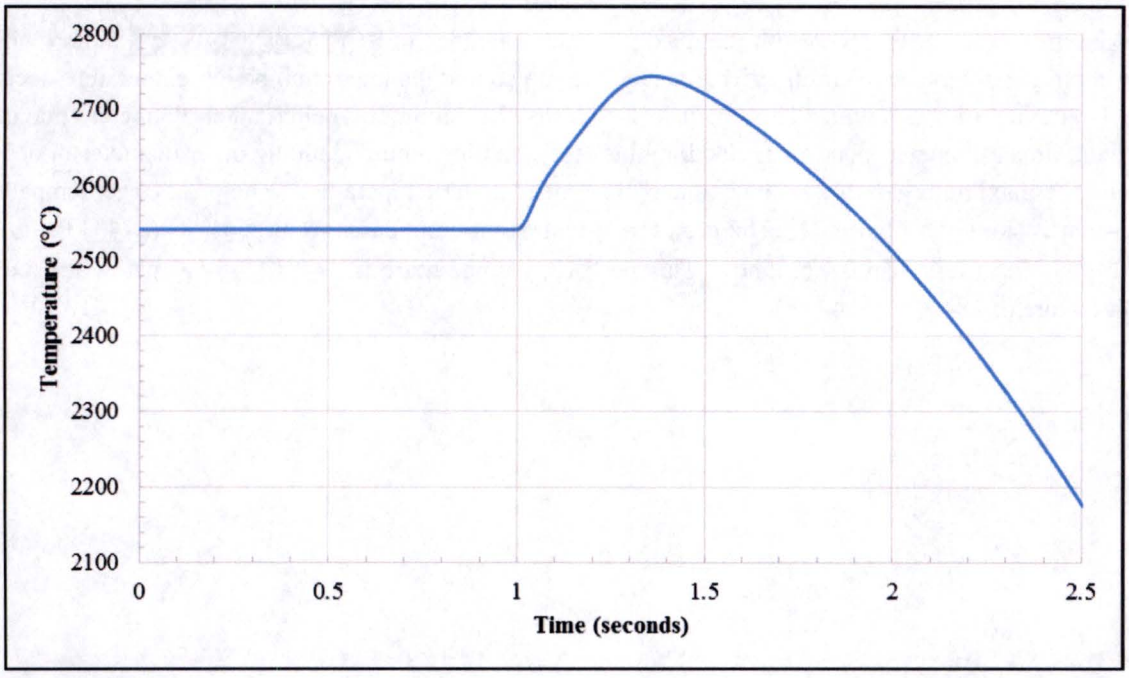

Figure 77
Peak Target Pellet Temperature During a Positive 0.006 Δk/k Reactivity Insertion

The pellet outer diameter and cladding inner and outer diameter temperature at the axial location where the peak pellet centerline temperature occurs is shown in Figure 78. The cladding outer diameter temperature shows a modest increase in temperature of around 17 °C (31 °F). The pellet outer diameter and cladding inner diameter temperatures become more closely coupled due to closure of the gap between the pellet and cladding and an increase in interface pressure. Cladding hoop strain for the [redacted] gap at the end of irradiation goes through a similar transient as for the [redacted] gap but increases from 0.28% to just under 0.60%. 5a, b, f

Peak heat generation within the target pellets is a factor of 3.74 greater than nominal. Heat capacity and thermal resistances result in the surface heat flux at the peak location being only a factor of 1.52 to 1.75 greater than nominal, depending on the initial gap size and burnup conditions. FRAPTRAN assesses critical heat flux (CHF) using one of five different CHF correlations. The Macbeth CHF correlation was chosen because of its validity at low pressures. The Macbeth CHFR reaches a minimum value of between 2.25 and 2.53 depending on initial gap size and burnup conditions. The Bernath CHFR reaches a minimum of 1.56 to 1.76 depending on the case. No target rod damage or radiological release would occur from this accident.

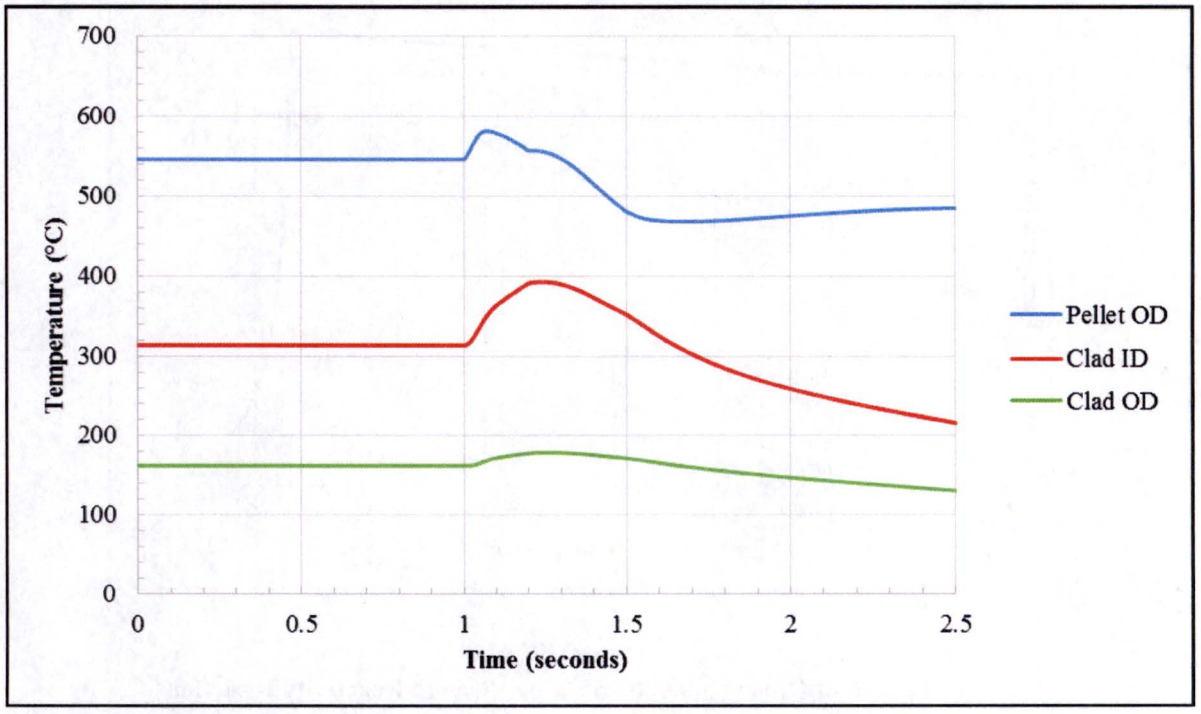

Figure 78
Pellet OD and Cladding Temperatures (ID and OD) at Peak Pellet Location During a Positive 0.006 Δk/k Reactivity Insertion

10.3 Control Blade Withdrawal

As presented in Section 13.2.2.1.2 of the MURR SAR, a positive reactivity ramp insertion rate of 0.0003 Δk/k/s, which is the Technical Specification limit on the maximum rate of reactivity insertion for all four (4) shim CBs operating simultaneously, was introduced to the reactor starting at subcritical cold conditions and at an initial power level of 10 MW. For subcritical cold conditions, the short period reactor scram terminates the transient within 150 sec before the power has reached 64 watts. No target pellet or cladding damage would occur at such a low power.

For full power conditions, the high power reactor scram terminates the transient after 4.53 seconds when reactor power rises from 10.0 MW to the 12.5 MW high power scram set point. The thermal-mechanical performance of the target rod during this transient was analyzed using FRAPCON and FRAPTRAN. The power transient that drives the heat generation in the target rods is shown in Figure 79. The figure includes 1 sec of steady-state operation at 100% power and the power transient after reactor SCRAM.

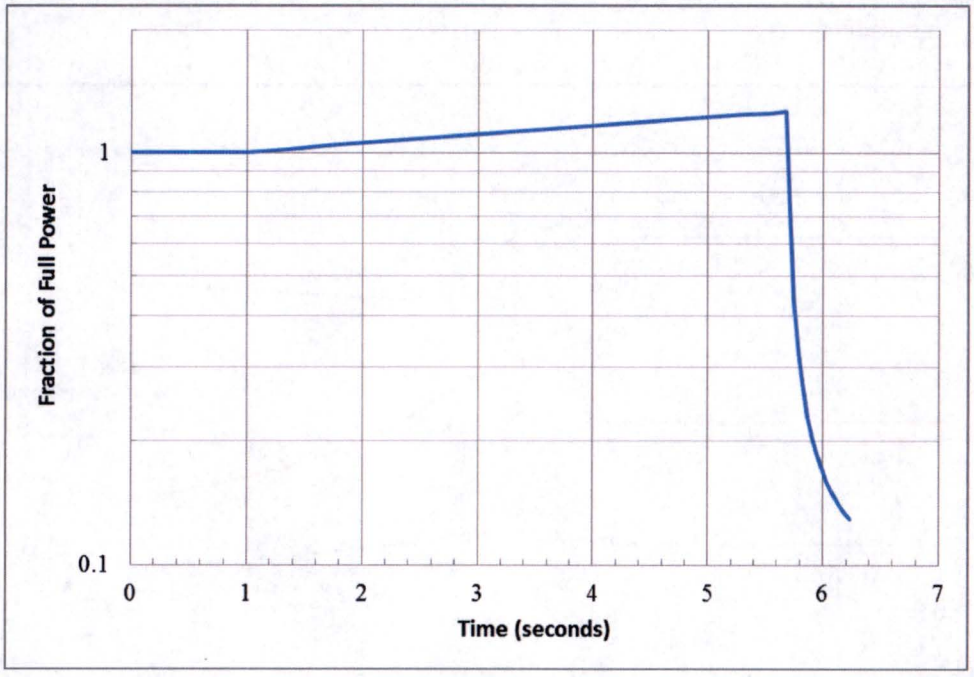

Figure 79
Power Transient During a 0.0003 Δk/k per Second Reactivity Insertion

The target rod analysis for the CB withdrawal examines the maximum powered target rod at the beginning and end of a three-week irradiation. A steady-state analysis of the three-week irradiation was performed at 100% power using FRAPCON to establish the initial conditions for the transient analysis. The FRAPCON analysis also assumes that the TA flow rate is 100% of nominal during the three-week irradiation. Mid-week and weekend shutdowns are also included in the power history for the TA.

The FRAPCON steady-state analysis defines the burnup, UO_2 and cladding deformation, and fission gas release that form the starting point for the FRAPTRAN analysis. The maximum cladding strain occurs with the minimum gap tolerance of [redacted]. The maximum cladding strain also occurs at the end of the three week irradiation due to the effects of burnup on gap closure and fission gas release. The strain transient that the cladding is predicted to undergo during the control blade withdrawal is shown in Figure 80. The hoop strain increases from about 0.28% to just under 0.61% but remains well under the 1% strain limit.

5a, b, f

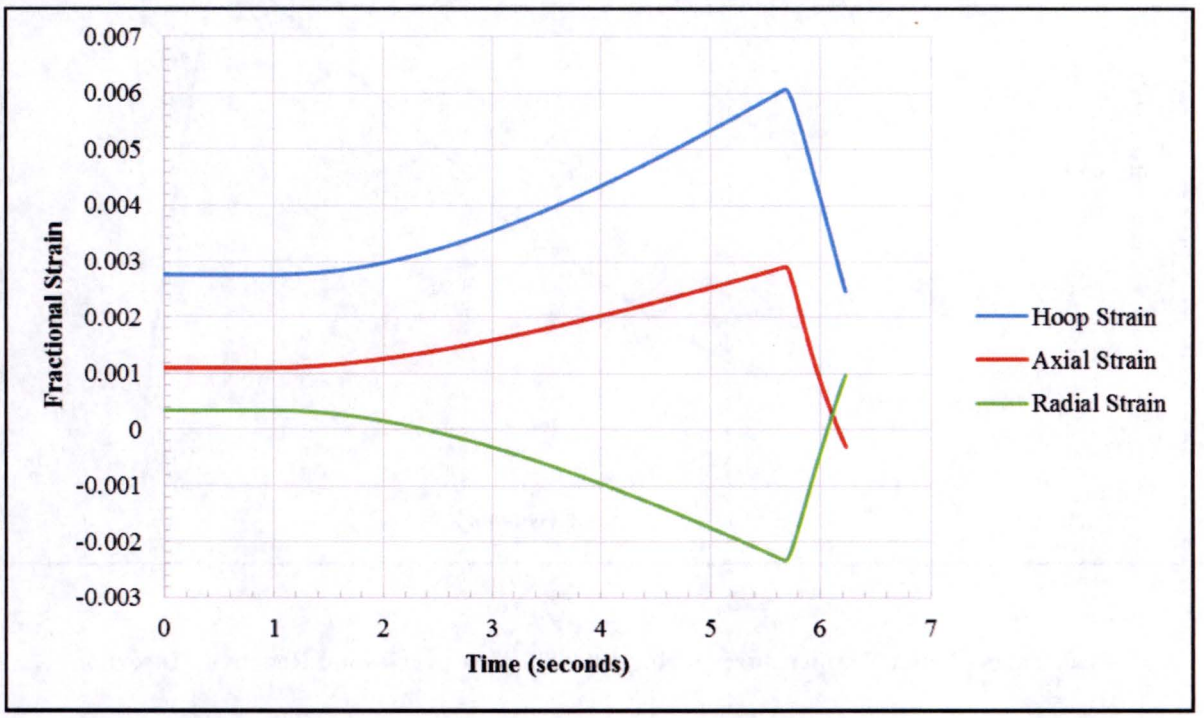

Figure 80
Cladding Strains at Peak Pellet Location During a 0.0003 Δk/k per Second Reactivity Insertion

For the case using the [redacted] gap between the pellet and cladding, the pellet centerline temperature increases just over 300 °C (540 °F) to 2375 °C (4307 °F) at the end of irradiation. The temperature of the cladding inner diameter increases to just under 315 °C (599 °F), and the cladding outer diameter temperature increases by less than 8 °C (14 °F).

5a, b, f

The FRAPTRAN analysis of the [redacted] gap case predicts the maximum pellet temperatures due to the higher thermal resistance between the pellet and cladding. The maximum pellet temperature increases from 2327 °C (4221 °F) to 2563 °C (4645 °F) at the beginning of irradiation as shown in Figure 81. The pellet outer diameter and cladding inner and outer diameter temperature at the axial location where the peak pellet centerline temperature occurs is shown in Figure 82. The pellet outer diameter and cladding inner diameter temperatures become more closely coupled due to closure of the gap between the pellet and cladding and an increase in interface pressure. The cladding inner diameter

5a, b, f

temperature shows a modest increase in temperature of around 35 °C (63 °F) to just over 321 °C (610 °F). Cladding hoop strain goes through a similar transient as shown in Figure 80 but increases from 0.13% to just over 0.14%.

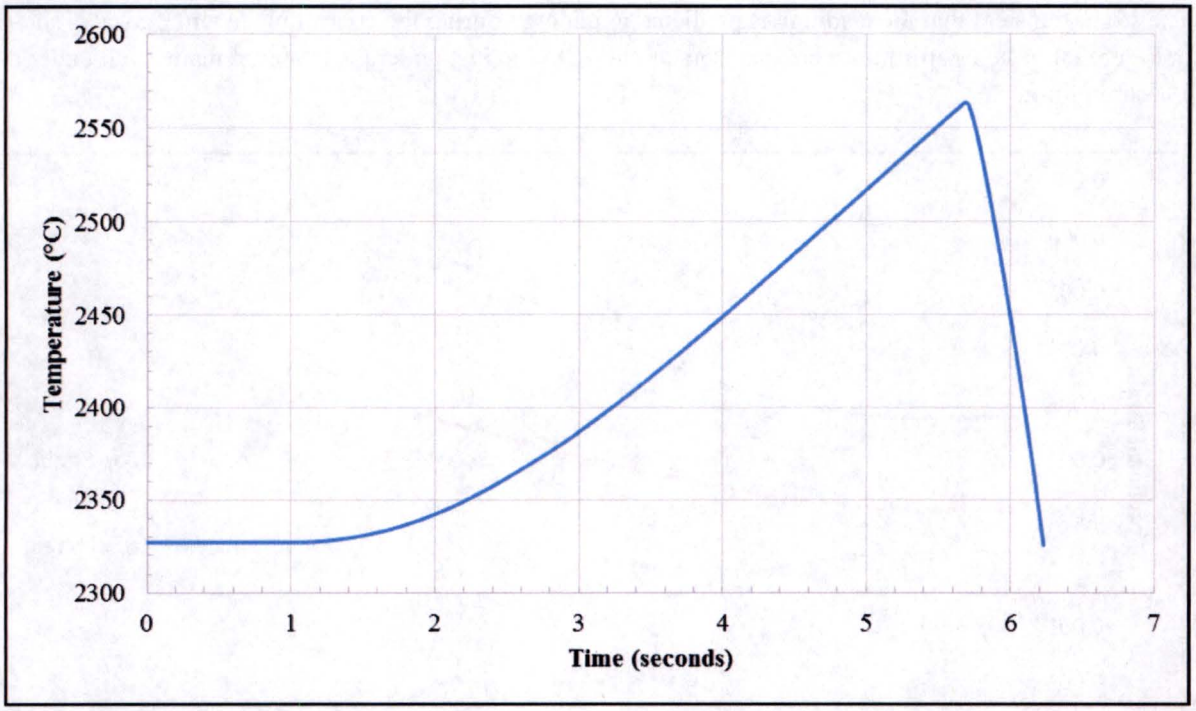

Figure 81
Peak Target Pellet Temperature During a 0.0003 Δk/k per Second Reactivity Insertion

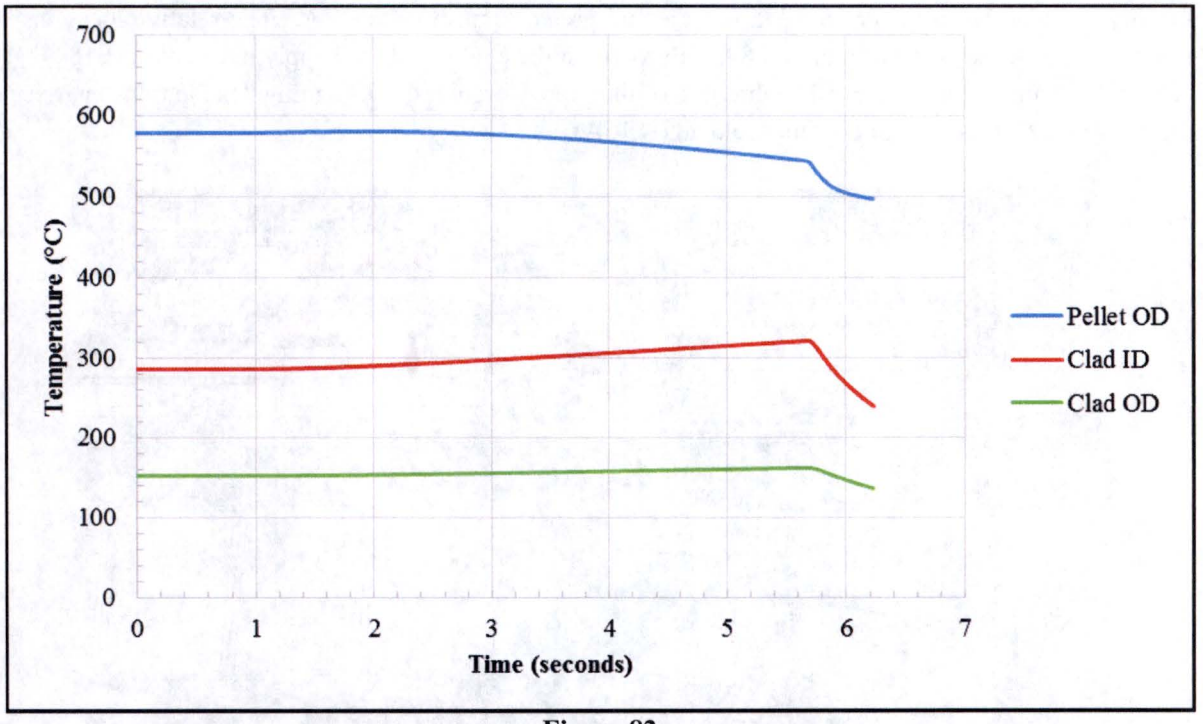

Figure 82
Pellet OD and Cladding Temperatures (ID and OD) at Peak Pellet Location During a 0.0003 Δk/k per Second Reactivity Insertion

10.4 Loss of Target Coolant

This accident assumes the double-ended break of one of the pipes in the TCS. The design and operation of the TCS are described in Section 3.

Pipe breaks can occur in a variety of locations either in or out of the reactor pool. Depending on the location of the break, the loss of coolant will cause either an increase or a decrease in flow at the flow sensors on either pipe leg supplying cooling water to the two (2) TAs. The hi/low flow set points are at 115% and 85% of nominal flow and result in a reactor scram and opening of the decay heat removal valves (natural circulation) located just above the refueling bridge level. Pump coast-down after pump trip can mitigate the early phase of the transient unless the offset pipe break prevents pump flow from reaching the TA.

Pipe breaks in the reactor pool differ from pipe breaks out of the reactor pool (in air) because the decay heat removal valves are assumed to not operate. A pipe break in the pool establishes a natural circulation loop between the TA and reactor pool regardless of whether the decay heat removal valves open. If the break is in the air, a natural circulation loop is only established if the decay heat removal valves open. Otherwise, the break prevents pool water from reaching the TA inlet and establishing a natural circulation loop.

The pipe break before the wye affects both TAs but a pipe break downstream of the wye at the joint with the flexible pipe has a lower cold leg volume and greater impact on the TA. The relative locations of these pipe breaks are shown in Figure 83. The water in the cold leg of the supply line is almost 18 °F (10 °C) cooler than the pool water. The draining of this water through the TAs mitigates the transient during the early phase of the loss of coolant accident (LOCA).

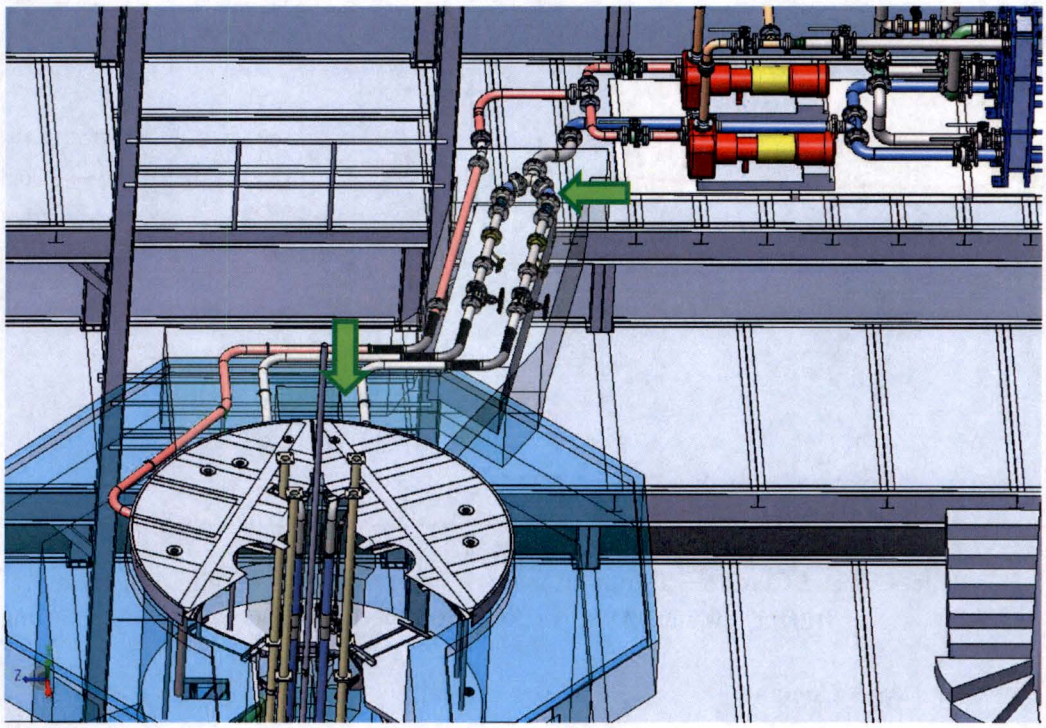

Figure 83
Pipe Break Locations Out of the Reactor Pool

Pipe breaks out of and in the reactor pool are covered in the accident analyses that follow.

10.5 Pipe Break Locations Out of the Reactor Pool

The pipe break in air just after the flexible pipe is a more credible pipe break than other locations closer to the TA because the joint is more vulnerable and the remaining pipe is of welded construction. The upper bridge structure protects the pipes where they bend downward into the reactor pool. The break is analyzed to occur in the supply line to TA 2 because it has the target rod with the highest power density, and the target rod with the highest power in addition to being the TA with the most power.

The LOCA for the SGE TEF was modeled using RELAP5 mod3.3 patch 03. RELAP5 was developed by the NRC to analyze thermal-hydraulic transients in pressurized water reactors. It can be used to analyze a variety of geometries and was used to analyze the LOCA and Loss of Flow Accident (LOFA) in Sections 13.2.3 and 13.2.4 of the MURR SAR for relicensing. The RELAP5 model for this accident

includes both TAs, TCS pump and heat exchanger, and decay heat removal valves. The double-ended guillotine rupture is modeled with three (3) valves – two of the valves connect to the reactor pool on either side of the break, and the third valve connects the two ends of the pipe across the break. Prior to accident initiation, the valves to the reactor pool are closed and the valve across the break is open. When the break is initiated, the valve connecting the two (2) pipe ends is closed and the two (2) valves from each end connected to the reactor pool are opened. All three (3) valves are assumed to completely change position in 0.5 seconds which is a reasonable assumption for a mechanically induced failure that displaces the two (2) ends of the pipe since the piping is not at high pressure.

The flow transient caused by a LOCA resulting from a double-ended pipe break is shown in Figure 84. The transient analysis starts with the reactor and TAs at 100% power and the TCS at 100% nominal flow to accurately simulate the expected response of the protection system. The decay heat removal valves are assumed to not operate. The break causes an increase in the flow measurement in the pipe supplying TA 2 and a decrease in the flow rate supplying TA 1.

The reactor is scrammed at 0.05 seconds when the mass flow rate to TA 2 is greater than 115%. A low flow signal occurs shortly thereafter at 0.08 seconds for TA 1 when its flow rate is less than 85%. The operator is assumed to immediately trip the TCS water pump on the high flow alarm. CB movement is delayed by 0.15 seconds after the reactor scram signal is generated. The mass flow entering TA 2 falls quickly because of the pipe break. The flow through TA 1 remains above [redacted]. The flow through TA 2 drops below [redacted] at around 9 seconds and experiences several slow flow reversals between 10 and 40 seconds after which boiling and chugging within both TAs is predicted.

5a, d, e, f

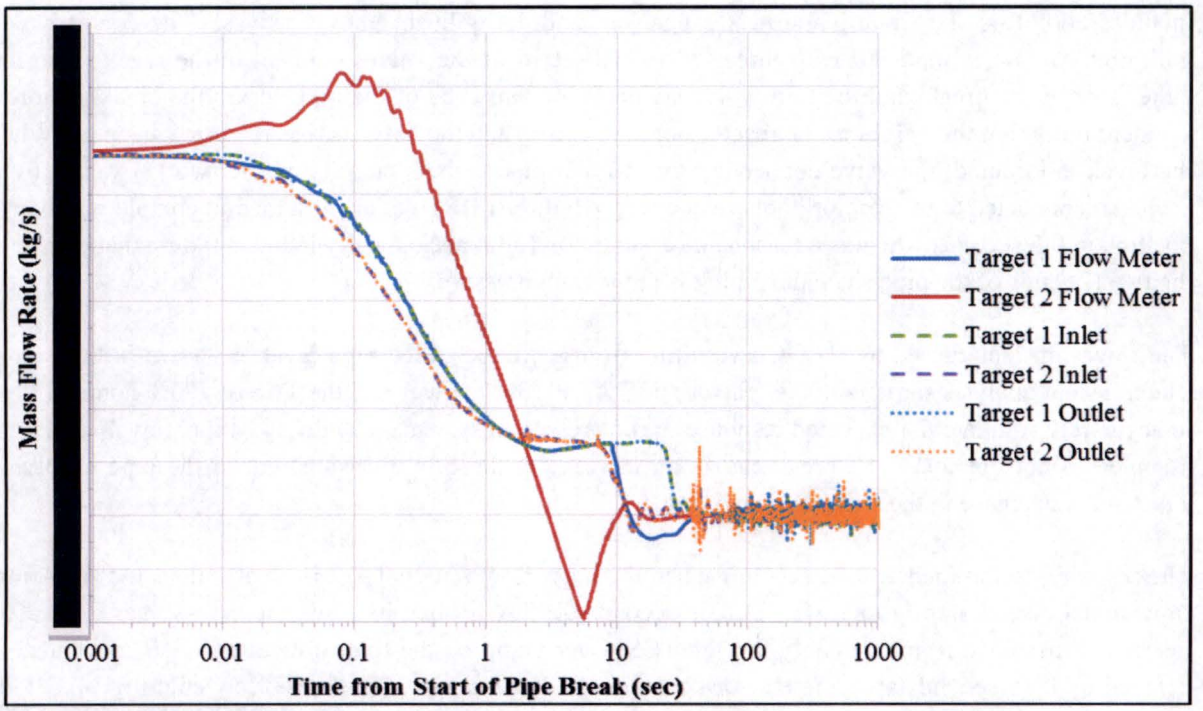

5a, d, e, f

Figure 84
Mass Flow Transient During a LOCA in Air Without Decay Heat Removal Valves Opening

In TA 2, target rod 17 has the maximum peak power density and rod 22 has the maximum rod power. In TA 1, rod 5 has the maximum peak power density and rod 6 has the maximum rod power though both rods are lower in power than the rods in TA 2. The heat generation in the target rods is shown in Figure 85. The heat generation drops at around 0.20 seconds when the CBs start inserting. The heat removal from the target rods presented in Figure 87and Figure 89 shows that stored energy removal is significant over the first 10 seconds. Mass flow oscillations due to chugging and boiling are also reflected in the oscillations in heat removal.

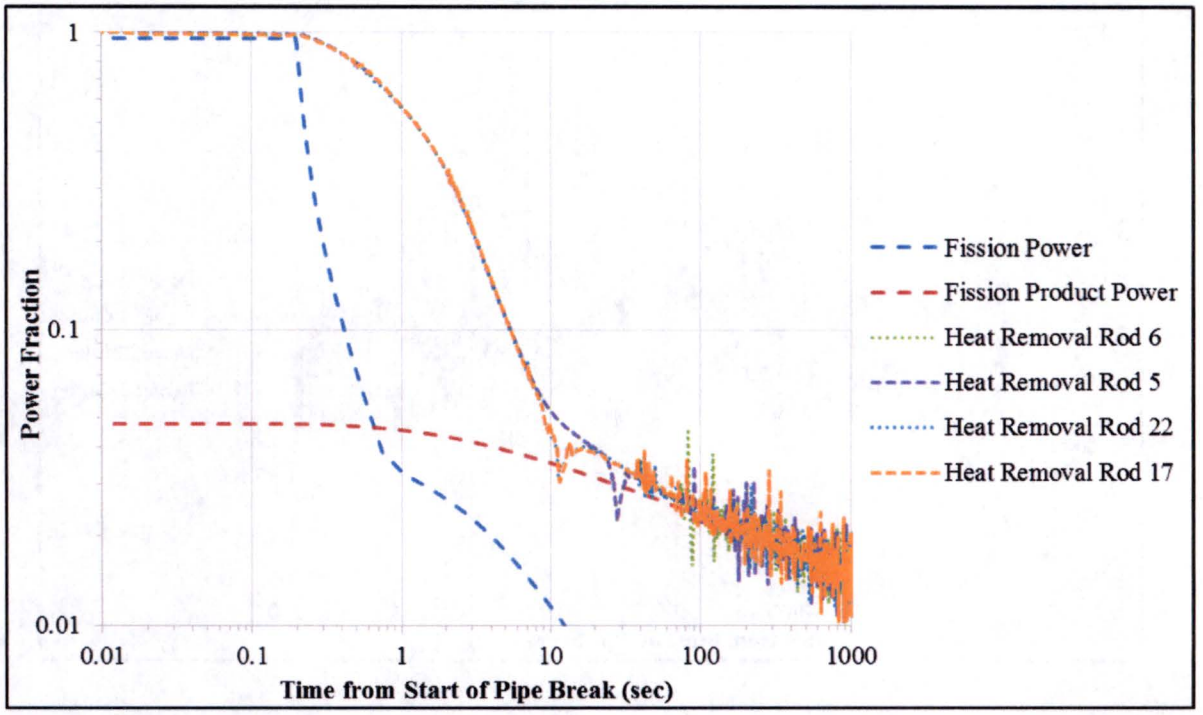

Figure 85
Target Power During a LOCA in Air Without Decay Heat Removal Valves Opening

Coolant temperatures at the inlet and outlet of the two (2) TAs are presented in Figure 86. Mass flow out of the TAs due to boiling are represented by outlet temperatures between 70 and 100 °C (160 and 212 °F). Mass flow back into the TAs are represented by the lower bounds of the temperature oscillations around 50 °C (120 °F). These flow oscillations also move water and thermal energy to the TA entrance which slowly raises that temperature.

Pellet centerline temperatures do not increase during this LOCA because of the reactor scram signal at 0.05 seconds, the UO_2 heat capacity, and the water flow through the TA caused by draining of the cooling line. The maximum temperatures of the cladding inner diameter (ID) are shown in Figure 87. The cladding ID temperature increases by 3.0 °C (5.4 °F) prior to CB insertion and afterwards, is lower than normal operating temperature. The increases in cladding ID temperature at around 10 and 30 seconds coincide with the decreases in flow rate at those times. Boiling within the TAs keeps the maximum cladding temperature just above saturation temperature.

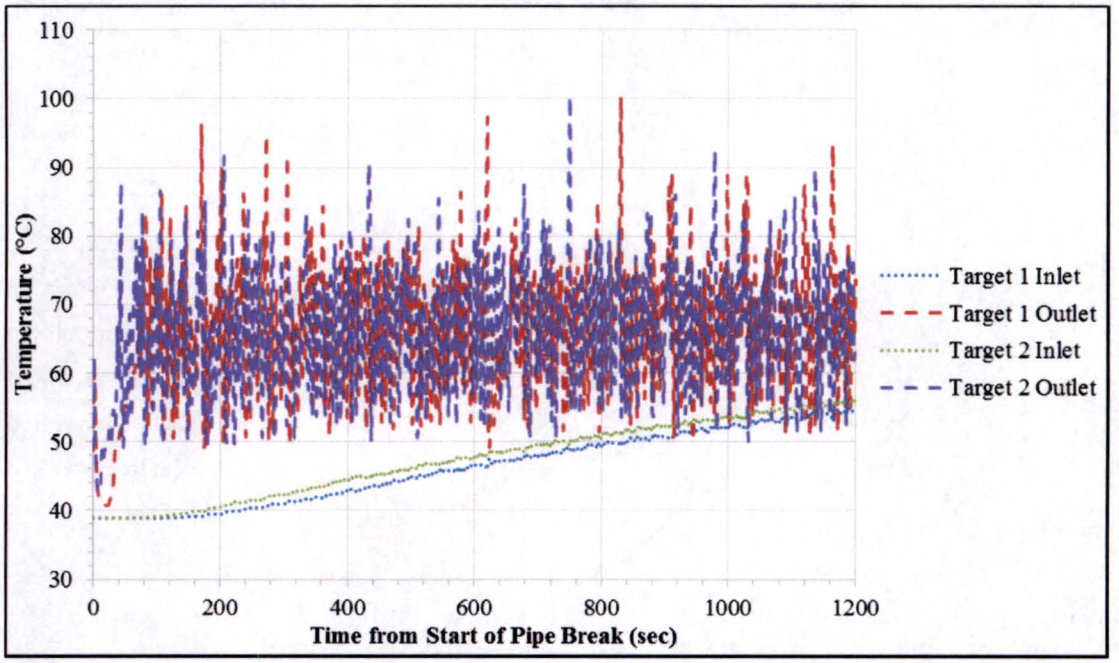

Figure 86
Coolant Temperatures During a LOCA in Air Without Decay Heat Removal Valves Opening

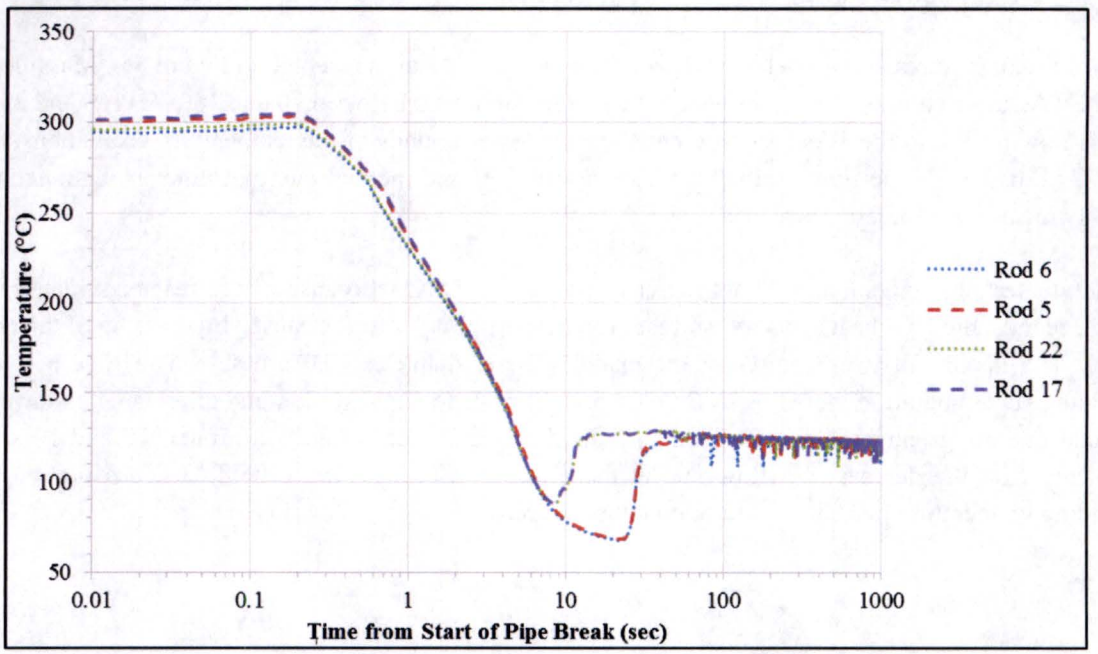

Figure 87
Maximum Cladding ID Temperatures During a LOCA in Air Without Decay Heat Removal Valves Opening

Because the pellet and cladding temperatures are near normal values, all cladding stresses and strains are also normal. Therefore, there is no cladding breach and no release of radioactivity associated with this LOCA.

If the one of the two decay heat removal valves for each TA were to operate, the consequences of the LOCA in air are even less significant. The flow transient due to a LOCA in air with the decay heat removal valves working is shown in Figure 88. The TA inlet flow is the same as the TA outlet flow and a small natural circulation flow is established after 20 seconds. TA 1 flow rate is higher around 10 seconds due to a small contribution of pump coast-down through the intact supply line to TA 1.

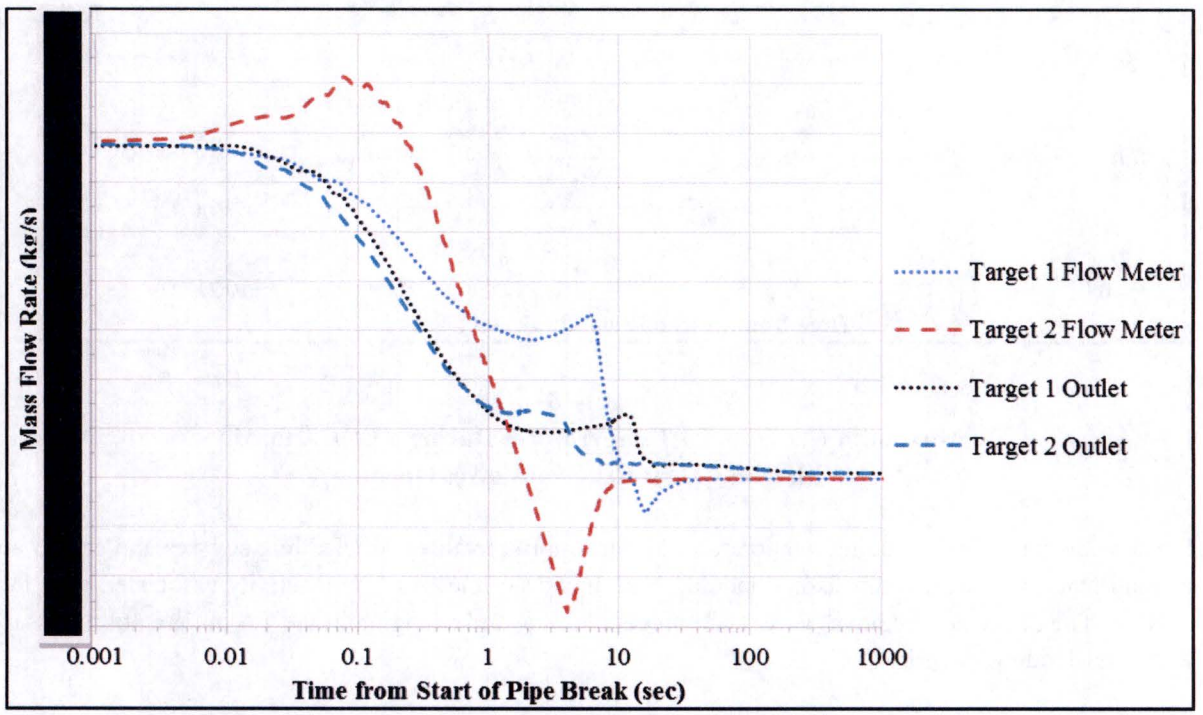

5a, d, e, f

Figure 88
Mass Flow Transient During a LOCA in Air With Decay Heat Removal Valves Opening

Pellet centerline temperatures also do not increase during this LOCA. The maximum temperatures of the cladding ID are shown in Figure 89. The cladding ID temperature increases by 3.0 °C (5.4 °F) prior to control blade insertion and afterwards, is lower than normal operating temperature. Natural circulation is sufficient to prevent chugging and cladding temperatures steadily decrease after 20 seconds. Peak vapor fraction is less than 1%.

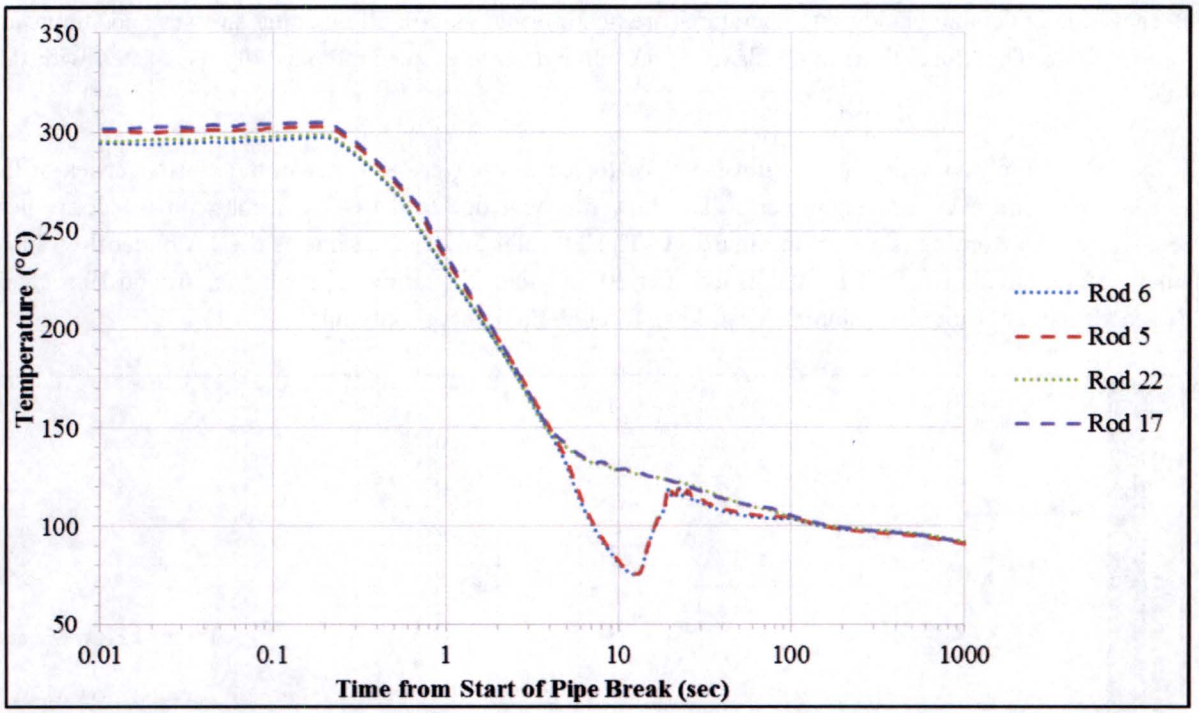

Figure 89
Maximum Cladding ID Temperatures During a LOCA in Air
With Decay Heat Removal Valves Opening

Because the pellet and cladding temperatures are near normal values, all cladding stresses and strains are also normal. Therefore, there is no cladding breach and no release of radioactivity associated with this LOCA. The decay heat removal valves can prevent boiling and chugging in the TA but are not necessary to assure cladding integrity.

10.6 Pipe Break Locations in the Reactor Pool

The target cooling lines supplying water to the TAs are protected by the upper bridge structure above the pool and the refueling bridge located below the normal pool water level. The cooling lines also have lateral supports and are joined to the TA by a flexible joint. It is nearly incredible to postulate a mechanistic failure of these cooling pipes which results in a complete offset rupture within the assumed rupture time of 0.5 sec. If the break occurs near the decay heat removal valves then it is essentially the same as opening the decay heat removal valves. The worst possible break location is the connection between the inlet pipe welded to the target housing and the flexible pipe as shown in Figure 90. Direct mechanical interaction in this area is very unlikely due to the congestion around this elevation.

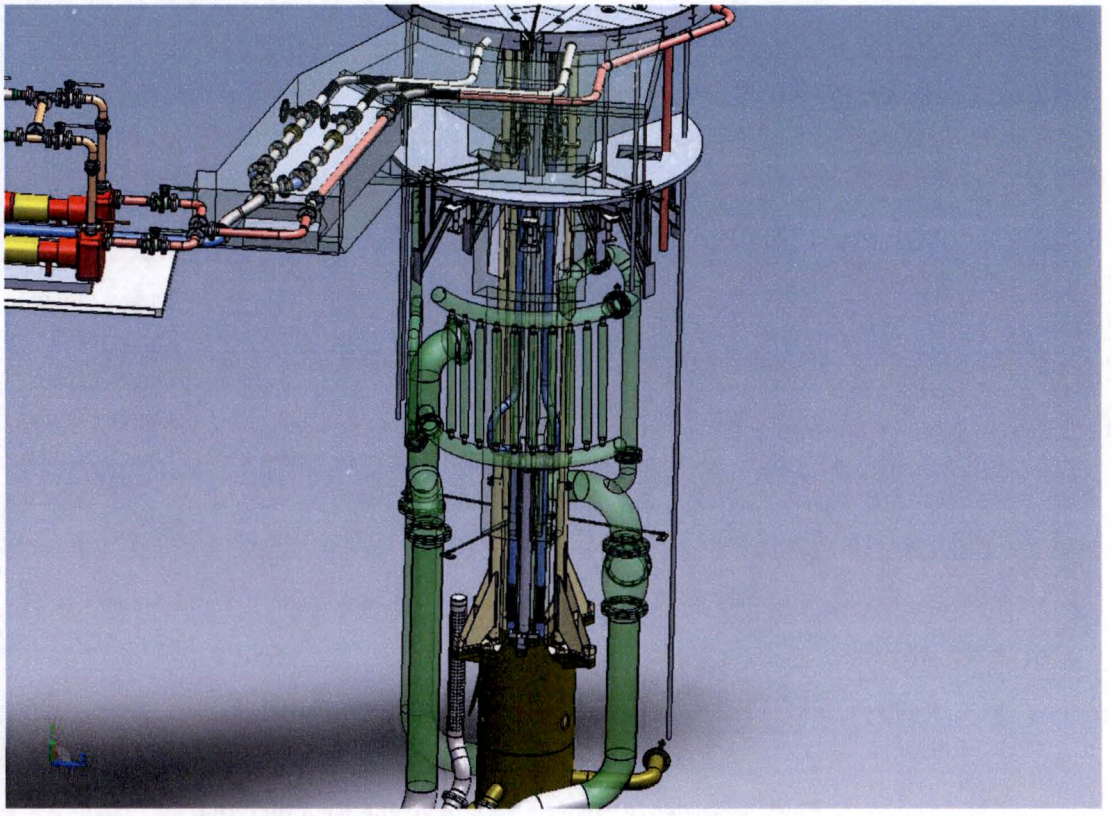

Figure 90
Pipe Break Location in the Reactor Pool

The LOCA in water used the same RELAP5 model as the LOCAs in air except that the break location was relocated as shown in Figure 90. The break time to complete offset rupture was also kept at 0.5 seconds although it is more likely that the break time would be either longer underwater or less than a complete offset rupture.

The flow transient caused by a LOCA in water resulting from a double-ended pipe break is shown in Figure 91. The transient analysis starts with the reactor and TA at 100% power and the TCS at 100% nominal flow to accurately simulate the expected response of the protection system. The decay heat removal valves are assumed to not operate though their operation would be ineffective in this accident. The break causes an increase in the flow measurement in the pipe supplying TA 2 and a decrease in the flow rate supplying TA 1.

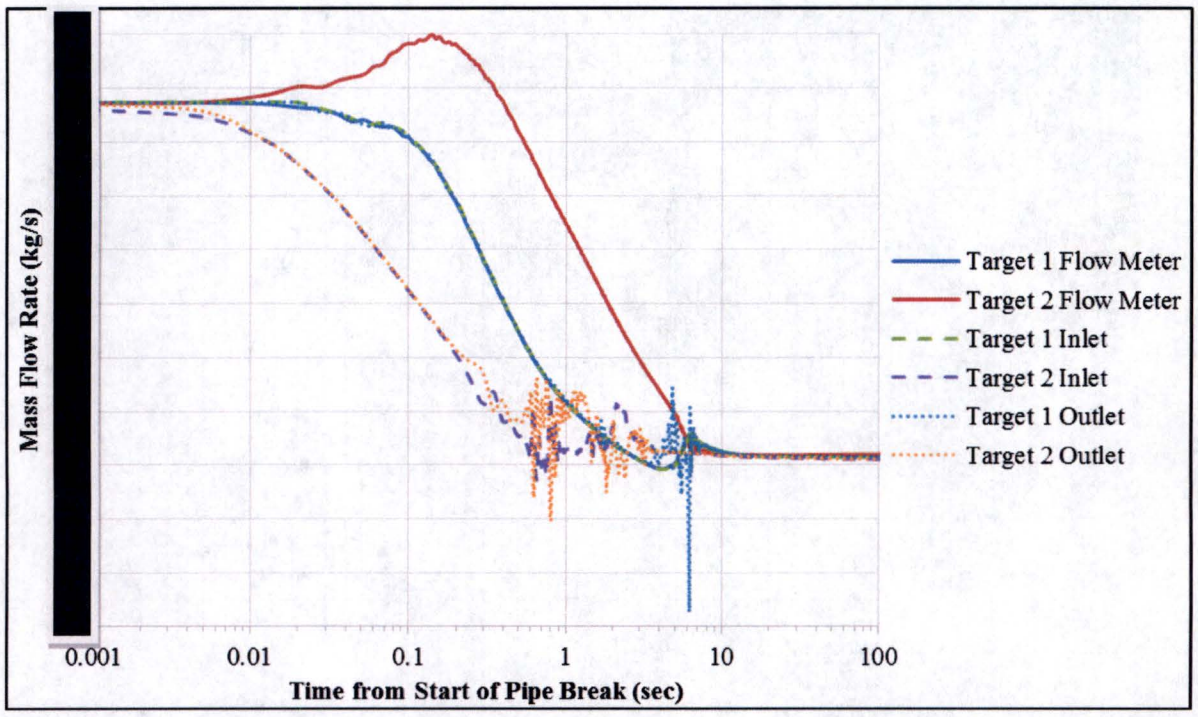

5a, d, e, f

Figure 91
Mass Flow Transient During a LOCA in the Reactor Pool

The reactor is scrammed at 0.09 seconds when the mass flow rate to TA 2 is greater than 115%. A low flow signal occurs shortly thereafter at 0.13 seconds for TA 1 when its flow rate is less than 85%. CB movement is delayed by 0.15 seconds after the reactor scram signal is generated. The mass flow entering TA 2 falls quickly because of the pipe break. The flow through TA 2 drops to zero at around 0.6 seconds and experiences several boiling and chugging oscillation for the next few seconds. The flow through TA 1 remains above zero for about 3 seconds before it also demonstrates some boiling and chugging oscillations. Natural circulation through TA 2 after 6 seconds is sufficient to prevent further boiling and chugging.

The heat generation in the target rods is shown in Figure 92. The heat generation drops at around 0.24 seconds when the CBs start inserting. Brief periods of transition and film boiling occur at the high heat flux locations of the target rods. The heat removal from the target rods presented in Figure 92 shows that stored energy removal is significant over the first 10 seconds. Mass flow oscillations due to chugging and boiling are also reflected in the oscillations in heat removal and occur while significant stored energy remains to be removed.

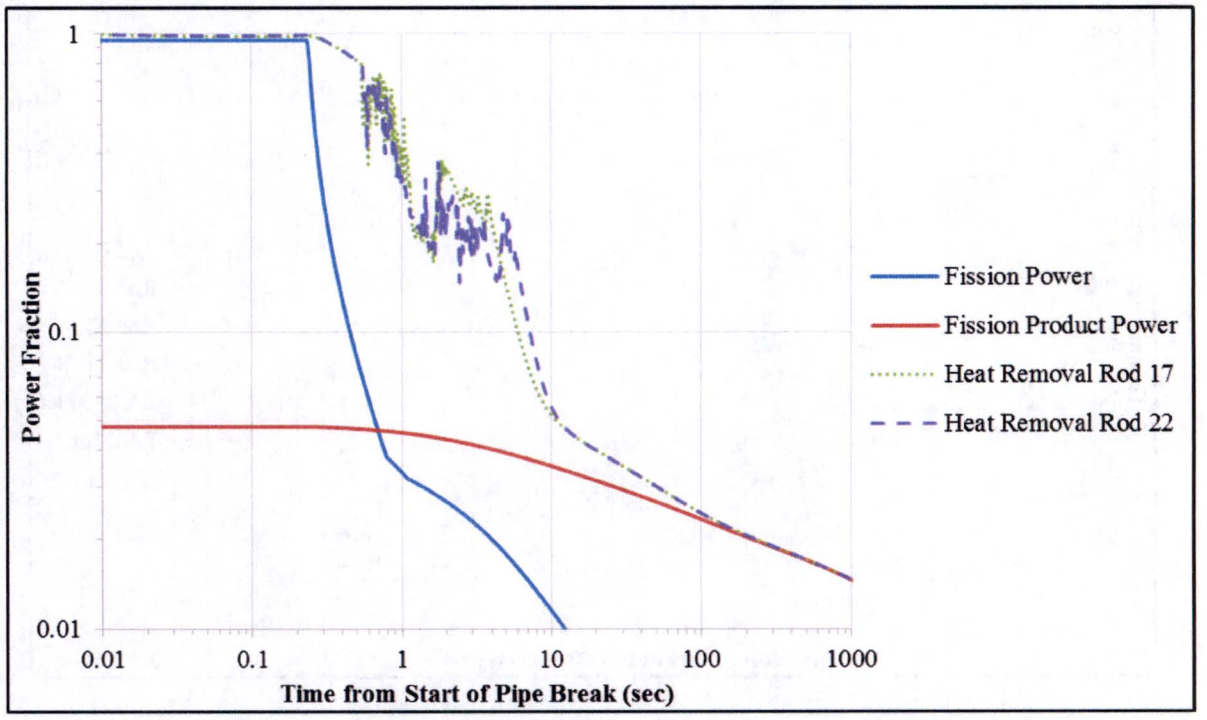

Figure 92
Target Power During a LOCA in the Reactor Pool

The maximum temperatures of the cladding ID and coolant entering and exiting TA 2 are shown in Figure 93. Cladding temperatures start experiencing rapid increases at around 0.6 seconds which corresponds to the rapid drop in flow rate. Peak cladding temperatures reach 849 °C (1560 °F) in target rod 22 and 827 °C (1520 °F) in target rod 17. Peak cladding temperatures in rods 5 and 6 steadily decline after the reactor scram except for a brief temperature excursion of around 100 °C (180 °F) between 6 and 7 seconds.

A FRAPTRAN analysis of cladding integrity during this LOCA in water transient was performed using minimum and maximum pellet-clad gap tolerances of [redacted] Cladding OD temperatures as a function of time and axial location were obtained from RELAP5 and used as the boundary condition for the FRAPTRAN analysis. FRAPCON results used in the insertion of excess reactivity transient analysis were used to define the burnup and fission gas release inputs for FRAPTRAN at BOL and EOL conditions. The maximum hoop strain occurs at EOL conditions in target rod 22 with the maximum gap tolerance of [redacted]. The cladding temperatures used in the FRAPTRAN analysis for rod 22 are presented in Figure 94. The maximum hoop strain of 0.54% at the peak strain location along with the radial and axial strains at that location are presented in Figure 95. These strains are much less than the 1% strain criteria so that cladding integrity is maintained.

5a, b, f

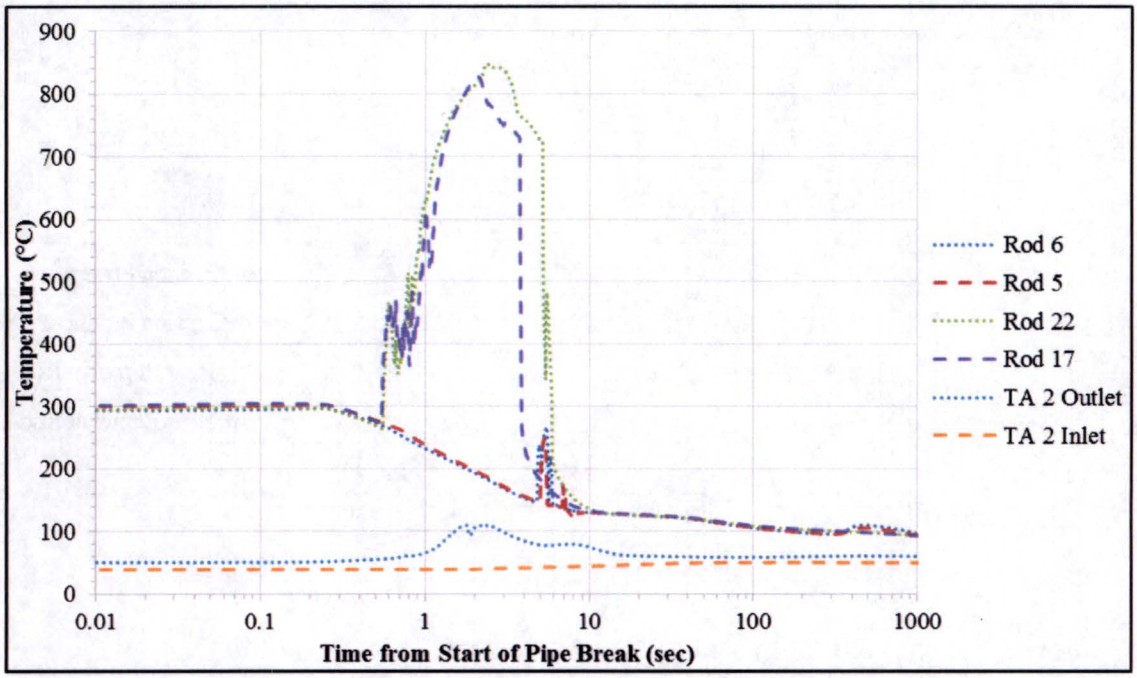

Figure 93
Maximum Cladding ID and Coolant Temperatures During a LOCA in the Reactor Pool

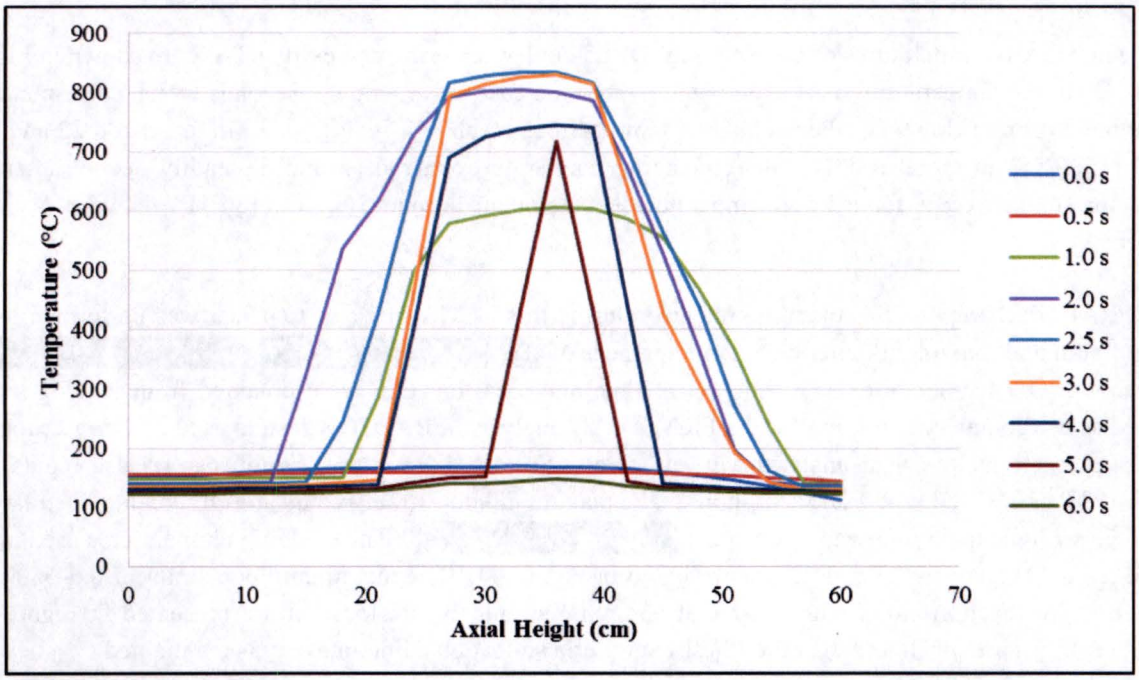

Figure 94
Cladding OD Temperature Profile in Target Rod 22 During a LOCA in the Reactor Pool

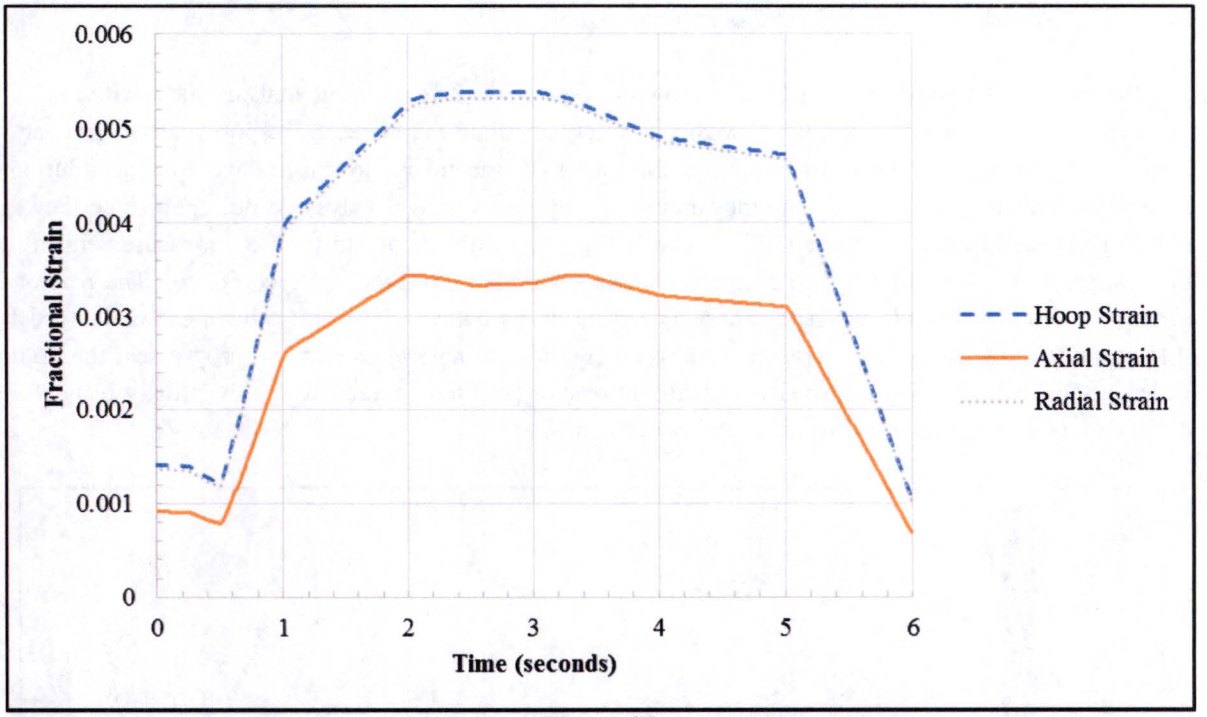

Figure 95
Cladding Fractional Strains in Rod 22 during a LOCA in the Reactor Pool

10.7 Loss of Target Flow

The loss of target flow accident can be initiated by inadvertent valve closures, pump failures, or loss of electrical power.

Pipe breaks discussed in the previous section also result in a loss of target flow. Inadvertent valve closure is prevented by securing the valves in the open position using a locking pin since there is no safety requirement associated with the operation of the manual isolation valves and they are only for maintenance purposes. Therefore, the most limiting initiating event is a loss of pump flow (LOPF) which can be caused by either loss of electrical power or pump failure. The LOPF event impacts both TAs and includes pump coast-down and fluid momentum to ease the transition from forced flow to natural circulation flow.

The TCS has redundant 100% capacity pumps. Only one of the pumps is required to operate and the other pump is an installed spare. If the operating pump fails, there is no automatic switchover to the backup pump. Redundant flow signals in the TCS will initiate protective actions including reactor scram when flow either reduces to 85% of nominal or increases to 115% of nominal. Additional actions taken due to the flow reduction are opening of the decay heat removal valves.

The LOPF was modeled using RELAP5 mod3.3 patch 03. The RELAP5 model is the same model used for the LOCA analyses described in Loss of Target Cooling.

The flow transient caused by this LOPF is shown in Figure 96. The transient analysis starts with the TCS at 100% power and 100% nominal flow to accurately simulate the expected response of the protection system. The LOPF accident is assumed to include a loss of secondary flow as one would expect during a loss of site power. The analysis assumes that the decay heat removal valves do not open since they are not an Engineered Safety Feature (ESF). The LOPF causes a decrease in the flow measurement in the pipes supplying TA 1 and TA 2. Pump coast-down takes about 10 seconds to complete. The reactor is scrammed at 0.14 seconds when the mass flow rate drops below 85%. CB movement is delayed by 0.15 seconds after the reactor scram signal is generated. As natural circulation progresses, the colder water in the TCS is slowly replaced with water at reactor pool temperature which eventually results in a decline in natural circulation flow at around 600 seconds.

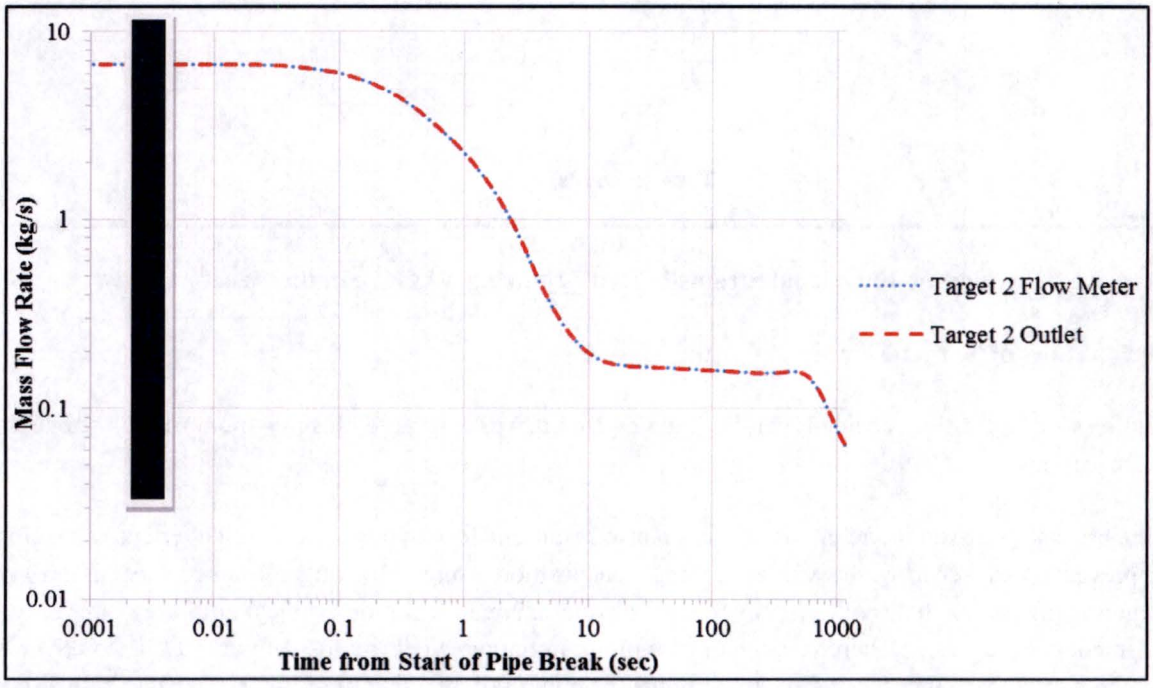

5a, d, e, f

Figure 96
Mass Flow Transient During Loss of Pump Flow

Maximum cladding ID temperatures and coolant temperatures are shown in Figure 97. Peak cladding temperatures rise slightly by 2.0 °C (3.6 °F) but then steadily decline after the reactor scram. Coolant exit temperature from TA 2 rises slightly at around 5 seconds and again after 600 seconds. At 600 seconds the inlet temperature starts to rise as reactor pool water has mixed with the cooler target cooling water. Eventually the TA inlet temperature will reach the maximum pool temperature of 50 °C (120 °F) at which point further increase in temperatures will cease.

Because the pellet and cladding temperatures are near normal values, all cladding stresses and strains are also normal. Therefore, there is no cladding breach and no release of radioactivity associated with this LOPF. The decay heat removal valves can improve the natural circulation cooling in the TA but are not necessary to assure cladding integrity.

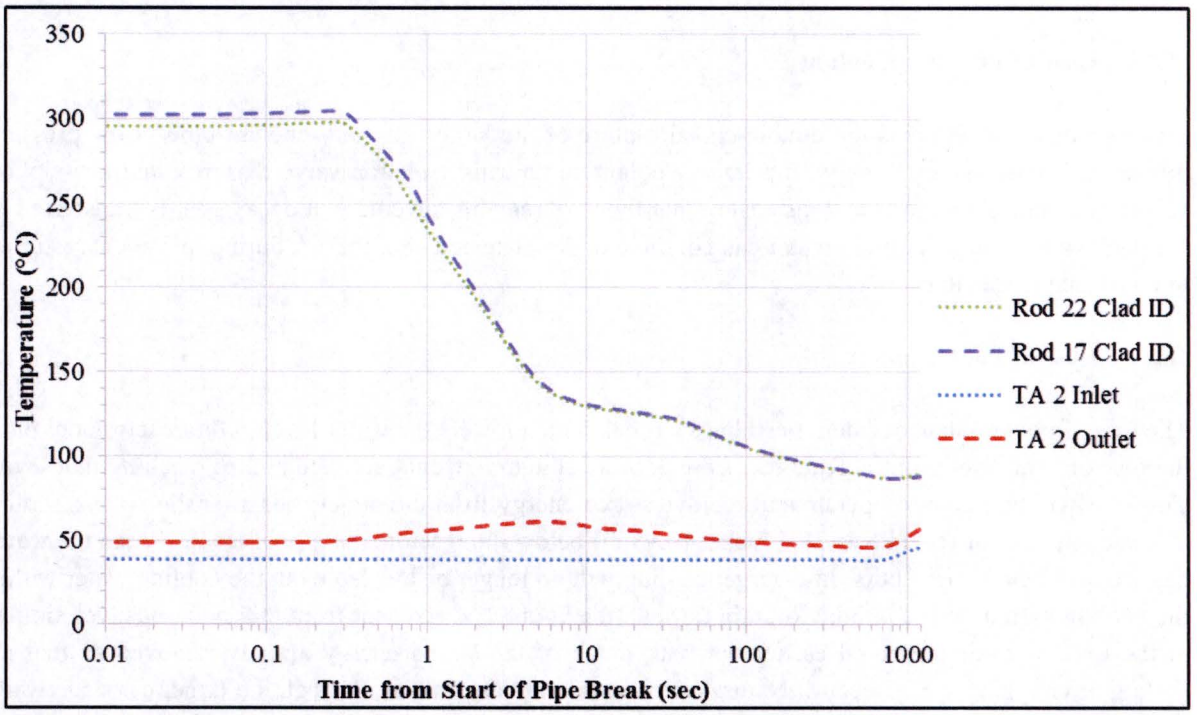

Figure 97
Maximum Cladding ID and Coolant Temperatures During Loss of Pump Flow

10.8 Mishandling of Target Cartridge or Target Rods

This event examines the potential to damage the target cartridge or target rods while being removed from its reflector position to its reactor pool transfer location. Multiple barriers separate the fission products in the target material from potential release locations within the TA.

The robust design of the target cartridge and target rods, and careful design of the tooling for handling the cartridge and rods will help prevent a handling accident from occurring while a target cartridge is being moved from its reflector position to its storage and transfer location within the reactor pool, or removing a target rod from the cartridge. This movement occurs no more than twice per week. The movement is carefully planned and does not start until after the reactor is shut down and the target rods are sufficiently cooled so the TCS can be shutdown.

Based on additional decay prior to handling, the consequences of mishandling the target cartridge or target rods are bounded by the TEF MHA.

10.9 Loss of Primary Coolant Flow

This reactor event can be caused by a variety of initiating events which result is flow stagnation and reversal in the MURR core. For all initiating events other than loss of electrical power, the target cooling water can continue to circulate and cool the TA during this event resulting in no consequences to it.

10.10 Loss of Primary Coolant

This reactor event assumes the double-ended rupture of the largest primary coolant pipe. Low pressure initiates a reactor scram along with primary coolant pump trips, isolation valve closures, and anti-siphon valves opening. Automatic actions ensure that the core remains covered and decay heat is transferred to the pool water. Target cooling water can continue to circulate and cool the TA during this event resulting in no consequences to it.

10.11 Loss of Pool Coolant

The loss of pool coolant accident postulates a break which lowers the water level in the reactor pool until the reactor scram set point is reached. Low pool level alarms would activate before reaching that level. The TCS will continue to operate and remove stored energy from the target rods after the reactor scram. The suction line for the TCS is 37.5 inches (0.95 m) below the reactor scram pool level. When the water has dropped below the suction line, target cooling will no longer be available but the cooling water within the cooling system will continue to drain through the TAs. The accident from this point behaves similar to the LOCA in air presented earlier but with much of the stored energy already removed so that no boiling or chugging would occur. Natural circulation and heat transfer through the target cartridge walls would be sufficient to maintain target rod cladding integrity and prevent any release of radioactivity.

10.12 Loss of Offsite Electrical Power

This event would cause the reactor to scram, pumps to shut down, and valves to fail to their safe shutdown positions due to their fail-safe design. Loss of electrical power would cause the decay heat removal valves to open thereby replacing the loss of forced flow from the shutdown of the target cooling water pumps with natural circulation flow. Pump coast-down and fluid momentum would provide additional flow during the transition from pump flow to natural circulation flow. This event is the same as the loss of target flow event analyzed earlier.

11. Technical Specifications

The new Technical Specifications associated with the SGE TEF are included as Attachment 2 to the License Amendment.

12. Proposed Confirmatory Testing

A variety of tests are planned to validate the design and demonstrate operation of the SGE TEF before installation and operation of the experiment in the reactor graphite reflector region. These tests are both

at the component and system level, and are designed to validate not only performance and safety at the system level, but to validate analytical modeling of component behavior.

12.1 Summary Description of Planned Tests

12.1.1 Target Pellet/Cladding Behavior Irradiation Testing

An irradiation test campaign will be performed to demonstrate the safety of the target rods. The chosen location for the test is the National Research Universal (NRU) reactor at Canadian Nuclear Laboratories (CNL), which can provide sufficient neutron flux and similar operating conditions to the nominal target rod design. The test will utilize capsules that replicate the geometry of the target rods. Following the irradiation test, a series of post-irradiation examinations (PIE) will be carried out to verify the performance of the target rod pellets and cladding.

CNL will fabricate eight (8) LEU irradiation test capsules using components fabricated by GA. Each capsule will contain up to 20 pellets of 5 mm diameter and 6 mm height. The capsule structure will be representative of the full TA's cladding design. This will include a Zircaloy-4 cladding tube and a nominal gap of 50 microns between the cladding and pellets (cold condition). Two ceramic spacers[3] will hold the UO_2 pellets in the center of the tube to prevent the metal end caps from reaching excessive temperatures. A low-carbon steel retaining spring is included for handling loads. The capsule will be filled with helium to improve the gap thermal conductivity between the cladding and pellets. The critical dimensions and attributes are provided in Table 53 and an illustration of the conceptual capsule design is shown in Figure 98, all representative of production target rods.

Table 53
Capsule Dimensions and Attributes

Cladding ID, mm	5.100 ± 0.025
Cladding wall thickness, mm	0.50 [redacted]
Pellet density, %TD	93 to 97
Pellet OD, mm	5.0 [redacted]
Pellet height, mm	6.0 [redacted]
UO_2 mass per capsule,* g	25.1
Pellet enrichment, †%	9.4
Helium fill pressure, atm	1
Tube material	Zircaloy-4

5a, b, f

[3] The peak neutron flux in the NRU reactor is essentially uniform over the length of the capsule. A ceramic spacer is therefore included in the test capsule to prevent end effect over heating of the capsule.

Ceramic spacer material	Aluminum Oxide

*Assumes 20 pellets per capsule at 95% theoretical density.
†Value determined by CNL neutronics analysis.

5a, b, d, e, f

Figure 98
Conceptual Design of Test Capsule

The capsules are designed to interface with CNL's existing equipment for handling nuclear targets used for the production of medical isotopes in the NRU reactor. The flow channel for the target capsules is formed long rod-like structure which replaces a fuel element. This structure contains four internal channels, each of which house an assembly of four (4) target elements linked end over end in a straight line, referred to as a stringer. The ends of the test capsules incorporate features which allow them to be incorporated into the stringer assemblies. For the irradiation test, each stringer will consist of two (2) loaded test capsules and two 92) filler capsules of solid aluminum. By utilizing the existing stringer design, the test capsules will allow for flexible handling, as each stringer can be removed separately.

The duration of the test irradiation period in the reactor is three (3) weeks, the maximum allowable irradiation time for target rods in MURR. The coolant flow conditions in the NRU reactor are similar to those in MURR. The coolant temperature ranges from 34 to 40 °C (93.2 to 104 °F), and the flow Reynolds number between 70,000 and 90,000 (80,000 for the target design in MURR). The coolant pressure is between 423 and 655 kPa (61.4 to 95 psi), which gives increased margin for boiling. Since there are multiple available irradiation locations, the target position was chosen to ensure that the targets reach the maximum design pellet power density of [redacted]. Given the highly thermalized neutron

5a, d, e, f

spectrum of the NRU reactor, the pellet enrichment was reduced to reach the desired power density. By matching the power density, coolant temperature and flow velocity, the test ensures that the irradiation conditions are sufficiently similar to the design condition in MURR.

Since FRAPCON/FRAPTRAN analysis shows that relocation strain occurring at shutdown contributes to the closure of the pellet-cladding gap, the test will incorporate multiple shutdown/restart cycles. [redacted] These shutdown/restart cycles will be simulated by removal of the test capsules from the flux field (the targets are compatible with online handling). The test schedule is given below in Table 54.

5a, d, e, f

Table 54
Irradiation Test Schedule

Test	Tasks	Start	End
Four Capsules to be Subjected to Irradiation Tests for Pellet/Cladding Behavior	Irradiations	11/25/16	4/10/2017
	Post-irradiation Examinations (PIE)	6/29/2017	8/14/2017
	Test Report Preparation	8/14/2017	10/3/2017

Following the irradiation, the capsules will be subjected to numerous PIE tests. Only four (4) of the eight (8) capsules are to be examined – the other four (4) will serve as back-up specimens. During the irradiation, the pellets may deform due to thermal strains, including "hour-glassing" and cracking, and release gaseous fission products. A visualization of potential pellet deformation during irradiation is shown in Figure 99. This deformation and gas build-up can lead to both mechanical and chemical interactions between the cladding and pellets, and verifying that these phenomena do not compromise the integrity of the cladding is important to the safety and operation of the target rods.

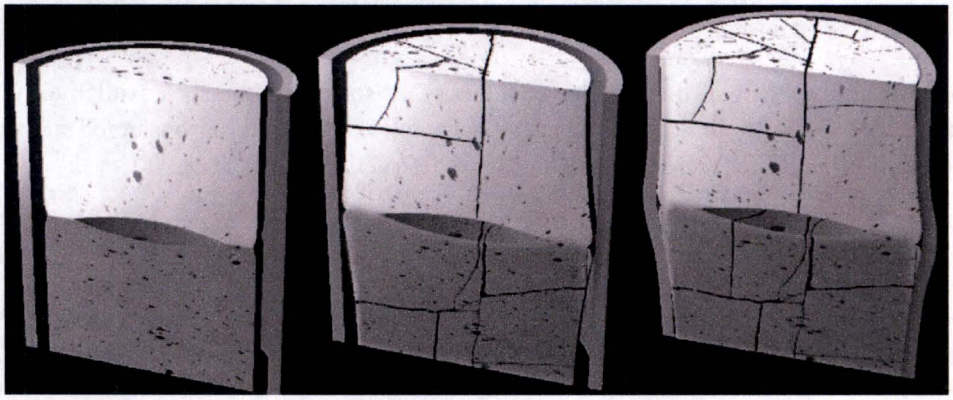

Figure 99
Visualization of Potential Pellet Deformation over Course of Irradiation (not to scale)

The following PIE tests will be performed on the capsules following the irradiation period:

[redacted]

5a, b, e, f

Data collected from the PIE will be provided to the NRC as soon as it becomes available. While the test is intended to verify GA's predictions of target rod behavior, the test will be considered successful as long as the test capsule remains hermetically sealed prior to destructive examination.

12.1.2 Critical Heat Flux Tests

The SGE target rods operate at very high power densities to maximize isotope yield. Analysis of the heat transfer in the target systems shows that cladding wall temperatures in the highest heat flux regions of the target exceed the coolant saturation temperature, leading to some subcooled nucleate boiling. The analysis predicts that the vapor content due to this boiling is confined to the surface of the target rods and is negligible in volume, and the NRC-accepted correlations show that the CHFR for the system will continue to provide sufficient margin. While the CHF with the various correlations shows that the CHFR

for the target rod cartridge provides sufficient margin, the safest approach is to verify that there are adequate margins in the CHFR via an experiment that shows significant margin exists between the system's maximum operating heat flux and the CHF for the configuration.

The overall objectives of the test are as follows:

- Demonstrate that for the system's maximum design heat flux, the cooling flow remains in the subcooled nucleate boiling regime, with minimal vapor generation at the wall.
- Experimentally determine the CHF for the system geometry and flow conditions, showing that sufficient safety margin is maintained.

This test is being conducted at the University of Wisconsin. A representative test section has been fabricated for insertion into a low pressure flow loop to perform the heat flux testing. The geometry of the target can be approximated by an annular channel. The cladding tube is at the center of the annulus, and a Pyrex tube will form the outer portion of the flow channel. The inner diameter of the Pyrex tube will be set to match the hydraulic diameter of the design target flow channel. A 3D model of the test section design is shown in Figure 100 and the conceptual section of the test rig minus the instrumentation is shown in Figure 101.

Heating is provided by direct resistive heating of an Inconel 625 tube. The power supply is rated to 100 kW and is capable of supplying a heat flux at the wall of 9 MW/m^2. Instrumentation to measure pressure drop, coolant temperature, Inconel tube temperature, and power supplied are all incorporated into the test section design. Coolant temperature and pressure in the test rig are adjustable to match target rod design conditions. Since the resistive heating provides a flat heat profile, the length of the heat tube was reduced by the peaking factor so that the total power was preserved while operating at the maximum heat flux.

The first test objective will be achieved by operating the flow loop while providing sufficient power to the heating rod to reach the desired heat flux. Nominal and worst-case [redacted] flow, [redacted] heat flux) conditions will be used. Cladding surface temperature will be calculated from internal thermocouple measurements, power supply output, and heating tube geometry. The bubble generation at heater surface will be captured with high speed camera.

5a, b, f

The second test objective will be achieved by slowly ramping the power to the heater until DNB occurs. DNB is detectable as an excursion event on the heater internal thermocouple. Coolant temperature will be adjusted to ensure that local conditions at the end of the heater where DNB occurs match the design temperature of the coolant at the maximum heat flux location in the target cartridge.

The test schedule is given below in Table 55.

Table 55
Critical Heat Flux Test Schedule

Test	Tasks	Start	End
Critical Heat Flux Tests	Complete Assembly and Instrumentation of Test Rig and Perform Initial Shakedown Testing	9/16/2016	12/30/2016
	Perform Flow Characterization and CHFR Tests	1/2/2017	2/15/2017
	Complete Final Report	2/15/2017	2/28/2017

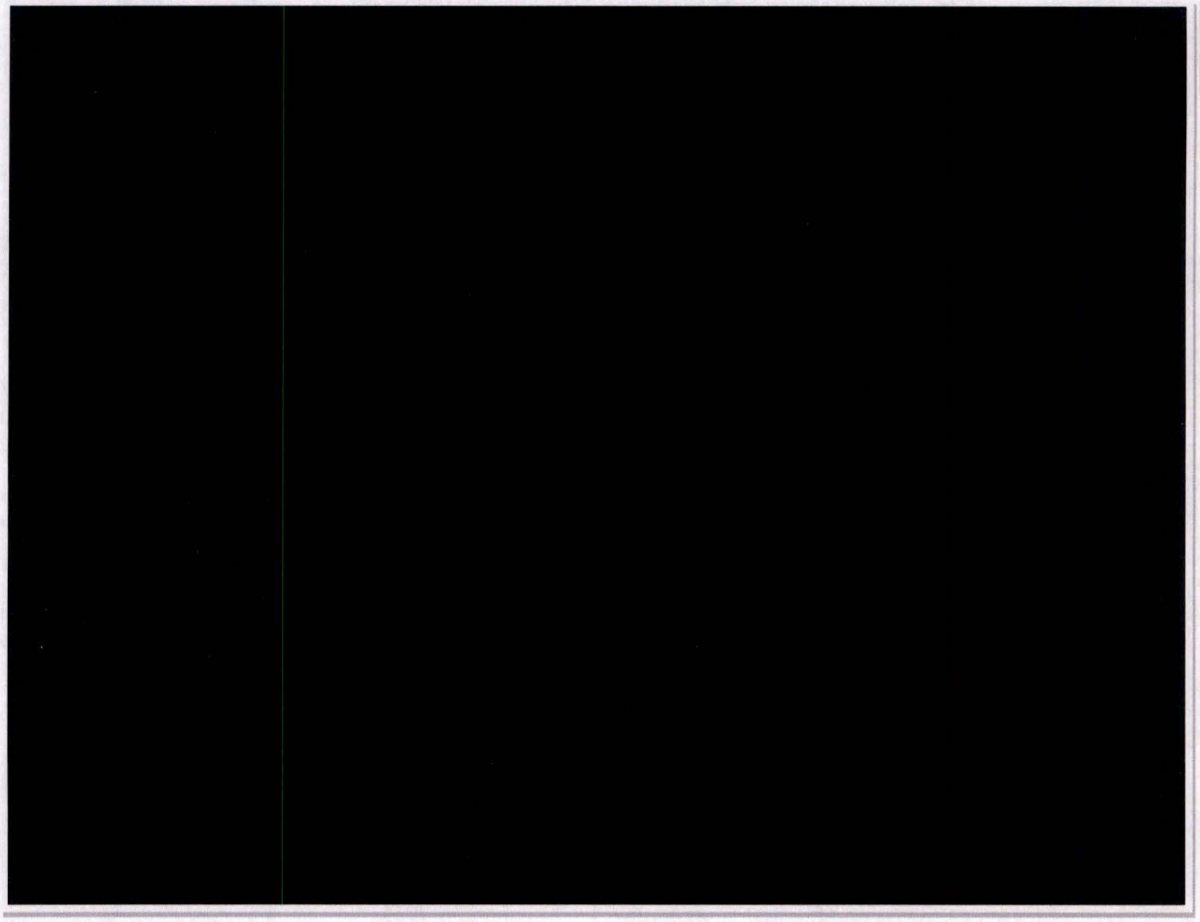

5a, b, e, f

Figure 100
Conceptual Schematic of CHF Test Flow Section

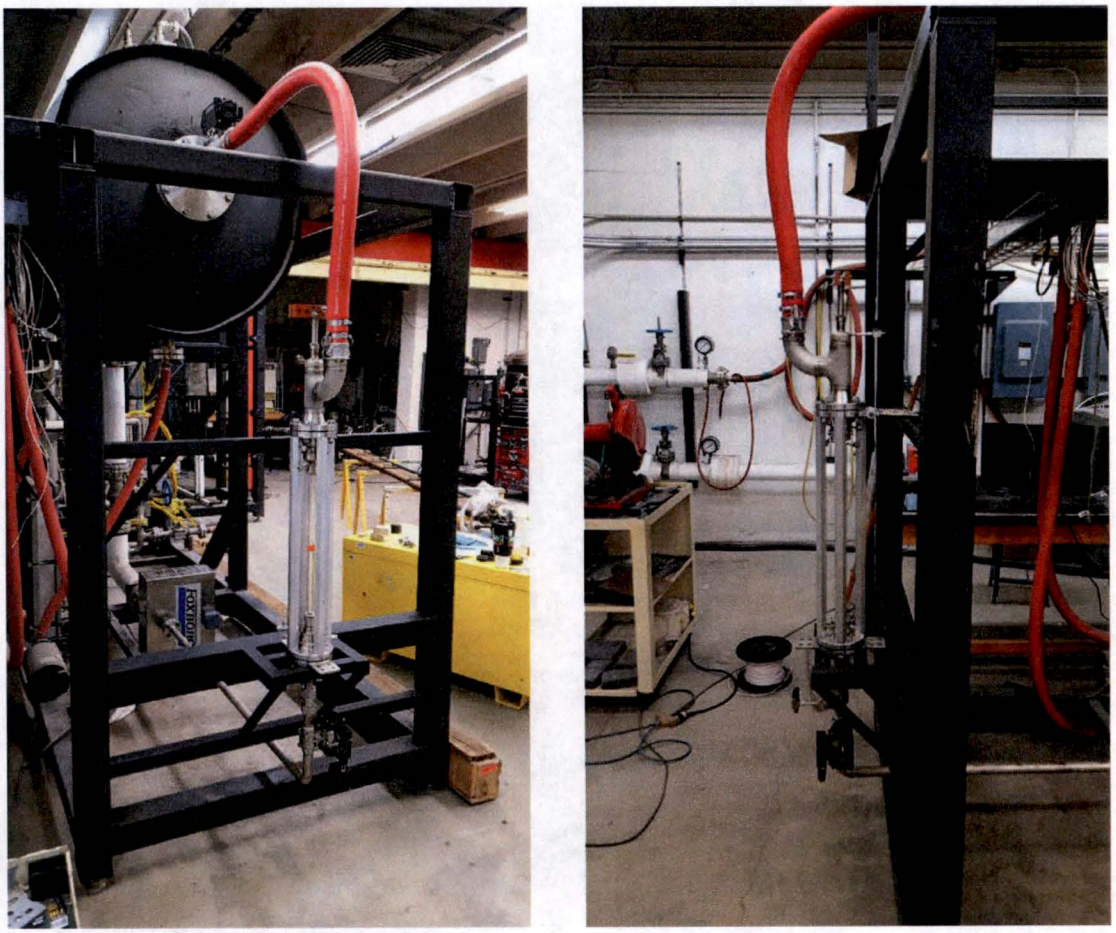

Figure 101
Uninstrumented Critical Heat Flux Test Section in Low Pressure Flow Loop Rig

12.1.3 System Integration and Cooling Flow Tests

The purpose of the system integration is to verify the installation and removal procedures for the target system components (target housing, target cartridge, target rods, and target loading and unloading station) and TCS piping upstream of the target housing. Operation of the pick-up tooling for the target rods and cartridges will also be demonstrated. In addition, after system integration is complete, flow and pressure drop tests will be performed to verify the functionality of the WCM and to confirm the pressure drop through the TA that was obtained by analysis. A representation of these systems will be assembled and tested at GA facilities. Figure 102 illustrates the test components, which include a surrogate pool, target system, and TCS.

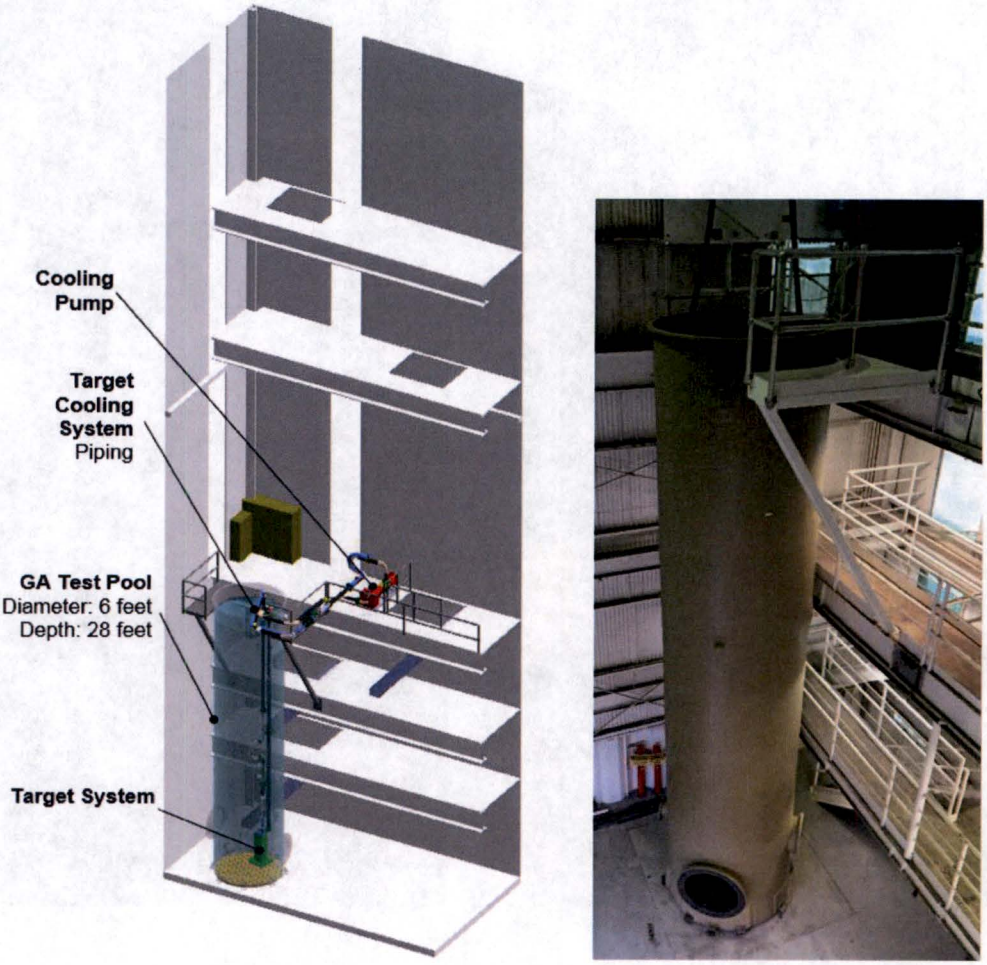

Figure 102
GA Test Setup Conceptual Arrangement

The surrogate pool will be a fiberglass tank; 6 feet (1.8 m) in diameter and 28 feet (8.5) tall. This height allows realistic underwater simulation of the system integration procedures. The TCS piping in the surrogate pool will be representative of the piping and pipe support structure that will be used at MURR. The goal is to mimic the attachment points and structural interferences as closely as possible.

The full scale production system at MURR consists of two target systems, however only one target system will be tested in this configuration at GA's test facilities. The test specifications and a comparison of the out-of-reactor test pool and the MURR pool are shown in Table 56.

Table 56
Testing Specifications

Parameters	GA Test Pool Specifications	MURR Pool Specifications
Pool Diameter	6 feet	10 feet
Pool Depth	28 feet	31 feet
Distance from Bottom of Target to Nominal Operating Water Level	26 feet	26 feet
WCM Inlet Pipe Inner Diameter	4 inches	4 inches
Number of Target Assemblies	1	2
WCM Outlet Pipe Inner Diameter	3 inches	3inches
Water Chemistry	~5.5 nominal pH Conductivity ~2 µS/cm	5.5 nominal pH Conductivity < 2 µS/cm

The test schedule is shown in Table 57.

Table 57
System Integration Test Schedule

Test	Tasks	Start	End
System Integration and Cooling Flow Tests	TA Installation Test	4/4/2017	4/10/2017
	TA Pressure Drop Test	4/20/2017	4/21/2017
	Target Rod & Cartridge Installation/Removal Test	4/24/2017	4/28/2017
	Test Report Preparation	5/8/2017	6/23/2017

13. References

1. "Irradiation Effect on Fatigue Behavior of Zircaloy-4 Cladding Tubes", Tenth International Symposium, ASTM STP 1245, 1994 pp. 549-558.
2. Nekhamkin, Y., Hasan, D., Elias, E. "Zirconium Ignition in an Exposed Fuel Channel," Conference on Reactor Physics and Technology II, Israel, pp. 45-48, February 2014.
3. [ASTM STP 1245] "Irradiation Effect on Fatigue Behavior of Zircaloy-4 Cladding Tubes", Tenth International Symposium, ASTM STP 1245, 1994, pp 549-558.
4. [https://www-nds.iaea.org/CRPdpa/, 2015] "Primary Radiation Damage Cross Sections, https://www-nds.iaea.org/CRPdpa/, 2015.
5. [304441M00014/B] "Maximum Neutron Damage of Al6061, Zircaloy-4 and SS316L" GA Document No. 30441M00014/B. General Atomics Proprietary Information.
6. [King, 1973] King, T. T., A. Jostons and K. Farrell, "Neutron irradiation damage in a precipitation-hardened aluminum alloy," Effects of Radiation on Substructure and Mechanical Properties of Metals and Alloys, ASTM STP 529, American Society for Testing and Materials, 1973, pp. 165-180.
7. [Jin 2015] Jin, H.J. and T.K. Kim, "Neutron Irradiation Performance of Zircaloy-4 under Research Reactor Operating Conditions," Annals of Nuclear Energy, 25 (2015) pp. 309-315.
8. [IAEA-TECDOC-1496] Thermal Physical Properties Database of Materials for Light Water and Heavy Water Reactors, IAEA-TECDOC-1496, June 2006.
9. [Byun 1996] Byun, T. S. and N. Hashimoto, "Strain hardening and long-range internal stress in the localized deformation of irradiated polycrystalline metals," Journal of Nuclear Materials 354 (2006) 123-1304-28.
10. Pawel, J. E. et. al., Irradiation performance of stainless steels for ITER applications," Journal of Nuclear Materials 239 (1996) 126 131.
11. University of Missouri Research Reactor Safety Analysis Report, submitted to the U.S. Nuclear Regulatory Commission August 2006.
12. [LANL 2003] "MCNP – A General Monte Carlo N-Particle Transport Core, Version 5," LA-UR-03-1987, Los Alamos National Laboratory, April 2003.
13. [Conlin 2013] Conlin, J. L. et al., "Continuous Energy Neutron Cross Section Data Tables Based upon ENDF/B-VII.1," LA-UR-13-20137, Los Alamos National Laboratory, Feb. 2013.
14. [Parsons 2012] Parsons, D. K., Conlin, J. L, "Release of Continuous Representation for S(α,β) ACE Data," LA-UR-12-00800, Los Alamos National Laboratory, February 2012.
15. [Kutikkad 2015] Kutikkad, K., Private Communication, University of Missouri Research Reactor, July 2015.

16. [Peters 2016] Peters N., Private Communication, University of Missouri Research Reactor, May 2016.

17. [Kiedrowski 2010] Kiedrowski, B. C. et al., "MCNP5-1.60 Feature Enhancement & Manual Clarifications," LA-UR-10-06217, Los Alamos national Laboratory, 2010.

18. M. C. White, "Photoatomic Data Library MCPLIB04: A New Photoatomic Library Based On Data from ENDF/B-VI Release 8," LA-UR-03-1019, Los Alamos National Laboratory, February 2003.

19. M. C. White, "Development and Implementation of Photonuclear Cross-Section Data for Mutually Coupled Neutron-Photon Transport Calculations in the Monte Carlo N-Particle (MCNP) Radiation Transport Code," LA-13744-T, Los Alamos National Laboratory, July 2000.

20. J. F. Briesmeister, Ed., "MCNPTM – A General Monte Carlo N-Particle Transport Code," LA-13709-M, Los Alamos National Laboratory, March 2000.

21. J. W. Durkee, Jr. et al., "The MCNP6 Delayed-Particle Feature," LA-UR-12-00283, Los Alamos National Laboratory, March 2012.

22. D. B. Pelowitz, Ed., "MCNP6TM User's Manual Version 1.0," LA-CP-13-00634, Los Alamos National Laboratory, May 2013.

23. [30441R00033 2016] GA Document No. 30441R00033/B. "Forced Convection Cooling of High Power Density Nuclear Target Rod with Two-Phase Considerations" (December 2016) General Atomics Proprietary Information.

24. [Del Valle 1985] V.H. Del Valle, D.B.R. Kenning, Subcooled flow boiling at high heat flux, Int. J. Heat Mass Transfer, 28 (1985), pp. 1907–1920).

25. [Jens 1951] Jens, W.H., and Lottes, P.A, "Analysis of heat transfer, burnout, pressure drop and density data for high pressure water", ANL-4627, 1951.

26. [Unal 1976] H.C. Unal, Maximum Bubble Diameter, Maximum Bubble-Growth Time and Bubble-Growth Rate During the Subcooled Nucleate Flow Boiling of Water up to 17.72 MN/m^2, Int. J. Heat Mass Transfer, 19 (1976), pp. 643–649.

27. [Chen 1966] Chen, J. C. "Correlation for Boiling Heat Transfer to Saturated Liquids in Convective Flow," in Ind. Eng. Chem. Proc. Dev., 5, 322, 1966.

28. [Glasstone & Sesonske, 1967] S. Glasstone and A. Sesonske, Nuclear Reactor Engineering, Chapter 6, "Heat Transfer to Boiling Liquids: Surface and Volume Boiling", Sec. 6.129-6.149, Van Nostrand Reinhold [1967].

29. [Bernarth 1960] Bernath, Louis, "A Theory of Local-Boiling Burnout and its Application to Existing Data", Chemical Engineering Progress Symposium Series, NO. 30, Vol 56, p. 95-116, 1960.

30. [FRAPTRAN 2011] FRAPTRAN 1.5: "A Computer Code for the Transient Analysis of Oxide Fuel Rods", NUREG/CR-7023, PNNL-19400, Vol. 1, Rev. 1 May 2014.

31. [Groeneveld 2007] Groeneveld, D.C., et al, The 2006 CHF Look-Up Table, Nuclear Engineering and Design 237 (2007) p. 1909-1922.

32. [Padoussis 2004] ASME Boiler and Pressure Vessel Code, Section III, Div 1, Appendix N, N-1345.1, p. 338, 2004.

33. [Farmer 2006] Farmer, M.T., Hoffman, E.A., Pfeiffer, P.F., Therios, I.U, Wei, T.Y.C, Generation IV Nuclear Energy System Initiative Pin Core Subassembly Design, ANL-GENIV-070, April , 2006, p. 57-59.

34. [30441R00035 2016] "Cooling of the MURR Beryllium Reflector" GA Document No. 30441R00035/A (December 2016) General Atomics Proprietary Information.

35. GA Doc. No. 30441R00022 – Moved to Applicable Documents Table 3-2.

36. "Decay Heat Power in Light Water Reactors," ANSI/ANS-5.1-2014, published by the American Nuclear Society.

37. "Method for Calculating the Fractional Release of Volatile Fission Products from Oxide Fuel," ANSI/ANS-5.4-2011, published by the American Nuclear Society.

38. [30441R00022 2016] "Source Term Analysis" GA Document No. 30441R00022/B (December 2016) General Atomics Proprietary Information.